Nuclear protein dynamics during pattern-triggered immunity in *Arabidopsis thaliana*

Inaugural-Dissertation

zur

Erlangung des Doktorgrades

der Mathematisch-Naturwissenschaftlichen Fakultät

der Universität zu Köln

vorgelegt von

Sayan Roy Choudhury

aus Varanasi, Indien

Köln, Januar 2021

Die vorliegende Arbeit wurde am Max-Planck-Institut für Pflanzenzüchtungsforschung in Köln in der Abteilung für Pflanzen-Mikroben Interaktionen in der Arbeitsgruppe von Dr. Kenichi Tsuda angefertigt.

Berichterstatter: Prof. Dr. Stanislav Kopriva
(Gutachter)

Prof. Dr. Iris Finkemeier

Prof. Dr. Kenichi Tsuda

Tag der mündlichen Prüfung: 30.11.2020

Publication

Stuttmann J, Peine N, Garcia AV, Wagner C, Choudhury SR, Wang Y, et al. (2016) Arabidopsis thaliana DM2h (R8) within the Landsberg RPP1-like Resistance Locus Underlies three different cases of EDS1-conditioned autoimmunity. PLoS Genet 12(4):e1005990

Table of Contents

List of figures

List of tables

List of Abbreviations

BAK1	BRI1-ASSOCIATED RECEPTOR KINASE 1
CDPK	calcium-dependent protein kinase
cfu	colony forming unit
DAMP	damage-associated molecular pattern
DEP	differentially expressed proteins
EFR	EF-TU RECEPTOR
EF-Tu	elongation factor Tu
EGF	epidermal growth factor
ETI	effector-triggered immunity
ETS	effector-triggered susceptibility
FLS2	FLAGELLIN-SENSING2
GO	Gene Ontology
LPS	Lipopolysaccharides
LRR	leucine-rich-repeat
LysM	lysine motif M
MAMP	microbe-associated molecular pattern
MAPK	mitogen-activated protein kinase
mfec	*min7,fls2,efr,cerk1*
MS	Murashige and Skoog
NLR	nucleotide-binding leucine-rich repeat
OD	optical density
PGN	peptidoglycans
PGPR	plant growth promoting rhizobacteria
PRR	pattern recognition receptor
PTI	pattern-triggered immunity
Pto DC3000	*Pseudomonas syringae* pv. *tomato* DC3000
RK	receptor kinase
RLCK	receptor like cytoplasmic kinases
RLP	receptor-like protein
RT-qPCR	reverse transcriptase quantitative polymerase chain reaction
TF	transcription factor
TX-100	Triton-X 100

Abstract

Perception of microbe-associated molecular patterns (MAMPs) by cell surface localized pattern recognition receptors (PRRs) triggers pattern-triggered immunity (PTI). PTI is associated with massive, rapid transcriptional reprogramming that occurs within 30 min after MAMP perception. However, it remains unclear how signal for MAMP recognition at the plasma membrane is relayed into the nucleus to trigger transcriptional reprograming. I hypothesized that investigating nuclear and total protein abundance changes during PTI would provide insights into this. However, existing protocols for nuclear isolation required for nuclear proteomics have shortcomings. In this study, I modified a nuclear isolation protocol to facilitate detection of nuclear proteins in *Arabidopsis thaliana*. Mass spectrometry-based comparison with an existing nuclear isolation protocol showed that my method not only increased detection of nuclear proteins but also reduced contaminants, especially plastidial proteins compared with the previous protocol. I used this method to investigate nuclear protein dynamics during the MAMP flg22-induced PTI. I found that flg22-induced PTI resulted in significant changes in nuclear protein abundances with distinct responses at different time points. For instance, the transcription factor WRKY47 showed increased abundance in the nucleus at 3 and 9 h after flg22 treatment but was not detected in the total fraction. Consistently, mutant plants deficient in *WRKY47* showed compromised resistance against a bacterial pathogen. These results point to the significance of nuclear proteomics. In addition, by comparing nuclear and total proteome changes upon flg22-treatment, I found proteins showing signatures of movements between the cytosol and nucleus including the kinases- NADK1 and PCRK1 showing signatures of nuclear import and a phosphatase- MKP1 and a transcription factor TOE1 showing signatures of nuclear export. I also profiled nuclear and total proteomes at earlier time points to investigate protein abundance changes which likely precede transcriptional reprogramming. A hypothesis for rapid transcriptional activation is de-repression: flg22 perception triggers inhibition or disappearance of high-turnover negative regulators, which leads to transcriptional activation of flg22-responsive genes. This is supported by the data that flg22 and the translational inhibitor cycloheximide triggers highly overlapped gene expression changes. However, I found that flg22 and cycloheximide triggered very different protein abundance changes, suggesting that flg22 and cycloheximide do not share the same mechanism but do activate the common set of genes. I found that nuclear proteome at 15 min after flg22-treatment showed downregulation of a number of proteins including RIN4-a negative regulator of PTI, SSP5-a phosphatase and transcriptional repressor, and MVQ1- a MPK3/6 substrate. Since, this downregulation was

observed exclusively at 15 min in the nuclear fraction, downregulation of some of those proteins may be important for transcriptional reprogramming in response to flg22. Taken together, this thesis advances the field of nuclear proteomes in plants and provides insights into nuclear protein dynamics during flg22-trigerred PTI.

1. Introduction

1.1 The plant immune system

In nature, plants are subjected to a wide variety of microbes. They can be pathogenic or beneficial to plants (Agler et al., 2016; Hacquard et al., 2017; Berens et al., 2017). Plants have evolved various mechanisms to recognize these microbes in order to stay healthy (Guan-Zhu, 2018).Plants have evolved pattern recognition receptors (PRRs) to sense microbial existence or invasion (Couto and Zipfel, 2016; Wan et al., 2019b; Albert et al., 2020). The PRRs localizes on the cell surface and recognize microbial molecules known as microbe-associated molecular patterns (MAMPs). This recognition results in pattern-triggered immunity (PTI) (Tsuda and Katagiri, 2010). These MAMPs are evolutionarily conserved and usually indispensable microbial components that cannot be easily changed (Cook et al., 2015; Erbs and Newman, 2012; Boller and Felix, 2009). Plants can also mount PTI-like immunity by recognizing plant-derived damage-associated molecular patterns (DAMPs) via PRRs (Couto and Zipfel, 2016; Gust et al., 2017).

Evolution enabled several adapted pathogens to enhance their virulence via acquiring pathogen effector molecules to suppress PTI resulting in effector-triggered susceptibility (ETS) (Jones and Dangl, 2006). As a counter defense, plants have acquired a second branch of immunity, called effector-triggered immunity (ETI), in which pathogen effector molecules are recognized by intracellular receptors, typically belonging to nucleotide-binding leucine-rich repeat (NLR) family proteins (Jones and Dangl, 2006; Cui et al., 2015; Guan-Zhu, 2018). The NLRs can be grouped as sensor NLRs or helper NLRs (Tamborski and Krasileva, 2020). Sensor NLRs can directly recognize effectors or indirectly recognize effector by monitoring host proteins called guardees or decoys. The helper NLRs assist sensor NLRs or other NLRs for immune activation. Some NLRs have an integrated decoy domain which mimics important plant immune proteins, such as WRKY transcription factors, and serves as sensor for effector to trigger ETI (Sarris et al., 2015; Le Roux et al., 2015). These sensor NLRs monitors the guardees or decoys that alone are not sufficient to trigger ETI (Kourelis and Hoorn, 2018). For example, the *P. syringae* effector HopZ1a interacts with the plasma membrane associated receptor like cytoplasmic kinases (RLCK) ZED1. HopZ1a interaction with ZED1 is required for recognition of HopZ1a by the NLR ZAR1 (Lewis et al., 2013). However, ZED1 alone does not contribute to immunity against *P. syringae* in the absence of ZAR1 suggesting a decoy function of ZED1. PTI and ETI share common signaling components, but ETI is more robust

compared to PTI and is often associated with rapid cell death response to restrict growth of some pathogens (Tsuda and Katagiri, 2010). Thus, PTI and ETI represents two branches of plant immunity which help plants to fight against pathogens.

The role of plant immunity in detecting and regulating pathogenic microbes has been widely studied. However, plant immunity also plays an important role in shaping the plant microbiota (Teixeira et al., 2019; Fitzpatrick et al., 2020). Like pathogens, non-pathogenic or beneficial microbes can also suppress or evade plant immunity in order to successfully colonize. They do so by variation or degradation of MAMPs, changing lifestyle or by altering the surrounding environment to escape detection (Teixeira et al., 2019; Fitzpatrick et al., 2020). For instance, plant growth promoting rhizobacteria (PGPR) was found to have beneficial or deleterious effects on *A. thaliana* dependent on phosphate availability (Morcillo et al., 2020). Another study found that PGPR can lower soil pH to suppress immunity and facilitate root colonization (Yu et al., 2019). A recent study showed that *A. thaliana* roots can utilize both MAMPs and DAMPs signals in order to activate antibacterial defense specifically against pathogenic bacteria but not against commensal bacteria (Zhou et al., 2020a).

Furthermore, PTI was shown to regulate the phyllosphere microbiota composition in *A. thaliana.* A quadruple mutant- *mfec* (lacking *MIN7* involved in vesicle trafficking pathway and lacking PRRs- *FLS2*, *EFR*, *CERK1*) was found to have reduced endophytic microbial diversity compared to Col-0 plants (Xin et al., 2016; Chen et al., 2020). Additionally, relative abundance of Firmicutes were greatly reduced and that of Proteobacteria increased in *mfec* mutant compared to Col-0 showing importance of PTI in regulating the microbiota composition. Thus, plant immune system not only help plants against pathogenic microbes but plays an important role in regulating the microbiota.

1.2 Pattern-triggered immunity (PTI)

Until now several PRR-MAMP pairs have been identified and widely studied. PRRs can be receptor kinases (RKs) or receptor-like proteins (RLPs) (Couto and Zipfel, 2016; Wan et al., 2019a; Albert et al., 2020). RKs consist of a ligand binding extracellular ectodomain, a single transmembrane domain and an intracellular cytoplasmic kinase domain. The RKs differ from RLPs that lack an intracellular kinase domain or any other domain capable of intracellular signal transduction. Therefore, RLPs depend on other RKs for downstream signaling. PRRs are also categorized based on what kind of ligand-binding ectodomain they contain. PRRs recognize a

wide variety of MAMPs. For instance, PRRs containing a Leucin-rich repeat (LRR) ectodomain bind proteins or peptides, PRRs containing lysine motifs (LysM) bind carbohydrate-based ligands, PRRs containing lectin-type ectodomain bind ATP and, PRRs containing epidermal growth factor (EGF)-like ectodomains bind cell wall derived oligogalacturonides (Couto and Zipfel, 2016; Albert et al., 2020).

The microbial MAMPs are often required for microbial fitness. The MAMPs cannot be easily changed which is exploited by plants (Cook et al., 2015; Erbs and Newman, 2012; Boller and Felix, 2009). For instance, flg22 is a 22 amino acid peptide derived from bacterial flagellin and is recognized by the LRR-RK FLAGELLIN-SENSING2 (FLS2) in most land plants (Felix et al., 1999; Gómez-Gómez and Boller, 2000; Guan-Zhu, 2018). Elf18 is the N terminus, 18 amino acid long, peptide from the bacterial elongation factor Tu (EF-Tu) and is recognized by the LRR-RK EF-TU RECEPTOR (EFR) (Kunze et al., 2004; Zipfel et al., 2006). Other bacterial MAMPs include bacterial cell wall forming peptidoglycans (PGN) and bacterial medium-chain 3-hydroxy fatty acids. In *A. thaliana* PGN is recognized via the LysM domain containing RLPs, LysM DOMAIN PROTEIN 1 and 3 (*At*LYM1 and *AtL*YM3) (Zipfel, 2014). Lipopolysaccharides (LPS) was previously reported to be recognized by a S-lectin domain containing RK LIPOOLIGOSACCHARIDE-SPECIFIC REDUCED ELICITATION (*At*LORE) which senses the conserved lipid A (LA) moiety of bacterial LPS (Ranf et al., 2015). However, recently it was found that *At*LORE recognizes bacterial medium-chain 3-hydroxy fatty acids that co-purifies with LPS and may not LPS itself (Kutschera et al., 2019).

Among MAMPs of fungal origin, chitin is the most extensively studied. Chitin is perceived differently in different species. In *A. thaliana*, chitin is recognized by a heterodimer consisting of the LysM-RKs CHITIN ELICITOR RECEPTOR KINASE 1 (CERK1) and LysM-CONTAINING RECEPTOR KINASE 5 (LYK5) which is primary chitin receptor in a ligand dependent manner, and partially by LysM-CONTAINING RECEPTOR KINASE 4 (LYK4) that constitutively interacts with LYK5 leading to dimerization and phosphorylation of CERK1 leading to downstream signalling (Cao et al., 2014; Xue et al., 2019; Liu et al., 2012b). In Rice, chitin is recognized by LysM-RLP chitin-elicitor binding protein (OsCEBiP) together with OsLYP4 and OsLYP6 which has dual specificity for both chitin and PGN (Liu et al., 2012a; Kouzai et al., 2014). CEBiP is a LysM-RP that lacks intracellular kinase domain and requires rice chitin-elicitor receptor kinase 1 (OsCERK1), which has an intracellular kinase domain, to activate chitin signalling.

Additionally, there are several MAMP-PRR pairs in other plant species. For instance, in *Solanum lycopersicum* the LRR-RK FLS3 recognizes a different flagellin epitope, flgII-28. The tomato LRR-RK COLD SCHOCK PROTEIN RECEPTOR (CORE) recognizes the csp22 epitope of the bacterial cold-shock protein (CSP). In *Nicotiana benthamiana* csp22 is recognized by the LRR-RLP *Nicotiana benthamiana* RECEPTOR-LIKE PROTEIN REQUIRED FOR CSP22 RESPONSIVENESS (NbCSPR) (Hind et al., 2016; Saur et al., 2016). However, Wang et al. 2016 reported that ectopic expression of NbCSPR under 35S promoter in *N. benthamiana* did not respond to csp22 as measure by oxidative burst assay. Instead, a CORE homologue-NbCORE with 79% amino acid identity in *N. benthamina* was shown to be responsive to csp22(Wang et al., 2016). In rice, LRR-RK OsXA21 recognizes the *Xanthomonas oryzae* pv. *oryzae* (Xoo) RaxX protein (Pruitt et al., 2015, 2017).

MAMP recognition by the PRRs leads to several downstream PTI responses that are temporally regulated. For instance, PRR activation leads to rapid phosphorylation and activation of downstream components leading to production of reactive oxygen species (ROS), calcium influx, activation of mitogen-activated protein kinases (MAPKs) and calcium-dependent protein kinases (CDPKs) pathways that are central to phosphorylating and activating downstream components, such as transcription factors (TFs), leading to transcriptional reprograming. However, it is mostly unknown where components of PTI signaling interact that leads to signal transduction inside the nucleus. For instance, whether MAPKs or CDPKs phosphorylate transcription factors (TFs) in the cytosol which in turn moves inside the nucleus or MAPKs or CDPKs themselves move inside the nucleus to phosphorylate TFs leading to transcriptional reprograming is still unknown. It is conceivable that some factors move from the cytosol to the nucleus to trigger transcriptional reprogramming which still needs to be identified.

1.3 Flg22 signaling

1.3.1 Flg22 perception and early signaling events

In *A. thaliana*, flg22 is sensed by the LRR-RK FLS2 that is associated with SOMATIC EMBRYOGENESIS RECEPTOR KINASE (SERK) family co-receptors BRI1-ASSOCIATED RECEPTOR KINASE 1 (BAK1, also known as SERK3), and BAK1-LIKE1/SERK4 (BKK1/SERK4) on the plasma membrane (Chinchilla et al., 2007; Roux et al., 2011; Schulze et al., 2010). The flg22 binding to FLS2 is contributed by LRRs 3-18 which forms a binding

groove in FLS2 where flg22 makes contact (Sun et al., 2013). Upon binding of flg22, FLS2 heterodimerizes with BAK1 within minutes (Boller and Felix, 2009; Chinchilla et al., 2007; Sun et al., 2013). Heterodimerization of FLS2 and BAK1 leads to their rapid phosphorylation initiating the intracellular signaling (Schulze et al., 2010; Schwessinger et al., 2011; Cao et al., 2013). Flg22 acts like a "molecular glue" which stabilizes FLS2-BAK1 complex upon flg22 binding. The functional importance of BAK1 was shown via *A. thaliana bak1* mutants that showed reduced flg22 response measured by reduced ROS production and higher susceptibility to weakly virulent bacterial strain, such as- *Pseudomonas syringae* pv. *tomato* DC3000 (*Pto* DC3000) without effector proteins or coronatine, compared to Col-0 (Roux et al., 2011). In addition to BAK1, another FLS2 co-receptor- BAK1-LIKE1/SERK4 (BKK1) is required for full activation of flg22 response (Roux et al., 2011). The *bak1/-bkk1* double mutants was found to have a greater reduction in flg22 responses, such as, reduced ROS production, MAPK activation, and defense gene induction compared to single mutants.

FLS2-BAK1 complex formation is tightly regulated to prevent mis-activation in absence of pathogen or prolonged activation of immune responses (Zhou and Zhang, 2020). For instance, flg22 induced FLS2-BAK1 complex formation is inhibited by BAK1-INTERACTING RECEPTOR-LIKE KINASE 2 & 3 (BIR2 & BIR3) that constitutively associates with BAK1 in absence of flg22 (Gao et al., 2009; Halter et al., 2014; Imkampe et al., 2017). In the presence of flg22, BAK1 is released and can initiate complex formation with FLS2 to allow flg22 triggered signalling. Recently, nuclear shuttle protein (NSP)-interacting kinase 1 (NIK1), a RK, was found to negatively impact flg22 induced PTI responses, such as, MAPK activation and induction of defence marker genes- *PP2C* and *WRKY29*. The *nik1-1* knockout mutants were more resistant to *Pto* DC3000 and *P. syringae* pv. *maculicola* (*Psm*) ES4326 (Li et al., 2019a). In the absence of flg22, NIK1 is associated with FLS2 and BAK1 to negatively regulate mis-activation of immune response. Interestingly, since NIK1 remains associated with FLS2/BAK1 irrespective of flg22, it was proposed that in presence of flg22, NIK1 would bind more tightly to FLS2/BAK1 and negatively regulates prolonged PTI activation (Li et al., 2019a). The phosphorylation of PRRs is critical for their activation, therefore, several protein phosphatases directly regulate PRR activation via inhibiting phosphorylation. For instance, phosphatases type 2C (PP2Cs) are important negative regulators of PRR complex formation (Felix et al., 1994; Chandra and Low, 1995). In *A. thaliana,* overexpression of kinase-associated protein phosphatase (KAPP) leads to reduced flg22 responsiveness and was found to be associated with the cytoplasmic domain of FLS2 in yeast-two-hybrid assay (Gómez-Gómez et al., 2001). Another *A. thaliana* protein phosphatase type 2A (PP2A) was found to be

constitutively associated with the FLS2 co-receptor BAK1 in planta (Segonzac et al., 2014). Flg22 treatment reduced BAK1-associated PP2A activity and treatment with PP2A inhibitor, cantharidin, could induce BIK1 phosphorylation and ROS production which suggests a negative role of PP2A during PTI response (Segonzac et al., 2014).

In addition to the LRR-RKs discussed above there are other FLS2 interacting partners. For instance, the plasma membrane localized LRR-RK- IMPAIRED OOMYCETE SUSCEPTIBILITY1 (IOS1) interacts constitutively with FLS2 and its co-receptor BAK1. IOS1 was shown to be important for early MAMP-responses, such as, induction of the PTI-marker gene *FLG22-INDUCED RECEPTOR-LIKE KINASE 1* (*FRK1*), callose deposition and, MAPK activation by positively regulating the FLS2-BAK1 complex formation during MAMP treatment (Yeh et al., 2016). Beside IOS1, a recently identified co-receptor is the malectin-like receptor kinase FERONIA (FER) that serves as a scaffold protein and facilitates interaction of PRRs, such as, FLS2 and EFR with their co-receptor BAK1 (Stegmann et al., 2017). Recently, FER was shown to regulate FLS2-BAK1 association independent of its kinase activity and regulates FLS2 mobility in plasma membrane nanodomains (Gronnier et al., 2020). Another plasma membrane localized and, FLS2 and EFR associated receptor is the LORELEI-LIKE GPI-ANCHORED PROTEIN 1 (LLG1), which is also a co-receptor of FER and promotes interaction with BAK1 in a ligand dependent manner (Shen et al., 2017; Xiao et al., 2019). LLG1 also contributes to flg22 activated downstream signaling and PTI responses, such as, BOTRYTIS-INDUCED KINASE 1 (BIK1) phosphorylation and reactive oxygen species (ROS) production (Shen et al., 2017). Thus, flg22 perception involves a complex association among receptors and coreceptors for a successful perception and signaling.

1.3.2 Signaling downstream of FLS2- from the plasma membrane to the cytosol

Activation of PRRs following MAMP perception leads to activation of several downstream signalling cascades such as phosphorylation and activation of RLCKs, ROS production, Ca^{+2} influx across plasma membrane, MAPKs, CDPKs cascades, and heterotrimeric G proteins (Tang et al., 2017). RLCKs are important intracellular components of downstream signalling which phosphorylate and activate downstream components (Zhou and Zhang, 2020). In *A. thaliana*, an important member of the RLCK family is BIK1 which is associated with FLS2 in absence of flg22. Upon flg22 perception, BIK1 associated with FLS2/BAK1 complex is phosphorylated by BAK1 releasing BIK1 from the plasma membrane.

Activated BIK1 plays a crucial role during signalling from plasma membrane downstream of several receptor kinases such as FLS2, EFR, PEPRs and, CERK1 (Tang et al., 2017). For instance, BIK1 and a RLCK VII member- PBS1- LIKE1 (PBL1) are required for flg22 triggered activation of calcium channel and Ca^{+2} influx in cytoplasm (Ranf et al., 2014; Tang et al., 2017). In *A. thaliana*, CNGC2 and CNGC4 form a heteromeric calcium-permeable channel that is kept under a resting state by calmodulin CAM7 (Zhou and Zhang, 2020). Flg22 binding leads to phosphorylation of CNGC4 by BIK1 that activates the calcium channel and positively regulates flg22-induced ROS burst (Tian et al., 2019). BIK1 facilitates flg22-induced ROS production by phosphorylating the RESPIRATORY BURST OXIDASE HOMOLOGUE PROTEIN D (RBOHD) (Kadota et al., 2014; Li et al., 2014). Being an important signalling component, BIK1 protein level is regulated by protein turnover. In *A. thaliana*, CPK28 regulates proteasomal-dependent turnover of BIK1 (Monaghan et al., 2014). Additionally, ROS production is regulated by calcium-dependent kinase 5 (CPK5) that phosphorylates N-terminus of RBOHD and is itself activated by increased cytosolic Ca^{+2} regulated by cyclic nucleotide-gated channel (CNGCs) (Delormel and Boudsocq, 2019; Tian et al., 2019). Recently, it was shown that a CYSTEINE-RICH RK (CRK2) is required for MAMP triggered ROS production (Kimura et al., 2020). CRK2 remains associated with RBOHD. Upon flg22 treatment, C-terminus in RBOHD is phosphorylated by CRK2, which is necessary for ROS production and defence against *Pto* DC3000. On the other hand, RBOHD itself is under tight regulation via AvrPphB SUSCEPTIBLE1-LIKE13 (PBL13). PBL13 is a member of RLCK-VII family, that associates and phosphorylates RBOHD in absence of flg22 and negatively impact ROS production (Lin et al., 2015). Other RLCKs interacting with FLS2 are PTI-COMPROMISED RLCK 1 (PCRK1) and PCRK2 which are important for flg22-triggered salicylic acid (SA) accumulation and resistance against bacterial pathogens. Additionally, BRASSINOSTEROID SIGNALING KINASE 1 (BSK1) of RLCK XII family also associates with FLS2 and is required for flg22-induced ROS production (Shi et al., 2013).

The signal transduction downstream of RLCKs are also mediated via phosphorylation and activation of MAPKs and CDPKs that are crucial early signalling events downstream of PRRs (Tena et al., 2011). In *A. thaliana* two distinct MAPK pathways are activated within minutes after flg22 perception. The first pathway comprises of MPK4 and MPK11 which are activated by upstream MAPK kinases- MKK1/MKK2 that are activated by MAPK kinase kinase- MEKK1 and MEKK2. The second pathway comprises of MPK3 and MPK6 which are activated by upstream MAPK kinases- MKK4/MKK5 that are activated by MAPK kinase kinase- MAPKKK3 and MAPKKK5 (Zhou and Zhang, 2020). RLCKs are also shown to

directly regulate MAPK cascade downstream of PRRs. For instance, BSK1 was shown to interact with and phosphorylate MAPKKK5 and the *bsk1* mutant showed reduced phosphorylation of MAPKKK5 compared to Col-0, which demonstrates a direct connection between plasma membrane-localized receptor activation to cytosolic MAPK cascade activation (Yan et al., 2018). Moreover, phosphorylation of MAPKKK5 was necessary for immunity against bacterial and fungal pathogens. Additionally, MPKKK5 phosphorylates several MKKs, such as, MKK4/5. In turn, MKK4/5 phosphorylate MPK3/6 which are important for downstream PTI induced transcriptional reprogramming. A previous report claimed that phosphorylation of MAPKKK5 by a RLCKVII-1 family member- PBL27, was required for initiating chitin-induced activation of MAP kinase signalling cascade (Yamada et al., 2016). However, subsequent report claimed RLCKVII-4 family members to phosphorylate MAPKKK5 at Ser-599 which is required for MAMPs-flg22, efl18, chitin, Pep2 induced MPK3/6 activation (Bi et al., 2018). MPK3/6 have been described to have redundant roles and positively regulate plant immunity (Su et al., 2017; Zhang et al., 2018). Thus, RLCKs constitutes an important link connecting downstream signalling after PRR activation at the plasma membrane during PTI.

Another class of kinases are the calcium dependent protein kinases (CDPKs) that are rapidly phosphorylated upon flg22 treatment, such as CDPK4/5/6/11 (Boudsocq et al., 2010). Transcriptional induction of flg22-responsive genes and flg22-induced ROS production were completely abolished in *cpk4cpk5cpk6cpk11* quadruple mutants. CDPKs act like sensor of increased cytosolic Ca^{+2} produced due to variety of stresses. Due to presence of an N-terminal serine/threonine kinase domain and a C-terminal CaM-like domain with EF-hand calcium binding sites, CDPKs are effective signal transducers (Bigeard et al., 2015; Bredow and Monaghan, 2019). CDPK5 was shown to be phosphorylated following flg22 or efl18 treatment and RBOHD was identified as a substrate of CDPK5 in response to flg22 (Dubiella et al., 2013). In the same study, CDPK5 and RBOHD was found to be required for flg22-induced activation of PTI marker gene expression- *NHL1* in distal untreated leaves and phosphorylation of RBOHD was compromised in *cdpk5* mutants. CDPK28 was found to associate and phosphorylate BIK1, a key RLCK downstream of several PRRs, to regulate BIK1 protein turnover and negatively regulate PTI (Monaghan et al., 2014). BIK1 protein accumulation was enhanced in *cdpk28* mutants and was reduced in CDPK28 overexpressing lines. Activation of CDPKs and MAPKs leads to one of the hallmarks of PTI response-nuclear transcriptional reprograming. Thus, CDPKs and MAPKs constitutes crucial intermediators connecting signal transduction from cytosol into the nucleus described in later sections.

1.3.3 Signaling downstream of FLS2- from the cytosol to the nucleus

The MAPKs and CDPKs mediate the intracellular signalling from cytosol to the nucleus upon pathogen perception by the PRRs. They have several substrates, such as TFs, other kinases that leads to one of the hallmarks of PTI response which is transcriptional reprograming. For instance, a comparative transcriptome analysis of *mpk3*, *mpk4*, and *mpk6* mutants found that 36% of flg22-upregulated genes and 68% of flg22-downregulated genes were affected in at least one of the *mpk* mutants (Frei dit Frey et al., 2014). MAPKs are known to interact and phosphorylate variety of TFs, such as, basic region/leucine zipper motif (bZIP), basic helix-turn-helix (bHLH), MYB, WRKY and, APETALA2/ETHYLENE-RESPONSE ELEMENT BINDING FACTOR (AP2/ERF) (Tsuda and Somssich, 2015; Zhang et al., 2018). For instance in *A. thaliana*, flg22 triggered activation of a bZIP transcription factor VIP1 via MAPK3 leads to its re-localization from the cytosol to the nucleus where it mediates the expression of *PATHOGENESIS-RELATED1* (*PR1*) and *MYB44* (Djamei et al., 2007; Pitzschke et al., 2009). Similarly, MPK3/6 are known to phosphorylate MYB44 that induces the *WRKY70* which regulates SA and JA mediated transcriptional responses (Persak and Pitzschke, 2013; Shim et al., 2013). Additionally, several WRKY TFs are identified as potential targets of MPK3/6. For instance, WRKY33 is phosphorylated via MPK3/6 which induces *CYP71A13* and *PAD3* involved in camalexin biosynthesis. Unlike phosphorylation dependent nuclear re-localization of VIP1, MYB44 localizes in the nucleus with MPK3 and MKK4, irrespective of its phosphorylation status. Thus, one of the fundamental questions in plant immunity is in which subcellular location do MAPKs and TFs interact? MAPKs may phosphorylate TFs in the cytosol which then re-locate inside the nucleus similar to VIP1. Alternatively, MAPKs may themselves translocate into the nucleus to phosphorylate transcription factors which in turn induce transcriptional reprograming (Kim and Zhang, 2004). For instance, in animals phosphorylation at a 3 amino acid domain (SPS) of extracellular signal-regulated kinase (ERK)-2 was shown to induce its nuclear translocation (Wainstein and Seger, 2016). In parsley, ERM kinase was reported to be translocated into the nucleus upon Pep-25 elicitor treatment (Ligterink et al., 1997). It is conceivable that some factors move from the cytosol into the nucleus to trigger transcriptional reprogramming. However, in plants subcellular dynamics of MAPKs upon pathogen perception is largely elusive.

Similar to MAPKs, CDPKs are also important mediators of transcriptional reprograming. In *A. thaliana,* 70% of genes upregulated by ectopic expression of constitutively active CPK5 and CPK11 were also found to be upregulated by flg22 in microarray data. Recently, WRKY33

was identified as a direct target of CDPK5 and CDPK6 regulating camalexin production induced by *Botrytis cinerea* infection (Zhou et al., 2020b). Interestingly, WRKY33 is also phosphorylated by MPK3/6 but at a different site than CDPK5/6 suggesting WRKY33 as a common substrate regulating camalexin biosynthesis via specific phosphorylation of different phosphosites (Zhou et al., 2020b; Mao et al., 2011). In addition, CDPK5 was found to positively regulate priming in non-infected leaves before secondary infections and results in *SARD1* dependent enhanced accumulation of N-hydroxy pipecolic (NHP) acid which is a critical regulator of systemic acquired resistance (SAR) (Guerra et al., 2020). Although several instances about importance of CDPKs in regulating TFs are known, however, subcellular location of such interaction remains unknown.

Since the MAPKs/CDPKs rely on phosphorylation of their substrates for signal transduction, phosphatases are crucial in controlling the activity of MAPKs/CDPKs to regulate immune responses. For example, overexpression of the protein phosphatase *AP2C1* in *A. thaliana* compromises flg22- and oligogalacturonides (OGs)-induced phosphorylation of the MPK3/6 and, expression of *FRK1* and At1g26380 (*RetOx)* but not of *PHOSPHATE-INDUCED1 (PHI1)*. Expression of *FRK1* is regulated by MAPKs, expression of *RetOx* is regulated by MAPKs and CDPKs whereas expression of *PHI* is specifically regulated by CDPKs (Galletti et al., 2011; Boudsocq et al., 2010). Thus, phosphatase AP2C1 specifically de-phosphorylates MAPKs. The phosphatase MITOGEN-ACTIVATED PROTEIN KINASE PHOSPHATASE 1 (MKP1), was found to negatively regulate activation of MPK3 and MPK6. The *mkp1* mutants showed enhanced resistance to *Pto* DC3000 in an MPK6 dependent manner (Anderson et al., 2011). Furthermore, upon elf26 treatment MPK6 phosphorylates MKP1 resulting in accumulation of MKP1 protein. MKP1 was proposed to be a high turnover protein as demonstrated by increased accumulation of MKP1 after proteasome inhibitior-MG132 treatment (Jiang et al., 2017). Interestingly, protein phosphatases 2C (PP2Cs) were recently shown to inactivate ABA induced MPK3/6 phosphorylation (Mine et al., 2017). Moreover, *Pto* DC3000 was found to suppress MPK3/6 activation via induction of the PP2C- *HAI1* to suppress immunity. Therefore, protein phosphatases are important regulators of kinases and corresponding immune responses. Nevertheless, similar to the CDPKs/MAPKs it is not known in which subcellular location the phosphatases interact with their substrates.

1.3.4 FLS2-mediated transcriptional reprogramming in the nucleus

MAPKs and CDPKs activation lead to nuclear transcriptional reprograming that results

in production of antimicrobials to establish immunity. Transcriptional response to MAMPs-flg22 and elf18 were found to be highly overlapping although they have different receptors (Zipfel et al., 2006, 2004). An overlap of transcriptional response between flg22-induced differentially expressed genes with other MAMPs and DAMPs like chitin, oligogalacturnoide (OG) and peptidoglycan (PGN) was observed (Wan et al., 2008; Denoux et al., 2008; Gust et al., 2007). Thus, different MAMP and DAMPs trigger largely overlapping transcriptional response.

Transcriptional response is regulated via transcription factors that often act downstream of MAPKs/CDPKs pathway that regulate the activity of transcription factors (Li et al., 2016). The analysis of promoter sequences of flg22-induced genes and *RKs* showed overrepresentation of W-box *cis*-acting DNA elements, that are binding site for WRKY TFs (Navarro et al., 2004; Zipfel et al., 2004). The WRKY TFs may also be important to inhibit undue gene induction via constitutively expressed WRKY TFs since induced WRKY gene expression was found to be slightly upregulated in constitutive WRKY TF mutant, although the induction levels were lower than that upon flg22 treatment. Since constitutive WRKY binding sites on induced WRKY genes co-localizes with DNAse hypersensitive sites (DHSs) it was suggested that constitutive WRKYs act as repressors and are replaced by induced WRKY TFs upon induction via flg22 (Birkenbihl et al., 2018). Thus, WRKY TFs are important regulators during MAMP triggered transcriptional reprograming. Another class of TFs overrepresented in the early PTI responsive genes is the calmodulin-binding transcriptional activator (CAMTA) motifs which is important for early PTI (Jacob et al., 2017). Previously, *CAMTA3* was shown to be a negative regulator of immunity based on elevated immune phenotype in *camta3* knockout mutant (Du et al., 2009). However, *camta3* phenotype was later attributed to activation via two NLR proteins and a guardee role of *CAMTA3* (Lolle et al., 2017). On the other hand, CAMTA3 was found to positively regulate early stress response genes via a CAMTA binding motif, *Rapid Stress Response Element* (*RSRE*), in response to various stresses including flg22 (Benn et al., 2014).

Being an important signalling point, TFs are under tight regulation. For instance, in the absence of pathogen, WRKY33 required for MAMP induced camalexin synthesis, is kept under inhibition within a nuclear complex of MPK4 and VQ motif-containing protein (VQP) MKS1 (Qiu et al., 2008). Upon flg22 perception, MPK4 phosphorylates MKS1. The MKS1-WRKY33 complex is released from MKP4. This allows WRKY33 to positively regulate transcription of its target *PHYTOALEXIN DEFICIENT3 (PAD3)* which is required for synthesis of camalexin. In a later study, WRKY33 was found to be phosphorylated by MPK3 and MPK6 and

phosphorylation was necessary for pathogen induced camalexin production(Mao et al., 2011). It will be interesting to know whether regulation of WRKY33 by MPK4 and MPK3/6 are as well interconnected. MPK3/6-targeted-VQ-motif-containing protein 1 (MVQ1) is another VQ-protein that was found to be a negative regulator of several WRKY TFs. MVQ1 is degraded upon flg22 treatment de-repressing WRKY TFs, thus allowing expression of target genes such as *NHL10* (Pecher et al., 2014). Thus, individual signaling components and their role in defense signaling are getting more known. However, how TFs relay signal transduction inside the nucleus, for instance, whether they move from the cytosol to the nucleus upon activation or get activated inside the nucleus needs to be further investigated.

Some of the discoveries in plant immune signaling points towards several possibilities which may further explain the mechanistic details of signaling from the plasma membrane to the nucleus. For instance, whether MAPKs and CDPKs phosphorylate TFs in the cytosol and phosphorylated TFs then translocate inside the nucleus, similar to VIP1. Alternatively, similar to animal ERK2, whether plant MAPKs and CDPKs can themselves translocate inside the nucleus where they phosphorylate TFs to regulate transcriptional reprogramming. It is conceivable that some factors move from the cytosol to the nucleus to trigger transcriptional reprograming. For instance, it was found that BIK1, which is associated with the plasma membrane, also showed a nuclear localization (Lal et al., 2018). BIK1 was found to interact with WRKY TFs-WRKY33, 50 and 57, in the nucleus, pointing to a mechanism that connects PRR perception at the plasma membrane to transcriptional reprogramming in the nucleus (Lal et al., 2018). However, since BIK1 nuclear localization is unaltered in both phosphodeficient and phosphomimic versions it is still unclear how BIK1's interaction with TFs is regulated upon pathogen attack.

In addition to cytosol to nuclear translocation, chloroplast proteins are also known to be re-located inside the nucleus to regulate nuclear encoded gene expression (Mullineaux et al., 2020). For example, upon treatment with flg22, SA and, hydrogen peroxide chloroplasts were found to induce stromal protrusion called stromules that surround the nucleus (Caplan et al., 2015). The stromule frequency was found to correlate with a chloroplast protein- N-RECEPTOR INTERACTING PROTEIN (NRIP1) that is required by the TIR-NB-LRR N immune receptor to recognize TMV helicase protein p50 (Caplan et al., 2008, 2015). In addition, it was later found that the perinuclear accumulation of stromules is specifically directed towards the nucleus and is facilitated by microtubules and actin filament organization during innate immune response (Kumar et al., 2018). Thus, stromule formation may be used by other chloroplast proteins to get transported inside the nucleus upon pathogen attack. Another

chloroplast localized protein PTM- a chloroplast envelope-bound plant homeodomain (PHD) transcription factor, was found to show nuclear localization under photooxidative stress. Upon various photooxidative stress inducing stimuli (norflurazon, lincomycin) PTM undergoes proteolytic cleavage and its amino terminal translocate inside the nucleus to transmit chloroplast signals to the nucleus, however, such signal transduction events are not known upon biotic stresses (Sun et al., 2011).

Another example of nuclear translocation is the endoplasmic reticulum (ER) localized EIN2 which is a positive regulator of ethylene signaling. EIN2 plays a central role in ethylene signalling as in *ein2* mutant are insensitive to ethylene (Ji and Guo, 2013). In the absence of ethylene, EIN2 is kept phosphorylated by CTR1 preventing cleavage and translocation of EIN2 (Ju et al., 2012). In the presence of ethylene, ethylene receptors and CTR1 are inactivated, resulting in dephosphorylation, and cleavage of C-terminal part of EIN2. The cleaved C-terminal part of EIN2 is translocated into the nucleus where it stabilizes EIN3 and activates downstream signalling. During PTI, MPK3/6 phosphorylates the rate limiting ethylene biosynthesis enzymes 1-aminocyclopropane-1-carboxylic acid synthases (ACS2 and ACS6) which enhances ethylene production. Additionally, MPK3/6 phosphorylates WRKY33 which binds to the promoter of ACS2 and ACS6 to further enhance ethylene production (Tsuda and Somssich, 2015).

In addition, to signalling components being translocated inside the nucleus to regulate transcription, another hypothesis for quick and massive induction of flg22 responsive genes is de-repression of transcription: at the basal state, transcription of flg22 responsive genes are suppressed by a negative regulator(s) and upon flg22 perception, transcription is de-repressed via removal or inactivation of such negative regulator(s). Previous studies suggested that de-repression could be a mechanism to induce transcriptional reprogramming in response to flg22 as several flg22-responsive genes are also induced upon treatment with the protein synthesis inhibitor cycloheximide (CHX) (Navarro et al., 2004; Jacob et al., 2017; Birkenbihl et al., 2018). In this scenario, it has been proposed that translation of negative regulator(s), assumed to be high turnover-proteins, is inhibited by CHX, which leads to reduced accumulation of the negative regulator(s) resulting in activation of transcription of flg22 responsive genes. Birkenbihl et al. 2018, investigating dynamics of WRKY TFs at both RNA and protein level upon flg22 treatment found two classes of WRKYs- constitutive and induced. In untreated samples constitutive WRKYs are bound to target genes. Upon flg22 treatment the constitutive WRKYs are replace by induced WRKYs suggesting a repressive role of the constitutive WRKYs during flg22 triggered transcriptional response. Protein translation inhibitors can

similarly induce transcription of immune genes by blocking continuous synthesis of high turn-over repressor proteins that are continuously degraded resulting in de-repression. Comparison of transcriptome response by conditional expression of the CC-domain of barley Mildew resistance locus A (MLA_{CC}-) and CHX treatment showed 87% overlap among upregulated genes (Jacob et al., 2017). This raises several possibilities. First, similar to CHX, MLA_{CC}- results in translation inhibition which leads to transcriptional activation via disappearance of high-turnover negative regulators. Alternatively, MLA_{CC}- and CHX activate common set of genes via different mechanisms.

Similarly, overlapping gene expression induced by PTI and CHX might be due to PTI inhibiting translation, and therefore PTI and CHX show similar gene expression profiles. On the other hand, PTI may not inhibit translation but converges with CHX's mode of action at some point such as reduced accumulation of negative regulators of PTI-responsive genes.

1.4 Subcellular proteomics in plant immune system

Much of our current knowledge about plant immune responses are based on genetics and transcriptomics studies (Zhou and Zhang, 2020; Albert et al., 2020). However, protein abundance cannot always be explained by gene expression, therefore, our understanding of plant immune responses at protein level is limited (Ali et al., 2014; Liu et al., 2016; Xu et al., 2017). For example, half of the differentially abundant proteins in response to *Phytophthora infestans* infection in potato (*Solanum tuberosum*) did not show corresponding change at the transcriptome level (Ali et al., 2014). Thus, in order to understand protein level regulation of plant immune responses proteomics is necessary. During the last decade, several proteomic approaches were applied to understand protein dynamics during immune responses in plants. Some of these studies analyzed total proteome (Jones et al., 2006; Wang et al., 2012; Parker et al., 2013; Lassowskat et al., 2014) and other focused on proteomes of specific subcellular organelles, such as, chloroplast and mitochondria (Jones et al., 2006), apoplast (Kaffamik et al., 2009; Cheng et al., 2009; Strehmel et al., 2017), plasma membrane (Benschop et al., 2007; Yadeta et al., 2017), cytoplasm (Rayapuram et al., 2018) and the nucleus (Fakih et al., 2016; Howden et al., 2017) to investigate changes during plant defense response. Among these, total phosphoproteome analysis to identify potential MAPK substrates in a dexamethasone (DEX) inducible system, identified several putative MAPK substrates out of which only seven were TFs-mostly WRKYs, among substrates identified with potential roles in plant defense (Lassowskat et al., 2014). On the other hand, another phosphoproteome analysis targeted to nuclear proteome identified 156 out 198 phosphoproteins with the gene ontology term

"nucleus" (Bigeard et al., 2014). This shows how targeted subcellular proteome analysis helps in identification of low abundant nuclear proteins, such as, transcription factors. The protein expression shows a wide range of protein abundances in any biological sample. Therefore, in order to reduce the range of protein abundances, for instance via fractionation, supports detection of low abundant proteins (Lundberg and Borner, 2019; Liu et al., 2019; Righetti and Boschetti, 2020; Itzhak et al., 2016).

The challenging part in subcellular proteomics is to obtain pure organellar fraction. Thus, proteins detected in a target organelle fraction may not be its true subcellular localization. Even more challenging is to assign localization of proteins that have multiple subcellular localizations such as signaling proteins. In order to assign protein localization and identify putative protein movements several approaches were used, such as Protein Correlation Profiling (PCP), localization of organelle proteins by isotope tagging (LOPIT), and Dynamic Organellar Maps have been used (Krahmer et al., 2018; Dunkley et al., 2006; Itzhak et al., 2016). These methods were used to produce organellar maps in mouse liver cells (PCP), *A. thaliana* callus (LOPIT) and, HeLA cells (Dynamic Organellar Maps). These methods are conceptually similar but differs in organelle separation technique and quantification method used. The cells are lysed to release organelles which are them partially separated by gradient centrifugation. These fractions have an overlapping proteome profiles and different organelles are represented by different fraction. Next, MS profile of each fraction is obtained that yields abundance distribution profile for each protein. Cluster analysis identifies protein groups with similar profiles. The profiles of organellar marker proteins are compared with the clusters to identify which cluster represents which organelle. Finally, the marker profile is used to train an algorithm that predicts subcellular localizations of unknown proteins (Lundberg and Borner, 2019). All these methods use multiple fractions to predict protein subcellular localization and protein movement where the non-target fractions are used as a reference to filter out incorrect localization. My purpose of including the total protein fraction together with nuclear protein fraction was to identify signaling proteins from cytosol to the nucleus during PTI.

1.4.1 Nuclear proteomics in plant immune system

MAMP perception leads to a rapid nuclear transcriptional reprograming that ultimately leads to PTI associated defense responses. Inside the nucleus, the compartmentalization of DNA of eukaryotic cells necessitates a mechanism to connect non-nuclear signals to the transcriptional machinery which demands for nuclear transport mechanisms. Common examples are nucleocytoplasmic translocation of TFs (Plotnikov et al., 2011; Persak and

Pitzschke, 2013), nuclear translocation of chloroplast proteins (Caplan et al., 2015; Sun et al., 2011) and, nuclear translocation of membrane bound transcription factors (Yao et al., 2017; Lal et al., 2018). In addition, nuclear transport plays a crucial role in regulating key cell-biological processes such as, uptake of signaling receptors such as R-proteins and regulating activity of transcription factors (Shen and Schulze-Lefert, 2007; Lundberg and Borner, 2019). Nevertheless, it is still unclear how these events are related and what directly communicates the perception of MAMPs, such as flg22, at the plasma membrane to transcriptional reprograming inside the nucleus. Therefore, understanding of nuclear protein dynamics can provide clues that can provide crucial information for mechanisms that connect MAMPs perception at the extracellular space to the nuclear transcriptional reprogramming. To date, limited information is available on nuclear protein dynamics during plant immune responses (Yin and Komatsu, 2016; Fakih et al., 2016; Tang et al., 2020; Howden et al., 2017).

In 2006, a two-dimensional gel electrophoresis (2-DE)-mass spectrometry (MS) based nuclear proteome analysis was applied on hot pepper leaves after tobacco mosaic virus infection (Lee et al., 2006). Due to technique limitations, only six protein significantly upregulated under virus infection condition was identified, including a 26S proteasome subunit RPN7. Further experiment suggested that RPN7 is located in the virus infected region and enhances hypersensitive response (HR) of leaves to against the virus infection. Later, the nuclear response in soybean leaves upon treatment of resistant and susceptible types of rust pathogen was carried out, and exhibits a differential regulation of 855 proteins (Cooper et al., 2011). At least 20 potential transcription factors, some of which similar to WRKY19, and also phosphatases and S-glycosyl hydrolases are specifically identified in the resistance interactions. To understand the protein expression in *A. thaliana* upon chitin triggered immunity, Fakih et al compared the nuclear proteomes of wild type Col-0 and *cerk1*, a receptor mutant, plants (Fakih et al., 2016). CERK1 is the membrane receptor for recognition of chitin signals and, leads to PTI in *A. thaliana*. They identified 8 proteins that were specifically identified in wild type and not in *cerk1* plants, and most of them were ribosomal proteins, however, none of them were known to be involved in MAMP response. From these results it is largely unknown which nuclear protein changes are relevant for MAMP response. More recently, a tomato nuclear proteome study during *Phytophthora capsici* infection gave further insights into nuclear protein dynamics and identified a family of AHL protein involved in immunity against *P.capsici.* A total number of 285 and 140 proteins were up- or down-regulated upon *P. capsici* infection, respectively. The abundance of AT-Hook-Like (AHL) family protein, AHL1, AHL5, and AHL9, were reduced upon pathogen infection, which were localized in the nucleus of tomato. Further experiments

suggested that AHL1, AHL5 and AHL9 are involved in PTI activation and resistance against *P. capsici*. In animal field Wühr et.al 2015 studied nucleocytoplasmic partitioning using nuclei isolated from frog oocytes via microdissection. Out of ca. 9000 proteins identified 55% proteins were cytoplasmic, 27% were nuclear and 17% were equally distributed between nuclear and cytoplasm. On investigating to what extent nuclear export affect nucleocytoplasmic protein partitioning, they found only 3% of proteome were actively exported out of the nucleus. However, there are few studies that investigated nuclear protein dynamics in plants during immune response partly due to the fact that efficient isolation of nuclear protein remains challenging. Thus, nuclear proteomics could be an important set up for the characterization of molecular components involved in plant immunity.

1.5. Thesis aims

One of the long-standing questions in plant immunity is where components of immune signalling pathways interact to relay signal perception at cell surface inside the nucleus. For instance, where does MAPKs phosphorylate TFs- whether components of MAPK cascade move inside the nucleus to interact with TFs or TFs and other signalling protein themselves move inside the nucleus to induce immune response? I hypothesized that flg22 perception leads to changes in nuclear protein abundance that induces PTI responses. Additionally, some signaling proteins might re-locate inside the nucleus connecting MAMP perception at plasma membrane to nuclear transcriptional reprograming.

In order to gain further insights into MAMP induced nuclear protein dynamics, I decided to profile nuclear proteome along with total proteome as a control. I found that the existing nuclear isolation protocol were standardized only based on western blotting with antibodies representing single organelles to test for purity and enrichment of nuclear proteins. This does not provide information about the overall quality of a purification method. Furthermore, the existing nuclear isolation methods showed contamination of proteins from other compartments, in particular, plastidial proteins. This would hinder the identification of low abundant nuclear proteins like TFs. Therefore, my first aim of my PhD was to improve the existing nuclear isolation protocol and test the overall improvement over existing protocols using LC-MS/MS.

To date nuclear proteomic studies in plants have focussed only on nuclear protein fraction to study nuclear protein dynamics in response to various stimuli. In my thesis, inclusion of total protein fraction together with nuclear protein fraction will not only be useful to investigate protein abundance change but can also help to identify potential protein movement associated with PTI. For instance, an increase in abundance in the nuclear fraction and no change in the total fraction for a particular protein could imply nuclear import. Therefore, I used total protein as a control to identify potential protein movement from cytosol into/out of nucleus upon flg22 treatment by LC-MS/MS.

Numerous studies have investigated transcriptional responses over broad temporal range during PTI. However, differences in nuclear protein dynamics during PTI is yet largely unknown. Therefore, my second thesis aim was to investigate nuclear protein dynamics at two time points- 3 h and 9 h, representing early and late PTI responses, after flg22 treatment. Among proteins showing quantitative change upon flg22 treatment, I could not only detect proteins that showed abundance change during the two time points tested but also detected handful of

proteins showing signatures of protein movement. In addition, I also detected proteins in the nuclear fraction whose role in plant immunity was yet unknown and its nuclear localization was not yet experimentally confirmed.

The 3 h and 9 h time points provided insights into the nuclear protein dynamics associated with early and late PTI but still earlier time points would provide information about protein abundance changes that might occur prior to transcriptional changes. This led to my next aim which was to identify proteins at early time points- 15, 30, 60 min after flg22 treatment. Additionally, I also included protein synthesis inhibitor cycloheximide (CHX) treatment for 60 min in my study since previous studies found that flg22-responsive genes are also induced upon CHX treatment. In this scenario, it has been proposed that de-repression of early flg22 genes is achieved by inhibition of translation of negative regulators which are high turnover proteins. This led me to test whether flg22 response overlap with CHX treatment at protein level similar to transcriptomic studies.

Until now there were no attempt to investigate nucleocytoplasmic dynamics of proteins during plant immune response. My thesis takes a first attempt in this direction to provide further insights into the nuclear protein dynamics over a wide temporal range during flg22-trigerred PTI and identifies a yet unknown TF that is a positive regulator of immunity.

2. Results

2.1 The establishment of a new nuclear isolation protocol for nuclear proteome analysis

To gain insights into nuclear protein dynamics during flg22 response, I decided to profile nuclear proteome as well as total cellular proteome as a control. However, a previous nuclear isolation protocol, henceforth referred as Folta-protocol, showed contamination of proteins from other compartments, in particular, plastids (Folta and Kaufman, 2007). Therefore, I attempted to improve Folta-protocol because contamination from other compartments will prevent identification of low abundant nuclear proteins by LC-MS/MS (Burgess et al., 2014). Compared to Folta-protocol, I modified various factors such as the homogenization method and the composition of extraction buffer as these would affect nuclear intactness and protein contamination from other compartments. For instance, I found that homogenization by chopping with razor blades performed better than other homogenization methods such as polytron, hand-held blender, paint shaker, or grinding snap-frozen leaves (Figure S1A, B). I also adjusted concentration of Triton-X 100 (TX-100), a non-ionic detergent, which prevents clumping of nuclei and facilitates its release from cells but also affects the integrity of chloroplast resulting in chloroplast protein contamination during nuclear isolation (Loureiro et al., 2007). Compared to Folta-protocol which uses 1% of TX-100, I found that a reduced concentration, at 0.85% of TX-100 resulted in reduced protein contamination from chloroplasts (Figure 1A, Figure S1C).

I assessed the nuclear protein enrichment and purity by immunoblotting (Figure 1B). I used transgenic *A. thaliana* plants expressing GFP-tagged Nup50a, which localize to the nucleoplasm (Tamura et al., 2010). I used anti-GFP antibody as a nuclear marker in addition to the classical histone-H3 (Howden et al., 2017; Tamura et al., 2010). In addition, I used antibodies against Rubisco large subunit (RbCl; chloroplast stroma), light-harvesting complex II (LHC; chloroplast thylakoid), cytosolic fructose-1,6-bisphosphatase (FBPase; cytosol), isocitrate dehydrogenase (IDH; mitochondria) and calnexin homolog 1/2 (CNX1/2; endoplasmic reticulum) to detect proteins from stroma, thylakoid, cytosol, mitochondria, and endoplasmic reticulum, respectively.

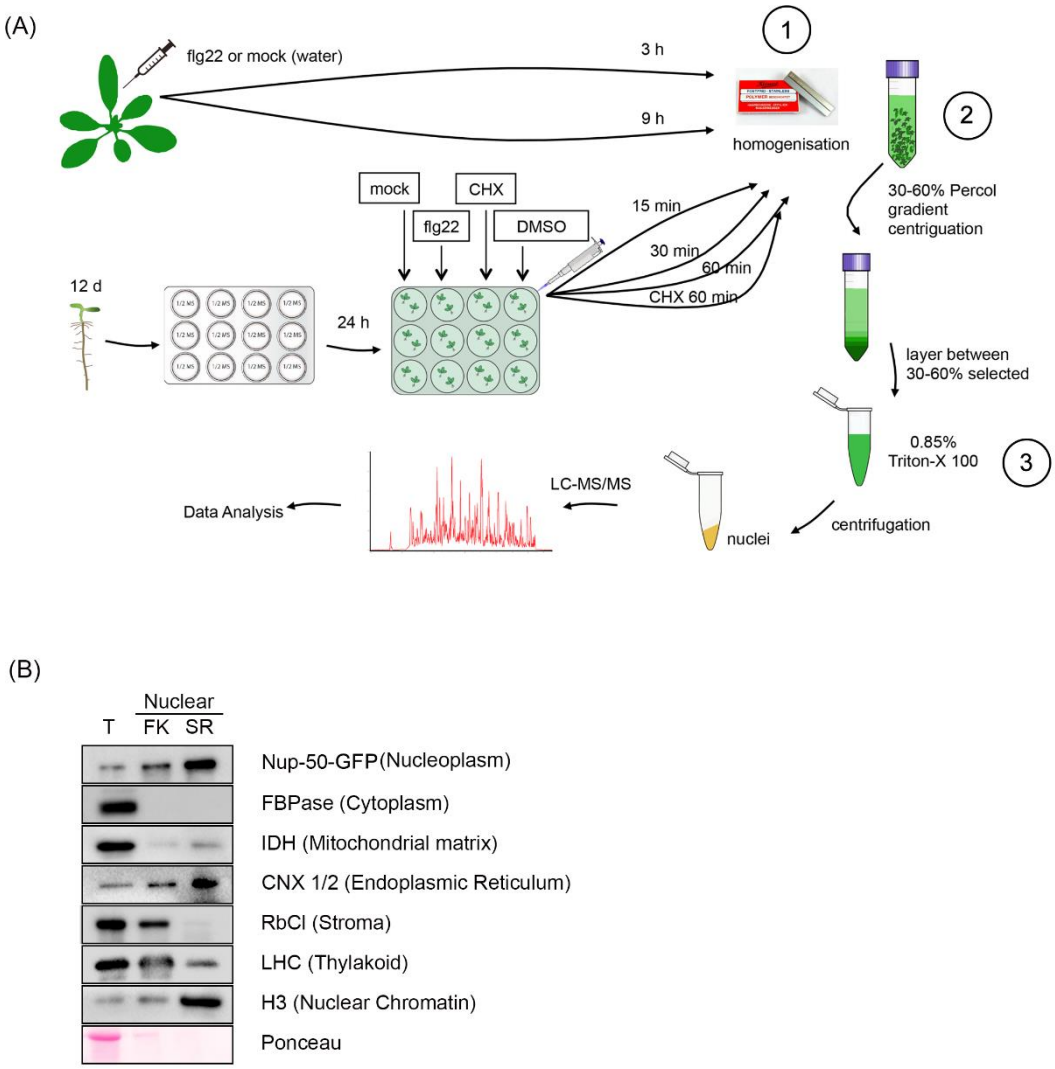

Figure 1: Establishment of a new protocol for nuclear protein isolation. (A) Schematic representation of the new nuclear protein isolation protocol (SR). Number in circles represents the following changes to Folta protocol- 1. chopping instead of blender, 2. TX-100 treatment excluded, and 3. 0.85% TX-100 instead of 1%. **(B)** Fresh leaves from 4-5 weeks old transgenic Col-0 plants expressing GFP-tagged Nup50a were used for nuclear and total protein isolation. Nuclear proteins were isolated by Folta-protocol ("FK") or by the new protocol ("SR"). Total protein (T) was isolated from total leaf extract. Extracted protein (2µg) was used for immunoblotting using anti-GFP (nucleoplasm), anti-H3 (nuclear chromatin), anti-RbCl (chloroplast), anti-LHC (thylakoid), anti-FBPase (cytosol), anti-IDH (mitochondria), and anti-CNX1/2 (endoplasmic reticulum) antibodies. Ponceau staining was used to assess protein loading and RuBisCO abundance. The experiment was performed with 3 independent biological replicates and a representative result is shown.

Compared to Folta-protocol (Figure 1A), my nuclear isolation protocol showed reduced contamination of thylakoid (anti-LHC) and stromal proteins (anti-RbCl). Both the protocols resulted in undetectable levels of cytosolic contaminations assessed by anti-FBPase. Although, my protocol showed higher contaminations from mitochondria and endoplasmic reticulum compared to Folta-protocol, my protocol showed higher nuclear enrichment as detected by anti-

GFP and anti-H3 antibodies (Figure 1B). As it is known that plastidial proteins occupy a major part of total cellular proteome, I concluded that my modified protocol would be a better method to detect low abundant nuclear proteins (Fröhlich et al., 2012). In addition, I observed consistent performances of my modified protocol in three independent experiments, which is important to obtain reproducible results (Figure S2).

To further assess the efficiency of my protocol for nuclear protein enrichment, I compared Folta and my protocol for quantitative nuclear proteomes using LC-MS/MS. As a control, I also investigated total cellular proteome. I assigned subcellular localization for the proteins identified by LC-MS/MS based on the predictions in SUBA4 reference database (Hooper et al., 2017). I analyzed protein subcellular localization in terms of both the abundance (Figure 2A) and number (Figure 2B). Quantitative nuclear proteome patterns in replicates using both Folta and my protocol showed high correlation (R^2 = 0.94 - 0.96) within the respective isolation protocols (Table 1), and the correlation values were similar to those obtained in other studies involving nuclear protein isolation which suggests that both methods produces reproducible results (Howden et al., 2017; Yin and Komatsu, 2016). However, correlations between Folta and my protocol were not high (R^2 = 0.47 - 0.52), which supports the immunoblotting results (Figure 1B) showing different levels of contamination from plastids, mitochondria and endoplasmic reticulum. In addition, the correlations between the total and nuclear fractions isolated using my protocol was lower (R^2 = 0.17 - 0.22) than those between the total and nuclear fraction isolated using Folta-protocol (R^2 = 0.38 - 0.48), which indicates that my protocol produces more different proteome patterns from the total proteome than Folta-protocol and suggests that my protocol enriches more nuclear proteins. Indeed, more nuclear proteins were detected in terms of both the abundance and number when using my protocol than Folta-protocol (Figure 2).

Consistent with immunoblotting results (Figure 1B), I observed lower contamination of plastidial proteins (26.3% vs 50%) but slightly higher contamination of ER (2.2% vs 1.4%) and mitochondrial (5.5% vs 5.3%) proteins with my protocol compared to the Folta-protocol (Table 2). Nevertheless, my protocol detected on average more nuclear proteins compared with Folta-protocol in the abundance (17% vs 3.6%) and the number (1932 vs 1083). These results indicate that my protocol has a higher power over Folta-protocol to detect nuclear proteins, which is crucial to examine nuclear protein dynamics in particular with the low abundance proteins such as transcription factors (Burgess et al., 2014).

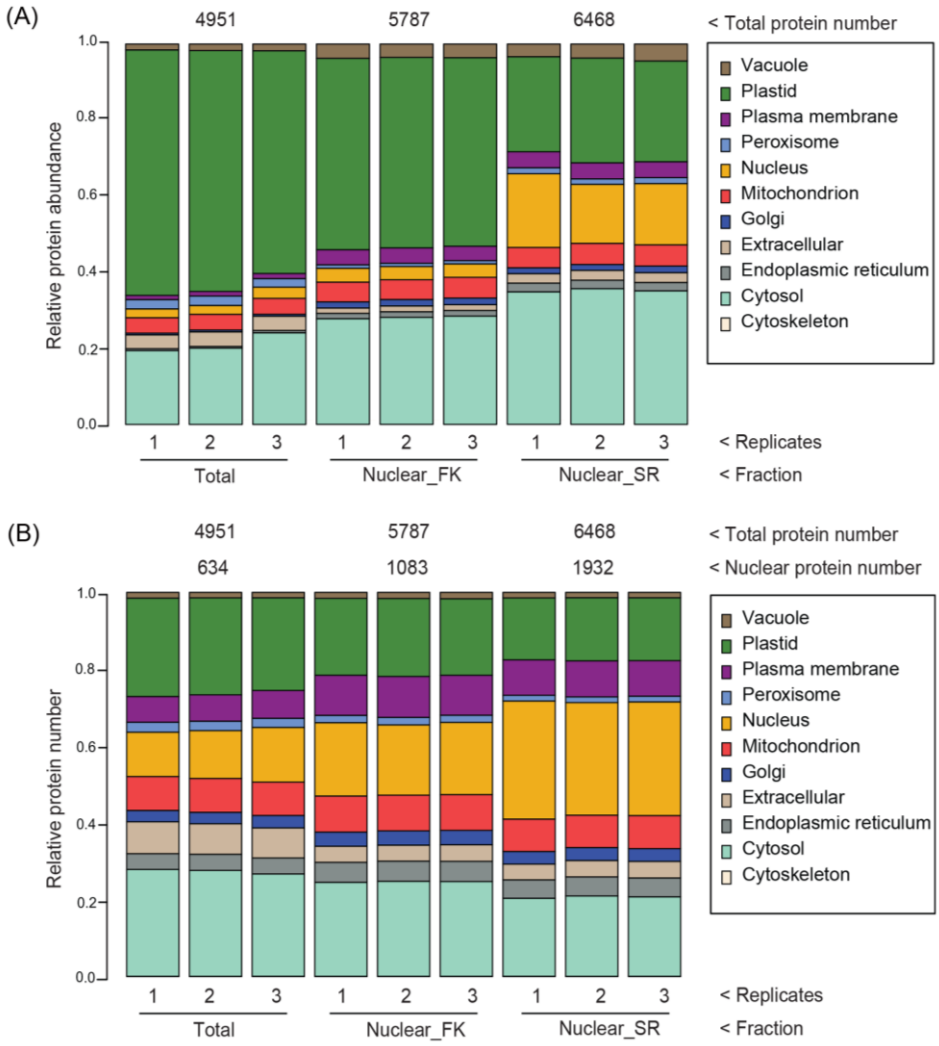

Figure 2: Nuclear proteins are highly enriched in the nuclear fraction using the newly established protocol. Total and nuclear proteins were isolated from leaves of 4-5-week-old Col-0 plants. Nuclear proteins were isolated using Folta-protocol (FK) or the new protocol described in this study (SR). Three replicates (protein samples were prepared from independent plant materials and processed simultaneously) were used for total proteins and each of the nuclear protein isolation was done by FK or SR-protocol. Relative protein abundance was calculated using intensity based absolute quantification (IBAQ) values. The individual columns represent each replicate showing relative protein abundance of proteins identified by LC-MS/MS and its subcellular localization as predicted by SUBA4 reference database. **(A)** Ratio of different subcellular localization of proteins based on their relative abundance (IBAQ value) in nuclear and total protein fraction**. (B)** Ratio of different subcellular localization of proteins based on the number of proteins in nuclear and total protein fraction. The first protein listed within each "Majority protein group" (see text) was used to assign the subcellular localization based on SUBA 4 reference database.

Table 1									
Total 1	1.00								
Total 2	0.96	1.00							
Total 3	0.93	0.94	1.00						
SR 1	0.17	0.18	0.20	1.00					
SR 2	0.19	0.20	0.22	0.95	1.00				
SR 3	0.18	0.20	0.22	0.94	0.96	1.00			
FK 1	0.38	0.41	0.47	0.47	0.51	0.50	1.00		
FK 2	0.40	0.43	0.48	0.48	0.52	0.51	0.96	1.00	
FK 3	0.39	0.42	0.48	0.47	0.52	0.51	0.93	0.94	1.00
	Total 1	**Total 2**	**Total 3**	**SR 1**	**SR 2**	**SR 3**	**FK 1**	**FK 2**	**FK 3**

Table 1: Two nuclear isolation protocols are reproducible. LFQ values were used to calculate correlation (R^2 values) in Perseus (version 1.5.2.6) among replicates of Folta-protocol (FK), the new protocol (SR), and the total fraction. Total and nuclear proteins were isolated from leaves of 4-5-week-old Col-0 plants. Three replicates were prepared from independent plant material.

Table 2						
	Relative protein abundance			**Average protein number**		
Localization	**Total**	**FK**	**SR**	**Total**	**Folta**	**SR**
Cytoskeleton	0.0	0.0	0.0	3.3	4.0	4.3
Cytosol	21.5	28.1	35.2	1352.3	1425.0	1335.0
Endoplasmic reticulum	0.5	1.4	2.2	206.3	302.7	316.3
Extracellular	3.8	1.5	2.6	396.3	244.7	273.0
Golgi	0.5	1.7	1.6	151.7	214.3	214.7
Mitochondrion	4.1	5.3	5.5	434.3	540.0	549.3
Nucleus	2.6	3.6	17.0	634.0	1083.7	1932.3
Peroxisome	2.4	0.9	1.5	121.7	110.3	96.0
Plasma membrane	1.2	3.9	4.2	344.0	608.0	601.3
Plastid	61.8	50.0	26.3	1236.0	1161.0	1054.0
Vacuole	1.7	3.6	3.8	71.7	93.3	91.7
Total	100	100	100	4951.7	5787.0	6468.0

Table 2: Subcellular localization patterns of proteins in the nuclear fractions. Relative protein abundance (%) and number of proteins detected in the nuclear fractions isolated using Folta (FK) or the new protocol (SR). Subcellular localization of proteins detected for the nuclear fractions as well as the total fraction was determined using SUBA4. The relative protein abundances (left) or the average number of proteins detected (right) are shown. The numbers are averaged over three independent biological replicates.

2.2 Nuclear protein dynamics during flg22 response

I profiled total and nuclear proteome in leaves of four-week-old *A. thaliana* Col-0 plants treated with flg22 or mock by LC-MS/MS to reveal nuclear protein dynamics during PTI. I took two time points, 3 h and 9 h after the treatment, to capture temporal nuclear protein dynamics because plant immune responses differ at these time points, such as differences in SA accumulation (Seyfferth and Tsuda, 2014). I performed two independent experiments each with three biological replicates. In total, I obtained 48 proteome results.

2.2.1 Subcellular protein localization patterns remain largely unchanged during flg22 response

Consistent with the previous analysis (Figure 2), I could enrich nuclear proteins in a reproducible manner (Figure 3). Briefly, I observed a very high correlation (R^2>0.92, Table S1) between biological replicates from the same conditions within the same experiment, and relatively high correlation (R^2>0.88) between biological replicates from different experiments. These high correlations were comparable or even higher compared to previous nuclear proteomics study (Howden et al., 2017). Overall proportion of subcellular localization of detected proteins in the abundance and number were comparable between flg22 and mock treatment (Table 3), with slight increase for nuclear proteins upon flg22 treatment (Table 4), suggesting at least dramatic protein movements into or out of the nucleus did not occur at 3 and 9 h after flg22 responses.

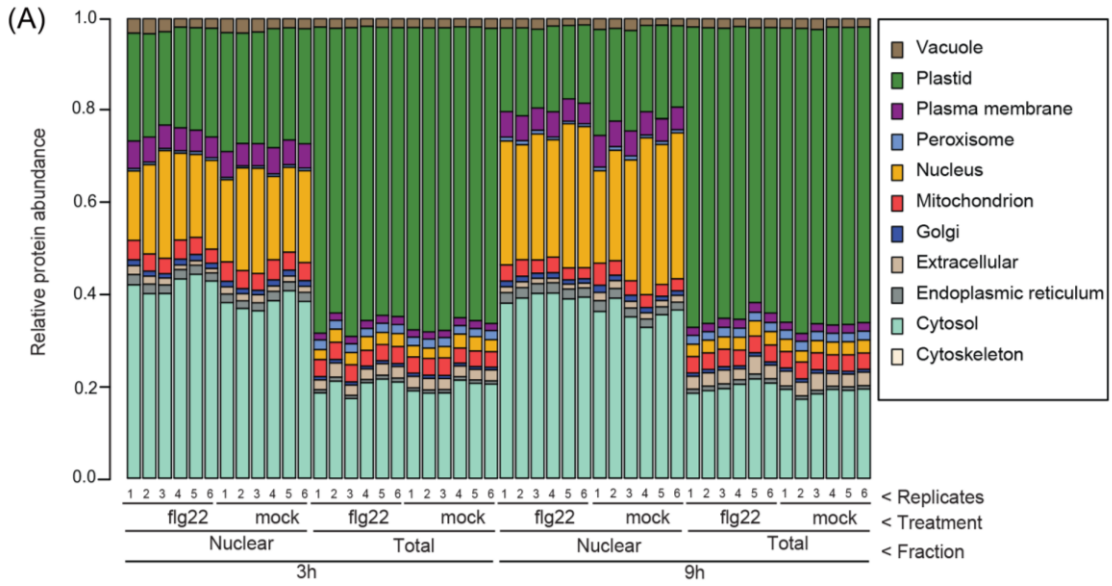

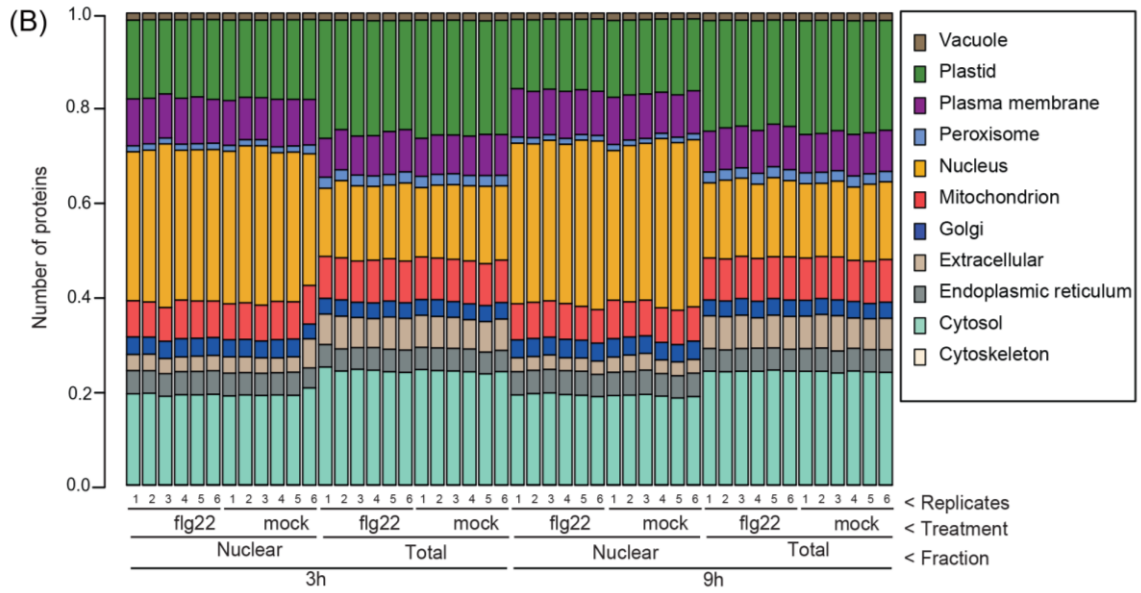

Figure 3: Subcellular localization of proteins detected in the nuclear and total proteome analysis. Total and nuclear proteins were isolated from leaves of 4-5-week-old Col-0 plants at 3 h or 9 h after 1 µM-flg22 or mock treatment. Six replicates (protein samples were prepared in two different days each containing three replicates prepared from independent plant materials) were prepared for each condition. Relative protein abundance was calculated using intensity based absolute quantification (IBAQ) values. The individual columns represent each replicate showing relative protein abundance of proteins identified by LC-MS/MS and its subcellular localization as predicted by SUBA4 reference database. **(A)** Subcellular localization of proteins based on their relative abundance (IBAQ value). **(B)** Subcellular localization of proteins based on protein number.

Table 3

Average number of proteins detected							
3h				9h			
Nuclear		Total		Nuclear		Total	
flg22	mock	flg22	mock	flg22	mock	flg22	mock
5147.5	5049.2	5444.3	5342.8	5073.3	4977.5	5656.2	5467.0

Table 3: Overview of the number of proteins detected by LC-MS/MS. The average number of proteins detected from 6-replicates for nuclear or total protein fractions at 3 h or 9 h after 1 µM-flg22 or mock treatment.

Table 4 (A): Proteins detected corresponding to each subcellular compartment at 3 h

	Nuclear				Total			
Localization	**flg22**	**mock**	**change**	**pval**	**flg22**	**mock**	**change**	**pval**
cytoskeleton	5.7	6.0	-0.3	0.145	5.0	5.0	0.0	NA
cytosol	984.3	956.7	27.7	0.073	1320.8	1284.2	36.7	0.175
endoplasmic reticulum	251.2	241.7	9.5	0.031	256.7	251.2	5.5	0.430
extracellular	169.5	166.3	3.2	0.511	358.5	350.2	8.3	0.593
golgi	192.3	187.5	4.8	0.261	181.8	182.0	-0.2	0.978
mitochondrion	395.2	396.7	-1.5	0.891	483.8	478.3	5.5	0.646
nucleus	1665.2	1631.2	34.0	0.251	859.0	837.7	21.3	0.587
peroxisome	66.7	63.7	3.0	0.040	124.0	121.3	2.7	0.509
plasma membrane	496.2	480.5	15.7	0.356	468.8	448.0	20.8	0.306
plastid	849.2	846.0	3.2	0.843	1302.3	1302.5	-0.2	0.992
vacuole	72.2	73.0	-0.8	0.653	83.5	82.5	1.0	0.744
Sum	5147.5	5049.2			5444.3	5342.8		

Table 4 (B): Proteins detected corresponding to each subcellular compartment at 9 h

	Nuclear				Total			
Localization	**flg22**	**mock**	**change**	**pval**	**flg22**	**mock**	**change**	**pval**
cytoskeleton	5.5	5.7	-0.2	0.687	5.2	5.0	0.2	0.341
cytosol	969.0	936.3	32.7	0.135	1363.7	1309.2	54.5	0.025
endoplasmic reticulum	250.8	245.0	5.8	0.391	267.7	261.8	5.8	0.216
extracellular	146.2	157.5	-11.3	0.165	389.8	374.3	15.5	0.334
golgi	193.3	188.5	4.8	0.336	195.0	183.7	11.3	0.020
mitochondrion	379.3	373.8	5.5	0.724	507.5	489.0	18.5	0.092
nucleus	1742.8	1696.0	46.8	0.101	922.2	871.7	50.5	0.077
peroxisome	62.3	58.5	3.8	0.192	128.7	123.7	5.0	0.017
plasma membrane	494.8	462.7	32.2	0.119	504.3	464.3	40.0	0.003
plastid	762.3	785.7	-23.3	0.286	1286.2	1298.5	-12.3	0.361
vacuole	66.8	67.8	-1.0	0.815	86.0	85.8	0.2	0.880
Sum	5073.3	4977.5			5656.2	5467.0		

Table 4: Subcellular protein localization patterns remain largely unchanged during flg22 response. SUBA4 predicted subcellular localization was used to compare contribution of each subcellular organelle in nuclear or total fraction at 3 h **(A)** and 9 h **(B)** after flg22 or mock treatment. The numbers corresponding to treatments indicates average number of proteins detected across 6-replicates. The third column (change) indicates difference between average number of proteins detected in flg22 vs mock treatment. A two-tailed *t*-test was used to calculate p-values (pval) corresponding to the change observed.

2.2.2 Responses to biotic stress were enriched both in nuclear and total fraction

To gain insights into what specific biological processes are associated with protein expression changes in the nucleus in response to flg22, I extracted quantitative proteins that are differentially expressed (DEPs, $|\log_2$ fold change$| > 1$; q-values < 0.05) and proteins showing consistent presence/absence pattern (expressed either in flg22 or mock treatment). Proteins consistently present in all six replicates in flg22 samples and consistently absent in all six replicates in mock samples were defined as "Increased" and when vice-versa then defined as "Decreased" (Table S4). I used the DEPs for gene ontology analysis. I used the BINGO plugin in Cytoscape and the available gene ontologies (GOs) to rank the GO terms in the order of statistical significance and showed the top ten GO terms (Figure 4). This analysis showed as expected that GO terms were enriched for proteins linked to biological processes in responses to various stimuli, including response to biotic stimulus and defense response in the nuclear fraction at 3 h after flg22 treatment. Similarly, DEPs in the total fraction were enriched for GO terms related to response to biotic stimulus and defense responses at both time points. Consistent to previous studies, many well-known proteins responsible for key processes such as transcriptional reprograming and SA accumulation during immunity responded to flg22 treatment. For example, the TFs- CBP60g and SARD1 protein expression in the nucleus were consistent to previous gene expression studies- CBP60g was increased (consistently present in flg22 samples) at 3 and 9 h and, SARD1 was upregulated at 9 h upon flg22 treatment which is consistent with their role in regulating *ICS1* transcription and SA biosynthesis at early and late time points, respectively (Wang et al., 2011a). In contrast, downregulated proteins did not yield significant GO terms (except for total fraction at 9 h). Compared to 3 h, I found that upregulated proteins in the nuclear fraction at 9 h are enriched for GO terms related to meristem activity. These GO terms were associated with two upregulated proteins, OBE1 and OBE2, which are transcription factors required for maintenance of apical meristem (Saiga et al., 2008). OBE1 interacted with HopO1-2, a type-3-effector from *Pto* DC3000, in a yeast-two-hybrid assay (Mukhtar et al., 2011; Lu and Yao, 2018). Although the biological significance of OBE1 in immunity is not known, a recent finding that maize heteromeric G-protein β subunit is a common signaling point between shoot meristem maintenance and immune response also suggests a connection between immunity and meristematic activity (Wu et al., 2020).

2.2.3 Identification of transcription factors involved in flg22 response

Transcriptional reprograming is a hallmark of PTI which occurs within 30 min after flg22 perception and is regulated by transcription factors (TFs) (Navarro et al., 2004; Li et al., 2016). TFs are generally low abundant nuclear proteins which necessitates enrichment of nuclear

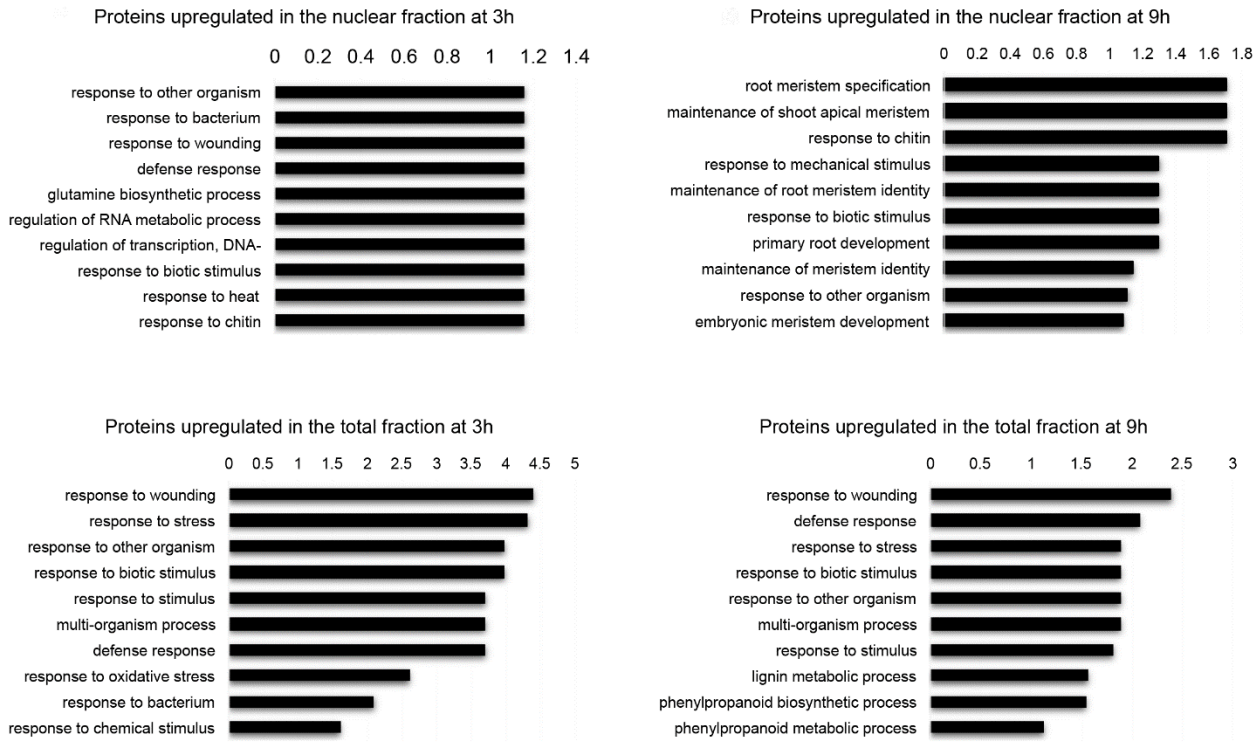

Figure 4: Gene Ontology (GO) term analysis for differentially regulated proteins in the nuclear and total fractions at 3 h and 9 h after flg22 treatment. The top 10 GO terms in descending order of statistical significance are shown for proteins that are upregulated at 3 h and 9 h in the nuclear **(A, B)** and total **(C, D)** fractions. GO terms associated with the downregulated proteins were enriched for only 9 h nuclear samples **(E).** The values on x-axis shows $-\log_{10}$ adjusted p-values. GO enrichment analysis was done with BingGO plugin for Cytoscape (FDR=0.1). As background a customized reference protein list was used which consisted of proteins that were detected at least twice in flg22 or mock conditions in nuclear or total fractions at 3 h or 9 h.

proteins in proteome analysis (Burgess et al., 2014). In order to extract TFs in my data, I used the PlantTFDB 4.0 database as a reference (Jin et al., 2017). Altogether, I identified 348 TFs in nuclear and/or total protein fraction at 3 h and/or 9 h time points (Table 5). Of these, I identified more TFs in the nuclear fraction (249/284 at 3 h / 9 h respectively) compared to total fraction (70/81 at 3 h / 9 h respectively), showing the significance of nuclear protein isolation to identify low abundance proteins localized in the nucleus (Table 5). Among the identified TFs, 14 were differentially expressed ($|\log_2$ fold change$| > 1$; q-value < 0.05) in the nuclear fraction at 3 h and/or 9 h in response to flg22 and none was differentially expressed in the total protein fraction

(Table S2A). I could capture TFs that are linked to key immune processes, such as SA biosynthesis at later stages of immunity (*SARD1*) and TFs that are involved in regulation of flg22 induced genes (*WRKY18, WRKY33, WRKY40)* (Tsuda and Somssich, 2015; Birkenbihl et al., 2017). Notably, I also found TFs which have not been implicated in immunity. Among them was WRKY47 which showed the highest induction amongst the TFs identified (more than 8 folds) in the nuclear fraction at 3 h and 9 h. Consistently, *WRKY47* expression was also highly induced in the transcriptome data starting from 2 h to 9 h (Table S2A) (Birkenbihl et al., 2018). These results suggest that WRKY47 is a novel TF involved in plant immunity. Therefore, the subcellular localization of WRKY47 and its involvement in immunity was further investigated. The subcellular localization of WRKY47 was investigated by transient expression in *Nicotiana benthamiana* and it was found that transiently expressed WRKY47, tagged with either N-terminal or C-terminal GFP, localize to the nucleus (Figure 5A), supporting its predicted role as a TF. Importantly, on comparing the growth of *Pto* DC3000 in *wrky47* mutant and wild type Col-0 plants, it was found that *Pto* DC3000 growth was enhanced in *wrky47* plants compared to the Col-0 plants, indicating that WRKY47 is a positive regulator of plant immunity against *Pto* DC3000 (Figure 5B-C).

In order to get further insights into how WRKY47 might be involved in immunity, I performed a protein-protein network analysis using the STRING database (Szklarczyk et al., 2015; Franceschini, 2015). I found that WRKY47 interacts with the LRR-RK IMPAIRED OOMYCETE SUSCEPTIBILITY1 (IOS1) which is a positive regulator of PTI (Figure 5D). IOS1 constitutively interacts with the flg22 receptor FLS2 and the co-receptor BAK1 and was shown to be important for early PTI-responses like induction of the immune marker gene *FRK1*, callose deposition, and MAPK activation by positively regulating the FLS2-BAK2 complex formation during PTI (Yeh et al., 2016). The interaction between the nuclear-localized WRKY47 and plasma membrane-localized IOS1, may imply a scenario similar to that upon *Xanthomonas oryzae (Xoo)* infection, the rice plasma membrane-localized PRR, XA21, is cleaved and re-localizes into the nucleus (Park and Ronald, 2012). However, biological significance of nuclear localization of XA21 cleavage product remains unknown since it was later found that the predicted nuclear localization sequence (NLS) that directs the cleavage product of XA21 to the nucleus was not required during *Xoo* mediated immunity (Wei et al., 2016).

Table 5				
	3 h		9 h	
	Nuclear	Total	Nuclear	Total
TFs detected	249	70	284	81
TFs Up/Down	32/18	5/6	27/48	2/6
TFs Increased/Decreased	8/1	1/0	12/2	6/0

Table 5: Nuclear fractionation facilitated the detection of transcription factors. The transcription factors (TFs) detected during LC-MS/MS at 3 h and/or 9 h after 1 µM-flg22 or mock treatment was identified using the PlantTFDB 4.0 database. The TFs showing quantitative change ($|\log_2$ fold change$| > 0.5$; q-value < 0.05) are referred as TFs Up/Down. The TFs which are consistently present in flg22 samples (in at least five replicates) and absent (in at least five replicates) in mock are defined as "TFs Increased" and vice-versa (as "TFs Decreased").

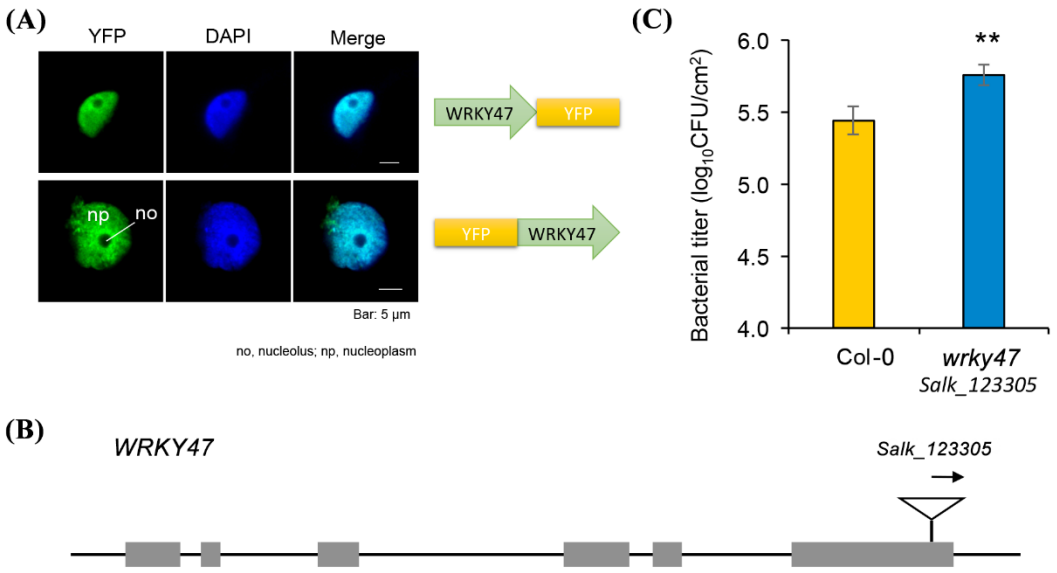

Figure 5: WRKY47 localizes to the nucleus and plays a positive role in plant immunity. (A) Transient expression of WRKY47-nYFP and WRKY47-cYFP under *A.thaliana* Ubiquitin-10 promoter (P_{UBQ10}) in *N. benthamiana*. Blue indicates DAPI-stained nuclei. **(B)** Genomic structure of the *wrky47* mutant. Grey boxes represent exons and T-DNA insertion site is indicated. **(C)** Leaves of 4 to 5-week-old Col-0 and *wrky47* plants were syringe-infiltrated with *Pto* (OD_{600} = 0.001). The bacterial titers were measured at 2 dpi. Bars represent means and standard errors calculated from one experiment with four biological replicates using mixed linear model. The statistically significant difference compared with Col-0 is indicated by the asterisk (P-value < 0.01). Data from Yiming Wang.

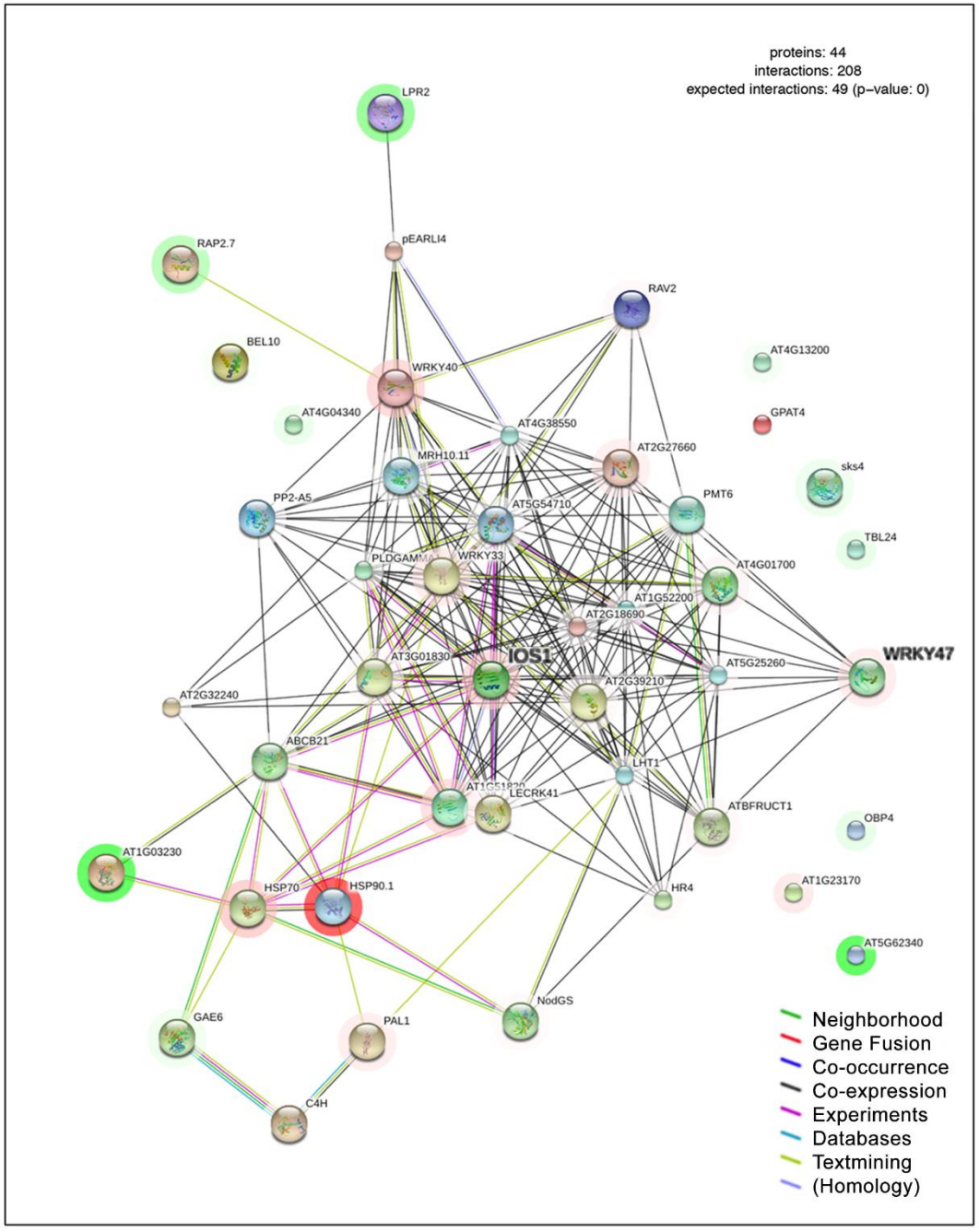

http://version10.string–db.org/10/p/4895485179

(D) WRKY47 interacts with IOS1. A set of 44 differentially expressed proteins ($|-\log_2 \text{value}| > 0.5$; q-value < 0.05) in the nuclear fraction at 3 h was selected to create the PPI network. The PPI network was created using STRINGdb in R and magnitude of protein abundance change was added into the PPI network. Color coded hallos around the protein nodes indicate upregulation (red) or downregulation (green) and the color intensities reflect magnitude of protein abundance change. Colored lines between the proteins indicate the various types of interaction evidence. Protein nodes which are enlarged indicate the availability of 3D protein structure information.

2.2.4 Quantitative proteome changes in nuclear proteome and transcriptome during flg22 response are highly correlated

In order to understand the relationship between gene and protein expression dynamics, I compared the transcriptome data consisting of Col-0 and *fls2*, a null mutant lacking the flg22 receptor FLS2, treated with flg22 with the current proteome dataset (Hillmer et al., 2017). In order to do correlation analysis, I imputed the missing values in my proteomics data set (O'connell et al., 2018). Since, protein compositions of nuclear and total protein fraction are different, I imputed those samples separately. For 6901 common proteins/genes, I used the $\log_2$ expression changes for correlation analysis.

I found differentially expressed proteins both in nuclear and total proteome in response to flg22 (DEPs, $|\log_2$ fold change$| > 1$; q-value < 0.05) (Table 6). I found that protein and gene expression patterns are similar for the differentially expressed proteins (Figure 6A-B). Additionally, I found a positive correlation between proteome and transcriptome data which supports the accuracy of the proteome data and suggests that proteome changes are likely explained by transcriptome changes at least in part. (Figure 6C, Table 7). I detected 30 and 106 DEPs in the nuclear fraction whereas I detected 29 and 101 DEPs in the total fraction at 3h and 9h respectively (Figure 6, Table S3).

Apart from differentially expressed proteins upon flg22 treatment, I found many proteins showing consistent presence/absence pattern between flg22 and mock treatments (Table S4). Among these proteins, I identified 20 TFs in the nuclear fraction (17 increased and 3 decreased, Table S2B). Many of the identified TFs were known to be involved in plant defense responses. For instance, I found several WRKY proteins (WRKY6, 22, and 29) increased in abundance in the nucleus at both 3 h and 9 h which were classified as flg22 induced group of *WRKYs* (Birkenbihl et al., 2018). Promoters of *WRKY6* and *WRKY29* showed increased H3K4 trimethylation which correlated with increased expression of defence response genes (Jaskiewicz et al., 2011) and *WRKY22* was found to be involved in flooding induced increased basal resistance (Hsu et al., 2013). The identification of immunity related TFs shows the robustness of my nuclear enrichment method to identify low abundant proteins during flg22 response.

Table 6				
Protein fraction/ Time	Number of proteins significantly* changing in abundance		Number of proteins with consistent presence/absence expression profile	
	Up	Down	Increased	Decreased
Nuclear/ 3 h	26	4	33	8
Nuclear/ 9 h	73	33	69	14
Total/ 3 h	28	1	24	2
Total/ 9 h	86	15	67	2

Table 6: The number of proteins whose abundance changes in response to flg22. Left, proteins showing quantitative change (* |-log2 value| > 1; q-value < 0.05) in response to flg22 vs mock treatment. Right, proteins which are consistently present (in all 6-replicates) in flg22 samples but absent in mock are defined as "Increased" and vice-versa (as "Decreased").

Table 7

Transcriptome	Proteome							
	3h				9h			
	DEP		ALL		DEP		ALL	
	Nuc	Tot	Nuc	Tot	Nuc	Tot	Nuc	Tot
1h	0.35	0.24	0.35	0.39	0.59	0.55	0.38	0.46
2h	0.76	0.55	0.36	0.4	0.75	0.71	0.43	0.52
3h	0.71	0.5	0.35	0.37	0.76	0.71	0.46	0.54
5h	0.36	0.48	0.3	0.31	0.76	0.73	0.44	0.52
9h	0.14	0.3	0.28	0.28	0.74	0.67	0.43	0.52

Table 7: Table showing Pearson correlation between transcriptome and proteome data. Pearson correlation are shown between transcriptome and proteome data- nuclear (Nuc) and total (Tot) proteome, at indicated time points. Proteome represents protein abundance change in Col-0 plants in response to flg22 vs mock treatment. Transcriptome represents transcriptome change in Col-0 vs *fls2* plants in response to flg22 treatment at indicated time-points. DEP- proteins showing quantitative change (|log2 value| > 1; q-value < 0.05). ALL- all proteins identified during LC-MS/MS in the nuclear (Nuc) or total (Tot) fractions at 3 h and/or 9 h after flg22/mock treatment.

2.2.5 Identification of candidate proteins which may directly relay signal for flg22-perception at the plasma membrane to transcriptional reprogramming in the nucleus

The mechanism by which flg22 perception on the plasma membrane triggers transcriptional reprogramming in the nucleus remains largely elusive. Some factors must move from the cytosol to the nucleus to activate transcriptional reprogramming. Proteins can be such factors. Indeed, it was found that BIK1, which associates with the plasma membrane, localizes in the nucleus upon activation by elf18. BIK1 interacts with WRKY TFs (WRKY33, 50, 57) in

the nucleus, pointing to a mechanism that connects MAMP perception at the plasma membrane to transcriptional reprogramming in the nucleus (Lal et al., 2018). To identify additional

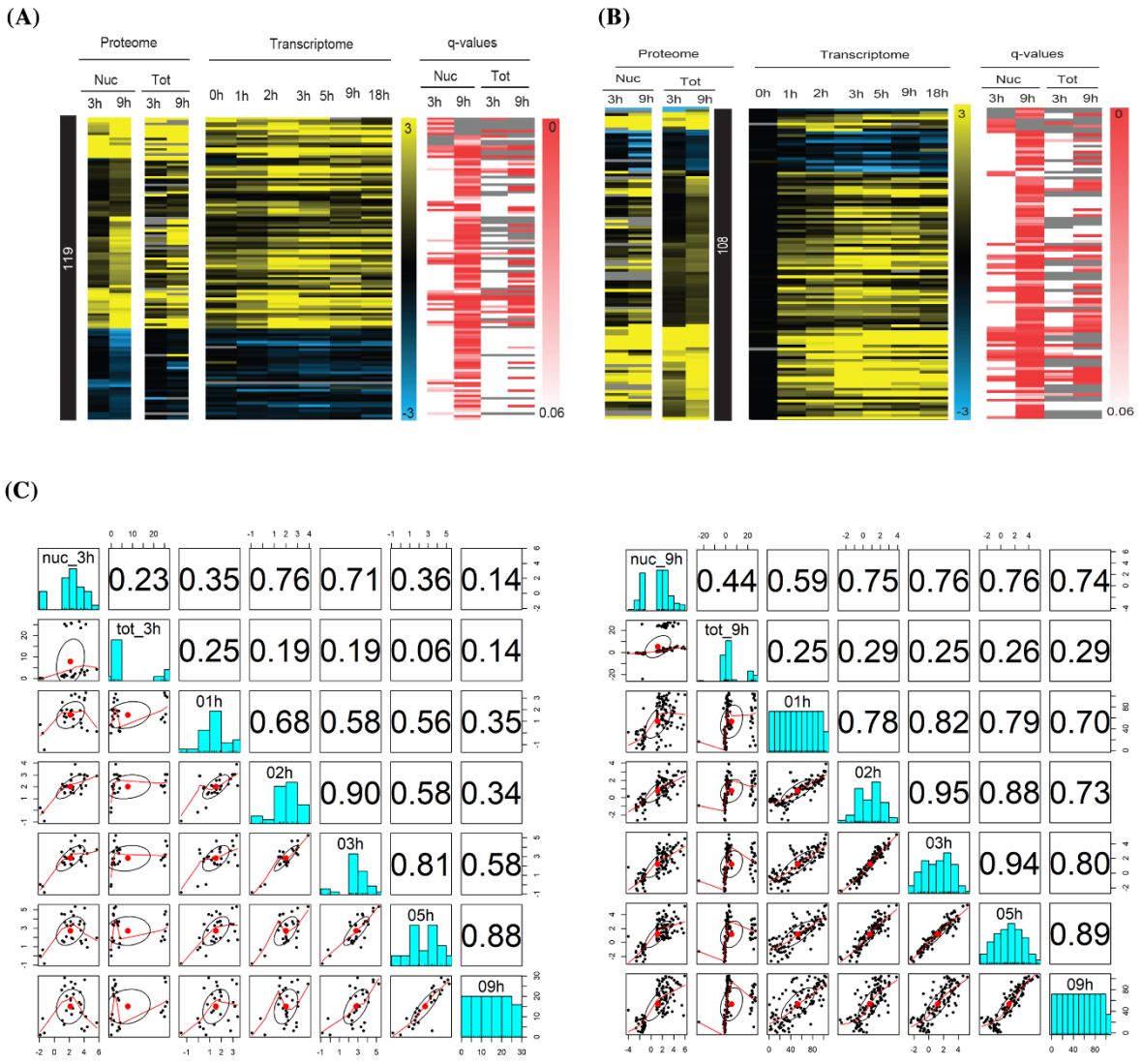

Figure 6: Quantitative protein changes closely mirrors transcriptome changes during flg22 response. Heatmaps shows differentially expressed proteins in nuclear and total protein fraction (DEPs) upon flg22/mock treatment. The first and second panel represents nuclear and total proteins, the third panel represents the transcriptome change, and the fourth panel represents q-values for the respective protein abundance change. Heatmap shows 119 DEPs in the nuclear fraction **(A)** and 108 DEPs in the total fraction **(B)** at 3 h and/or 9 h after 1 µM-flg22 infiltration. **(C)** Correlation of DEPs identified in the nuclear proteome at 3 h (first panel) and 9 h (second panel) with the transcriptome data (Col-0 vs *fls2* plants in response to flg22 treatment). Pearson correlation coefficients are shown.

proteins which relay the signal of flg22 perception to transcriptional reprogramming, I searched for proteins which show an increased abundance in the nuclear fraction but no change in the total protein fraction (or greater increase in the nuclear fraction than total fraction). In addition, I also looked for nuclear proteins that decreased in abundance in the nuclear fraction which

could be negative regulators of transcriptional reprograming. I selected proteins (both quantitative and proteins showing presence/absence pattern) using these criteria for 3 h and 9 h (Table S5). Among these, several proteins caught my attention, including WRKY47, because they may explain signal flow to the nucleus, such as, TFs and kinases (Table 8). Among these proteins, NAD Kinase 1 (NADK1, AT3G21070) increased >4-fold in the nuclear fraction with no change in the total fraction 3 h after flg22 treatment (Table 8). NADK1 is known to convert NAD^+ to $NADP^+$ in the cytosol (Waller et al., 2010; Hashida and Kawai-Yamada, 2019). Recent studies in animal and plant established the significance of enzymatic activity of TIR domains of TNLs in depletion of NAD^+ and pathogen recognition (Horsefield et al., 2019; Wan et al., 2019a). Activation of some NLRs leads to their nuclear accumulation where they regulate transcription (Tsuda and Somssich, 2015). The NAD^+ cleavage by TIR domains of plant NLRs leads to accumulation of second messengers like ADPR and cADPR which trigger calcium signalling that leads to downstream signalling (Wan et al., 2019a). Several plant TIR-NLRs such as RPS4, RPP1, RBA1 and BdTIR, required ENHANCED DISEASE SUSCEPTIBILITY 1 (EDS1) for cell death phenotype in response to pathogen (barley powdery mildew resistance protein MLA10) unlike animal TIR-NLR SARM1 (sterile alpha and TIR motif containing 1) (Wan et al., 2019a). At the same time, nuclear accumulation of EDS1 was shown to induce autoimmunity (Stuttmann et al., 2016). In yeast, enzymes required for biosynthesis of NAD^+ are nuclear localized (Kawai and Murata, 2008). Thus, similar to enzymatic activity of plant NLRs that require EDS1 for NAD+ depletion and ultimately to cell death, nuclear accumulation of NADK1 in response to flg22 can regulate nuclear $NAD^+/NADP^+$ homeostasis resulting in secondary signalling cues to relay MAMP perception during PTI.

Another protein was the Pattern-Triggered Immunity Compromised Receptor-like Cytoplasmic Kinase 1 (PCRK1, AT3G09830) which associates with the flg22 receptor FLS2 at the plasma membrane and was shown to be important for defense against *Pma* ES4326 and regulation of SA biosynthesis (Sreekanta et al., 2015; Kong et al., 2016). I found that PCRK1 increased in abundance in the nuclear fraction compared to total faction (>4 fold) at 3 h. The PCRK1 is predicted to be nuclear localized as per the SUBA4 database that uses different subcellular targeting prediction algorithms. On the other hand, PCRK1 and its functionally redundant homolog, PCRK2, that shares 80% amino acid sequence homology were found to be plasma membrane localized and associated with the flg22 receptor, FLS2 in the absence of flg22. Similar to BIK1, one of the explanations for observing increased PCRK1 abundance in the nuclear fraction would be that PCRK1 re-localizes from plasma membrane to the nucleus during flg22 response (Lal et al., 2018).

Table 8

Protein ID	Ratio[a] Proteome				Ratio[b] Transcriptome					SUBAcon	Description
	Nuc	Tot	Difference	pval	1h	2h	3h	5h	9h		
AT3G21070	2.30	-0.58	2.88	0.00	4.22	1.41	1.20	0.83	0.04	cytosol	NAD kinase 1 (NADK1)
AT4G01720	3.59	-0.14	3.74	0.00	0.82	1.36	2.92	2.75	2.65	nucleus	WRKY family transcription factor (WRKY47)
AT3G09830	2.08	-0.38	2.46	0.01	2.25	1.01	1.32	1.41	0.78	nucleus	Protein kinase superfamily protein (PCRK1)
AT3G55270	-2.99	-0.39	-2.60	0.01	-0.09	0.43	0.08	0.45	0.13	nucleus	mitogen-activated protein kinase phosphatase 1 (MKP1)
AT2G28550	-1.73	0.32	-2.05	0.00	-1.46	-0.92	-0.83	-0.85	-0.55	nucleus	related to AP2.7 (TOE1)

Table 8: Table showing potential candidates involved in relaying flg22 perception. A subset of proteins that shows change in nuclear abundance but no change in the total protein fraction at 3 h. The complete list of such proteins at 3 and 9 h can be found in Table S5. Proteome changes in nuclear (Nuc) and total (Tot) fractions and difference between them (Difference) are shown. A two-tailed *t*-test was used to calculate p-values (pval) corresponding to the difference between protein abundance change in the nuclear and total fraction calculated over 6-biological replicates. Ratio[a] represents protein abundance change in Col-0 plants in response to flg22 vs mock treatment. Ratio[b] represents transcriptome change in Col-0 vs *fls2* plants in response to flg22 treatment at indicated time-points. SUBA4 predicted subcellular localizations (SUBAcon) and descriptions are indicated for the proteins shown.

Among the downregulated proteins in the nuclear fraction, I found Target of Early Activation Tagged (TOE1, AT2G28550) and MAPK PHOSPHATASE 1 (MKP1, AT3G55270) interesting. These proteins were annotated as nuclear localized as per SUBA4 database and were downregulated in the nuclear fraction with no change in the total fraction at 3 h (Table 8). Among these, TOE1, a transcription factor, was shown to negatively regulate FLS2-mediated immunity by binding to the *FLS2* promoter (Zou et al., 2018). TOE1's reduced protein abundance in the nucleus may de-represses *FLS2* expression during flg22 response. Another downregulated protein I found in the nucleus was MKP1 (AT3G55270) which is a phosphatase that inactivates immune-related MAPKs, MPK3 and MPK6, thereby negatively regulating plant immunity (Bartels et al., 2009; Anderson et al., 2011; Jiang et al., 2017). I found that MKP1 accumulation decreased in the nucleus at 3 h. Since, MAPK phosphorylation is observed only up to 30 min, a reduction of MKP1 at 3 h may positively contribute towards a second round of MAPK activation by other MAMPs and provide a conducive cellular environment for phosphorylation of TFs and/or other components involved in PTI. At 9 h MKP1 showed no protein abundance change in the nucleus. This is indicative of a scenario that by 9 h MKP1 regains basal level to supress sustained activation of TFs and/or other components making a negative feedback loop. For example, PROTEIN PHOSPHATASE 2A (PP2A) dephosphorylates BAK1 to supress immune response (Segonzac et al., 2014). The identified

proteins whose accumulation in the nucleus change, such as NADK1, PCRK1, TOE1, and MKP1 are interesting candidates to further investigate their role in flg22-mediated immunity.

2.3 Flg22-induced genes are also induced by translational inhibitors

A hypothesis for quick and massive induction of flg22 responsive genes is de-repression of transcription: at the basal state, transcription of flg22 responsive genes are suppressed by negative regulator(s) and upon flg22 perception, transcription is de-repressed via removal or inactivation of such negative regulator(s). Additionally, several flg22-responsive genes were found to be induced upon treatment with the protein synthesis inhibitor cycloheximide (CHX) which suggests that de-repression could be a mechanism to induce transcriptional reprogramming in response to flg22 (Navarro et al., 2004; Jacob et al., 2017). In this scenario, it has been proposed that translation of negative regulator(s), assumed to be high turnover-proteins, is inhibited by CHX, which leads to reduced accumulation of the negative regulator(s), resulting in activation of transcription of flg22 responsive genes. On comparing transcriptome responses to flg22 (Winkelmüller, 2018) and CHX treatments available in public databases (Goda et al., 2008; Drechsel et al., 2013), there was a substantial overlap between genes upregulated 1 h after flg22 treatment and 3 h and/or 4 h after CHX treatment (Figure S5).

To confirm these transcriptome results, I performed expression analysis of flg22 marker genes, *PROPEP3* and *WRKY30,* by RT-qPCR upon treatment with different translational inhibitors and flg22 (Figure 7). I chose two time points- 2 h and 4 h because preliminary RT-qPCR experiment showed that CHX induced flg22 responsive genes only from 1 h onwards (Figure S6), which is consistent with protein degradation studies in human neural cell lines which found CHX activity starts from 45 min (Heier and Didonato, 2009). As expected, flg22 induced *PROPEP3* and *WRKY30* at 2 h and 4 h. Consistent with the transcriptome results, CHX also induced these two genes at 2 h and 4 h. The CHX used in this and previous studies was derived from microbes, which raises a possibility that such gene induction by CHX can be due to contamination of microbial molecules that are recognized in *A. thaliana* Col-0 plants to trigger PTI. In order to investigate the possibility of MAMP contamination in the CHX in my experiments, I additionally used a synthetic source of CHX, which is unlikely contaminated with MAMPs. CHX from the synthetic source similarly induced these two genes at 2 h and 4 h, suggesting that induction of flg22-responsive genes was due to CHX effects.

Next, I tested if gene induction by CHX, overlapped with flg22 response, is due to its activity of translational inhibition or other effects caused by CHX. To this end, I tested other translational inhibitors-anisomycin, puromycin and chloramphenicol which inhibits translation by different mechanism in eukaryotes (anisomycin and puromycin) and in prokaryotes (chloramphenicol) (Figure 7). I found that similar to CHX, anisomycin induced both genes. Puromycin induced *WRKY30* but did not induce *PROPEP3*. Lastly, chloramphenicol, which specifically inhibits only prokaryotic translation including chloroplast and mitochondrial translation (Smith-Johannsen and Gibbs, 1972), neither induced *PROPEP3* nor *WRKY30,* suggesting that induction of flg22-responsive genes is specific to cytosolic eukaryotic translation inhibition. Thus, flg22 treatment and cytosolic translational inhibition lead to induced expression of the same set of genes. This raises several possibilities. First, flg22 inhibits translation, and therefore flg22 and CHX treatments show similar gene expression profiles. Second, flg22 does not inhibit translation but converges with CHX's mode of action at some point such as reduced accumulation of negative regulators of flg22-responsive genes. The first possibility can be tested by performing a global translation profiling using ribosome foot-printing to identify genes whose translation is altered by flg22 and CHX treatments.

2.4 Nuclear protein dynamics during early flg22-response

In this thesis, I discovered WRKY47 as a positive regulator of immunity. In addition, I identified NADK1, PCRK1, TOE1, and MKP1, as potential regulators of flg22-mediated responses in the nucleus. While these findings provided insights into how plants might mediate flg22-mediated responses in the nucleus such as transcriptional reprogramming, how flg22 perception is relayed into the nucleus remained obscure. Therefore, I decided to profile earlier nuclear protein dynamics to identify proteins that relay flg22 perception into the nucleus thereby mediating transcriptional reprogramming.

I conducted additional nuclear and total proteome experiments at early time points (15, 30, and 60 min) after flg22 treatment. As flg22-triggered transcriptional reprograming occurs within 30 min (Li et al., 2016), I expected that I can capture protein dynamics before and after transcriptional reprogramming occurs and that proteins whose abundance changes at these time points might be involved in information relay of flg22 perception at the plasma membrane to the nucleus. Similar to my 3 h-9 h experiments, I also included total protein fraction as it would give us insights into nuclear specific events, such as protein movements, during early flg22 response. I also performed and analyzed nuclear and total protein fractions upon CHX treatment to test whether protein abundance changes overlap between CHX and flg22 treatments as

observed for gene expression changes. For CHX treatment, I chose 60 min as my preliminary RT-qPCR experiments showed that CHX induced expression of flg22-responsive genes, *PROPEP3* and *WRKY30,* at 60 min and not at 30 min (Figure S6). Additionally, as the leaf infiltration method used for 3 h and 9 h experiments are not suitable for short time periods, due to the time required for treatment and sample collection, I used 12-day old seedlings and immediately isolated nuclear and total proteins. In total, I analyzed 72 proteome samples.

2.4.1 Protein subcellular localization remain largely unchanged during early flg22 response.

Similar to the 3 h-9 h results, I could enrich nuclear proteins in a reproducible manner (Figure 8, S7 and, S8) and observed a very high correlation (R^2>0.8, Table S6) between replicates within the same conditions (i.e. same treatment-flg22/mock, at the same time point). In comparison to the 3 h-9 h results (Table 4), I detected a smaller number of proteins in the nuclear fraction than in the total fraction in early time points proteome data (Table 9) because this could be due to differences arising from different tissues used (i.e. seedlings include roots). A direct comparison of previous 3 and 9 h proteomes may not be very informative. Therefore, I focused on comparisons within seedling samples. Within the seedling samples, I observed high reproducibility and similar number of detected proteins (Table S6). In addition, overall proportion of subcellular localization of detected proteins largely did not change for all compartments at 15, 30, and 60 min after flg22 treatment, suggesting at least dramatic protein movements into one direction unlikely occurred during early flg22 response.

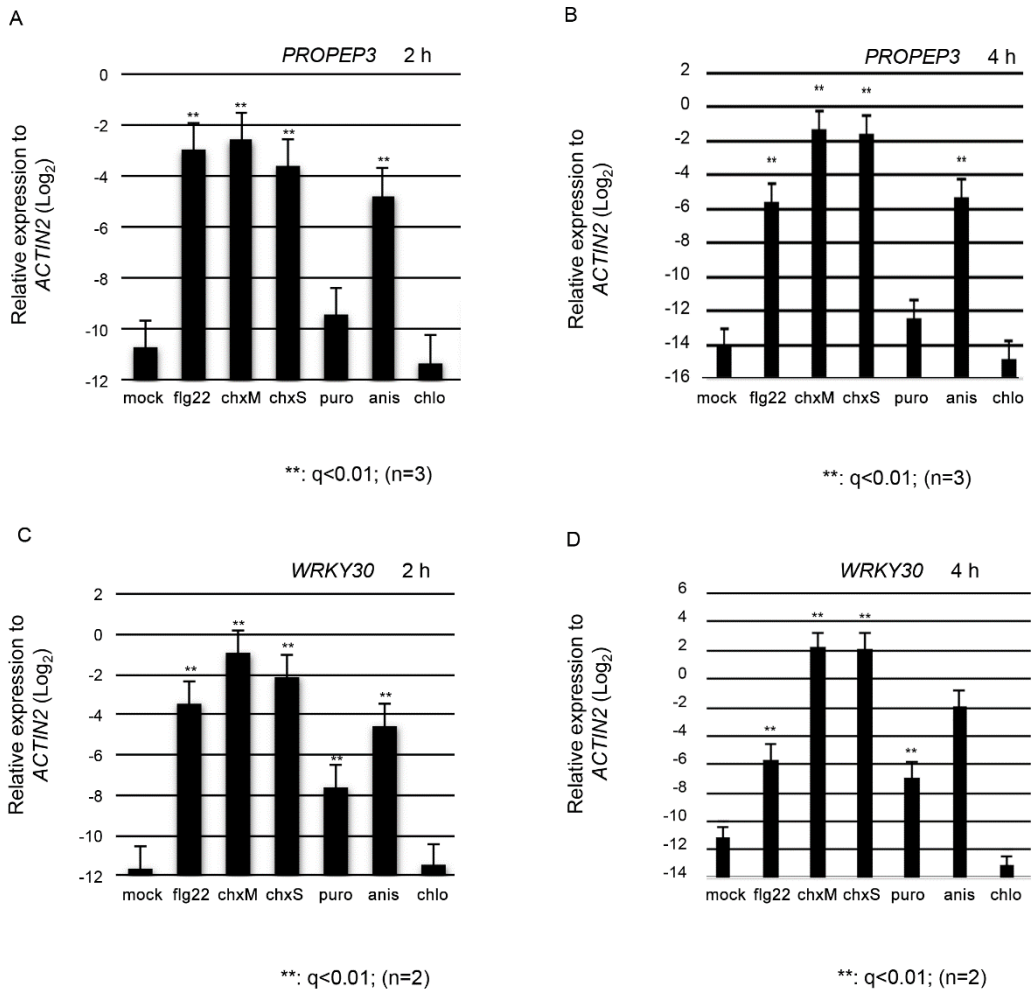

Figure 7: Translational inhibitors strongly induces expression of early flg22-responsive genes. Expression of flg22-responsive genes *PROPEP3* and *WRKY30* were tested after treatment of 12-day-old *A. thaliana* seedlings with 1 µM-flg22/mock and different protein translational inhibitors **(A-D)**. Protein translation inhibitors used were 100 µM-cycloheximide (chxS, synthetic source and chxM, microbial source), 200 µM-puromycin (puro), 100 µM-anisomysin (anis), and 100 µM-chloramphenicol (chlo). Bars represents the standard error from independent experiments ('n'). Asterisks indicate significant difference between mock and treatment samples (mixed linear model followed by Student's *t*-test; **, p<0.001)

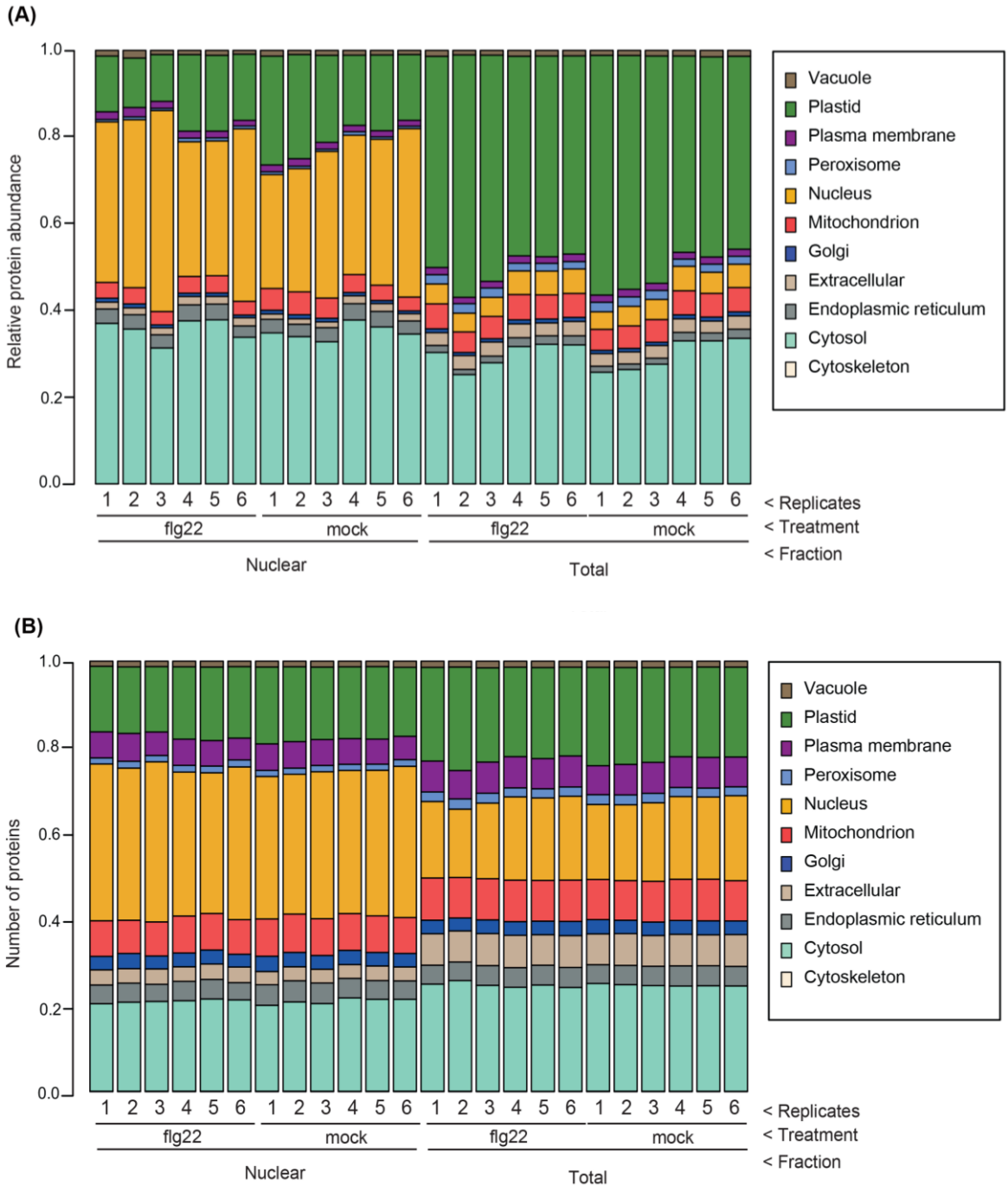

Figure 8: Subcellular localization of proteins detected in the nuclear and total proteome analysis. Total and nuclear proteins were isolated from Col-0 seedlings (12-day old) at 15 min after 1 µM-flg22 or mock (water) treatment. Six replicates (protein samples were prepared in two different days each containing three replicates prepared from independent plant materials) were prepared for each condition. Relative protein abundance was calculated using intensity based absolute quantification (IBAQ) values. The individual columns represent each replicate showing relative protein abundance of proteins identified by LC-MS/MS and its subcellular localization as predicted by SUBA4 reference database. **(A)** Ratio of different subcellular localization of proteins based on their relative abundance (IBAQ value). **(B)** Ratio of different subcellular localization of proteins based on protein

Table 9				
	Nuclear		Total	
Time	flg22	mock (water)	flg22	mock (water)
15 min	4683.8	4598.5	5680.0	6068.3
30 min	5781.7	5788.3	7059.3	7081.0
60 min	5782.3	5786.3	7029.3	7061.3
	CHX	mock (DMSO)	CHX	mock (DMSO)
60 min	5751.7	5723.0	7057.0	7007.3

Table 9: The number of proteins detected in early time point samples. Average number of proteins detected after 1 µM-flg22/ mock (water) or 100 µM-CHX/mock (DMSO) treatment in nuclear or total fraction at 15, 30, and 60 min. For flg22 treatment at 15 min six replicates (protein samples were prepared in two different days each containing three replicates prepared from independent plant materials) were used. For flg22 treatment at 30 and 60 min, and CHX treatment at 60 min three replicates prepared from independent plant materials were used.

2.4.2 Cycloheximide and flg22 converge at the transcriptome level inducing similar gene expression

On comparing the nuclear and total proteome upon flg22 and CHX treatments during early time points, I found proteins whose abundance show significant changes in protein abundance in nuclear and total proteome in response to flg22 and CHX (Table 10). I detected 97, 27 and 29 DEPs after 15, 30 and 60 min respectively of flg22 treatment and 24 DEPs after 60 min of CHX treatment in the nuclear fractions. (Table 10, Figure 9A). I found that protein dynamics in the nuclear fraction at 15 min were largely different from flg22 treated samples at other time points and CHX treated samples (Figure 9A, Figure S10). On the other hand, I observed some overlap (5 upregulated & 1 downregulated proteins common) between nuclear proteome at 30 and 60 min after flg22 treatment (Figure 9B). However, unlike the similarity at transcriptome level, protein expression after flg22 and CHX treatment were largely dissimilar. The difference among transcriptome and proteome responses (overlapping gene expression and non-overlapping protein expression) suggests that flg22 and CHX treatments induce the same genes but by different mechanisms (Merchante et al., 2017; Ding et al., 2014).

In order to investigate functional differences between flg22 and CHX response, I performed a gene ontology enrichment using BINGO plugin in Cytoscape and depicted the top 10 GO terms (Figure 10, Figure S11). Among the flg22 induced upregulated proteins in the nuclear fraction, at 15 and 30 min did not yield any significant GO terms, however, at 60 min GO terms for defense response and biotic stimulus were enriched as expected.

Table 10

Protein fraction	Time (Treatment)	Number of proteins significantly changing in abundance		Number of proteins with consistent presence/absence expression profile	
		Up	Down	Increased	Decreased
Nuclear	15 min (flg22)	18	79	10	7
	30 min (flg22)	15	13	6	3
	60 min (flg22)	20	9	11	3
	60 min (CHX)	6	18	11	8
Total	15 min (flg22)	11	12	5	9
	30 min (flg22)	6	15	0	2
	60 min (flg22)	20	9	6	8
	60 min (CHX)	7	10	4	4

Table 10: The number of proteins whose abundance changes during early flg22 and CHX response. Left, proteins showing quantitative change (|log2 value| > 1, p-value<0.05) upon flg22 (or CHX) vs mock treatment. Right, proteins which are consistently present in flg22 (or CHX) samples but absent in mock are defined as "Increased" and vice-versa (as "Decreased") in the nuclear or total fractions at indicated time points.

Whereas among flg22 induced downregulated proteins in the nuclear fraction at 15 min, I found GO terms enriched for "photosynthesis", and photosynthesis related processes. This observation was similar to a previous studies in *A. thaliana* that found downregulation of photosynthetic related GO terms in down regulated genes at translational level during AvrRpm1 induced ETI response (Meteignier et al., 2017), in downregulated genes during coronatine (COR) treatment (Attaran et al., 2014), and suppression of photosynthesis related genes upon infection with *Pto* DC3000 or *hrpA* treatment (Lewis et al., 2015; De Torres Zabala et al., 2015). Additionally, Attaran et al. 2014 found that although a global repression of photosynthetic genes was observed they didn't detect decrease in photosynthetic efficiency. Degradation of photosynthesis related proteins alters the redox state of a cell which are critical signaling cues (Pierella Karlusich et al., 2017; Su et al., 2018). Similarly, downregulation of photosynthesis related proteins very early might serve as signaling cues for transcriptional reprograming during PTI. Unlike the GO terms enriched in the nuclear fraction upon flg22 treatment, CHX treatment resulted in different GO term enrichment like "response to organic substance", "response to endogenous stimulus" etc., which were different from flg22 treatment (Figure 10). I found that flg22 and CHX treatment resulted in different protein abundance change in the total fraction as

well (Figure S10), which indicates that effects of CHX and flg22 on both nuclear and total protein accumulation are very different in contrast to transcriptome changes suggesting flg22 and CHX induce expression of similar genes with different mechanisms.

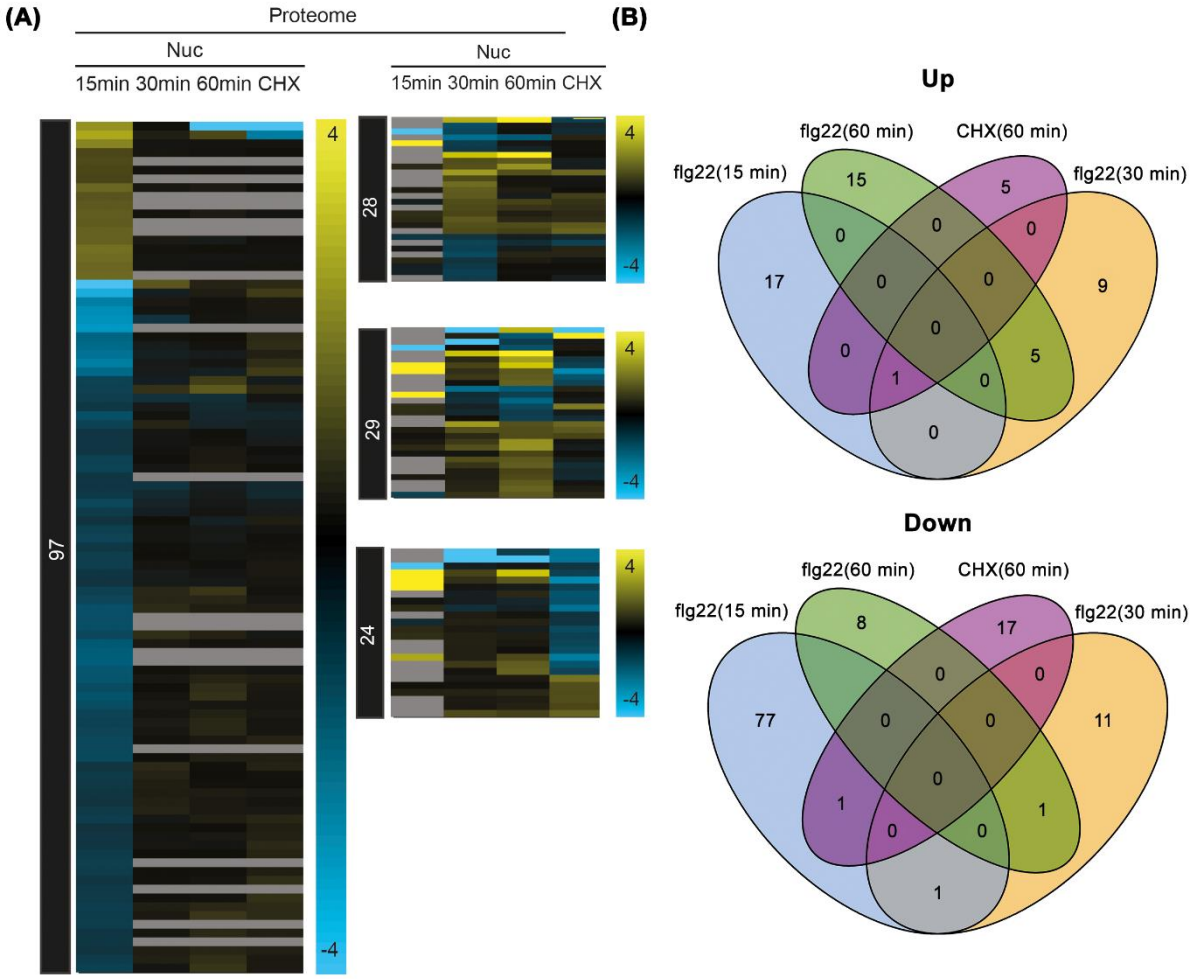

Figure 9: Early protein response to flg22 and cycloheximide are largely dissimilar. Heatmap showing DEPs ($|\log_2$ fold change$| > 1$; p-value < 0.05) in the nuclear fraction. **(A)** Left panel shows 97 DEPs at 15 min after 1 µM-flg22 treatment averaged across six replicates. Right-top panel shows 28 DEPs at 30 min and right-middle panel shows 29 DEPs at 60 min after 1 µM-flg22 treatment averaged across three replicates. Right-bottom panel shows 24 DEPs at 60 min after 100 µM-CHX treatment averaged across three replicates. **(B)** Venn diagram shows overlap of upregulated and downregulated proteins in the nuclear fraction after flg22 or CHX treatment at indicated time points.

2.4.3 Protein downregulation in the nucleus may precede flg22-triggered transcriptional reprograming

Nuclear protein dynamics at 15 min was strikingly different from that at 30, and 60 min (Figure 9A). Out of 97 DEPs detected in the nuclear fraction at 15 min, I found 79 proteins

were downregulated. I used seedlings, extracted proteins, and performed proteome analysis in the same way for 15, 30, and 60 min samples, yet I observed this downregulation only in the nuclear fraction at 15 min. This excludes the possibility of simple artifacts coming from technical issues with seedling experiments and suggests that protein downregulation is a specific response in the nuclear fraction at 15 min.

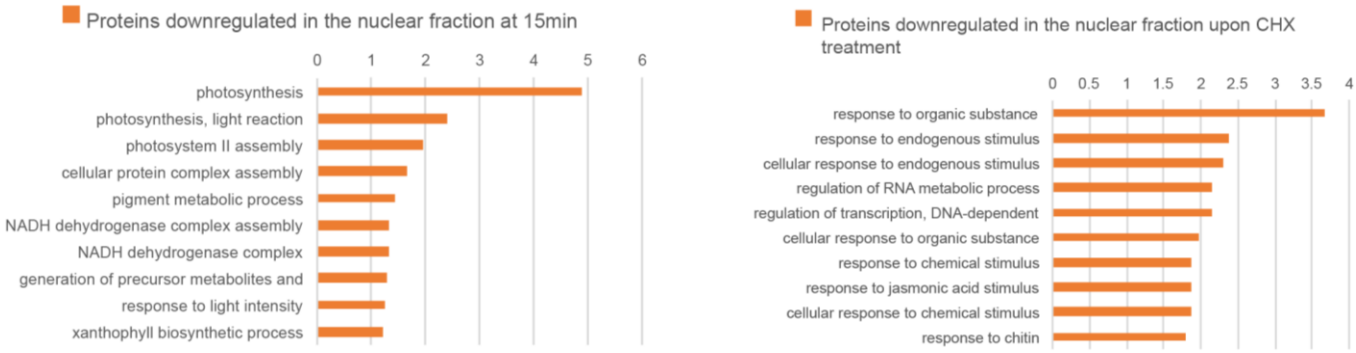

Figure 10: Early protein response to flg22 and CHX results in enrichment of different GO terms. Top ten GO terms are arranged according to their decreasing –log10 adjusted p-values for downregulated proteins ($|\log_2$ fold change$| > 1$; p-value < 0.05) after 1 µM-flg22 treatment after 15 min or 100 µM-CHX treatment after 60min in the nuclear fraction. GO enrichment analysis was done with BingGO plugin for Cytoscape (FDR=0.1). As background a customized reference protein list was used which consisted of proteins that were detected at least twice in the flg22 or mock conditions in nuclear or total fractions at 15, 30, and 60 min or after CHX treatment for 60 min.

2.4.4 Protein that may be involved in early flg22 response

At 15 min time point, 79 proteins were down-regulated in the nuclear fraction (Figure 9A, Table S7A). As these protein abundance changes precede transcriptional reprogramming, some of changes may be important for flg22-triggered transcriptional reprogramming and perhaps these down-regulated proteins may be negative regulators. In order to identify potential negative regulators during early flg22 response, I focused on downregulated proteins in the nuclear fraction which are predicted to be nuclear localized (Table 11). Among downregulated proteins in the nuclear fraction at 15 min, I found (SCP1-like small phosphatase (SSP5, AT5G11860) and, RPM1-interacting protein 4 (RIN4, AT3G25070) interesting. SSP5 is a RNA polymerase II carboxyl-terminal domain (RNA pol II CTD) phosphatase, capable of Ser5-PO_4 dephosphorylation and serve as a transcriptional repressor (Feng et al., 2010; Hajheidari et al., 2013). Experiments in *A. thaliana* protoplasts showed SSP5 to be localized in both cytosol and nuclei. Therefore, the downregulation of SSP5 in the nucleus upon flg22 treatment could play a role in the induction of immune genes via de-repression (Feng et al., 2010).

RIN4 is tethered to plasma membrane by C-terminal acylation, and is a negative regulator of PTI (Ray et al., 2019; Goslin et al., 2019; Afzal et al., 2011). Several pathogen effectors, like AvrRpt2, target RIN4 to inhibit PTI. RIN4 is cleaved by AvrRpt2 into 3 fragments. Two of these fragments, ACP2 and ACP3, contain a plant-specific nitrate-induced (NOI) domain which are then released from plasma membrane and suppress PTI (Afzal et al., 2011). Subcellular localization of these fragments after, being released from the plasma membrane, is unclear. Effectors like AvrRpt2 also cleaves other NOI domain containing proteins which are predicted to be plasma membrane localized such as RIN4 (Goslin et al., 2019). However, one of these NOI proteins, a RIN 4 family protein (AT5G40645), was found to show nuclear localization. The downregulation of RIN4 in the nucleus can be the non-membrane RIN4 proteins that are not properly targeted to plasma membrane. An alternative explanation can be in absence of pathogens plants use such non-targeted RIN4 to suppress PTI which upon MAMP perception are quickly removed from the nucleus to induce immune response.

Among other downregulated proteins I found MPK3/6-targeted-VQ-motif-containing protein 1 (MVQ1, AT1G28280) to be interesting. MVQ1, a nuclear localized protein, belongs to the groups of VQ-motif containing proteins that was found to be phosphorylated by MAP kinases-MPK3 and MPK6, and were named MPK3/6-targeted-VQ-motif-containing protein 1 (MVQ1) (Pecher et al., 2014). Flg22 treatment resulted in phosphorylation of MVQ1 as shown by mobility shift assay and resulted in decrease in MVQ1 abundance (Pecher et al., 2014). I found MVQ1 protein abundance decreased upon flg22 treatment in the nucleus at all time points tested which is consistent with previous report of reduced MVQ1 protein level upon flg22 treatment. Additionally, MVQ1 overexpression was found to inhibit flg22 induced *NHL10*, a early flg22-marker gene (Boudsocq et al., 2010), promoter activity in *A. thaliana* protoplasts (Weyhe, 2019). MVQ1 was shown to negatively affect WRKY- mediated gene expression via binding to WRKYs with the VQ-motif (Pecher et al., 2014; Weyhe, 2019). Recently, a comparative transcriptomic study found that about 400 flg22-induced genes were suppressed in MVQ1 overexpressing line compared to Col-0 and compromised resistance against *Botrytis cinerea* infection indicating a negative regulatory role of MVQ1 in plant immunity (Weyhe, 2019). Compared to Col-0, *mvq1* plants were more sensitive to flg22-treatment as observed by upregulation of a higher number of defense related genes (Weyhe, 2019). I also observed that MVQ1 abundance decreased upon CHX treatment in the nuclear fraction which is consistent with previous report of enhanced degradation of MVQ1 upon flg22 and CHX co-treatment (Pecher et al., 2014).This suggests that MVQ1 is a high turnover protein whose rapid removal from the nucleus could be important for de-repression of early immune genes.

In addition to the downregulated proteins, upregulated proteins are also interesting, such as TFs. Among upregulated proteins in the nuclear fraction at 15 min were PHD type transcription factor with transmembrane domains (PTM, AT5G35210), Calmodulin-binding transcription activator protein 2 (CAMTA2, AT5G64220) and, Calmodulin-binding transcription activator protein 3/Signal Responsive 1 (CAMTA3/SR1, AT2G22300). PTM is a chloroplast envelope-bound plant homeodomain (PHD) transcription factor that localizes in chloroplast membrane. Upon various photooxidative stress inducing stimuli (norflurazon, lincomycin) PTM undergoes proteolytic cleavage and its amino terminal translocate inside the nucleus to transmit chloroplast signals to the nucleus (Sun et al., 2011).. I found that PTM increased >2-fold in the nuclear fraction specifically at 15 min upon flg22 treatment (Table 11). It remained unchanged in the nuclear fractions at other time points tested and was undetected in the total fraction. Interestingly, the upregulation of PTM in the nuclear fraction at 15 min coincided with downregulation of proteins involved in electron transport chain as found in GO-term analysis (Figure 10). The downregulation of electron transport chain and photosynthesis related proteins leads to ROS production (Su et al., 2018; Pierella Karlusich et al., 2017). PTM was shown to sense ROS accumulation. A plausible role of PTM could be to sense the ROS accumulation in response to flg22 which then undergoes cleavage and translocation into the nucleus to trigger transcriptional reprograming. In this scenario PTM cleavage products may use stromules to get translocated into the nucleus to mediate the expression of nuclear encoded defense during flg22 response (Caplan et al., 2015). This led me to check which part of PTM was detected in my nuclear fraction. I detected 15 peptides, all arising from N-terminal region of PTM in my nuclear fraction (Figure 11). Most of these peptides were detected in flg22 treated nuclear fraction (25 detections in flg22 vs 10 detection in mock) suggesting flg22 dependent accumulation of N-terminal part of PTM (Figure 11). Specific upregulation of PTM in the nuclear fraction together with its central role in transmitting chloroplast derived retrograde signaling suggests that it may be an important signaling factor connecting MAMP perception to nuclear transcriptional reprograming.

One of the proteins that were upregulated in the nuclear fraction in 15 min were *CALMODULIN-BINDING TRANSCRIPTIONAL ACTIVATORs-CAMTA2* and *CAMTA3* (Table 11). The *CAMATA3* was shown to be a negative regulator of immunity based on elevated immune phenotype in *camta3* knockout mutant and *CAMTAs* were shown to be involved in PTI

Table 11: Potential candidates involved in early flg22 response

Protein ID	Proteome								SUBAcon	Description
	Nuc				Tot					
	15min	30min	60min	CHX	15min	30min	60min	CHX		
Downregulated proteins										
AT3G25070	-1.21	-0.49	-0.14	-0.33	-0.28	0.28	-0.32	-0.19	plasma membrane	RPM1 interacting protein 4 (RIN4)
AT5G11860	-1.21	NA	NA	NA	NA	NA	NA	NA	cytosol	SCP1-like small phosphatase 5 (SSP5)
AT1G28280	-25.16	-25.81	-1.23	-2.38	-22.82	NA	NA	NA	nucleus	VQ motif-containing protein (MVQ1)
Upregulated proteins										
AT5G35210	1.10	NA	NA	NA	NA	NA	NA	NA	nucleus	metalloendopeptidases;zinc ion binding;DNA binding (PTM)
AT5G64220	1.60	NA	NA	NA	-0.21	NA	NA	NA	nucleus	Calmodulin-binding transcription activator protein 2 (CAMTA2)
AT2G22300	1.32	NA	NA	NA	-0.22	NA	NA	NA	nucleus	Calmodulin-binding transcription activator protein 3 (CAMTA3)

Table 11: Table showing potential candidates involved in early flg22 response. A subset of proteins that shows change in nuclear protein abundance during early flg22 response. The complete list of such proteins after flg22 or cycloheximide (CHX) treatment can be found in Table S7.

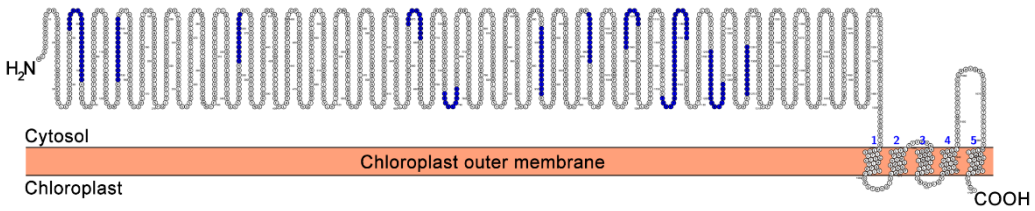

AASSNILEQMK, ASLMDIFSYIASR, AVELPNQVNGVQAR, DFDDNEVFLGK, DSQIPEVVGFK, HQNAVIPVIK, IFSGLFPLK, IVSYDTGLYR, KIPGLNYGDASYIPR, NQNILLAGR, NVEDTGVDFR, QSTAPQFTINVR, TRVPTNINHR, VATGLLENVPR, VSYGVFFGNQK
N-terms: Phobius
TMRs: UniProt

SN	Peptides	Score	Number of detections	
			flg22	mock
1	AASSNILEQMK	81.95	1	0
2	ASLMDIFSYIASR	98.353	1	0
3	AVELPNQVNGVQAR	82.417	2	0
4	DFDDNEVFLGK	93.649	1	1
5	DSQIPEVVGFK	50.353	0	1
6	HQNAVIPVIK	77.318	3	0
7	IFSGLFPLK	75.109	2	2
8	IVSYDTGLYR	80.219	4	1
9	KIPGLNYGDASYIPR	46.68	1	0
10	NQNILLAGR	91.9	3	1
11	NVEDTGVDFR	64.04	1	0
12	QSTAPQFTINVR	74.944	1	2
13	TRVPTNINHR	71.524	2	0
14	VATGLLENVPR	57.348	1	2
15	VSYGVFFGNQK	62.582	2	0

Figure 11: N-terminal end of PTM was enriched in the nuclear fraction during flg22 response. Top panel shows the transmembrane structure of PTM visualized in Protter (version 1.0) and peptides detected for its identification are highlighted blue. Bottom panel shows number of times peptides are detected among the six-replicates of flg22/mock treated nuclear fractions for the identification of PTM by LC-MS/MS.

and ETI signalling (Du et al., 2009; Karasov et al., 2017). However, *camta3* phenotype was later attributed to activation via two NLR proteins and a guardee role of CAMTA3 (Lolle et al., 2017). Using a two NLR P-loop dominant negative mutants, *dsc1-dn* and dsc2-dn, it was shown that *camta3* phenotype is suppressed in the *camta3/dsc1-dn/dsc2-dn* triple mutants and the *camta3* autoimmune phenotype is contributed by DSC1 and DSC2 NLRs. Additionally, *CAMTA3* was found to positively regulate early stress response genes via a CAMTA-binding motif, *Rapid Stress Response Element* (*RSRE*), in response to various stresses including flg22 (Benn et al., 2014). In line with previous studies, different *CAMTAs*, including *CAMTA2* and *CAMTA3*, were found to be induced within 15 min of various treatments including SA, JA, and H_2O_2 (Yang and Poovaiah, 2002). I found CAMTA2 was upregulated during flg22 treatment at 15, 30 and 60 min and CHX treatment at 60 min in the nucleus and CAMTA3 was upregulated in the nucleus upon flg22 treatment at 15 min and CHX treatment at 60 min. These results together with a positive role of CAMTA3 in the induction of early stress response genes suggests that CAMTAs may serve as a positive regulator of early flg22-induced PTI.

3. Discussion

3.1 The establishment of a new nuclear isolation protocol for nuclear proteome analysis

Despite several attempts to conduct nuclear proteome analysis, there is still much room for method improvement. For instance, I found that Folta protocol showed contamination of proteins from other compartments, in particular, plastidial proteins (Figure 1A). Nuclear protein isolation protocol from Sikorskaite et al., 2013 also showed contamination of stromal proteins as could be seen from Coomassie staining around 50 kDa which corresponds to RbCl, a stromal protein (Sikorskaite et al., 2013). Many publications used either mechanical homogenisation or with liquid nitrogen to homogenise plant tissue which may affect not only nuclear integrity but also break chloroplasts that may leak into the nuclear protein fraction. I found that modifying the homogenization technique, chopping instead of using a blender or with liquid nitrogen and mortar-pestle, helped to reduce chloroplast contamination (Figure S1A, B). Vlasák et al. found that in comparison to snap-freezing with liquid nitrogen, homogenization using blender performed better to keep nuclei intact (Vlasák, 1981). However, Zhang et al. found that liquid nitrogen performed better compared to blender for nuclei isolation from tomato leaves (Zhang et al., 1995). Nevertheless, other protocols using blender for homogenisation recommends use of lowest speed setting which suggests that the shearing force from mechanical homogenisation would affect nuclear integrity (Folta and Kaufman, 2007; Sikorskaite et al., 2013). Therefore, I used chopping with razor blades. Furthermore, compared to Folta-protocol, TX-100 at a final concentration of 0.85 %, instead of 1 %, and only before the second centrifugation step resulted in reduced chloroplast protein contamination.

Nuclear isolation protocols were evaluated for the quality of method by immunoblotting experiments for marker proteins and/or microscopy images using DAPI staining (Goto et al., 2019; Howden et al., 2017; Fakih et al., 2016; Sikorskaite et al., 2013). However, both methods cannot show the overall quality of the fractionation procedure. For instance, nuclear enrichment is often shown by immunoblotting with nuclear histone-H3. However, histone-H3 may not serve as the best marker for nuclear enrichment. Since histone-H3 is tightly associated with chromatin, histone-H3 signal can be detected even from broken nuclei (Annunziato, 2008). Therefore, I used transgenic plants expressing GFP-tagged Nup50a, localized to the nucleoplasm, in addition to histone H3 to access nuclear enrichment (Tamura et al., 2010). However, MS based proteome profiling is a more reliable method to reveal the overall quality

of a nuclear isolation protocol as recently also used by Goto et al. 2019 on *A. thaliana* cell cultures to demonstrate nuclear method isolation improvements (Goto et al., 2019).

Goto et al. 2019 used a high concentration sucrose gradient to isolate nuclei from *A. thaliana* cell culture and identified 1539 nuclear proteins using LC-MS/MS. Another nuclear proteomic study investigating chitosan-induced nuclear proteome changes in *A. thaliana* identified 232 nuclear proteins (Fakih et al., 2016). In comparison, I identified 1932 nuclear proteins as per SUBA4 subcellular predictions. This is an 25% increase in nuclear protein detection as compared to Goto et al. which can allow us to identify flg22-responsive proteins that are not yet implicated in immunity. The increased number of nuclear proteins identified in my method compared to Goto et al. can be contributed by not only the improvement in nuclear fractionation method but also sample preparation for LC-MS/MS and starting material used. For instance, Goto et al. used a sequential protein extraction method to extract soluble, peripheral and membrane proteins and *A. thaliana* cell cultures as starting material which may as well aid in protein detection. However, one of the challenging aspects in nuclear proteomics is to distinguish contaminants from bonafide nuclear proteins. Therefore, an approach independent of obtaining pure organellar fraction to assign subcellular localization as done in animal field might be further helpful in finding nuclear proteins. In addition, having several protein fractions can give further insights into putative subcellular protein movements. For example, methods such as PCP and LOPIT make use of several protein fractions and generate protein abundance profiles for each fraction (Lundberg and Borner, 2019). These abundance profiles for each fraction are compared to profiles of organellar marker proteins to identify which fractions represent which organelles. The presence of several fractions corresponding to different organelles serves as a reference and would help in detection of protein movement into/out of the nucleus in response to external stimulus.

3.2 Nuclear protein dynamics during early and late flg22-response

MAMP perception by PRRs at the cell surface leads to several downstream PTI responses that include transcriptional reprograming inside the nucleus. However, it is mostly unknown where PTI signaling components, such as MAPKs or TFs, interact to relay signal transduction inside the nucleus. I hypothesized that some factors move from cytosol to the nucleus to relay PTI signaling inside the nucleus. For instance, the plasma membrane associated-BIK1 was found to localize in the nucleus upon elf18 treatment where it interacts with WRKY TFs, indicating a mechanism that connects MAMP perception at the plasma membrane to nuclear transcriptional reprograming (Lal et al., 2018). In order to select proteins involved in signal

transduction from the plasma membrane inside the nucleus, I searched for proteins that showed upregulation in the nuclear fraction with no change in the total fraction. Based on this hypothesis, I found NADK1 interesting. NADK1 increased more than 4-fold in the nuclear fraction with no change in the total fraction at 3 h after flg22 treatment (Table 8). NADK1 converts NAD+ to NADP+ in the cytosol (Waller et al., 2010; Hashida and Kawai-Yamada, 2019). Recently, in plants enzymatic activity of TIR domain was established in depletion of NAD^+ and pathogen recognition (Wan et al., 2019a). It is known that activation of some NLRs leads to their nuclear accumulation (Tsuda and Somssich, 2015). On the other hand, NAD^+ cleavage by TIR domains of plant NLRs leads to accumulation of second messengers such as ADPR and cADPR which trigger calcium signaling (Wan et al., 2019a). Induction of nuclear calcium is known to play an important role in the perception of nodulation (Nod) and mycorrhizal (Myc) factors released by rhizobial and arbuscular mycorrhizal symbionts, respectively (Charpentier, 2018). Briefly, rhizobial Nod factor (Nf) induced increase nuclear calcium leads to activation of calcium pump, SERCA-type calcium ATPase (MCA8) (Capoen et al., 2011). MCA8 is proposed to release Ca^{2+} back into the lumen of the nuclear envelope. Increased nuclear Ca^{2+} activates calcium and calmodulin dependent kinases and activates signal transduction to the downstream components such transcription factor CYCLOPs (Yano et al., 2008; Singh et al., 2014). Nuclear accumulation of NADK1 in response to flg22 may regulate nuclear NAD+/NADP+ homeostasis resulting in secondary signaling cues, such as increased nuclear Ca^{2+}, to relay MAMP perception during PTI. In addition, using nuclear import/export inhibitors in combination with nuclear proteomics may further help to focus on MAMP responsive protein movements during PTI.

Among proteins showing quantitative change in response to flg22 treatment in the nuclear and total protein fractions I detected several TFs that have not been implicated in immunity (Table S2A). Among them I found WRKY47, a TF yet unknown in immunity, to be highly upregulated at 3 h and 9 h after flg22 treatment. Based on pathogen growth assay, WRKY47 was found to be a positive regulator of plant immunity against *Pto* DC3000 (Figure 5B-C). WRKY47 belongs to group II of WRKY TF gene family consisting of 74 genes based on number and structure of WRKY domains and a zinc-finger motif (Eulgem et al., 2000; Wang et al., 2011b). Phylogenetic analysis based on nucleotide sequence found WRKY47 together with WRKY40 in group IIa (Wang et al., 2011b). WRKY40 was found to be a negative regulator during basal immunity whereas a positive regulator during AvrRpt2-induced ETI (Seyfferth, 2016). Additionally, *WRKY47* was found to be in group of induced *WRKY*s upon 1 or 2 h after flg22 treatment based on gene expression (Birkenbihl et al., 2018). Consistently, I

found *WRKY47* gene expression was also induced from 2 h after flg22 treatment (Table S2A). However, WRKY47 protein level was similar to that of control at 2 h unlike induced WRKYs after flg22 treatment (Birkenbihl et al., 2018), possibly due to a delay in protein synthesis. Based on pathogen growth assay and its proposed role as induced WRKYs, WRKY47 may function as a positive regulator during flg22-induced PTI.

On comparing protein and gene expression patterns for the proteins showing quantitative change, I found a positive correlation with the transcriptome data. Since the transcriptome and proteome data were generated independently, a positive correlation between transcriptome and proteome data shows that protein responses are not random and indicates a high accuracy of both omics datasets (Figure 6C, Table 7). A comparative proteome-transcriptome study investigating high temperature stress response in yeast during ethanol fermentation found a relatively high correlation (R=0.5593-0.7080) between DEPs and differentially expressed genes (DEGs) showing same expression trends (Li et al., 2019b). Similar, overall correlation between proteome and transcriptome changes (R=0.41) were also observed in *A. thaliana* upon elf18 treatment (Xu et al., 2017). Consistently, I observed that 3 h proteome is similar to transcriptome at 2 h (R^2 = 0.76/.55 for nuclear/total proteome, respectively) and, 9 h proteome is similar to transcriptome at previous time points, which is consistent with the central dogma (Figure 6C, Table 7). This suggests that proteome changes mirrors transcriptome changes at 3 and 9 h and transcriptome independent protein abundance changes may be more prevalent in early time points. Nevertheless, it is known that the dynamics of mRNA and protein synthesis can have large variations which must be considered while comparing proteome and transcriptome correlations (Lee et al., 2011; Liu et al., 2016). For instance, a delay in mRNA to protein synthesis was observed in fission yeast during oxidative stress and during life cycle transition in *Plasmodium falciparum* (Lackner et al., 2012; Roch et al., 2004). Such delay between mRNA expression to protein synthesis can be as long as 12 h for certain proteins, for example Trafd1, as reported in mouse dendritic cells upon LPS treatment (Jovanovic et al., 2015). Thus, in order to compare proteome and transcriptome a more targeted approach considering specific proteins and delay in protein synthesis may give us further insights into dependency of proteome on transcriptional changes.

3.3 Nuclear proteins dynamics at very early time points

From 3 h and 9 h time points, I identified WRKY47 as a positive regulator of immunity. In addition, I identified NADK1, PCRK1, TOE1, and MKP1, as potential regulators of flg22-

mediated responses in the nucleus. Nevertheless, still earlier time points can provide information about protein dynamics independent of transcriptional changes.

A hypothesis for flg22 induced quick and massive transcriptional reprograming is via de-repression of transcription. At the basal state, transcription of flg22 responsive genes are suppressed by negative regulator(s) and upon flg22 perception, transcription is de-repressed via removal or inactivation of such negative regulator(s). Previous studies found an overlapping transcriptional response upon flg22 and CHX treatment which suggests that de-repression could be a mechanism to induce transcriptional reprograming (Navarro et al., 2004; Jacob et al., 2017). Therefore, it was proposed that translation of negative regulator(s) which are high turnover proteins was inhibited by CHX, which leads to reduced accumulation of negative regulator(s), resulting in activation of flg22-induced transcriptional response. By comparing transcriptome responses to flg22 (Winkelmüller, 2018) and CHX treatments available in public databases (Goda et al., 2008; Drechsel et al., 2013), there was a substantial overlap between genes upregulated 1 h after flg22 treatment and 3 h and/or 4 h after CHX treatment (Figure S5). Consistently, I found expression of flg22 marker genes, *PROPEP3* and *WRKY30*, were upregulated by flg22 and CHX treatment (Figure 7). Similar to CHX, anisomycin also induced both genes. Puromycin, however, induced only *WRKY30* but failed to significantly induce *PROPEP3* which might be due to slow mode of inhibition of puromycin or low concentration used. Puromycin and anisomysin inhibit eukaryotic translation via different mechanisms and they are structurally different from CHX, thus they would have different off target effect. All three inhibitors, however, could induce *PROPEP3* and *WRKY30* (although puromycin *failed* to significantly induce *PROPEP3*). Additionally, chloramphenicol, that specifically inhibits bacterial translation (Smith-Johannsen and Gibbs, 1972), neither induced *PROPEP3* nor *WRKY30*. Together these results suggest that upregulation of flg22-responsive genes is specific to cytosolic eukaryotic translation inhibition. Expression of same set of genes by flg22 and CHX raises several possibilities. For instance, flg22 inhibits translation, and therefore, CHX induces similar gene expression as flg22 treatment. Alternatively, flg22 does not inhibit translation but converges with CHX's mode of action at some point such as accumulation of negative regulators of flg22-responsive genes. To test whether flg22 inhibits global translation to induce early flg22-responsive genes ribosome foot printing can be used to identify genes whose translation is altered (Brar and Weissman, 2015). On the other hand, to test whether negative regulators are indeed high turnover proteins, we can monitor protein degradation rates via targeted approach such as CHX-chase assay or using a MS based approach by metabolic labelling such as SILAC(Eldeeb et al., 2019)

An overlapping transcriptional response upon flg22 and CHX treatment led me to test whether protein level also show similar trends. Therefore, I included CHX treatment for 60 min in my proteomics experiment for early time points that included 15, 30 and 60 min of flg22 treatment. However, unlike the similarity at transcriptome level, protein expression after flg22 and CHX treatment were dissimilar both in nuclear and total protein fractions (Figure 9B). The difference among transcriptome and proteome responses (overlapping gene expression and non-overlapping protein expression) suggests that flg22 and CHX treatments induce the same genes by different mechanisms, such as phosphorylation of initiation factors, composition of ribosomal proteins, protein composition of the translational machinery and conformation of mRNAs (Merchante et al., 2017; Ding et al., 2014). Additionally, CHX mediated transcriptome response can be due to inhibition of protein synthesis of repressors, that are continuously degraded. Whereas flg22-mediated transcriptome response can be due to gene activators. Alternatively, due to differences in protein synthesis and gene expression dynamics as discussed above (Lee et al., 2011; Lackner et al., 2012; Jovanovic et al., 2015), comparing a later time point after CHX treatment to an earlier time point after flg22-treatment may show some overlap at protein level.

One of the striking features of nuclear protein dynamics upon flg22 treatment during early time points is downregulation of proteins in the nuclear fraction at 15 min. Out of 97 DEPs detected in the nuclear fraction at 15 min, 79 proteins were downregulated (Figure 9A). I observed this downregulation exclusively in the nuclear fraction at 15 min. This suggests that at least artifacts coming from technical issues during nuclear fractionation can be excluded as the downregulation was specific to 15 min nuclear sample. This downregulation of proteins, which may be negative regulators, detected in the nuclear fraction may precede transcriptional reprograming. Recently, in budding yeast global translation inhibition, using translational inhibitors like CHX, was found to de-repress ribosome biogenesis genes (Cheng and Brar, 2019). Interestingly, in human cell lines global translational downregulation (reduced by 65%) resulted in phosphorylation and activation of a MAPKKK-TAK1-D, that can phosphorylate downstream targets like MKK4 and MKK3/6 triggering activation of p38 MAPK and stress activated protein kinase (SAPK)/Jun amino-terminal kinases (JNK) (Cheng and Brar, 2019). However, in plants effects of global translational inhibition on immunity is yet unknown. Nevertheless, examples of removal of negative regulators for transcriptional induction is known. For instance, degradation of jasmonate ZIM-domain (JAZ), a negative regulator of jasmonate (JA) signaling, upon perception of jasmonoyl-isoleucine (JA-Ile) alleviates the TF

MYC2 from repression enabling MYC2 to regulate expression of early JA-responsive genes (Tsuda and Somssich, 2015).

Among the flg22 induced downregulated proteins in the nuclear fraction at 15 min, I found GO terms enriched for "photosynthesis", and photosynthesis related processes. This observation was similar to a previous study in *A. thaliana* that found downregulation of photosynthetic related GO terms in down regulated genes at translational level during AvrRpm1 induced ETI response and in downregulated genes during coronatine (COR) treatment (Meteignier et al., 2017; Attaran et al., 2014). In the same study, Attaran et al. 2014 found that although a global repression of photosynthetic genes was observed they didn't detect decrease in photosynthetic efficiency. Degradation of photosynthesis related proteins alters the redox state of a cell which are critical signaling cues (Pierella Karlusich et al., 2017; Su et al., 2018). Similarly, downregulation of photosynthesis related proteins very early might serve as signaling cues for transcriptional reprograming during PTI.

4. Materials and Methods

4.1 Materials

4.1.1 Plant Materials

Arabidopsis thaliana accession Col-0 was used as the wild type (WT) and *wrky47* mutant used was in the same background. Transient expression assay was performed in *Nicotiana benthamiana* (*N.benthamiana*).

Mutant	**Gene locus**	**Cause of mutation**	**Accession**	**Reference**
wrky47	AT4G01720	T-DNA	Col-0	Alonso et al., 2003

4.1.2 Bacterial Material

Bacteria	**Strain**	**Resistance**	**Purpose**
Pseudomonas syringae pv. t*omato* DC3000 (*Pto* DC3000)	*Pto* DC3000/pLAFR	Rifampicin and Tetracycline	pathogen assay
Escherichia coli (*E. coli*)	DH10B		competent cells
Agrobacterium tumefaciens (*A. tumefaciens*)	Gv31010 pMP90	Rifampicin and Gentamycin	competent cells

4.1.3 Primers

Locus	**Plant**	**Forward sequence**	**Reverse sequence**
ACTIN2	*A.thaliana*	TAAGGTCGTTGCACCACCTG	GCTGGAATGTGCTGAGGGAA
PROPEP3	*A.thaliana*	CTTGCGATCTTTCGTCATCA	GTTCTTCCCTCTCGCTTTGA
WRKY30	*A.thaliana*	GCTGGACGATGGATTCAGTT	AGTGGCTTCACATCCTTGAGA

4.1.4 Chemicals

Chemical	**Working Concentration**	**Company**
Flg22	5µM in sterile water	ZBiolab Inc. (Westfield USA)
TritonX-100	10% in sterile water	Sigma-aldrich, USA
EvaGreen DNA Dye	5 % in RT-qPCR mix	Biotium (Hayward, USA)
Percoll	100 %	Sigma-aldrich, USA

Antibody	**Working Concentration**	**Company**
Anti-GFP	1:2500	Abcam (Cambridge; UK)
Anti-cFBPase	1:5000	Agrisera (Sweden)
Anti-IDH	1:5000	Agrisera (Sweden)
Anti-CNX1/2	1:2500	Agrisera (Sweden)
Anti-RbCl	1:10000	Agrisera (Sweden)
Anti-LHC	1:5000	Agrisera (Sweden)
Anti-H3	1:5000	Agrisera (Sweden)
Anti-Rabbit IgG	1:10000	Sigma-Aldrich (Steinheim; Germany)

Anti-Mouse Ig HP	1:10000	GE Healthcare (Freiburg; Germany)

Kit/Enzyme	**Purpose**	**Company**
peqGOLD TriFast™	RNA Extraction	Peqlab, Darmstadt
Super signal west/femto maximum sensitivity substrates	Detection system for Immunoblotting	Thermo Scientific (Darmstadt; Germany)
SuperScript II Reverse Transcriptase	cDNA synthesis	Thermo Fischer Scientific (USA)

4.1.5 Media and solutions

Name	**Contents**
½ Murashige & Skoog (MS) (pH 5.8)	2.45g/l MS medium with vitamins and MES buffer
	1% (w/v) sucrose
	0.5% (w/v) plant agar
Sterilizing bleach solution	1.5 % (v/v) NaClO
	0.02 % (v/v) Triton X-100
King's B (KB) (pH 6.9)	10 g/l bacto Proteose peptone No. 3
	15 g/l Glycerol
	1.5 g/l K_2HPO_4
	15 g/l bacto agar
	After autoclaving: 5 ml/l sterile 1 M $MgSO_4$
Luria-Bertani (LB) (pH 7.0)	1 % (w/v) tryptone
	1 % (w/v) NaCl
	0.5 % (w/v) yeast extract
	1.5 % (w/v) agar
DNA extraction buffer	50 mM Tris-HCl
	200 mM NaCl
	0.2 mM EDTA
	0.5 % SDS
	100 µg/ml of Proteinase K (freshly added)
RNA precipitation solution	1.2 M NaCl
	0.8 M trisodium citrate
cDNA precipitation solution	50 µl of 100% ethanol in total 52 µl solution
	2 µl of 3M sodium acetate in total 52 µl solution
10 % APS	1 g APS
	10 ml H2O
Electrophorese buffer (10x)	250 mM tris-HCl (pH 8.3)
	1.92 M glycin
	1 % (w/v) SDS
Ponceau staining solution	5 % (v/v) acetic acid
	1 % (w/v) Ponceau S
PCR buffer (10x) (pH 8.8)	200 mM Tris-HCl
	100 mM KCl
	100 mM $(NH_4)_2$ SO_4
	20 mM $MgCl_2$
	10% Triton X-100
SDS-PAGE running buffer	192 mM glycin
	25 mM tris-HCl (pH 8.3)
	0.1 % (w/v) SDS
Separating gel buffer	1.5 M tris-HCl (pH 6.8)
	0.3 % (w/v) SDS
Stacking gel buffer	0.5 M tris-HCl (pH 6.8)
	0.3 % (w/v) SDS
TBST-T	20 mM tris-HCl (pH 7.6)

	137 mM NaCl
	0.05 % (v/v) Tween-20
TE	1 mM EDTA pH 8.0
	10 mM tris-HCl pH 7.4
Transfer (blotting) buffer	25 mM tris-HCl (pH 8.0)
	192 mM glycin
	0.1 % (v/v) SDS
	20 % (w/v) methanol

4.2 Methods

4.2.1 Plant growth on soil

A. thaliana Col-0 seeds were stratified for 3-4 days at 4 °C in water in the dark. The seeds were sown onto commercial soil (Stender, Schermbeck Germany) in 9 X 9 pots. Seedlings were separated into fresh soil after 12-14 days and growing was continued for 2-3 weeks (10 h light/ 14 h darkness, 23/20 °C, 60 % humidity). 4-5-week-old plants were transferred to long day chamber 2 days prior to the experiments (12 h light/ 12 h darkness, 22 °C, 54/58 % humidity). For infection, soil-grown-plants were transferred to another chamber at 22 °C with a 12 h photoperiod and 60 % relative humidity three days before bacterial inoculation.

4.2.2 Plant growth on ½ MS-plate

For seedlings seeds were sterilized by shaking in 2 ml of a bleach solution for 10 min. Then, seeds were washed 5 times with sterile water and stratified in sterile water for 3-4 days. Sterilized seeds were diluted in 0.1 % (w/v) plant agar. The seeds were transferred onto ½ MS agar plates using a 1 ml filter tip (equal distance between seeds) and grown in Percival growth chamber (CU-36LX5D, Percival, USA) at 22 °C, 10 h L/D for eleven days. Eleven-day-old seedlings were transferred to liquid ½ MS-Medium (same composition as MS-Agar) one day before treatment.

4.2.3 Bacterial growth

Pto DC3000 was grown on King'B (KB) media for two days at 28°C. Before use bacteria were transferred to liquid KB medium and incubated overnight at 28°C and 200 rpm until they reached an OD600 between 0.8 and 1. *E. coli* were grown on LB media at 37°C and 190 rpm with antibiotics. *A. tumefaciens* were grown on YEB media for two days at 28°C or in liquid YEB media 16-20 h at 28°C and 200 rpm with antibiotics.

4.2.4 Chemical treatment

11-day-old seedlings were transferred from ½ MS-Agar to 24-well plates each with 1.6 ml of ½ MS-Medium 24 h prior to treatments. 10-12 seedlings per sample were transferred to each well. For the flg22 and cycloheximide (synthetic) treatments, ½ MS-Medium was removed and replenished with 1600 µl of 1 µM flg22 or 100 µM cycloheximide prepared in ½ MS-Medium was added to the medium containing the seedlings. Six wells were combined for one replicate to reduce experimental variance and were used immediately for nuclear protein isolation. One seedling from each of the six well were harvested in liquid nitrogen at indicated time points for preparation of total protein. The samples were stored at –80°C until use.

For qPCR experiments 5-10 seedlings per well were used. The antibiotics cycloheximide (both microbial and synthetic), puromycin, anisomycin and chloramphenicol were added in concentrations of 100 µM, 200 µM, 100 µM and 100 µM respectively similar to above. Three wells were combined for one sample to reduce experimental variance when the seedlings were harvested in liquid nitrogen at indicated time points. The samples were stored at –80°C until use.

4.2.5 RNA isolation, cDNA synthesis, RT-qPCR, and statistical analysis

Seedling samples were ground in 2 mL Eppendorf tubes with 4 metal. The grounded materials were mixed with 0.5 ml TRIfast for seedlings, or 1 ml TRIfast for leaves, by vortexing. Chloroform (one fifth volume of added TRIfast) was added to the mixture and centrifuged for 15 min at 14,000 rpm at 4 °C. The supernatant was transferred into a new 1.5 ml tube, isopropanol was added (same volume as the supernatant), and incubated 10 min at room temperature followed by centrifugation for 15 min at 14,000 rpm at 4 °C. The pellet was suspended in 200 µl of nuclease free water, mixed with 100 µl of RNA precipitation solution, 100 µl of isopropanol, and incubated for 10 min at RT. The RNA pellet was collected by centrifugation for 15 min at 14000 rpm at 4 °C, washed with 400 µl of 75 % ethanol and centrifuged again for 2 min at 12000 rpm at room temperature. The pellet was dried and suspended in 50 µl of nuclease free water. RNA concentration was measured by NanoDrop photometer (PeqLab, Erlangen, Germany).

SuperScript II reverse transcriptase (Invitrogen, Thermo Fisher Scientific; USA) was used for cDNA synthesis. The mixture was heated up by PCR thermocycler and then synthesized cDNA was precipitated by cDNA precipitation solution. The cDNA was collected by

centrifugation for 20 min at 14000 rpm at room temperature, the pellet was washed with 75% ethanol, and centrifuged for 5 min at 14000 rpm at room temperature. The supernatant was removed and the pellet was dried for 5 min. The cDNA pellet was suspended in 200 µl of nuclease free water.

Reaction mix for cDNA synthesis:

50 µM oligo dT20	1 µl
10 mM each dNTP mix	1 µl
250 ng/µl RNA	11 µl
0.1 M DDT	2 µl
5XFirst-strand buffer	4 µl
SuperScript II reverse transcriptase	1 µl

RT-qPCR was performed on a CFX Connect Real-Time PCR Detection System (Biorad, USA) using the following reaction mix and program. The target gene was quantified relative to the expression of *A. thaliana ACTIN2* (*ACT2*). The ΔCt values were calculated by subtracting the Ct-value of the target gene from Ct-value of *ACT2*. The ΔCt values were used for further statistical analysis.

Reaction mix for RT-qPCR:

cDNA	4 µl
2.5 µM Primer forward	2 µl
2.5 µM Primer reverse	2 µl
10x PCR buffer	2.5 µl
10 mM dNTP	0.5 µl
Eva Green Dye	1.25 µl
Homemade Taq polymerase	0.5 µl
Sterile water	12.25 µl

Programm for RT-qPCR:

Initial Denaturation	95 °C	3 min	
Denaturation	95 °C	15 sec	40 cycles
Annealing	60 °C	30 sec	
Elongation	72 °C	30 sec	
Final Elongation	55 °C	1 min	

The following models were fit to the relative Ct values compared to *ACT2*: Ctgyr = GYgy+Rr+egyr, where GY, genotype:treatment interaction, and random factors; R, biological replicate; e, residual; Ctytr = YTyt+Rr+eytr, where YT, treatment:time interaction; Ctgytr =

GYTgyt+Rr+egytr, where GYT, genotype:treatment:time interaction. The mean estimates of the fixed effects were used as the modelled relative Ct values, visualized as relative log_2 expression values, and compared by two-tailed *t*-test.

4.2.6 Bacterial growth assay

Bacterial growth assay was performed as in (Wang et al., 2018). Briefly, *Pto* DC3000 was grown in KB medium with 50 µg/ml rifampicin overnight. The bacteria were harvested, washed, and diluted to OD_{600} = 0.001 with sterile water. The bacterial suspension was syringe (needleless) infiltrated in 4-5-week old leaves. Three leaf discs (approximately $1cm^2$) collected was defined as a technical replicate and 4-independent plants were used in each experiment. The experiment was performed once with four-biological replicates.

Means and standard errors were calculated from one experiment with four-biological replicates using the mixed linear model in R. The following model was fit to the bacterial growth data; log10 CFUgyr = GYgy+Rr+egyr, where GY, genotype:treatment interaction, and random factors; R, biological replicate; e, residual. The mean estimates of the fixed effects were used as the modelled bacterial titers, and compared by two-tailed *t*-test.

4.2.7 Cloning and confocal microscopy

The construction of constructs and confocal microscopy was done as in Wang et al., 2019. Briefly, coding region of *WRKY47* fused with cYFP/n-YFP and expressed under under *A.thaliana* Ubiquitin-10 promoter (P_{UBQ10}). Bacterial transformation was done as in Seyferth, 2019. Briefly, electrocompetent *A. tumefaciens* cells (Gv3101 pMP90) were transformed with the above construct. Single *A. tumefaciens* colony was grown in selective YEB media overnight (28 °C; 200 rpm). The bacterial cells were harvested, cleaned and diluted to reach a final concentration of OD_{600} = 0.5. Bacterial suspension was syringe (needleless) infiltrated into abaxial *N. benthamiana* leaves. The plants were kept at RT for 2 d until confocal microscopy. Confocal microscopy was done with an LSM700 confocal microscopy (Zeiss Microscopy, Germany) at standard settings (Wang et al., 2019). The experiment was performed once with more than three-technical replicates.

4.2.8 Total and nuclear protein extraction

Total proteins were isolated from leaves of 4-5-week-old *A. thaliana* Col-0 plants or 12-days old seedlings. For total proteins isolation from mature plants 4 leaves per plant per pot

were harvested after flg22 or mock (water) treatment at indicated time points to reduce experimental variation. Samples were frozen in liquid nitrogen and leaf material was homogenized for 6 min using metal balls and a paint shaker. To this 100 µl of preheated SDT-lysis buffer at 95 °C was added and incubated at 95 °C for 5 min. The lysate was centrifuged at 16,000 g for 15 min at RT and supernatant was transferred to a fresh 1.5 ml Eppendorf tube to ensure separation of cell debris and leaf material from the protein containing supernatant. This step was repeated once more. The supernatant was stored at -80 °C until further use. For total protein isolation from seedlings 1-2 seedlings per well pooled from 6 well were used to reduce experimental variation. Samples were frozen in liquid nitrogen and protein extraction proceeded as in case discussed above.

Nuclear protein isolation was done freshly from leaves of 4-5 week old Col-0 plants or 12-days old seedlings. For nuclear protein isolation from mature plants 4 leaves per plant from four plants per pot pooled over four pots were used (64 leaves). In case of nuclear protein isolation from seedlings ~72 seedlings pooled over six well were used. Sample pooling was done to reduce experimental variation. Nuclear protein extraction was done using following steps:

1) 10 ml 1X NEB buffer was used per sample. Initially chopped with razor blades using 5 ml NEB buffer for leaves and 2 ml NEB buffer for seedlings to achieve a slurry. The plant materials were chopped for 5 min on ice.
2) The homogenate was filtered twice through Miracloth (Calbiochem, catalogue no. 475855-1R). First filtration using single layer and second filtration using double layers of Miracloth into a 50 ml falcon tube. The filtrate was topped up to 10 ml with 1X NEB buffer.
3) Percoll (Sigma Aldrich, catalogue no. P1644) solutions- 30 % and 80 % were prepared as described in step 11. Place 6 ml of 30 % Percoll in a round-bottom centrifugation tube (pre-cooled) and underlay with 6 ml of 80 % slowly using an automatic pipette in order to get a sharp interphase.
4) Load the homogenate (10 ml) on the 30 % - 80 % Percoll gradient prepared in the previous step. Centrifuge at 3400 rpm, for 30 min at 4 °C
5) Collect the layer at 30 % - 80 % interphase from the Percoll gradient using a 5 ml pipette. Collect up to 2 ml of interphase layer in a 15 ml falcon tube.
6) Top up the falcon up to 14 ml with 1X Gradient buffer containing 1 % TX-100 (final to achieve a final concentration of 0.85 %). Transfer the solution in a round bottom centrifugation tube (pre-cooled).

7) Underlay the solution in the centrifugation tube with 6 ml of 30 % Percoll solution. Centrifuge at 3400 rpm for 10 min at 4 °C. After centrifugation the nuclei settles at the bottom of the centrifugation tube. Carefully decant the supernatant so as not to lose the pellet.
8) Suspend the pellet in 1 ml 1X sample buffer and transfer in 2 ml Eppendorf tubes. Centrifuge gently at 1000 g for 10 min to pellet nuclei. Remove the supernatant.
9) Add preheated SDT buffer (50µl) to the pellet and incubate at 95 °C for 10 min. Centrifuge at maximum speed (13000 g) and collect supernatant.
10) Protein concertation was measured using the Pierce™ 660 nm Protein-assay (catalogue no.22660) kit as per manufacturer's protocol.
11) Following solutions were used for nuclear protein isolation:

Nuclear Extraction Buffer (NEB)

(1X)	**Stock**	**100ml (2X)**
Hexylene glycol (2 M)	7.8 M	51.28 ml
PIPES KOH pH 7 (20 mM)	0.4 M	10 ml
$MgCl_2$ (10 mM)	1 M	2 ml
2-mercaptoethanol (5 mM)	14.3 M	17.5 µl in 50 ml 1X
Distilled water		

Gradient Buffer (GB)

(1X)	**Stock**	**100ml (5X)**
Hexylene glycol (0.5 M)	7.8 M	32.05 ml
PIPES KOH pH 7 (5 mM)	0.4 M	6.25 ml
$MgCl_2$ (10 mM)	1 M	5 ml
2-mercaptoenathol (5 mM)	14.3 M	17.5 µl in 50 ml 1X

Percoll 80 % (30 ml)

GB 5X	6 ml
Percoll	24 ml

Percoll 30 % (30 ml)

GB 5X	6 ml
Percoll	9 ml

Distilled water	15 ml

Gradient 1X (1 % TX-100)

	12 ml per sample
GB 5X	10 ml
2-mercaptoenathol (5 mM)	17.5 µl
TX-100 (25 %)	2 ml
Distilled water	Top up to 50 ml

Additional details for stock solution preparations:

i. PIPES KOH 0.4 M (24.2 g PIPES KOH in 200 ml water),
ii. MgCl2 1 M (47.6 g / 500 ml)
iii. 25% TX-100 (2.5 ml TX-100 100 % + 7.5ml water)
iv. 5 M 2-mercaptoethanol (3.5 ml 2-mercaptoethanol (14.3 M stock) + 6.5 ml water)
v. Hexylene glycol 7.8 M (Sigma aldrich, catalogue no. 112100) - Molarity calculated from following information: d=0,925g/ml, MW=118.17g, Weight=500g)
vi. For LC-MS/MS analysis 10-30 µg protein was sent to the MS facility.
vii. SDT-lysis buffer (4 % (w/v) SDS, 100 mM Tris-HCl pH 7.6, 0.1 M DTT).

4.2.9 Immunoblotting, immunodetection, and Ponceau-staining

The extracted proteins were mixed with 1X protein loading dye (Biorad) and separated as per Laemmli, 1970 in 1 x SDS-PAGE running buffer using Mini-PROTEAN II cells apparatus (Bio-Rad). Proteins were first runned in a 4 % acrylamide stacking gel at 80 V for 30 min, followed by their separation in a 12.5 % acrylamide resolving gel according to their molecular weight at 120 V for 90 min.

Proteins were blotted from the gel onto a PVDF membrane at 100 V for 60 min using the Mini Trans-Blot system (Bio-Rad) filled with transfer (blotting) buffer and cooled with an ice-pack. Proteins on the membrane were saturated by an incubation with 5 % milk powder diluted in TBS-T for 60 min at RT while shaking. The blot was washed 3 times with TBS-T each time with 5 min shaking. First antibody was used (dilution in section 4.1.4) with 2.5 % milk/TBS-T and was incubated overnight at 4 °C (50 rpm). Next day, the primary antibody solution was completely removed, blot was washed 3 times with TBS-T each time with 5 min shaking, and incubated for 60 min at RT with the secondary antibody (dilution in section 4.1.4) with 2.5 % milk/TBS-T. Proteins were detected after a 5 min incubation with the SuperSignal™ West

Pico/Femto Maximum Sensitivity substrate (Thermo Fisher Scientific) using the ChemiDocTM MP system (Bio-Rad).

Equal protein loading was evaluated using Ponceau staining. The PVDF membrane was incubated with Ponceau staining solution for 5 min at RT while shaking. Staining solution was removed and the membrane was washed 3 times with TBS-T each time with 5 min shaking. The air-dried membrane was used to evaluate protein loading.

4.2.10 Mass spectrometry

Mass spectrometry was performed by the Protein Mass Spectrometry Service at Max Planck Institute for Plant Breeding Research, Cologne and the following method was made available by Dr. Sara Christina Stolze.

"Sample Preparation and fractionation: Proteins were digested using a filter aided sample preparation protocol (FASP) adapted from Wiśniewski et al., 2009. In brief, protein concentration was determined using Pierce 660nm Protein Assay and in case of total protein extract 50 µg were used, for nuclear extracts the protein amount was <50 µg, so the entire sample was processed. Next, 1/10 vol of 1M DTT (100 mM final) was added and samples were incubated for 5 min at 95 °C. Samples were then diluted with 8M urea in 0.1 M Tris/HCl pH-8.5 (UA) to a compatible detergent concentration (0.5% SDS, max.) and loaded onto filters (Sartorius, Vivacon 500, VN01H22, 30k Da cutoff) by centrifuging for 10 min at 14000 g. Samples were then washed with UA by centrifugation for 10 min at 14000 g and alkylated using 100 µL 55 mm chloracetamide in UA and incubation for 20 min in the dark, followed by centrifugation for 10 min at 14000 g. After washing 3x with UA, the filter was transferred to a new Eppendorf tube and 50 µL of LysC solution (stock: 0.5 µg/µL Lys-C (WAKO) in 50 mM NH4HCO3 (ABC), working solution: dilute with UA to an enzyme:protein ratio 1:100) was added and the sample was mixed and subsequently incubated for 3h at RT. Next, 300 µL of trypsine solution (stock: 1 µg/µL in 1 mM HCl, working solution: dilute with UA to an enzyme:protein ratio 1:100) was added, the sampes were mixed and incubated o/N at RT. After centrifugation, 50 µL of ABC were added and samples were centrifuged for 10 min at 14000 g, the flow through containing the peptides was acidified with TFA to 0.5% final concentration. The flow through was desalted using stage tips with C18 Empore disk membranes (3 M) (Rappsilber et al., 2003).

Next samples were submitted to SDB-RPS fractionation using a protocol adapted from (Borner and Fielding, 2014). In brief, stage tips were prepared with 2 layers of SDB-RPS membrane and activated with 100 µL acetonitrile, followed by equilibration with 100 µL equilibration buffer (30% (v/v) MeOH, 1% (v/v) TFA) and 100 µL 0.2% TFA. Next, peptides were immobilized on the membrane and washed with 100 µL 0.2% TFA. Peptides were then eluted into 3 consecutive fractions using SDB-RPS buffer 1 (100 mM NH4HCO2, 40% (v/v) ACN, 0.5% FA), SDB-RPS buffer 2 (150 mM NH4HCO2, 60% (v/v) ACN, 0.5% FA) and finally SDB-RPS buffer 3 (5% Ammonia (v/v), 80% (v/v) ACN). The collected fractions were evaporated to dryness to remove residual ammonia.

LC-MS/MS data acquisition: Dried peptides were re-dissolved in 2% ACN, 0.1% TFA for analysis and adjusted to a final concentration of 0.1 µg/µl. Samples were analysed using an EASY-nLC 1200 (Thermo Fisher) coupled to a Q Exactive Plus mass spectrometer (Thermo Fisher). Peptides were separated on 16 cm frit-less silica emitters (New Objective, 0.75 µm inner diameter), packed in-house with reversed-phase ReproSil-Pur C18 AQ 1.9 µm resin (Dr. Maisch). Peptides (0.5 µg) were loaded on the column and eluted for 115 min using a segmented linear gradient of 5% to 95% solvent B (0 min : 5%B; 0-5 min -> 5%B; 5-65 min -> 20%B; 65-90 min ->35%B; 90-100 min -> 55%; 100-105 min ->95%, 105-115 min ->95%) (solvent A 0% ACN, 0.1% FA; solvent B 80% ACN, 0.1%FA) at a flow rate of 300 nL/min. Mass spectra were acquired in data-dependent acquisition mode with a TOP15 method. MS spectra were acquired in the Orbitrap analyzer with a mass range of 300–1750 m/z at a resolution of 70,000 FWHM and a target value of 3×106 ions. Precursors were selected with an isolation window of 1.3 m/z. HCD fragmentation was performed at a normalized collision energy of 25. MS/MS spectra were acquired with a target value of 105 ions at a resolution of 17,500 FWHM, a maximum injection time (max.) of 55 ms and a fixed first mass of m/z 100. Peptides with a charge of +1, greater than 6, or with unassigned charge state were excluded from fragmentation for MS2, dynamic exclusion for 30s prevented repeated selection of precursors.

Data processing: Raw data were processed using MaxQuant software (version 1.5.7.4, http://www.maxquant.org/) (Cox and Mann, 2008) with label-free quantification (LFQ) and iBAQ enabled (Tyanova et al., 2016a). MS/MS spectra were searched by the Andromeda search engine against a combined database containing the sequences from *A.thaliana* (TAIR10_pep_20101214; ftp://ftp.arabidopsis.org/home/tair/Proteins/TAIR10_protein_lists/) and sequences of 248 common contaminant proteins and decoy sequences. Trypsin specificity was required and a maximum of two missed cleavages allowed. Minimal peptide length was

set to seven amino acids. Carbamidomethylation of cysteine residues was set as fixed, oxidation of methionine and protein N-terminal acetylation as variable modifications. Peptide-spectrum-matches and proteins were retained if they were below a false discovery rate of 1%."

4.2.11 Bioinformatic and statistical analysis of LC-MS/MS data

PERSEUS (version 1.5.2.6) (Tyanova et al., 2016b) was used to analyse the protein identification and quantification data from MaxQuant. The raw intensities were log_2-transformed for downstream analysis. To identify proteins showing significant change in abundance (flg22 vs mock or CHX vs mock), a two-sample *t*-test with a false discovery rate (FDR) of 0.05 was performed in PERSEUS. The resulting p-values were corrected for multiple testing by calculating the FDR (or q-value) using p.adjust function with Benjamini-Hochberg method in R. The GO-term enrichment analysis was performed using the BinGO plugin within the Cytoscape environment. A Hypergeometric test by Benjamini-Hochberg FDR correction for GO-enrichment was calculated in the BinGO plugin. As background a customized reference protein list was used which consisted of proteins that were detected at least twice in at least one condition (flg22 or mock and CHX or mock).

5. References

Afzal, A.J., da Cunha, L., and Mackey, D. (2011). Separable fragments and membrane tethering of Arabidopsis RIN4 regulate its suppression of PAMP-triggered immunity. Plant Cell **23**: 3798–3811.

Agler, M.T., Ruhe, J., Kroll, S., Morhenn, C., Kim, S.-T., Weigel, D., Kemen, E.M., and Waldor, M.K. (2016). Microbial Hub Taxa Link Host and Abiotic Factors to Plant Microbiome Variation. PLoS Biol. **14 (1)**: e1002352.

Albert, I., Hua, C., Nürnberger, T., Pruitt, R.N., and Zhang, L. (2020). Surface Sensor Systems in Plant Immunity. Plant Physiol. **182**: 1582–1596.

Ali, A., Alexandersson, E., Sandin, M., Resjö, S., Lenman, M., Hedley, P., Levander, F., and Andreasson, E. (2014). Quantitative proteomics and transcriptomics of potato in response to Phytophthora infestans in compatible and incompatible interactions. BMC Genomics **15**: 1–18.

Anderson, J.C., Bartels, S., Besteiro, M.A.G., Shahollari, B., Ulm, R., and Peck, S.C. (2011). Arabidopsis MAP Kinase Phosphatase 1 (AtMKP1) negatively regulates MPK6-mediated PAMP responses and resistance against bacteria. Plant J. **67**: 258–268.

Annunziato, A.T. (2008). DNA Packaging: Nucleosomes and Chromatin. Nat. Educ.: 1(1):26.

Attaran, E., Major, I.T., Cruz, J.A., Rosa, B.A., Koo, A.J.K., Chen, J., Kramer, D.M., He, S.Y., and Howe, G.A. (2014). Temporal dynamics of growth and photosynthesis suppression in response to jasmonate signaling. Plant Physiol. **165**: 1302–1314.

Bartels, S., Anderson, J.C., Gonza, M.A., Peck, S.C., Ulm, R., Buchala, A., and Me, J. (2009). MAP KINASE PHOSPHATASE1 and PROTEIN TYROSINE PHOSPHATASE1 Are Repressors of Salicylic Acid Synthesis and SNC1-Mediated Responses in Arabidopsis. Plant Cell **21**: 2884–2897.

Benn, G., Wang, C., Hicks, D.R., Stein, J., Guthrie, C., and Dehesh, K. (2014). A key general stress response motif is regulated non-uniformly by CAMTA transcription factors. Plant J. **80**: 82–92.

Benschop, J.J., Mohammed, S., O'Flaherty, M., Heck, A.J.R., Slijper, M., and Menke, F.L.H. (2007). Quantitative phosphoproteomics of early elicitor signaling in Arabidopsis. Mol. Cell. Proteomics **6**: 1198–1214.

Berens, M.L., Berry, H.M., Mine, A., Argueso, C.T., and Tsuda, K. (2017). Evolution of Hormone Signaling Networks in Plant Defense. Annu. Rev. Phytopathol. **55**: 18.1-18.25.

Bi, G., Zhou, Z., Wang, W., Li, L., Rao, S., Wu, Y., Zhang, X., Menke, F.L.H., Chen, S., and Zhou, J.-M. (2018). Receptor-like Cytoplasmic Kinases Directly Link Diverse Pattern Recognition Receptors to the Activation of Mitogen-activated Protein Kinase Cascades in Arabidopsis. Plant Cell **30**: 1543–1561.

Bigeard, J., Colcombet, J., and Hirt, H. (2015). Signaling mechanisms in pattern-triggered immunity (PTI). Mol. Plant **8**: 521–539.

Bigeard, J., Rayapuram, N., and Bonhomme, L. (2014). Proteomic and phosphoproteomic analyses of chromatin-associated proteins from Arabidopsis thaliana. Proteomics **14**: 1–51.

Birkenbihl, R.P., Kracher, B., Ross, A., Kramer, K., Finkemeier, I., and Somssich, I.E. (2018). Principles and characteristics of the Arabidopsis WRKY regulatory network during early MAMP-triggered immunity. Plant J.: 96: 487-502.

Birkenbihl, R.P., Liu, S., and Somssich, I.E. (2017). Transcriptional events defining plant immune responses. Curr. Opin. Plant Biol. **38**: 1–9.

Boller, T. and Felix, G. (2009). A renaissance of elicitors: perception of microbe-associated molecular patterns and danger signals by pattern-recognition receptors. Annu. Rev. Plant Biol. **60**: 379–406.

Borner, G.H.H. and Fielding, A.B. (2014). Using in-solution digestion, peptide fractionation, and a q exactive mass spectrometer to analyze the proteome of clathrin-coated vesicles. Cold Spring Harb. Protoc. **2014**: 1192–1195.

Boudsocq, M., Willmann, M.R., McCormack, M., Lee, H., Shan, L., He, P., Bush, J., Cheng, S.H., and Sheen, J. (2010). Differential innate immune signalling via Ca 2+ sensor protein kinases. Nature **464**: 418–422.

Brar, G.A. and Weissman, J.S. (2015). Ribosome profiling reveals the what, when, where and how of protein synthesis. Nat. Rev. Mol. Cell Biol. **16**: 651–664.

Bredow, M. and Monaghan, J. (2019). Regulation of plant immune signaling by calcium-dependent protein kinases. Mol. Plant-Microbe Interact. **32**: 6–19.

Burgess, M.W., Keshishian, H., Mani, D.R., Gillette, M.A., and Carr, S.A. (2014). Simplified and Efficient Quantification of Low-abundance Proteins at Very High Multiplex via Targeted Mass Spectrometry. Mol. Cell. Proteomics **13**: 1137–1149.

Cao, Y., Aceti, D.J., Sabat, G., Song, J., Makino, S. ichi, Fox, B.G., and Bent, A.F. (2013). Mutations in FLS2 Ser-938 Dissect Signaling Activation in FLS2-Mediated Arabidopsis Immunity. PLoS Pathog. **9**: e1003313.

Cao, Y., Liang, Y., Tanaka, K., Nguyen, C.T., Jedrzejczak, R.P., Joachimiak, A., and Stacey, G. (2014). The kinase LYK5 is a major chitin receptor in Arabidopsis and forms a chitin-induced complex with related kinase CERK1. Elife **3**: e03766.

Caplan, J.L., Kumar, A.S., Park, E., Padmanabhan, M.S., Hoban, K., Modla, S., Czymmek, K., and Dinesh-Kumar, S.P. (2015). Chloroplast Stromules Function during Innate Immunity. Dev. Cell **34**: 45–57.

Caplan, J.L., Mamillapalli, P., Burch-Smith, T.M., Czymmek, K., and Dinesh-Kumar, S.P. (2008). Chloroplastic Protein NRIP1 Mediates Innate Immune Receptor Recognition of a Viral Effector. Cell **132**: 449–462.

Capoen, W., Sun, J., Wysham, D., Otegui, M.S., Venkateshwaran, M., Hirsch, S., Miwa, H., Downie, J.A., Morris, R.J., Ané, J.M., and Oldroyd, G.E.D. (2011). Nuclear membranes control symbiotic calcium signaling of legumes. Proc. Natl. Acad. Sci. U. S. A. **108**: 14348–14353.

Charpentier, M. (2018). Calcium signals in the plant nucleus: Origin and function. J. Exp. Bot. **69**: 4165–4173.

Chen, T. et al. (2020). A plant genetic network for preventing dysbiosis in the phyllosphere. Nature **580**: 653–657.

Cheng, F.Y., Blackburn, K., Lin, Y.M., Goshe, M.B., and Williamson, J.D. (2009).

Absolute protein quantification by LC/MS e for global analysis of salicylic acid-induced plant protein secretion responses. J. Proteome Res. **8**: 82–93.

Cheng, Z. and Brar, G.A. (2019). Global translation inhibition yields condition-dependent de-repression of ribosome biogenesis mRNAs. Nucleic Acids Res. **47**: 5061–5073.

Chinchilla, D., Zipfel, C., Robatzek, S., Kemmerling, B., Nürnberger, T., Jones, J.D.G., Felix, G., and Boller, T. (2007). A flagellin-induced complex of the receptor FLS2 and BAK1 initiates plant defence. Nature **448**: 497–500.

Cook, D.E., Mesarich, C.H., and Thomma, B.P.H.J. (2015). Understanding Plant Immunity as a Surveillance System to Detect Invasion. Annu. Rev. Phytopathol **53**: 541–63.

Couto, D. and Zipfel, C. (2016). Regulation of pattern recognition receptor signalling in plants. Nat. Rev. Immunol. **16**: 537–552.

Cox, J. and Mann, M. (2008). MaxQuant enables high peptide identification rates, individualized p.p.b.-range mass accuracies and proteome-wide protein quantification. Nat. Biotechnol. **26**: 1367.

Cui, H., Tsuda, K., and Parker, J.E. (2015). Effector-Triggered Immunity: From Pathogen Perception to Robust Defense. Annu. Rev. Plant Biol. **66**: 487–511.

Delormel, T.Y. and Boudsocq, M. (2019). Tansley review Properties and functions of calcium-dependent protein kinases and their relatives in Arabidopsis thaliana. New Phytol. **224**: 585–604.

Denoux, C., Galletti, R., Mammarella, N., Gopalan, S., Werck, D., De Lorenzo, G., Ferrari, S., Ausubel, F.M., and Dewdney, J. (2008). Activation of defense response pathways by OGs and Flg22 elicitors in Arabidopsis seedlings. Mol. Plant **1**: 423–445.

Ding, Y., Tang, Y., Kwok, C.K., Zhang, Y., Bevilacqua, P.C., and Assmann, S.M. (2014). In vivo genome-wide profiling of RNA secondary structure reveals novel regulatory features. Nature **505**: 696–700.

Djamei, A., Pitzschke, A., Nakagami, H., Rajh, I., and Hirt, H. (2007). Trojan Horse Strategy in Agrobacterium Transformation: Abusing MAPK Defense Signaling. Science. **453**: 453–457.

Drechsel, G., Kahles, A., Kesarwani, A.K., Stauffer, E., Behr, J., Drewe, P., Rätsch, G., and Wachter, A. (2013). Nonsense-mediated decay of alternative precursor mRNA splicing variants is a major determinant of the Arabidopsis steady state transcriptome. Plant Cell **25**: 3726–42.

Du, L., Ali, G.S., Simons, K.A., Hou, J., Yang, T., Reddy, A.S.N., and Poovaiah, B.W. (2009). Ca2+/calmodulin regulates salicylic-acid-mediated plant immunity. Nature **457**: 1154–1158.

Dubiella, U., Seybold, H., Durian, G., Komander, E., Lassig, R., Witte, C.P., Schulze, W.X., and Romeis, T. (2013). Calcium-dependent protein kinase/NADPH oxidase activation circuit is required for rapid defense signal propagation. Proc. Natl. Acad. Sci. U. S. A. **110**: 8744–8749.

Dunkley, T.P.J. et al. (2006). Mapping the Arabidopsis organelle proteome. Proc. Natl. Acad. Sci. U. S. A. **103**: 6518–23.

Eldeeb, M.A., Siva-Piragasam, R., Ragheb, M.A., Esmaili, M., Salla, M., and Fahlman,

R.P. (2019). A molecular toolbox for studying protein degradation in mammalian cells. J. Neurochem. **151**: 520–533.

Erbs, G. and Newman, M.A. (2012). The role of lipopolysaccharide and peptidoglycan, two glycosylated bacterial microbe-associated molecular patterns (MAMPs), in plant innate immunity. Mol. Plant Pathol. **13**: 95–104.

Eulgem, T., Rushton, P.J., Robatzek, S., and Somssich, I.E. (2000). The WRKY superfamily of plant transcription factors. Trends Plant Sci. **5**: 199–206.

Fakih, Z., Ahmed, M.B., Letanneur, C., and Germain, H. (2016). An unbiased nuclear proteomics approach reveals novel nuclear protein components that participates in MAMP-triggered immunity. Plant Signal. Behav. **11**: e1183087.

Felix, G., Duran, J.D., Volko, S., and Boller, T. (1999). Plants have a sensitive perception system for the most conserved domain of bacterial flagellin. Plant J. **18**: 265–276.

Feng, Y., Kang, J.S., Kim, S., Yun, D.J., Lee, S.Y., Bahk, J.D., and Koiwa, H. (2010). Arabidopsis SCP1-like small phosphatases differentially dephosphorylate RNA polymerase II C-terminal domain. Biochem. Biophys. Res. Commun. **397**: 355–360.

Fitzpatrick, C.R., Salas-González, I., Conway, J.M., Finkel, O.M., Gilbert, S., Russ, D., Teixeira, P.J.P.L., and Dangl, J.L. (2020). The Plant Microbiome: From Ecology to Reductionism and Beyond. Annu. Rev. Microbiol. **74**: 81–100.

Folta, K.M. and Kaufman, L.S. (2007). Isolation of Arabidopsis nuclei and measurement of gene transcription rates using nuclear run-on assays. Nat. Protoc. **1**: 3094–3100.

Franceschini, A. (2015). STRINGdb Package Vignette.: 1–13.

Frei dit Frey, N. et al. (2014). Functional analysis of Arabidopsis immune-related MAPKs uncovers a role for MPK3 as negative regulator of inducible defences. Genome Biol. **15**: R87.

Fröhlich, A., Gaupels, F., Sarioglu, H., Holzmeister, C., Spannagl, M., Durner, J., and Lindermayr, C. (2012). Looking deep Inside: Detection of low-abundance proteins in leaf extracts of Arabidopsis and phloem exudates of pumpkin. Plant Physiol. **159**: 902–914.

Galletti, R., Ferrari, S., and de Lorenzo, G. (2011). Arabidopsis MPK3 and MPK6 play different roles in basal and oligogalacturonide-or flagellin-induced resistance against Botrytis cinerea. Plant Physiol. **157**: 804–814.

Gao, M., Wang, X., Wang, D., Xu, F., Ding, X., Zhang, Z., Bi, D., Cheng, Y.T., Chen, S., Li, X., and Zhang, Y. (2009). Regulation of Cell Death and Innate Immunity by Two Receptor-like Kinases in Arabidopsis. Cell Host Microbe **6**: 34–44.

Goda, H. et al. (2008). The AtGenExpress hormone and chemical treatment data set: Experimental design, data evaluation, model data analysis and data access. Plant J. **55**: 526–542.

Gómez-Gómez, L. and Boller, T. (2000). FLS2: An LRR receptor-like kinase involved in the perception of the bacterial elicitor flagellin in Arabidopsis. Mol. Cell **5**: 1003–1011.

Goslin, K., Eschen-Lippold, L., Naumann, C., Linster, E., Sorel, M., Klecker, M., de Marchi, R., Kind, A., Wirtz, M., Lee, J., Dissmeyer, N., and Graciet, E. (2019). Differential n-end rule degradation of RIN4/NOI fragments generated by the AvrRpt2

effector protease. Plant Physiol. **180**: 2272–2289.

Goto, C., Hashizume, S., Fukao, Y., Hara-Nishimura, I., and Tamura, K. (2019). Comprehensive nuclear proteome of Arabidopsis obtained by sequential extraction. Nucleus **10**: 81–92.

Gronnier, J., Franck, C.M., Stegmann, M., DeFalco, T.A., Cifuentes, A.A., Dünser, K., Lin, W., Yang, Z., Kleine-Vehn, J., Ringli, C., and Zipfel, C. (2020). FERONIA regulates FLS2 plasma membrane nanoscale dynamics to modulate plant immune signaling. bioRxiv: 2020.07.20.212233.

Guan-Zhu, H. (2018). Origin and evolution of the plant immune system. New Phytol. **222**: 70–83.

Guerra, T., Schilling, S., Hake, K., Gorzolka, K., Sylvester, F.P., Conrads, B., Westermann, B., and Romeis, T. (2020). Calcium-dependent protein kinase 5 links calcium signaling with N-hydroxy-l-pipecolic acid- and SARD1-dependent immune memory in systemic acquired resistance. New Phytol. **225**: 310–325.

Gust, A.A., Biswas, R., Lenz, H.D., Rauhut, T., Ranf, S., Kemmerling, B., Götz, F., Glawischnig, E., Lee, J., Felix, G., and Nürnberger, T. (2007). Bacteria-derived peptidoglycans constitute pathogen-associated molecular patterns triggering innate immunity in Arabidopsis. J. Biol. Chem. **282**: 32338–32348.

Gust, A.A., Pruitt, R., and Nürnberger, T. (2017). Sensing Danger : Key to Activating Plant Immunity. Trends Plant Sci. **22**: 779–791.

Hacquard, S., Spaepen, S., Garrido-Oter, R., and Schulze-Lefert, P. (2017). Interplay Between Innate Immunity and the Plant Microbiota INTRODUCTION TO THE PLANT MICROBIOTA. Annu. Rev. Phytopathol **55**: 565–89.

Hajheidari, M., Koncz, C., and Eick, D. (2013). Emerging roles for RNA polymerase II CTD in Arabidopsis. Trends Plant Sci. **18**: 633–643.

Halter, T. et al. (2014). The leucine-rich repeat receptor kinase BIR2 is a negative regulator of BAK1 in plant immunity. Curr. Biol. **24**: 134–143.

Hashida, S.N. and Kawai-Yamada, M. (2019). Inter-Organelle NAD Metabolism Underpinning Light Responsive NADP Dynamics in Plants. Front. Plant Sci. **10**: 960.

Heier, C.R. and Didonato, C.J. (2009). Translational readthrough by the aminoglycoside geneticin (G418) modulates SMN stability in vitro and improves motor function in SMA mice in vivo. Hum. Mol. Genet. **18**: 1310–1322.

Hillmer, R.A., Tsuda, K., Rallapalli, G., Asai, S., Truman, W., Papke, M.D., Sakakibara, H., Jones, J.D.G., Myers, C.L., and Katagiri, F. (2017). The highly buffered Arabidopsis immune signaling network conceals the functions of its components. PLoS Genet. **13**: e1006639.

Hind, S.R. et al. (2016). Tomato receptor FLAGELLIN-SENSING 3 binds flgII-28 and activates the plant immune system. Nat. Plants **2**: 1–8.

Hooper, C.M., Castleden, I.R., Tanz, S.K., Aryamanesh, N., and Millar, A.H. (2017). SUBA4: The interactive data analysis centre for Arabidopsis subcellular protein locations. Nucleic Acids Res. **45**: D1064–D1074.

Horsefield, S. et al. (2019). NAD+ cleavage activity by animal and plant TIR domains in cell

death pathways. Science. **365**: 793–799.

Howden, A.J.M., Stam, R., Heredia, V.M., Motion, G.B., Have, S., Hodge, K., Marques, T.M., Amaro, M., and Huitema, E. (2017). Quantitative analysis of the tomato nuclear proteome during Phytophthora capsici infection unveils regulators of immunity. New Phytol. **215**: 309–322.

Hsu, F., Chou, M., Chou, S., Li, Y., Peng, H., and Shih, M. (2013). Submergence Confers Immunity Mediated by the WRKY22 Transcription Factor in Arabidopsis. Plant Cell **25**: 2699–2713.

Imkampe, J. et al. (2017). The Arabidopsis Leucine-rich Repeat Receptor Kinase BIR3 Negatively Regulates BAK1 Receptor Complex Formation and Stabilizes BAK1. Plant Cell **29**: 2285–2303.

Itzhak, D.N., Tyanova, S., Cox, J., and Borner, G.H.H. (2016). Global, quantitative and dynamic mapping of protein subcellular localization. Elife **5**: e16950.

Jacob, F., Kracher, B., Mine, A., Seyfferth, C., Blanvillain-Baufumé, S., Parker, J.E., Tsuda, K., Schulze-Lefert, P., and Maekawa, T. (2017). A dominant-interfering camta3 mutation compromises primary transcriptional outputs mediated by both cell surface and intracellular immune receptors in Arabidopsis thaliana. New Phytol. **217**: 1667–1680.

Jaskiewicz, M., Conrath, U., and Peterha, C. (2011). Chromatin modification acts as a memory for systemic acquired resistance in the plant stress response. EMBO Rep. **12**: 50–55.

Ji, Y. and Guo, H. (2013). From Endoplasmic Reticulum (ER) to Nucleus : EIN2 Bridges the Gap in Ethylene Signaling. Mol. Plant **6**: 11–14.

Jiang, L., Anderson, J.C., Besteiro, M.A.G., and Peck, S.C. (2017). Phosphorylation of Arabidopsis MAP Kinase Phosphatase 1 (MKP1) Is Required for PAMP Responses and Resistance against Bacteria. Plant Physiol. **175**: 1839–1852.

Jin, J., Tian, F., Yang, D.-C., Meng, Y.-Q., Kong, L., Luo, J., and Gao, G. (2017). PlantTFDB 4.0: toward a central hub for transcription factors and regulatory interactions in plants. Nucleic Acids Res. **45**: D1040–D1045.

Jones, A.M.E., Thomas, V., Bennett, M.H., Mansfield, J., and Grant, M. (2006). Modifications to the arabidopsis defense proteome occur prior to significant transcriptional change in response to inoculation with Pseudomonas syringae. Plant Physiol. **142**: 1603–1620.

Jones, J.D.G. and Dangl, J.L. (2006). The plant immune system. Nature **444**: 323–329.

Jovanovic, M. et al. (2015). Dynamic profiling of the protein life cycle in response to pathogens. Science. **347**: 1259038.

Ju, C. et al. (2012). CTR1 phosphorylates the central regulator EIN2 to control ethylene hormone signaling from the ER membrane to the nucleus in Arabidopsis. Proc. Natl. Acad. Sci. U. S. A. **109**: 19486–19491.

Kadota, Y., Sklenar, J., Derbyshire, P., Stransfeld, L., Asai, S., Ntoukakis, V., Jones, J.D., Shirasu, K., Menke, F., Jones, A., and Zipfel, C. (2014). Direct Regulation of the NADPH Oxidase RBOHD by the PRR-Associated Kinase BIK1 during Plant Immunity. Mol. Cell **54**: 43–55.

Kaffamik, F.A.R., Jones, A.M.E., Rathjen, J.P., and Peck, S.C. (2009). Effector proteins of the bacterial pathogen Pseudomonas syringae alter the extracellular proteome of the host plant, Arabidopsis thaliana. Mol. Cell. Proteomics **8**: 145–156.

Karasov, T.L., Chae, E., Herman, J.J., and Bergelson, J. (2017). Mechanisms to Mitigate the Trade-Off between Growth and Defense. Plant Cell **29**: 666–680.

Kawai, S. and Murata, K. (2008). Structure and function of NAD kinase and NADP phosphatase: Key enzymes that regulate the intracellular balance of NAD(H) and NADP(H). Biosci. Biotechnol. Biochem. **72**: 919–930.

Kim, C.Y. and Zhang, S. (2004). Activation of a mitogen-activated protein kinase cascade induces WRKY family of transcription factors and defense genes in tobacco. Plant J. **38**: 142–151.

Kimura, S. et al. (2020). CRK2 and C-terminal Phosphorylation of NADPH Oxidase RBOHD Regulate Reactive Oxygen Species Production in Arabidopsis. Plant Cell **32**: 1063–1080.

Kong, Q., Sun, T., Qu, N., Ma, J., Li, M., Cheng, Y., Zhang, Q., Wu, D., and Zhang, Z. (2016). Two Redundant Receptor-Like Cytoplasmic Kinases Function Downstream of Pattern Recognition Receptors to Regulate Activation of SA Biosynthesis. Plant Physiol. **171**: 1344–1354.

Kourelis, J. and Hoorn, R.A.L. Van Der (2018). Defended to the Nines : 25 Years of Resistance Gene Cloning Identifies Nine Mechanisms for R Protein Function. Plant Cell **30**: 285–299.

Kouzai, Y., Nakajima, K., Hayafune, M., Ozawa, K., Kaku, H., Shibuya, N., Minami, E., and Nishizawa, Y. (2014). CEBiP is the major chitin oligomer-binding protein in rice and plays a main role in the perception of chitin oligomers. Plant Mol. Biol. **84**: 519–528.

Krahmer, N., Najafi, B., Schueder, F., Zeigerer, A., Heinz, G., Borner, H., Krahmer, N., Najafi, B., Schueder, F., Quagliarini, F., Steger, M., and Seitz, S. (2018). Reveal Subcellular Reorganization in Diet-Induced Hepatic Steatosis Organellar Proteomics and Phospho-Proteomics Reveal Subcellular Reorganization in Diet-Induced Hepatic Steatosis. Dev. Cell **47**: 205–221.

Kumar, A.S., Park, E., Nedo, A., Alqarni, A., Ren, L., Hoban, K., Modla, S., McDonald, J.H., Kambhamettu, C., Dinesh-Kumar, S.P., and Caplan, J.L. (2018). Stromule extension along microtubules coordinated with actin-mediated anchoring guides perinuclear chloroplast movement during innate immunity. Elife **7**: e23625.

Kunze, G., Zipfel, C., Robatzek, S., Niehaus, K., Boller, T., and Felix, G. (2004). The N Terminus of Bacterial Elongation Factor Tu Elicits Innate Immunity in Arabidopsis Plants. Plant Cell **16**: 3496–3507.

Kutschera, A. et al. (2019). Bacterial medium-chain 3-hydroxy fatty acid metabolites trigger immunity in Arabidopsis plants. Science. **364**: 178–181.

Lackner, D.H., Schmidt, M.W., Wu, S., Wolf, D.A., and Bähler, J. (2012). Regulation of transcriptome, translation, and proteome in response to environmental stress in fission yeast. Genome Biol. **13**.

Lal, N.K. et al. (2018). The Receptor-like Cytoplasmic Kinase BIK1 Localizes to the

Nucleus and Regulates Defense Hormone Expression during Plant Innate Immunity. Cell Host Microbe **23**: 485-497.e5.

Lassowskat, I., Böttcher, C., Eschen-Lippold, L., Scheel, D., and Lee, J. (2014). Sustained mitogen-activated protein kinase activation reprograms defense metabolism and phosphoprotein profile in Arabidopsis thaliana. Front. Plant Sci. **5**: 1–20.

Lee, M.V., Topper, S.E., Hubler, S.L., Hose, J., Wenger, C.D., Coon, J.J., and Gasch, A.P. (2011). A dynamic model of proteome changes reveals new roles for transcript alteration in yeast. Mol. Syst. Biol. **7**: 1–12.

Lewis, J.D., Lee, A.H.Y., Hassan, J.A., Wana, J., Hurleya, B., Jhingree, J.R., Wang, P.W., Lo, T., Youn, J.Y., Guttman, D.S., and Desveaux, D. (2013). The Arabidopsis ZED1 pseudokinase is required for ZAR1-mediated immunity induced by the Pseudomonas syringae type III effector HopZ1a. Proc. Natl. Acad. Sci. U. S. A. **110**: 18722–18727.

Lewis, L.A. et al. (2015). Transcriptional Dynamics Driving MAMP-Triggered Immunity and Pathogen Effector-Mediated Immunosuppression in Arabidopsis Leaves Following Infection with Pseudomonas syringae pv tomato DC3000. Plant Cell **27**: 3038–3064.

Li, B. et al. (2019a). The receptor-like kinase NIK1 targets FLS2/BAK1 immune complex and inversely modulates antiviral and antibacterial immunity. Nat. Commun. **10**: 1–14.

Li, B., Meng, X., Shan, L., and He, P. (2016). Transcriptional Regulation of Pattern-Triggered Immunity in Plants. Cell Host Microbe **19**: 641–650.

Li, L., Li, M., Yu, L., Zhou, Z., Liang, X., Liu, Z., Cai, G., Gao, L., Zhang, X., Wang, Y., Chen, S., and Zhou, J.M. (2014). The FLS2-associated kinase BIK1 directly phosphorylates the NADPH oxidase RbohD to control plant immunity. Cell Host Microbe **15**: 329–338.

Li, P., Fu, X., Chen, M., Zhang, L., and Li, S. (2019b). Proteomic profiling and integrated analysis with transcriptomic data bring new insights in the stress responses of Kluyveromyces marxianus after an arrest during high-temperature ethanol fermentation. Biotechnol. Biofuels **12**: 1–13.

Ligterink, W., Kroj, T., zur Nieden, U., Hirt, H., and Scheel, D. (1997). Receptor-mediated activation of a MAP kinase in pathogen defense of plants. Science **276**: 2054–2057.

Lin, Z.J.D., Liebrand, T.W.H., Yadeta, K.A., and Coaker, G. (2015). PBL13 is a serine/threonine protein kinase that negatively regulates arabidopsis immune responses. Plant Physiol. **169**: 2950–2962.

Liu, B. et al. (2012a). Lysin motif-containing proteins LYP4 and LYP6 play dual roles in peptidoglycan and chitin perception in rice innate immunity. Plant Cell **24**: 3406–3419.

Liu, T., Liu, Z., Song, C., Hu, Y., Han, Z., She, J., Fan, G., Wang, J., Jin, C., Chang, J., Zhou, J.M., and Chai, J. (2012b). Chitin-induced dimerization activates a plant immune receptor. Science. **336**: 1160–1164.

Liu, Y., Beyer, A., and Aebersold, R. (2016). On the Dependency of Cellular Protein Levels on mRNA Abundance. Cell **165**: 535–550.

Liu, Y., Lu, S., Liu, K., Wang, S., Huang, L., and Guo, L. (2019). Proteomics: A powerful tool to study plant responses to biotic stress. Plant Methods **15**: 1–20.

Lolle, S., Greeff, C., Petersen, K., Sømark, K., Mundy, J., Petersen, M., Lolle, S., Greeff, C., Petersen, K., Roux, M., Jensen, M.K., and Bressendorff, S. (2017). Matching NLR Immune Receptors to Autoimmunity in Article Matching NLR Immune Receptors to Autoimmunity in camta3 Mutants Using Antimorphic NLR Alleles. Cell Host Microbe **21**: 518–529.

Loureiro, J., Rodriguez, E., Dolezel, J., and Santos, C. (2007). Two New Nuclear Isolation Buffers for Plant DNA Flow Cytometry: A Test with 37 Species. Ann. Bot.: 875–888.

Lu, Y. and Yao, J. (2018). Chloroplasts at the crossroad of photosynthesis, pathogen infection and plant defense. Int. J. Mol. Sci. **19**: 1–37.

Lundberg, E. and Borner, G.H.H. (2019). Spatial proteomics: a powerful discovery tool for cell biology. Nat. Rev. Mol. Cell Biol. **20**: 285–302.

Mao, G., Meng, X., Liu, Y., Zheng, Z., Chen, Z., and Zhang, S. (2011). Phosphorylation of a WRKY transcription factor by two pathogen-responsive MAPKs drives phytoalexin biosynthesis in Arabidopsis. Plant Cell **23**: 1639–1653.

Merchante, C., Stepanova, A.N., and Alonso, J.M. (2017). Translation regulation in plants : an interesting past , an exciting present and a promising future. Plant J. **90**: 628–653.

Meteignier, L.V., El-Oirdi, M., Cohen, M., Barff, T., Matteau, D., Lucier, J.F., Rodrigue, S., Jacques, P.E., Yoshioka, K., and Moffett, P. (2017). Translatome analysis of an NB-LRR immune response identifies important contributors to plant immunity in Arabidopsis. J. Exp. Bot. **68**: 2333–2344.

Mine, A., Berens, M.L., Nobori, T., Anver, S., Fukumoto, K., Winkelmüller, T.M., Takeda, A., Becker, D., and Tsuda, K. (2017). Pathogen exploitation of an abscisic acid- and jasmonate-inducible MAPK phosphatase and its interception by Arabidopsis immunity. Proc. Natl. Acad. Sci. U. S. A. **114**: 7456–7461.

Monaghan, J., Matschi, S., Shorinola, O., Rovenich, H., Matei, A., Segonzac, C., Malinovsky, F.G., Rathjen, J.P., Maclean, D., Romeis, T., and Zipfel, C. (2014). The calcium-dependent protein kinase CPK28 buffers plant immunity and regulates BIK1 turnover. Cell Host Microbe **16**: 605–615.

Morcillo, R.J. et al. (2020). Rhizobacterium-derived diacetyl modulates plant immunity in a phosphate-dependent manner. EMBO J. **39**: e102602.

Mukhtar, M.S. et al. (2011). Independently Evolved Virulence Effectors Converge onto Hubs in a Plant Immune System Network. Science. **333**: 596–601.

Mullineaux, P.M., Exposito-Rodriguez, M., Laissue, P.P., Smirnoff, N., and Park, E. (2020). Spatial chloroplast-to-nucleus signalling involving plastid–nuclear complexes and stromules. Philos. Trans. R. Soc. B Biol. Sci. **375**: 20190405.

Navarro, L. et al. (2004). The Transcriptional Innate Immune Response to g22. Interplay and Overlap with Avr Gene-Dependent Defense Responses and Bacterial Pathogenesis. Plant Physiol. **135**: 1113–1128.

O'connell, J.D., Paulo, J.A., O'brien, J.J., and Gygi, S.P. (2018). Proteome-Wide Evaluation of Two Common Protein Quantification Methods. J. Proteome Res. **17**: 1934–1942.

Park, C.J. and Ronald, P.C. (2012). Cleavage and nuclear localization of the rice XA21 immune receptor. Nat. Commun. **3**: 1–6.

Parker, J., Koh, J., Yoo, M.J., Zhu, N., Feole, M., Yi, S., and Chen, S. (2013). Quantitative proteomics of tomato defense against Pseudomonas syringae infection. Proteomics **13**: 1934–1946.

Pecher, P., Eschen-Lippold, L., Herklotz, S., Kuhle, K., Naumann, K., Bethke, G., Uhrig, J., Weyhe, M., Scheel, D., and Lee, J. (2014). The Arabidopsis thaliana mitogen-activated protein kinases MPK3 and MPK6 target a subclass of 'VQ-motif'-containing proteins to regulate immune responses. New Phytol. **203**: 592–606.

Persak, H. and Pitzschke, A. (2013). Tight Interconnection and Multi-Level Control of Arabidopsis MYB44 in MAPK Cascade Signalling. PLoS One **8**: e57547.

Pierella Karlusich, J.J., Zurbriggen, M.D., Shahinnia, F., Sonnewald, S., Sonnewald, U., Hosseini, S.A., Hajirezaei, M.R., and Carrillo, N. (2017). Chloroplast redox status modulates genome-wide plant responses during the non-host interaction of Tobacco with the hemibiotrophic bacterium Xanthomonas campestris pv. Vesicatoria. Front. Plant Sci. **8**: 1–21.

Pitzschke, A., Djamei, A., Teige, M., and Hirt, H. (2009). VIP1 response elements mediate mitogen-activated protein kinase 3-induced stress gene expression. Proc. Natl. Acad. Sci. U. S. A. **106**: 18414–18419.

Plotnikov, A., Zehorai, E., Procaccia, S., and Seger, R. (2011). The MAPK cascades: Signaling components, nuclear roles and mechanisms of nuclear translocation. Biochim. Biophys. Acta - Mol. Cell Res. **1813**: 1619–1633.

Pruitt, R.N. et al. (2015). The rice immune receptor XA21 recognizes a tyrosine-sulfated protein from a Gram-negative bacterium. Sci. Adv. **1**: e1500245.

Pruitt, R.N., Joe, A., Zhang, W., Feng, W., Stewart, V., Schwessinger, B., and Ronald, P.C. (2017). A microbially derived tyrosine-sulfated peptide mimics a plant peptide hormone. New Phytol. **215**: 725–736.

Qiu, J.L. et al. (2008). Arabidopsis MAP kinase 4 regulates gene expression through transcription factor release in the nucleus. EMBO J. **27**: 2214–2221.

Ranf, S., Eschen-Lippold, L., Frhlich, K., Westphal, L., Scheel, D., and Lee, J. (2014). Microbe-associated molecular pattern-induced calcium signaling requires the receptor-like cytoplasmic kinases, PBL1 and BIK1. BMC Plant Biol. **14**: 1–15.

Ranf, S., Gisch, N., Schäffer, M., Illig, T., Westphal, L., Knirel, Y.A., Sánchez-Carballo, P.M., Zähringer, U., Hückelhoven, R., Lee, J., and Scheel, D. (2015). A lectin S-domain receptor kinase mediates lipopolysaccharide sensing in Arabidopsis thaliana. Nat. Immunol. **16**: 426–433.

Rappsilber, J., Ishihama, Y., and Mann, M. (2003). Stop And Go Extraction tips for matrix-assisted laser desorption/ionization, nanoelectrospray, and LC/MS sample pretreatment in proteomics. Anal. Chem. **75**: 663–670.

Ray, S.K., Macoy, D.M., Kim, W.Y., Lee, S.Y., and Kim, M.G. (2019). Role of RIN4 in Regulating PAMP-Triggered Immunity and Effector-Triggered Immunity: Current Status and Future Perspectives. Mol. Cells **42**: 503–511.

Rayapuram, N., Bigeard, J., Alhoraibi, H., Bonhomme, L., Hesse, A.M., Vinh, J., Hirt, H., and Pflieger, D. (2018). Quantitative phosphoproteomic analysis reveals shared and specific targets of Arabidopsis mitogen-activated protein kinases (MAPKs) MPK3,

MPK4, and MPK6. Mol. Cell. Proteomics **17**: 61–80.

Righetti, P.G. and Boschetti, E. (2020). Low-abundance plant protein enrichment with peptide libraries to enlarge proteome coverage and related applications. Plant Sci. **290**: 110302.

Roch, K.G. Le, Johnson, J.R., Florens, L., Zhou, Y., Santrosyan, A., Grainger, M., Yan, S.F., Williamson, K.C., Holder, A.A., Carucci, D.J., Iii, J.R.Y., and Winzeler, E.A. (2004). Global analysis of transcript and protein levels across the. Genome Res.: 2308–2318.

Le Roux, C., Parker, J.E., and Deslandes, L. (2015). A Receptor Pair with an Integrated Decoy Converts Pathogen Disabling of Transcription Factors to Article A Receptor Pair with an Integrated Decoy Converts Pathogen Disabling. Cell **161**: 1074–1088.

Roux, M., Schwessinger, B., Albrecht, C., Chinchilla, D., Jones, A., Holton, N., Malinovsky, F.G., Tör, M., de Vries, S., and Zipfel, C. (2011). The Arabidopsis leucine-rich repeat receptor-like kinases BAK1/SERK3 and BKK1/SERK4 are required for innate immunity to hemibiotrophic and biotrophic pathogens. Plant Cell **23**: 2440–2455.

Saiga, S., Furumizu, C., Yokoyama, R., Kurata, T., Sato, S., Kato, T., Tabata, S., Suzuki, M., and Komeda, Y. (2008). The Arabidopsis OBERON1 and OBERON2 genes encode plant homeodomain finger proteins and are required for apical meristem maintenance. Development **135**: 1751–1759.

Sarris, P.F., Duxbury, Z., Sohn, K.H., Jones, J.D.G., Sklenar, J., and Derbyshire, P. (2015). A Plant Immune Receptor Detects Pathogen Effectors that Target WRKY Transcription Factors. Cell **161**: 1089–1100.

Saur, I.M.L., Kadota, Y., Sklenar, J., Holton, N.J., Smakowska, E., Belkhadir, Y., Zipfel, C., and Rathjen, J.P. (2016). NbCSPR underlies age-dependent immune responses to bacterial cold shock protein in Nicotiana benthamiana. Proc. Natl. Acad. Sci. U. S. A. **113**: 3389–3394.

Schulze, B., Mentzel, T., Jehle, A.K., Mueller, K., Beeler, S., Boller, T., Felix, G., and Chinchilla, D. (2010). Rapid heteromerization and phosphorylation of ligand-activated plant transmembrane receptors and their associated kinase BAK1. J. Biol. Chem. **285**: 9444–9451.

Schwessinger, B., Roux, M., Kadota, Y., Ntoukakis, V., Sklenar, J., Jones, A., and Zipfel, C. (2011). Phosphorylation-dependent differential regulation of plant growth, cell death, and innate immunity by the regulatory receptor-like kinase BAK1. PLoS Genet. **7**: e1002046.

Segonzac, C., Macho, A.P., Sanmartín, M., Ntoukakis, V., Sánchez-Serrano, J.J., and Zipfel, C. (2014). Negative control of BAK 1 by protein phosphatase 2A during plant innate immunity . EMBO J. **33**: 2069–2079.

Seyfferth, C. and Tsuda, K. (2014). Salicylic acid signal transduction: the initiation of biosynthesis, perception and transcriptional reprogramming. Front. Plant Sci. **5**: 1–10.

Shen, Q., Bourdais, G., Pan, H., Robatzek, S., and Tang, D. (2017). protein LLG1 associates with and modulates FLS2 to regulate innate immunity. Proc. Natl. Acad. Sci. **114**: 2–7.

Shen, Q.H. and Schulze-Lefert, P. (2007). Rumble in the nuclear jungle: Compartmentalization, trafficking, and nuclear action of plant immune receptors. EMBO J. **26**: 4293–4301.

Shi, H., Shen, Q., Qi, Y., Yan, H., Nie, H., Chen, Y., Zhao, T., Katagiri, F., and Tang, D. (2013). BR-signaling kinase1 physically associates with flagellin SENSING2 and regulates plant innate immunity in Arabidopsis. Plant Cell **25**: 1143–1157.

Shim, J.S., Jung, C., Lee, S., Min, K., Lee, Y.W., Choi, Y., Lee, J.S., Song, J.T., Kim, J.K., and Choi, Y. Do (2013). AtMYB44 regulates WRKY70 expression and modulates antagonistic interaction between salicylic acid and jasmonic acid signaling. Plant J. **73**: 483–495.

Sikorskaite, S., Rajamäki, M.-L., Baniulis, D., Stanys, V., and Valkonen, J.P. (2013). Protocol: Optimised methodology for isolation of nuclei from leaves of species in the Solanaceae and Rosaceae families. Plant Methods **9**: 31.

Singh, S., Katzer, K., Lambert, J., Cerri, M., and Parniske, M. (2014). CYCLOPS, A DNA-binding transcriptional activator, orchestrates symbiotic root nodule development. Cell Host Microbe **15**: 139–152.

Smith-Johannsen, H. and Gibbs, S.P. (1972). Effects of chloramphenicol on chloroplast and mitochondrial ultrastructure in Ochromonas Danica. J. Cell Biol. **52**: 598–614.

Sreekanta, S., Bethke, G., Hatsugai, N., Tsuda, K., Thao, A., Wang, L., Katagiri, F., and Glazebrook, J. (2015). The receptor-like cytoplasmic kinase PCRK1 contributes to pattern-triggered immunity against Pseudomonas syringae in Arabidopsis thaliana. New Phytol. **207**: 78–90.

Stegmann, M., Monaghan, J., Smakowska-Luzan, E., Rovenich, H., Lehner, A., Holton, N., Belkhadir, Y., and Zipfel, C. (2017). The receptor kinase FER is a RALF-regulated scaffold controlling plant immune signaling. Science. **355**: 287–289.

Strehmel, N., Hoehenwarter, W., Mönchgesang, S., Majovsky, P., Krüger, S., Scheel, D., and Lee, J. (2017). Stress-related mitogen-activated protein kinases stimulate the accumulation of small molecules and proteins in Arabidopsis thaliana root exudates. Front. Plant Sci. **8**: 1–13.

Stuttmann, J., Peine, N., Garcia, A. V., Wagner, C., Choudhury, S.R., Wang, Y., James, G.V., Griebel, T., Alcázar, R., Tsuda, K., Schneeberger, K., and Parker, J.E. (2016). Arabidopsis thaliana DM2h (R8) within the Landsberg RPP1-like Resistance Locus Underlies Three Different Cases of EDS1-Conditioned Autoimmunity. PLOS Genet. **12**: e1005990.

Su, J., Yang, L., Zhu, Q., Wu, H., He, Y., Liu, Y., Xu, J., Jiang, D., and Zhang, S. (2018). Active photosynthetic inhibition mediated by MPK3/MPK6 is critical to effector-triggered immunity. PLoS Biol. **16**: 1–29.

Su, J., Zhang, M., Zhang, L., Sun, T., Liu, Y., Lukowitz, W., Xu, J., and Zhang, S. (2017). Regulation of stomatal immunity by interdependent functions of a pathogen-responsive MPK3/MPK6 cascade and abscisic acid. Plant Cell **29**: 526–542.

Sun, X., Feng, P., Xu, X., Guo, H., Ma, J., Chi, W., Lin, R., Lu, C., and Zhang, L. (2011). A chloroplast envelope-bound PHD transcription factor mediates chloroplast signals to the nucleus. Nat. Commun. **2:477**.

Sun, Y., Li, L., Macho, A.P., Han, Z., Hu, Z., Zipfel, C., Zhou, J.-M., and Chai, J. (2013). Structural Basis for flg22-Induced Activation of the Arabidopsis FLS2-BAK1 Immune Complex. Science. **342**: 624–629.

Szklarczyk, D. et al. (2015). STRING v10: Protein-protein interaction networks, integrated over the tree of life. Nucleic Acids Res. **43**: D447–D452.

Tamborski, J. and Krasileva, K. V. (2020). Evolution of Plant NLRs: From Natural History to Precise Modifications. Annu. Rev. Plant Biol. **71**: 355–378.

Tamura, K., Fukao, Y., Iwamoto, M., Haraguchi, T., and Hara-Nishimura, I. (2010). Identification and Characterization of Nuclear Pore Complex Components in Arabidopsis thaliana. Plant Cell **22**: 4084–4097.

Tang, D., Wang, G., and Zhou, J.M. (2017). Receptor kinases in plant-pathogen interactions: More than pattern recognition. Plant Cell **29**: 618–637.

Tang, Y., Huang, A., and Gu, Y. (2020). Global profiling of plant nuclear membrane proteome in Arabidopsis. Nat. Plants **6**: 838–847.

Teixeira, P.J.P., Colaianni, N.R., Fitzpatrick, C.R., and Dangl, J.L. (2019). Beyond pathogens: microbiota interactions with the plant immune system. Curr. Opin. Microbiol. **49**: 7–17.

Tena, G., Boudsocq, M., and Sheen, J. (2011). Protein kinase signaling networks in plant innate immunity. Curr. Opin. Plant Biol. **14**: 519–529.

Tian, W., Hou, C., Ren, Z., Wang, C., Zhao, F., Dahlbeck, D., Hu, S., Zhang, L., Niu, Q., Li, L., Staskawicz, B.J., and Luan, S. (2019). A calmodulin-gated calcium channel links pathogen patterns to plant immunity. Nature **572**: 131–135.

De Torres Zabala, M. et al. (2015). Chloroplasts play a central role in plant defence and are targeted by pathogen effectors. Nat. Plants **1**: 15074.

Tsuda, K. and Katagiri, F. (2010). Comparing signaling mechanisms engaged in pattern-triggered and effector-triggered immunity. Curr. Opin. Plant Biol. **13**: 459–465.

Tsuda, K. and Somssich, I.E. (2015). Transcriptional networks in plant immunity. New Phytol. **206**: 932–947.

Tyanova, S., Temu, T., and Cox, J. (2016a). The MaxQuant computational platform for mass spectrometry-based shotgun proteomics. Nat. Protoc. **11**: 2301–2319.

Tyanova, S., Temu, T., Sinitcyn, P., Carlson, A., Hein, M.Y., Geiger, T., Mann, M., and Cox, J. (2016b). The Perseus computational platform for comprehensive analysis of (prote)omics data. Nat. Methods **13**: 731–740.

Vlasák, J. (1981). Effect of different disintegration techniques and media on yield and appearance of isolated nuclei. Biol. Plant. **23**: 406–413.

Wainstein, E. and Seger, R. (2016). The dynamic subcellular localization of ERK: mechanisms of translocation and role in various organelles. Curr. Opin. Cell Biol. **39**: 15–20.

Waller, J.C., Dhanoa, P.K., Schumann, U., Mullen, R.T., and Snedden, W.A. (2010). Subcellular and tissue localization of NAD kinases from Arabidopsis: Compartmentalization of de novo NADP biosynthesis. Planta **231**: 305–317.

Wan, J., Zhang, X.C., Neece, D., Ramonell, K.M., Clough, S., Kim, S.Y., Stacey, M.G., and Stacey, G. (2008). A LysM receptor-like kinase plays a critical role in chitin signaling and fungal resistance in Arabidopsis. Plant Cell **20**: 471–481.

Wan, L., Essuman, K., Anderson, R.G., Sasaki, Y., Monteiro, F., Chung, E.-H., Osborne Nishimura, E., DiAntonio, A., Milbrandt, J., Dangl, J.L., and Nishimura, M.T. (2019a). TIR domains of plant immune receptors are NAD +-cleaving enzymes that promote cell death Downloaded from. Science. **365**: 799–803.

Wan, W.L., Fröhlich, K., Pruitt, R.N., Nürnberger, T., and Zhang, L. (2019b). Plant cell surface immune receptor complex signaling. Curr. Opin. Plant Biol. **50**: 18–28.

Wang, H., Wang, S., Lu, Y., Alvarez, S., Hicks, L.M., Ge, X., and Xia, Y. (2012). Proteomic analysis of early-responsive redox-sensitive proteins in Arabidopsis. J. Proteome Res. **11**: 412–424.

Wang, L., Albert, M., Einig, E., Fürst, U., Krust, D., and Felix, G. (2016). The pattern-recognition receptor CORE of Solanaceae detects bacterial cold-shock protein. Nat. Plants **2**: 16185.

Wang, L., Tsuda, K., Truman, W., Sato, M., Nguyen, L. V., Katagiri, F., and Glazebrook, J. (2011a). CBP60g and SARD1 play partially redundant critical roles in salicylic acid signaling. Plant J. **67**: 1029–1041.

Wang, Q., Wang, M., Zhang, X., Hao, B., Kaushik, S.K., and Pan, Y. (2011b). WRKY gene family evolution in Arabidopsis thaliana. Genetica **139**: 973–983.

Wang, Y., Garrido-Oter, R., Wu, J., Winkelmüller, T.M., Agler, M., Colby, T., Nobori, T., Kemen, E., and Tsuda, K. (2019). Site-specific cleavage of bacterial MucD by secreted proteases mediates antibacterial resistance in Arabidopsis. Nat. Commun. **10**: 2853.

Wang, Y., Schuck, S., Wu, J., Yang, P., Döring, A.C., Zeier, J., and Tsuda, K. (2018). A MPK3/6-WRKY33-ALD1-Pipecolic Acid Regulatory Loop Contributes to Systemic Acquired Resistance. Plant Cell **30**: 2480–2494.

Wei, T., Chen, T., Ho, Y.T., and Ronald, P.C. (2016). Mutation of the rice XA21 predicted nuclear localization sequence does not affect resistance to Xanthomonas oryzae pv . oryzae. PeerJ **4**: e2507.

Weyhe, M. (2019). Transcriptional regulation of defence gene expression by a VQ-motif containing protein.

Winkelmüller, T.M. (2018). Comparative transcriptomics within Arabidopsis thaliana accessions and across Brassicaceae species reveal evolutionary conserved and lineage-speficic expression signatures in pattern triggered immunity.

Wiśniewski, J.R., Zougman, A., and Mann, M. (2009). Combination of FASP and StageTip-based fractionation allows in-depth analysis of the hippocampal membrane proteome. J. Proteome Res. **8**: 5674–5678.

Wu, Q., Xu, F., Liu, L., Char, S.N., Ding, Y., Je, B. Il, Schmelz, E., Yang, B., and Jackson, D. (2020). The maize heterotrimeric G protein β subunit controls shoot meristem development and immune responses. Proc. Natl. Acad. Sci. U. S. A. **117**: 1799–1805.

Xiao, Y., Stegmann, M., Han, Z., DeFalco, T.A., Parys, K., Xu, L., Belkhadir, Y., Zipfel,

C., and Chai, J. (2019). Mechanisms of RALF peptide perception by a heterotypic receptor complex. Nature **572**: 270–274.

Xin, X.F., Nomura, K., Aung, K., Velásquez, A.C., Yao, J., Boutrot, F., Chang, J.H., Zipfel, C., and He, S.Y. (2016). Bacteria establish an aqueous living space in plants crucial for virulence. Nature **539**: 524–529.

Xu, G., Greene, G.H., Yoo, H., Liu, L., Marqués, J., Motley, J., and Dong, X. (2017). Global translational reprogramming is a fundamental layer of immune regulation in plants. Nature **545**: 487.

Xue, D.X., Li, C.L., Xie, Z.P., Staehelin, C., and Napier, R. (2019). LYK4 is a component of a tripartite chitin receptor complex in Arabidopsis thaliana. J. Exp. Bot. **70**: 5507–5516.

Yadeta, K.A., Elmore, J.M., Creer, A.Y., Feng, B., Franco, J.Y., Rufian, J.S., He, P., Phinney, B., and Coaker, G. (2017). A Cysteine-Rich Protein Kinase Associates with a Membrane Immune Complex and the Cysteine Residues Are Required for Cell Death. Plant Physiol. **173**: 771–787.

Yamada, K. et al. (2016). The Arabidopsis CERK1-associated kinase PBL27 connects chitin perception to MAPK activation. EMBO J. **35 (22)**: 2468–2483.

Yan, H., Zhao, Y., Shi, H., Li, J., Wang, Y., and Tang, D. (2018). BRASSINOSTEROID-SIGNALING kinase1 phosphorylates MAPKKK5 to regulate immunity in arabidopsis. Plant Physiol. **176**: 2991–3002.

Yang, T. and Poovaiah, B.W. (2002). A calmodulin-binding/CGCG box DNA-binding protein family involved in multiple signaling pathways in plants. J. Biol. Chem. **277**: 45049–45058.

Yano, K. et al. (2008). CYCLOPS, a mediator of symbiotic intracellular accommodation. Proc. Natl. Acad. Sci. U. S. A. **105**: 20540–20545.

Yao, S., Deng, L., and Zeng, K. (2017). Genome-wide in silico identification of membrane-bound transcription factors in plant species. PeerJ **5**: e4051.

Yeh, Y., Panzeri, D., Kadota, Y., Huang, Y., Huang, P., and Tao, C. (2016). The Arabidopsis Malectin-Like / LRR-RLK IOS1 Is Critical for BAK1-Dependent and BAK1-Independent Pattern-Triggered Immunity. Plant Cell **28**: 1701–1721.

Yin, X. and Komatsu, S. (2016). Nuclear Proteomics Reveals the Role of Protein Synthesis and Chromatin Structure in Root Tip of Soybean during the Initial Stage of Flooding Stress. J. Proteome Res. **15**: 2283–2298.

Yu, K., Liu, Y., Tichelaar, R., Savant, N., Lagendijk, E., van Kuijk, S.J.L., Stringlis, I.A., van Dijken, A.J.H., Pieterse, C.M.J., Bakker, P.A.H.M., Haney, C.H., and Berendsen, R.L. (2019). Rhizosphere-Associated Pseudomonas Suppress Local Root Immune Responses by Gluconic Acid-Mediated Lowering of Environmental pH. Curr. Biol. **29**: 3913-3920.e4.

Zhang, H. -B, Zhao, X., Ding, X., Paterson, A.H., and Wing, R.A. (1995). Preparation of megabase-size DNA from plant nuclei. Plant J. **7**: 175–184.

Zhang, M., Su, J., Zhang, Y., Xu, J., and Zhang, S. (2018). Conveying endogenous and exogenous signals: MAPK cascades in plant growth and defense. Curr. Opin. Plant Biol. **45**: 1–10.

Zhou, F., Emonet, A., Dénervaud Tendon, V., Marhavy, P., Wu, D., Lahaye, T., and Geldner, N. (2020a). Co-incidence of Damage and Microbial Patterns Controls Localized Immune Responses in Roots. Cell **180**: 440-453.

Zhou, J., Wang, X., He, Y., Sang, T., Wang, P., Dai, S., Zhang, S., and Meng, X. (2020b). Differential Phosphorylation of the Transcription Factor WRKY33 by the Protein Kinases CPK5/CPK6 and MPK3/MPK6 Cooperatively Regulates Camalexin Biosynthesis in Arabidopsis. Plant Cell **32**: 2621–2638.

Zhou, J.M. and Zhang, Y. (2020). Plant Immunity: Danger Perception and Signaling. Cell **181**: 978–989.

Zipfel, C. (2014). Plant pattern-recognition receptors. Trends Immunol. **35**: 345–351.

Zipfel, C., Kunze, G., Chinchilla, D., Caniard, A., Jones, J.D.G., Boller, T., and Felix, G. (2006). Perception of the Bacterial PAMP EF-Tu by the Receptor EFR Restricts Agrobacterium-Mediated Transformation. Cell **125**: 749–760.

Zipfel, C., Robatzek, S., Navarro, L., Oakeley, E.J., Jones, J.D.G., Felix, G., and Boller, T. (2004). Bacterial disease resistance in Arabidopsis through flagellin perception. Nature **428**: 15–18.

Zou, Y., Wang, S., Zhou, Y., Bai, J., Huang, G., Liu, X., Zhang, Y., Tang, D., and Lu, D. (2018). Transcriptional Regulation of the Immune Receptor FLS2 Controls the Ontogeny of Plant Innate Immunity. Plant Cell **30**: 2779–2794.

6. Supplement

6.1 Supplementary figures

Figure S1:

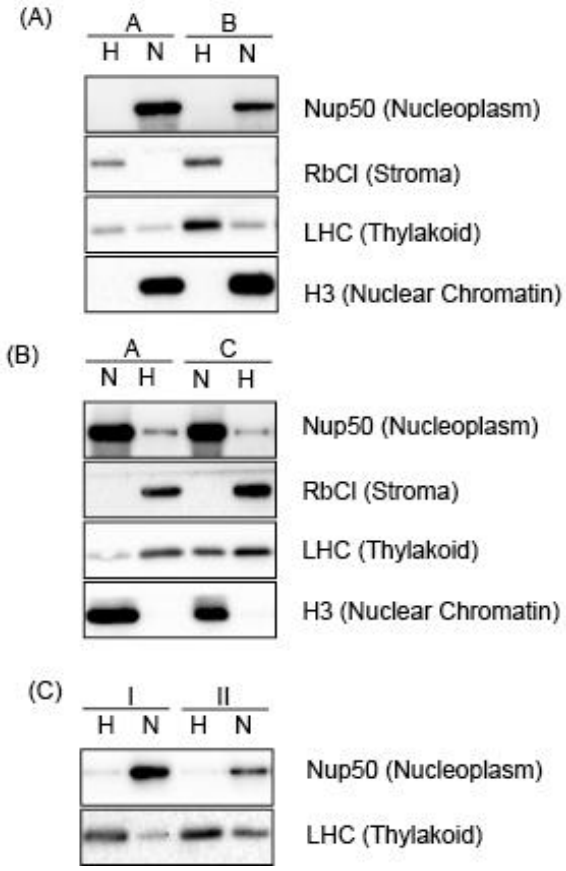

Figure S1: Comparison of modifications to the nuclear protein isolation. Fresh leaves from 4-5 weeks old transgenic Col-0 plants expressing GFP-tagged Nup50a were used for nuclear (N) and total protein isolation (H). Nuclear proteins were isolated by the new protocol ("SR") or Folta protocol (FK). **(A & B)** Comparison of homogenization chopping (A) vs a blender (B) & chopping (A) vs paint-shaker (C). **(C)** Comparison of Triton X-100 used only at second centrifugation step (I) vs used at both centrifugation steps (II). Homogenate was used for total proteins (H). 2 µg of protein was used for immunoblotting using anti-GFP (nucleoplasm), anti-H3 (nuclear chromatin), anti-RbCl (chloroplast) and, anti-LHC (thylakoid) antibodies.

Figure S2:

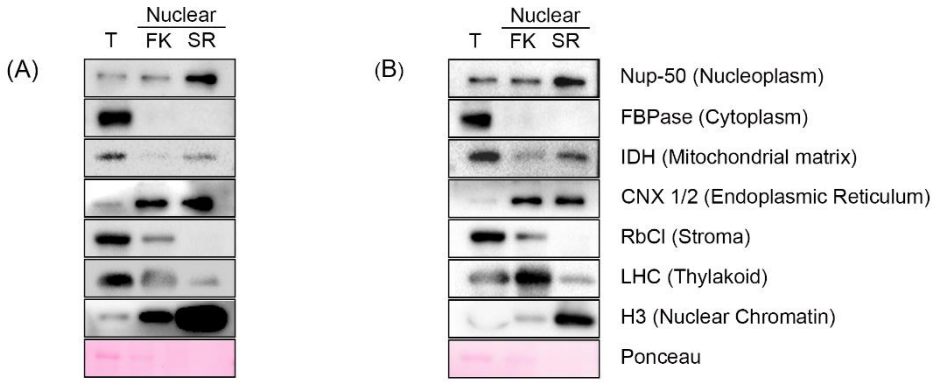

Figure S2: Establishment of new protocol for nuclear protein isolation. Fresh leaves from 4-5 weeks old transgenic Col-0 plants expressing GFP-tagged Nup50a were used for nuclear and total protein isolation. Nuclear proteins were isolated by the Folta et al. protocol ("FK") and by the new protocol ("SR"). Total proteins (T) were isolated from total leaf extract (1g leaf material). Extracted protein (2µg) was used for immunoblotting using anti-GFP (nucleoplasm), anti-H3 (nuclear chromatin), anti-RbCl (chloroplast), anti-LHC (thylakoid), anti-FBPase (cytosol), anti-IDH (mitochondria) and anti-CNX1/2 (endoplasmic reticulum) antibodies. Ponceau staining was used to assess protein loading and RuBisCO abundance. The figure shows two replicates, (A) & (B), out of the three biological replicates for the immunoblotting experiment.

Figure S3:

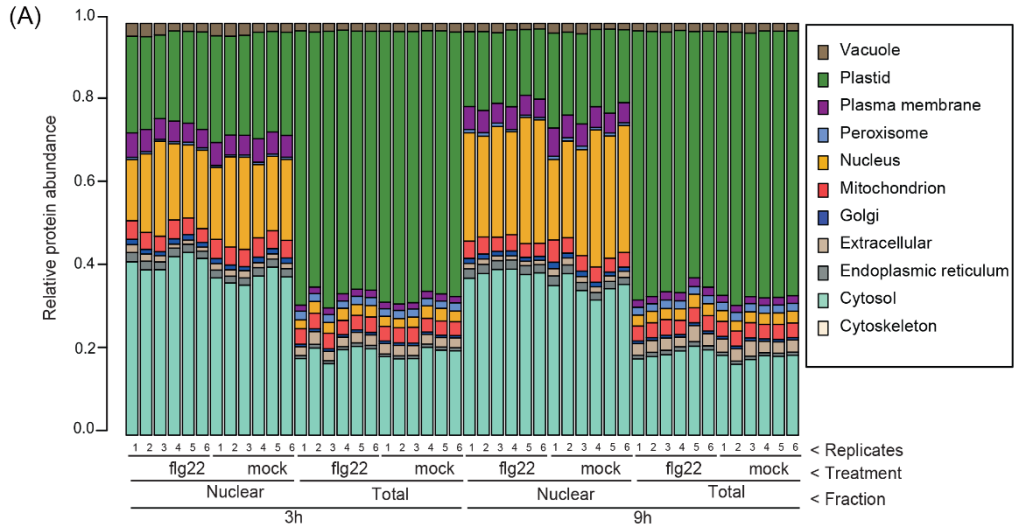

Figure S3: Relative protein abundance of all proteins identified in each protein group. Subcellular localization of all the proteins identified in each "Majority protein group" was used to calculate enrichment of subcellular organelles using SUBA 4 reference database. The IBAQ values assigned to each "Majority protein group" was divided by the total number of proteins identified within each "Majority protein group" and the

Figure S4:

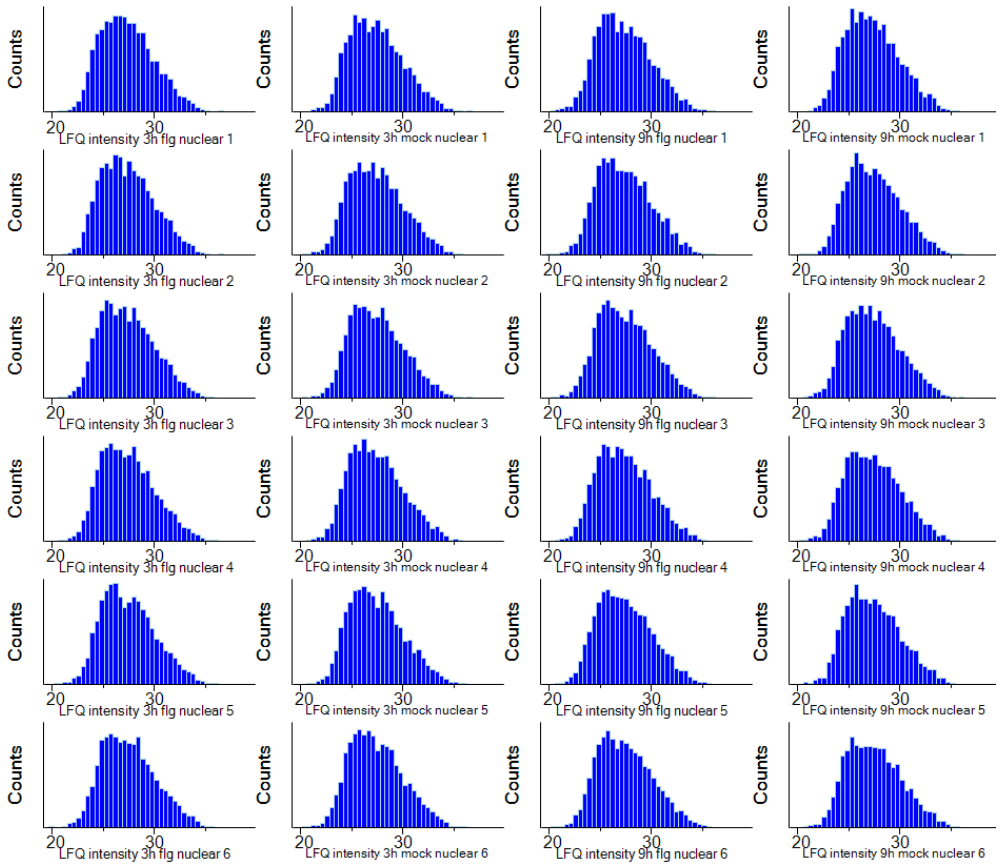
Counts
20
30
LFQ intensity 3h flg nuclear 1
LFQ intensity 3h mock nuclear 1
LFQ intensity 9h flg nuclear 1
LFQ intensity 9h mock nuclear 1
LFQ intensity 3h flg nuclear 2
LFQ intensity 3h mock nuclear 2
LFQ intensity 9h flg nuclear 2
LFQ intensity 9h mock nuclear 2
LFQ intensity 3h flg nuclear 3
LFQ intensity 3h mock nuclear 3
LFQ intensity 9h flg nuclear 3
LFQ intensity 9h mock nuclear 3
LFQ intensity 3h flg nuclear 4
LFQ intensity 3h mock nuclear 4
LFQ intensity 9h flg nuclear 4
LFQ intensity 9h mock nuclear 4
LFQ intensity 3h flg nuclear 5
LFQ intensity 3h mock nuclear 5
LFQ intensity 9h flg nuclear 5
LFQ intensity 9h mock nuclear 5
LFQ intensity 3h flg nuclear 6
LFQ intensity 3h mock nuclear 6
LFQ intensity 9h flg nuclear 6
LFQ intensity 9h mock nuclear 6

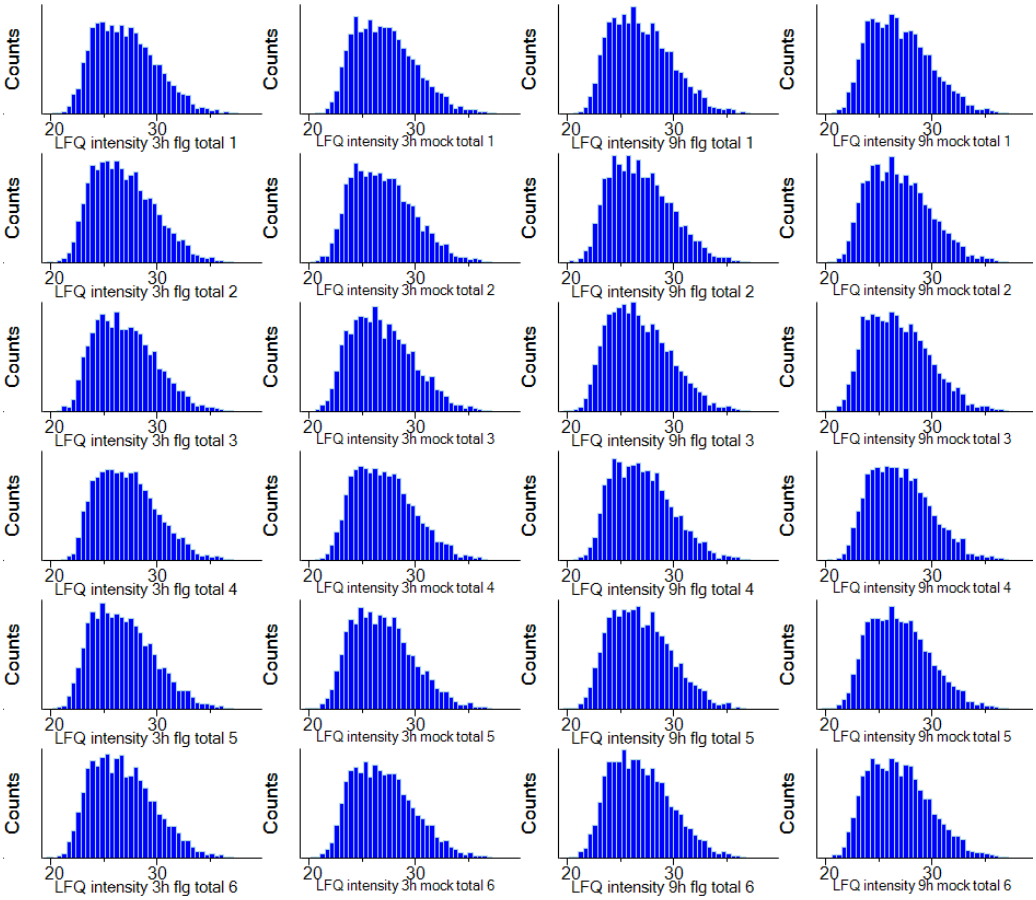

Figure S4: LFQ intensities show a normalized distribution. Histogram showing distribution of $\log_2$ transformed LFQ intensity (blue bars) for replicates of nuclear and total fractions at 3 h and 9 h after 1 µm-

Figure S5:

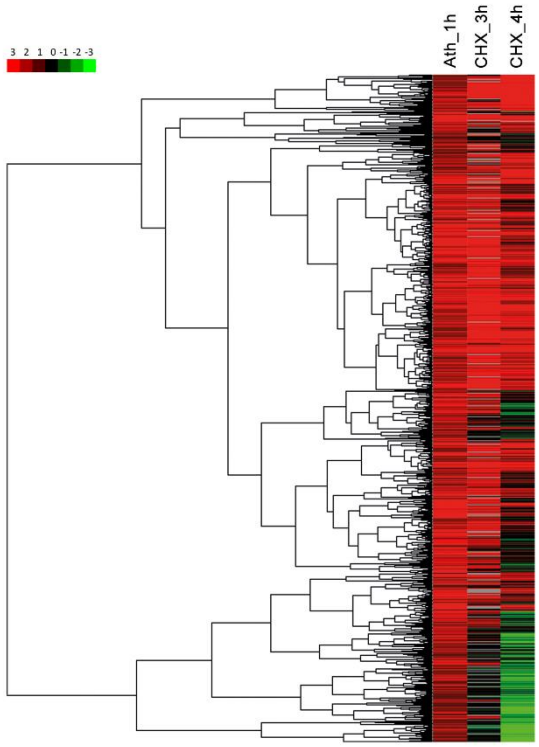

Figure S5: Transcriptome responses overlap during flg22 and CHX treatment. Genes that were induced more than 2-folds 1 h after 1 µm-flg22 treatment (Ath_1h) were selected and compared to CHX treatment, 10 µm for 3 h (CHX_3h) or 35 µm for 4 h (CHX_4h) from public data (Goda et al., 2008; Drechsel et al., 2013). Out of 237 genes 167 flg22-induced genes were also induced upon CHX treatment at 3 h and/or 4 h (Data from Thomas Winkelmüller)

Figure S6:

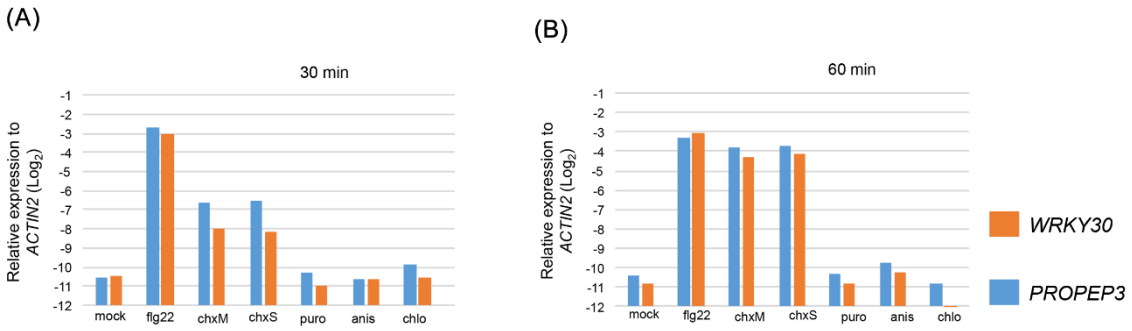

Figure S6: Cycloheximide induces flg22-responsive genes from 1 h onwards. Expression of flg22-responsive genes *PROPEP3* and *WRKY30* were tested after treatment of 12-day-old *A. thaliana* seedlings with mock or flg22 (1 µM) and different protein translational inhibitors. Protein translation inhibitors used were 100 µM- cycloheximide (chxS, synthetic source and chxM, microbial source), 200 µM-puromycin (puro), 100 µM-anisomysin (anis), and 100 µM-chloramphenicol (chlo).

Figure S7:

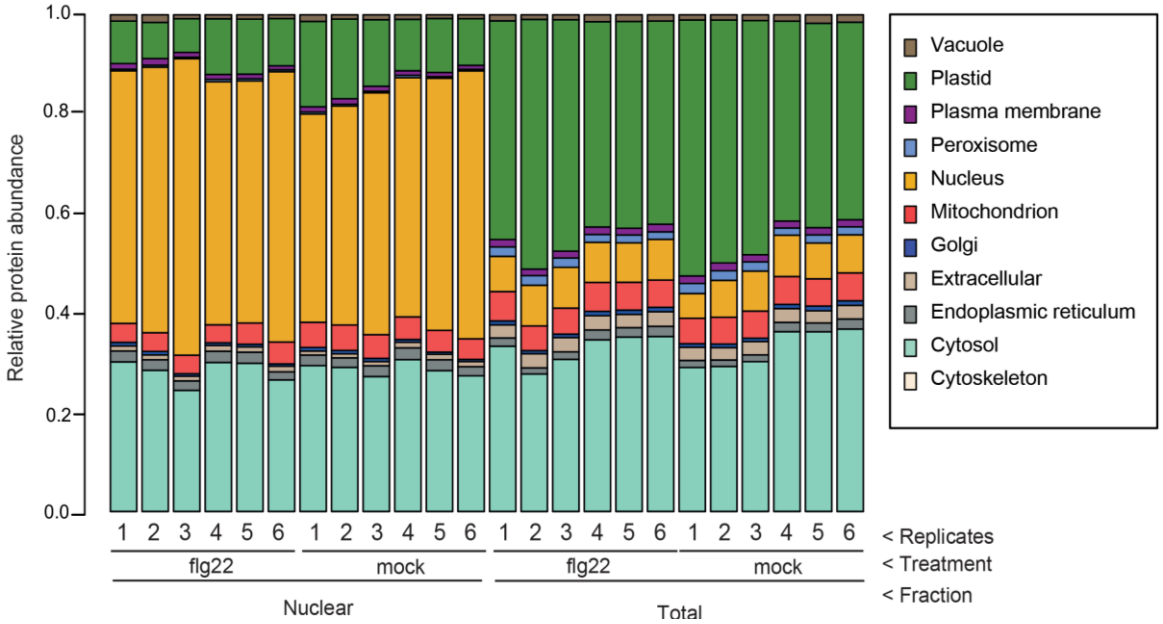

Figure S7: Subcellular localization of proteins detected in the nuclear and total proteome analysis. Col-0 seedlings (12-day old) were treated with 1 µM-flg22, water (mock). Nuclear and total proteins were isolated after 15min of flg22/water(mock) treatment. Six replicates (protein samples were prepared in two different days each containing three replicates prepared from independent plant materials) were prepared for each condition. Relative protein abundance was calculated using intensity based absolute quantification (IBAQ) values. The individual columns represent each replicate showing relative protein abundance of proteins identified by LC-MS/MS and its subcellular localization as predicted by SUBA4 reference database. Subcellular localization of all the proteins identified in each "Majority protein group" was used to calculate enrichment of subcellular organelles using SUBA 4 reference database. The IBAQ values assigned to each "Majority protein group" was divided by the total number of proteins identified within each "Majority protein group" and the resultant IBAQ values were assigned to each member within the group

Figure S8:

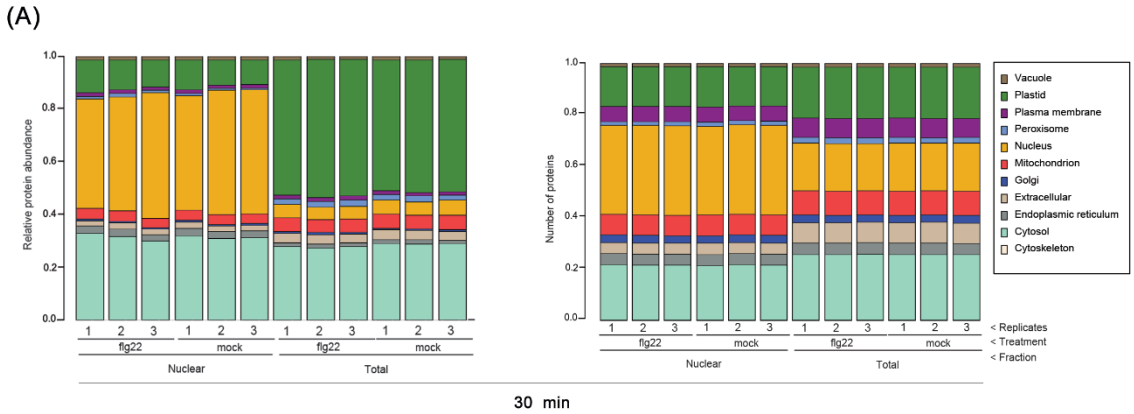

(B)

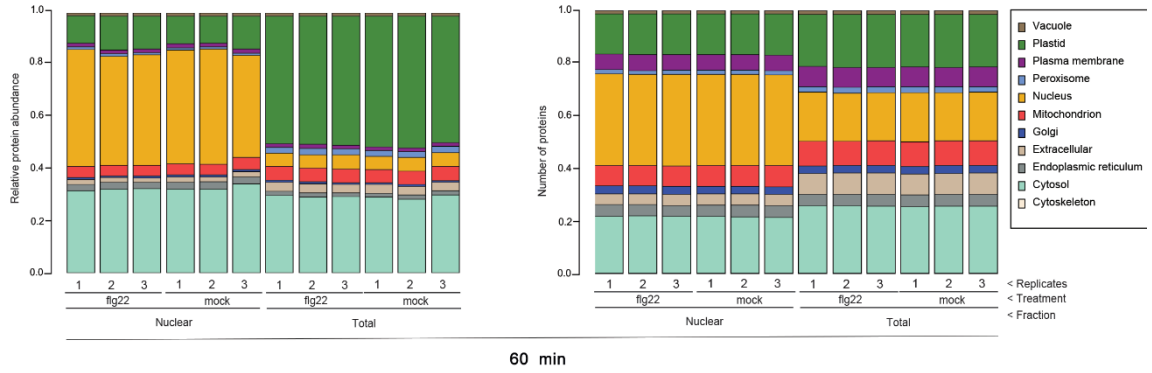

(C)

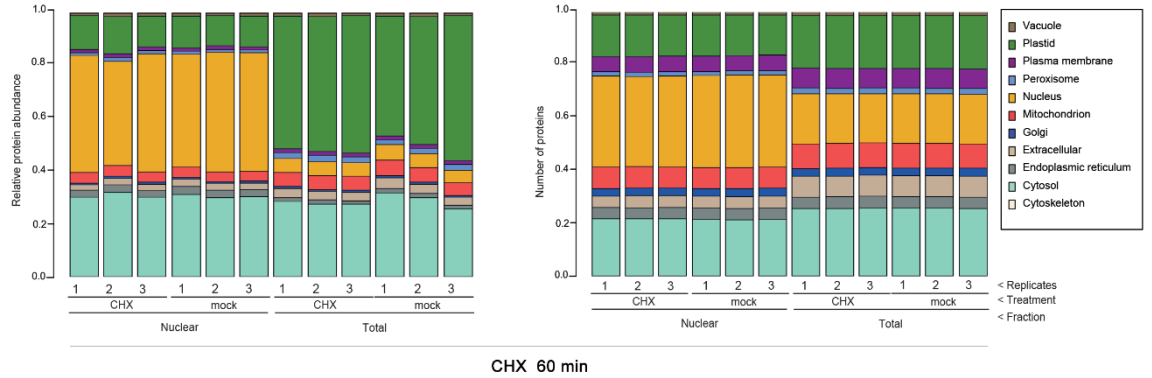

Figure S8: Subcellular localization of proteins detected in the nuclear and total proteome analysis. Col-0 seedlings (12-day old) were treated with 1 µM-flg22, water (mock) or 100 µM-cycloheximide in ½ MS solution. Nuclear and total proteins were isolated after 30 (A), and 60 min (B) of flg22/water(mock) treatment or after 60 min (C) of CHX/DMSO (mock) treatment. Three replicates (protein samples were prepared on the same day from independent plant materials) were prepared for each condition. Relative protein abundance was calculated using intensity based absolute quantification (IBAQ) values. The individual columns represent each replicate showing relative protein abundance of proteins identified by LC-MS/MS and its subcellular localization as predicted by SUBA4 reference database. Subcellular localization of all the proteins identified in each "Majority protein group" was used to calculate enrichment of subcellular organelles using SUBA 4 reference database. The first panel shows subcellular localization of proteins based on their relative abundance (IBAQ value) in the nuclear and total protein fraction. The second panel shows subcellular localization of proteins based on the number of proteins. The first protein listed within each "Majority protein group" (see text) was used to assign the subcellular localization based on SUBA4 reference database.

Figure S9:

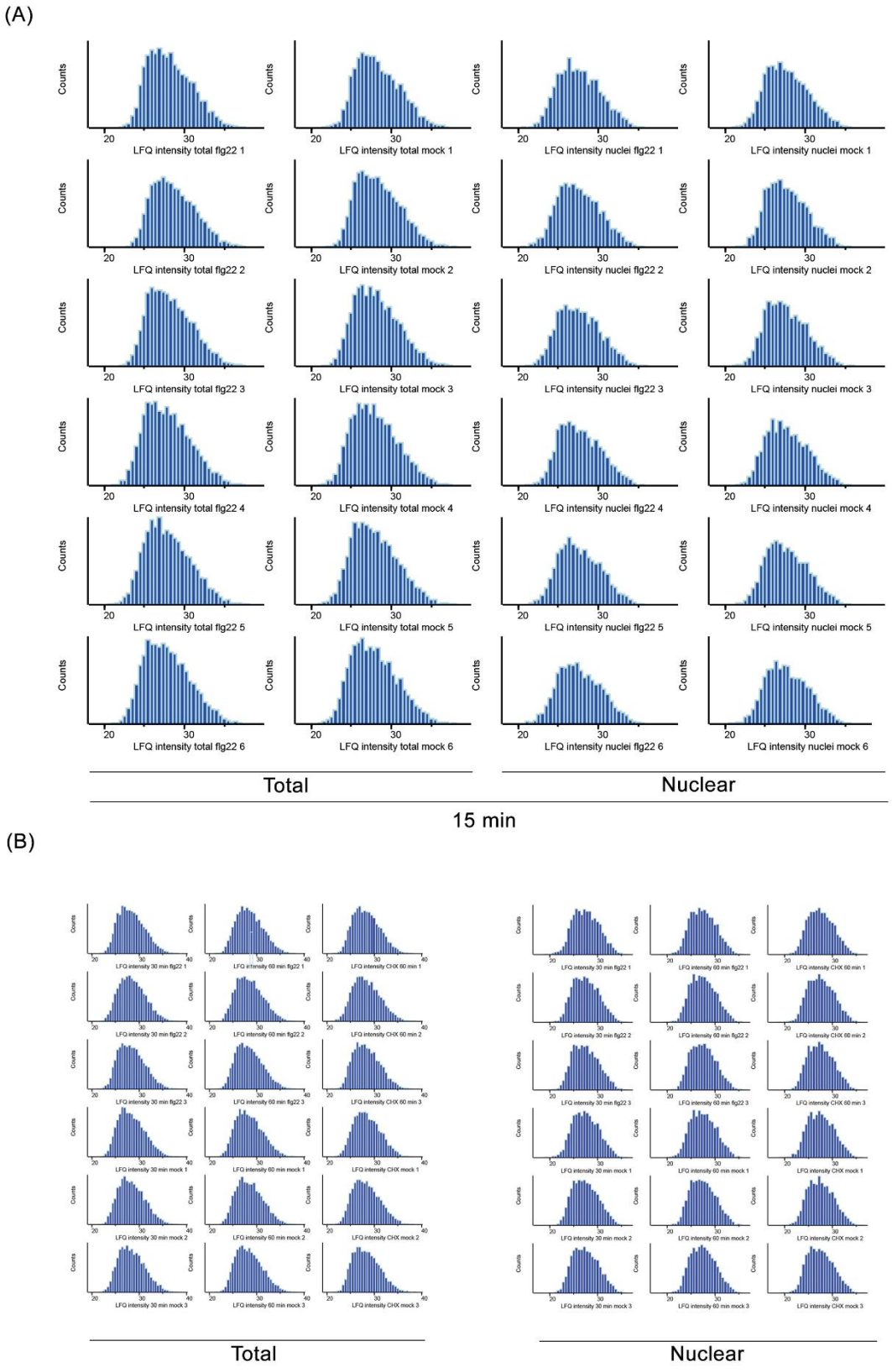

Figure S9: LFQ intensities show a normalized distribution. The histogram shows distribution of log_2 transformed LFQ intensity (blue bars) for replicates of nuclear and total fractions after 1 µM-flg22-treatment at 15, 30, and 60 min and after 100 µM-CHX treatment in ½ MS solution at 60 min.

Figure S10:

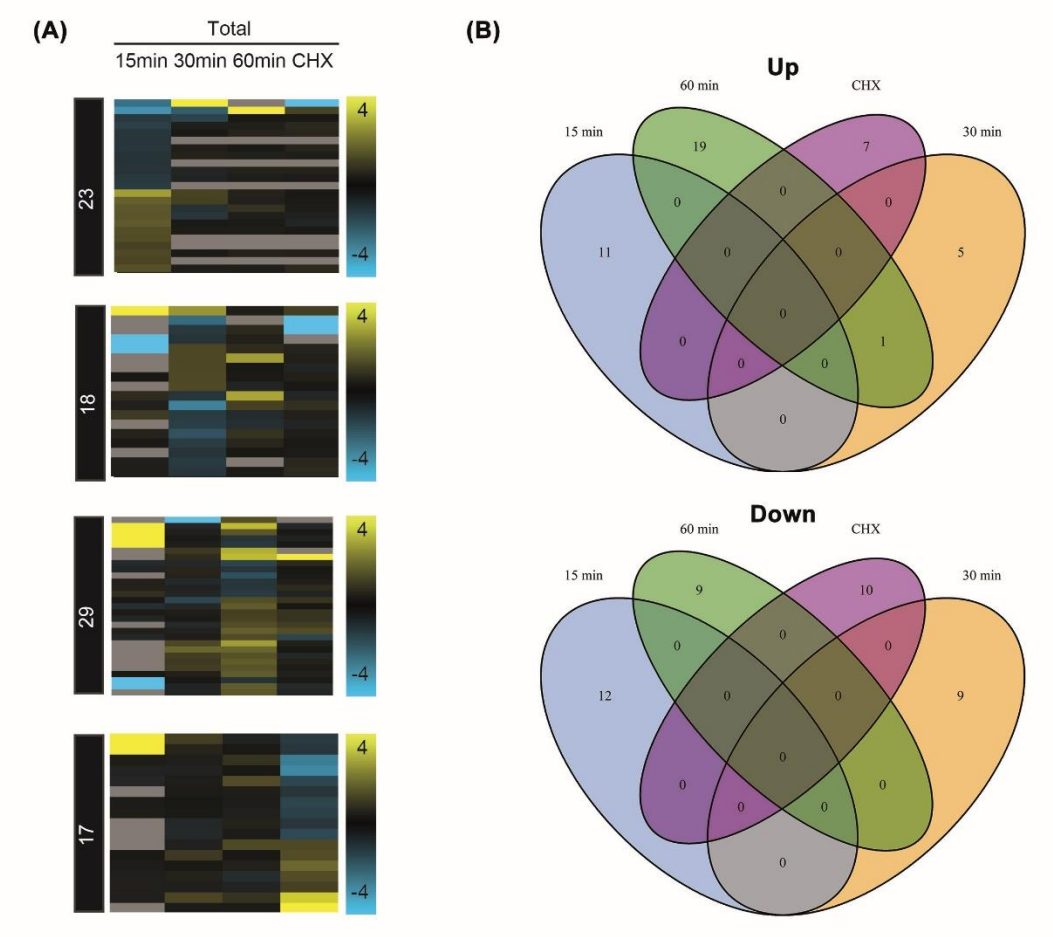

Figure S10: Early protein response to flg22 and cycloheximide largely do not overlap. Heatmap showing DEPs ($|\log_2$ fold change$| > 1$; p-value < 0.05) in the total fraction. **(A)** First panel shows 23 DEPs at 15 min after 1 µM-flg22 treatment averaged across six replicates. Second panel shows 18 DEPs at 30 min and third panel shows 29 DEPs at 60 min after 1 µM-flg22 treatment averaged across three replicates. Fourth panel shows 17 DEPs at 60 min after 100 µM-CHX treatment averaged across three replicates. **(B)** Venn diagram shows overlap of upregulated and downregulated proteins in the total fraction after flg22 or CHX treatment at indicated time points.

Figure S11:

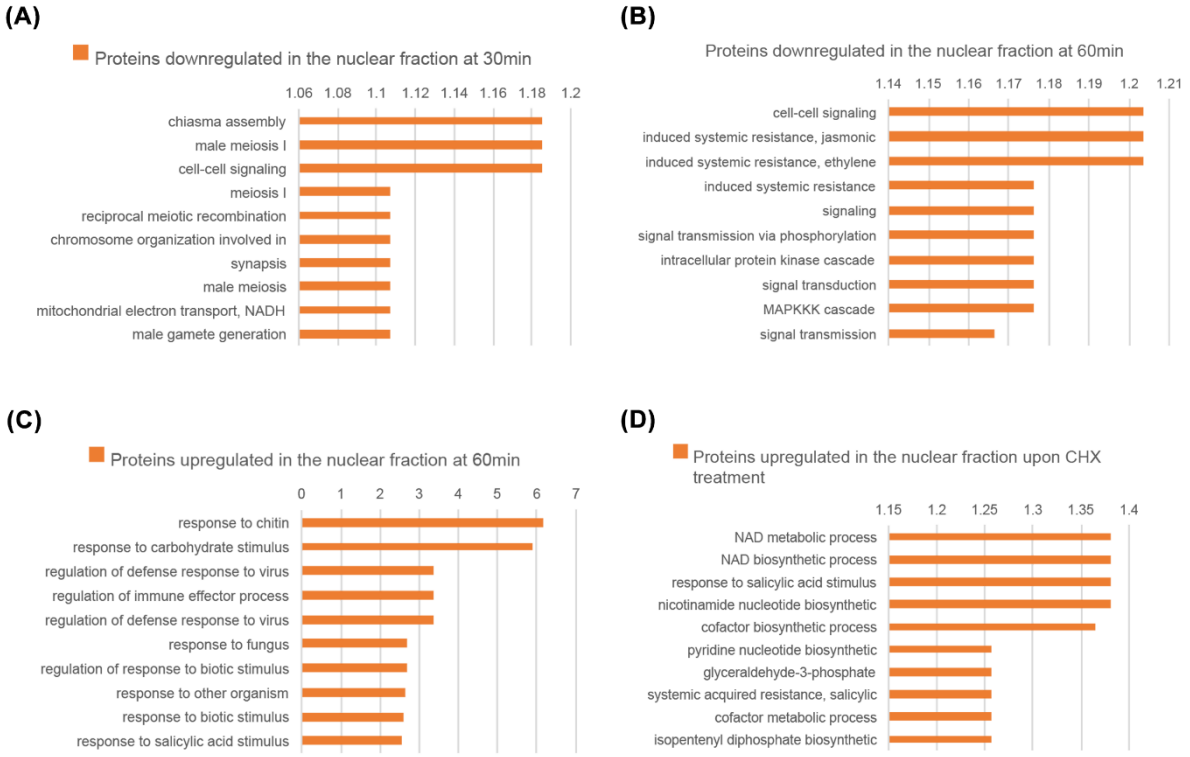

Figure S11: Early protein response to flg22 and CHX results in enrichment of different GO terms. Top ten GO terms are arranged according to their decreasing $-\log_{10}$ adjusted p-values for downregulated **(A, B)** and upregulated **(C, D)** proteins (|log2 fold change| > 1; p-value < 0.05) after 1 µM-flg22 treatment after 30, and 60 min or 100 µM-CHX treatment after 60min in the nuclear fraction. GO enrichment analysis was done with BingGO plugin for Cytoscape (FDR=0.1). As background a customized reference protein list was used which consisted of proteins that were detected at least twice in the flg22 or mock conditions in nuclear or total

6.2 Supplementary Tables

Table S1:

Table S1 (A): Correlation among replicates in the nuclear fraction at 3 h

Nuclear													
flg22 3h	flg 1	1.00											
	flg 2	0.95	1.00										
	flg 3	0.92	0.95	1.00									
	flg 4	0.90	0.90	0.88	1.00								
	flg 5	0.88	0.88	0.86	0.96	1.00							
	flg 6	0.87	0.88	0.86	0.93	0.96	1.00						
mock 3h	mock 1	0.92	0.92	0.91	0.89	0.86	0.85	1.00					
	mock 2	0.90	0.92	0.92	0.90	0.88	0.89	0.93	1.00				
	mock 3	0.90	0.93	0.94	0.87	0.85	0.85	0.93	0.96	1.00			
	mock 4	0.89	0.88	0.85	0.95	0.93	0.91	0.90	0.90	0.87	1.00		
	mock 5	0.88	0.88	0.86	0.94	0.95	0.93	0.90	0.91	0.88	0.97	1.00	
	mock6	0.89	0.89	0.86	0.95	0.95	0.93	0.90	0.91	0.88	0.97	0.97	1.00
		flg 1	flg 2	flg 3	flg 4	flg 5	flg 6	mock 1	mock 2	mock 3	mock 4	mock 5	mock6
		flg22 3h						mock 3h					
		Nuclear											

Table S1 (B): Correlation among replicates in the nuclear fraction at 9 h

Nuclear													
flg22 9h	flg 1	1.00											
	flg 2	0.98	1.00										
	flg 3	0.97	0.96	1.00									
	flg 4	0.93	0.93	0.92	1.00								
	flg 5	0.93	0.91	0.92	0.96	1.00							
	flg 6	0.91	0.89	0.91	0.94	0.97	1.00						
mock 9h	mock 1	0.84	0.84	0.82	0.84	0.82	0.80	1.00					
	mock 2	0.91	0.91	0.90	0.88	0.86	0.85	0.89	1.00				
	mock 3	0.93	0.93	0.92	0.88	0.87	0.86	0.86	0.93	1.00			
	mock 4	0.88	0.87	0.88	0.91	0.93	0.93	0.84	0.87	0.88	1.00		
	mock 5	0.87	0.86	0.86	0.90	0.92	0.92	0.85	0.88	0.87	0.96	1.00	
	mock6	0.90	0.89	0.90	0.91	0.93	0.92	0.83	0.89	0.91	0.95	0.94	1.00
		flg 1	flg 2	flg 3	flg 4	flg 5	flg 6	mock 1	mock 2	mock 3	mock 4	mock 5	mock6
		flg22 9h						mock 9h					
		Nuclear											

Table S1 (C): Correlation among replicates in the total fraction at 3 h

Total													
flg22 3h	flg 1	1.00											
	flg 2	0.96	1.00										
	flg 3	0.95	0.96	1.00									
	flg 4	0.93	0.93	0.93	1.00								
	flg 5	0.95	0.95	0.94	0.96	1.00							
	flg 6	0.95	0.95	0.95	0.95	0.97	1.00						
mock 3h	mock 1	0.96	0.95	0.95	0.92	0.93	0.94	1.00					
	mock 2	0.96	0.96	0.96	0.93	0.95	0.95	0.97	1.00				
	mock 3	0.96	0.96	0.96	0.92	0.94	0.95	0.96	0.97	1.00			
	mock 4	0.92	0.93	0.92	0.96	0.95	0.94	0.93	0.94	0.93	1.00		
	mock 5	0.92	0.92	0.93	0.95	0.96	0.95	0.92	0.94	0.93	0.96	1.00	
	mock6	0.93	0.93	0.93	0.93	0.94	0.95	0.94	0.95	0.94	0.94	0.94	1.00
		flg 1	flg 2	flg 3	flg 4	flg 5	flg 6	mock 1	mock 2	mock 3	mock 4	mock 5	mock6
		flg22 3h						mock 3h					
		Total											

Table S1 (D): Correlation among replicates in the total fraction at 9 h

Total													
flg22 9h	flg 1	1.00											
	flg 2	0.96	1.00										
	flg 3	0.963	0.961	1.00									
	flg 4	0.94	0.94	0.94	1.00								
	flg 5	0.94	0.95	0.95	0.95	1.00							
	flg 6	0.95	0.95	0.95	0.96	0.96	1.00						
mock 9h	mock 1	0.95	0.94	0.94	0.92	0.92	0.92	1.00					
	mock 2	0.95	0.95	0.95	0.92	0.92	0.93	0.97	1.00				
	mock 3	0.95	0.94	0.95	0.91	0.92	0.92	0.97	0.97	1.00			
	mock 4	0.934	0.931	0.929	0.946	0.934	0.943	0.953	0.951	0.947	1.00		
	mock 5	0.94	0.94	0.94	0.94	0.94	0.95	0.95	0.95	0.95	0.97	1.00	
	mock6	0.94	0.94	0.94	0.94	0.94	0.95	0.95	0.95	0.95	0.97	0.98	1.00
		flg 1	flg 2	flg 3	flg 4	flg 5	flg 6	mock 1	mock 2	mock 3	mock 4	mock 5	mock6
		flg22 9h						mock 9h					
		Total											

Table S1: Table showing level of correlation between samples for each treatment and replicate. LFQ intensities were used to calculate correlation (R^2 values) in Perseus (version 1.5.2.6). The R^2 values are indicated for nuclear fraction at 3 h **(A)**, & 9 h **(B)**, and total fraction at 3 h **(C)** & 9 h **(D)** after 1 µM-flg22 or mock treatment. Six replicates (protein samples were prepared in two different days each containing three replicates prepared from independent plant materials) were prepared for each condition.

Table S2:

Table S(A): Transcription factors differentially expressed in the nuclear fraction at 3h and/or 9h in response to flg22

Protein ID	Ratio[a]				Ratio[b]					SUBAcon	Description
	Proteome				Transcriptome						
	3h		9h								
	Nuc	Tot	Nuc	Tot	1h	2h	3h	5h	9h		
AT1G47900	-0.5	-22.8	-1.5	NA	-0.1	-0.2	-0.6	-0.3	-0.5	nucleus	Plant protein of unknown function (DUF869)
AT1G13260	2.6	NA	1.8	NA	-0.5	1.0	1.0	0.9	1.5	nucleus	related to ABI3/VP1 1 (RAV1)
AT4G18880	25.4	NA	2.1	NA	1.6	1.0	1.5	1.0	1.2	nucleus	heat shock transcription factor A4A
AT3G07780	1.0	NA	2.5	NA	0.6	0.7	0.8	0.7	0.4	plastid	Protein of unknown function (DUF1423/OBE1)
AT2G38470	3.6	23.5	2.7	NA	1.2	2.1	2.6	1.6	1.5	nucleus	WRKY DNA-binding protein 33
AT1G73805	0.5	NA	3.1	NA	0.5	0.0	0.1	0.6	0.7	nucleus	Calmodulin binding protein-like (SARD1)
AT4G01720	3.6	NA	5.2	NA	0.8	1.4	2.9	2.7	2.6	nucleus	WRKY family transcription factor 47
AT2G28550	-1.3	NA	-1.1	NA	-1.5	-0.9	-0.8	-0.9	-0.5	nucleus	related to AP2.7 (RAP2.7/TOE1)
AT1G68840	2.5	NA	26.0	NA	1.6	1.7	2.8	1.8	1.9	nucleus	related to ABI3/VP1 2 (RAV2)
AT5G48160	0.2	NA	2.6	22.1	-0.2	0.2	0.5	0.6	0.4	nucleus	Protein of unknown function (DUF1423/OBE2)
AT1G80840	4.3	25.1	25.8	NA	3.4	2.1	2.0	1.7	1.3	nucleus	WRKY DNA-binding protein 40
AT4G24240	1.6	23.2	3.8	23.9	1.2	1.7	3.3	2.6	2.2	nucleus	WRKY DNA-binding protein 7
AT4G31800	0.4	-0.3	2.7	22.7	0.6	0.4	1.1	1.3	1.8	nucleus	WRKY DNA-binding protein 18
AT5G08330	0.0	-0.5	-1.5	-24.2	-0.4	-0.9	-1.0	-1.3	-1.2	nucleus	TCP family transcription factor (TCP21)

Table S2(B): Transcription factors showing consitent presence/absence expression profile in the nuclear fraction at 3h and/or 9h

Protein ID	Ratio[a]				Ratio[b]					SUBAcon	Description
	Proteome				Transcriptome						
	3h		9h								
	Nuc	Tot	Nuc	Tot	1h	2h	3h	5h	9h		
AT2G25000	NA	NA	26.22	NA	-0.09	-0.07	1.38	1.57	1.72	nucleus	WRKY DNA-binding protein 60
AT2G42280	NA	NA	25.17	NA	-0.12	0.10	0.09	0.44	0.43	nucleus	basic helix-loop-helix (bHLH) DNA-binding superfamily protein
AT5G52830	NA	NA	25.88	NA	0.91	1.66	1.64	2.20	1.47	nucleus	WRKY DNA-binding protein 27
AT1G68520	NA	NA	-24.14	NA	-2.47	-2.58	-2.72	-2.25	-0.97	nucleus	B-box type zinc finger protein with CCT domain
AT4G23550	28.25	24.55	26.45	24.32	1.31	2.90	3.46	3.73	1.73	nucleus	WRKY family transcription factor
AT4G01250	28.13	NA	26.39	NA	2.24	3.24	4.04	3.49	2.35	nucleus	WRKY family transcription factor
AT5G64750	28.06	22.32	0.04	NA	0.69	1.85	3.16	3.34	1.50	nucleus	Integrase-type DNA-binding superfamily protein
AT1G62300	28.05	NA	27.33	NA	2.69	2.04	2.47	1.69	1.38	nucleus	WRKY family transcription factor
AT4G18880	25.38	NA	2.08	NA	1.61	1.05	1.46	0.99	1.16	nucleus	heat shock transcription factor A4A
AT2G30250	25.25	NA	25.19	NA	0.50	0.51	1.60	1.76	1.31	nucleus	WRKY DNA-binding protein 25
AT5G08790	24.98	0.68	24.60	-0.15	2.00	0.93	1.03	1.21	0.46	nucleus	NAC (No Apical Meristem) domain transcriptional regulator superfamily protein
AT1G10170	24.88	NA	0.03	NA	-0.39	0.27	0.28	0.64	0.13	nucleus	NF-X-like 1
AT4G18170	24.56	NA	NA	NA	1.87	1.03	1.37	1.06	0.33	nucleus	WRKY DNA-binding protein 28
AT5G15130	23.21	NA	24.77	NA	0.19	NA	NA	NA	1.44	nucleus	WRKY DNA-binding protein 72
AT1G80840	4.26	25.14	25.84	NA	3.43	2.07	2.01	1.72	1.29	nucleus	WRKY DNA-binding protein 40
AT1G68840	2.51	NA	25.99	NA	1.56	1.74	2.82	1.82	1.94	nucleus	related to ABI3/VP1 2
AT2G43010	-0.12	NA	-24.28	NA	-0.82	-1.00	-1.62	-2.23	-1.37	nucleus	phytochrome interacting factor 4
AT2G22540	-23.86	NA	-0.25	NA	-0.62	-1.91	-1.23	-1.33	-0.77	nucleus	K-box region and MADS-box transcription factor family protein
AT4G23810	-24.48	NA	24.71	NA	0.86	1.53	2.26	1.79	2.27	nucleus	WRKY family transcription factor
AT3G61150	-24.76	NA	24.83	NA	-0.12	0.45	0.97	0.32	0.05	nucleus	homeodomain GLABROUS 1

Table S2: Transcription factors detected in the nuclear protein fractions. The transcription factors (TFs) detected during LC-MS/MS at 3 h and/or 9 h after 1 µM-flg22 or mock treatment was identified using the PlantTFDB 4.0 database. **(A)** The TFs differentially expressed ($|\log_2$ fold change$| > 1$; q-value<0.05) in the nuclear fraction at 3 h and/or 9 h. **(B)** TFs showing consistent presence/absence pattern in the nuclear fraction at 3 h and/or 9 h. The TFs which are consistently present in flg22 samples (in at least five replicates) and absent (in at least five replicates) in mock are defined as “TFs Increased” and vice-versa (as “TFs Decreased”).

Table S3:

Table S3 (A): Differentially expressed proteins in nuclear fraction at 3 h

Protein ID	Ratio[a]				Ratio[b]					SUBAcon	Description
	Proteome				Transcriptome						
	3h		9h								
	Nuc	Tot	Nuc	Tot	1h	2h	3h	5h	9h		
AT5G52640	5.7	4.2	5.4	3.9	0.1	2.9	3.7	1.9	1.0	cytosol	heat shock protein 90.1
AT3G12580	4.4	3.6	2.9	2.9	0.2	2.9	3.3	0.9	0.5	cytosol	heat shock protein 70
AT1G80840	4.3	25.1	25.8	NA	3.4	2.1	2.0	1.7	1.3	nucleus	WRKY DNA-binding protein 40
AT1G51800	4.1	1.5	6.0	3.1	3.0	3.0	4.7	5.2	4.7	plasma membrane	Leucine-rich repeat protein kinase family protein
AT1G51820	4.1	2.9	27.7	27.0	2.8	2.7	3.6	3.5	NA	plasma membrane	Leucine-rich repeat protein kinase family protein
AT1G23170	3.7	4.0	5.7	4.9	0.4	1.9	2.5	1.3	0.1	cytosol	Protein of unknown function DUF2359, transmembrane
AT4G01720	3.6	NA	5.2	NA	0.8	1.4	2.9	2.7	2.6	nucleus	WRKY family transcription factor
AT2G38470	3.6	23.5	2.7	NA	1.2	2.1	2.6	1.6	1.5	nucleus	WRKY DNA-binding protein 33
AT2G37040	3.5	2.6	1.4	3.0	1.9	3.0	4.0	3.7	3.7	cytosol	PHE ammonia lyase 1
AT2G27660	3.4	26.4	4.8	26.0	3.1	3.0	4.1	3.4	2.9	nucleus	Cysteine/Histidine-rich C1 domain family protein
AT4G01700	2.8	2.2	3.2	3.0	3.3	3.9	5.2	5.3	4.0	extracellular	Chitinase family protein
AT2G39210	2.6	1.2	4.1	4.1	1.2	1.5	3.5	4.4	3.6	plasma membrane	Major facilitator superfamily protein
AT3G13790	2.5	0.7	3.7	2.0	0.5	2.0	2.7	3.4	3.9	extracellular	Glycosyl hydrolases family 32 protein
AT1G68840	2.5	NA	26.0	NA	1.6	1.7	2.8	1.8	1.9	nucleus	related to ABI3/VP1 2
AT3G53180	2.3	0.5	2.6	1.1	1.9	2.0	2.1	1.9	1.4	cytosol	glutamate-ammonia ligases;catalytics;glutamate-ammonia ligases
AT3G01830	2.3	25.5	26.8	25.5	3.2	3.0	3.2	2.6	2.1	nucleus	Calcium-binding EF-hand family protein
AT1G52200	2.3	25.7	27.0	26.5	1.6	2.5	4.7	4.8	4.2	plasma membrane	PLAC8 family protein
AT5G25260	2.2	3.6	4.4	5.1	1.9	2.6	3.8	3.7	2.9	cytosol	SPFH/Band 7/PHB domain-containing membrane-associated protein family
AT3G50480	2.2	3.2	29.8	5.4	1.4	1.5	2.2	3.3	3.0	cytosol	homolog of RPW8 4
AT2G18690	1.7	1.2	2.0	1.7	2.0	2.1	2.8	3.3	3.4	plasma membrane	
AT5G54710	1.6	24.4	2.4	23.9	1.3	2.0	2.8	2.1	1.7	plasma membrane	Ankyrin repeat family protein
AT5G40780	1.4	1.8	2.6	2.8	1.7	1.4	2.1	3.6	4.0	plasma membrane	lysine histidine transporter 1
AT4G36670	1.4	25.3	28.3	27.8	0.9	1.5	3.0	4.5	4.8	plasma membrane	Major facilitator superfamily protein
AT3G62150	1.3	0.6	0.6	0.9	1.4	2.0	2.3	1.5	0.5	plasma membrane	P-glycoprotein 21
AT2G20960	1.1	1.2	0.8	0.5	2.6	2.2	2.4	1.6	1.1	nucleus	Arabidopsis phospholipase-like protein (PEARLI 4) family
AT1G65390	1.0	1.0	2.3	3.4	1.9	1.8	3.5	4.5	3.7	plastid	phloem protein 2 A5
AT2G28550	-1.3	NA	-1.1	NA	-1.5	-0.9	-0.8	-0.9	-0.5	nucleus	related to AP2.7
AT1G71040	-1.6	-0.1	-0.7	0.0	0.0	-0.2	-0.2	0.6	1.2	extracellular	Cupredoxin superfamily protein
AT1G03230	-1.9	0.1	-1.5	-0.3	0.7	0.2	0.0	0.0	-0.3	extracellular	Eukaryotic aspartyl protease family protein
AT5G62340	-1.9	-0.2	-2.0	-0.7	NA	NA	NA	NA	NA	extracellular	Plant invertase/pectin methylesterase inhibitor superfamily protein

Table S3 (B) Differentially expressed proteins in nuclear fraction at 9 h

Protein ID	Ratio[a]				Ratio[b]					SUBAcon	Description
	Proteome				Transcriptome						
	3h		9h								
	Nuc	Tot	Nuc	Tot	1h	2h	3h	5h	9h		
AT1G51800	4.1	1.5	6.0	3.1	3.0	3.0	4.7	5.2	4.7	plasma membrane	Leucine-rich repeat protein kinase family protein
AT1G23170	3.7	4.0	5.7	4.9	0.4	1.9	2.5	1.3	0.1	cytosol	Protein of unknown function DUF2359, transmembrane
AT5G52640	5.7	4.2	5.4	3.9	0.1	2.9	3.7	1.9	1.0	cytosol	heat shock protein 90.1
AT4G01720	3.6	NA	5.2	NA	0.8	1.4	2.9	2.7	2.6	nucleus	WRKY family transcription factor
AT2G27660	3.4	26.4	4.8	26.0	3.1	3.0	4.1	3.4	2.9	nucleus	Cysteine/Histidine-rich C1 domain family protein
AT3G05500	0.4	0.9	4.6	5.6	0.2	0.4	0.7	1.5	3.2	cytosol	Rubber elongation factor protein (REF)
AT5G25260	2.2	3.6	4.4	5.1	1.9	2.6	3.8	3.7	2.9	cytosol	SPFH/Band 7/PHB domain-containing membrane-associated protein family
AT1G66090	27.5	4.2	4.1	27.0	1.6	2.6	1.4	1.6	1.4	plastid	Disease resistance protein (TIR-NBS class)
AT2G39210	2.6	1.2	4.1	4.1	1.2	1.5	3.5	4.4	3.6	plasma membrane	Major facilitator superfamily protein
AT5G61560	2.3	22.7	3.9	23.4	1.6	2.6	3.5	3.2	2.0	nucleus	U-box domain-containing protein kinase family protein
AT4G24240	1.6	23.2	3.8	23.9	1.2	1.7	3.3	2.6	2.2	nucleus	WRKY DNA-binding protein 7
AT2G20010	1.0	1.0	3.8	1.5	1.1	1.2	1.5	1.3	0.5	nucleus	Protein of unknown function (DUF810)
AT2G17720	1.7	0.7	3.7	2.3	0.9	1.3	1.9	2.3	2.3	endoplasmic reticulum	2-oxoglutarate (2OG) and Fe(II)-dependent oxygenase superfamily protein
AT3G13790	2.5	0.7	3.7	2.0	0.5	2.0	2.7	3.4	3.9	extracellular	Glycosyl hydrolases family 32 protein
AT5G02490	2.5	2.5	3.5	4.0	0.4	2.0	3.0	2.3	2.1	cytosol	Heat shock protein 70 (Hsp 70) family protein
AT4G24690	0.2	NA	3.4	26.9	-0.2	-0.2	0.3	0.6	1.7	nucleus	ubiquitin-associated (UBA)/TS-N domain-containing protein / octicosapeptide/Phox/Bemp1 (PB1) domain-containing protein
AT3G52400	2.2	2.0	3.3	2.9	1.6	1.7	3.6	2.9	2.3	plasma membrane	syntaxin of plants 122
AT4G01700	2.8	2.2	3.2	3.0	3.3	3.9	5.2	5.3	4.0	extracellular	Chitinase family protein
AT1G73805	0.5	NA	3.1	NA	0.5	0.0	0.1	0.6	0.7	nucleus	Calmodulin binding protein-like
AT5G26340	1.7	1.7	3.0	26.8	1.9	1.6	2.4	2.6	2.8	plasma membrane	Major facilitator superfamily protein
AT1G14740	1.1	NA	2.9	24.5	0.5	0.7	1.5	1.3	1.3	nucleus	Protein of unknown function (DUF1423)
AT3G12580	4.4	3.6	2.9	2.9	0.2	2.9	3.3	0.9	0.5	cytosol	heat shock protein 70
AT5G48540	2.6	1.3	2.8	1.7	2.8	3.1	3.9	3.8	3.1	extracellular	receptor-like protein kinase-related family protein
AT4G31800	0.4	-0.3	2.7	22.7	0.6	0.4	1.1	1.3	1.8	nucleus	WRKY DNA-binding protein 18
AT2G22500	1.2	1.1	2.7	1.4	1.2	1.0	1.7	1.9	1.7	mitochondrion	uncoupling protein 5

AT4G11890	24.9	24.0	2.7	25.6	2.1	2.0	2.2	2.5	2.4	cytosol	Protein kinase superfamily protein
AT2G38470	3.6	23.5	2.7	NA	1.2	2.1	2.6	1.6	1.5	nucleus	WRKY DNA-binding protein 33
AT3G53180	2.3	0.5	2.6	1.1	1.9	2.0	2.1	1.9	1.4	cytosol	glutamate-ammonia ligases;catalytics;glutamate-ammonia ligases
AT5G40780	1.4	1.8	2.6	2.8	1.7	1.4	2.1	3.6	4.0	plasma membrane	lysine histidine transporter 1
AT3G19930	0.6	24.6	2.6	2.7	0.5	1.1	1.9	2.4	2.1	plasma membrane	sugar transporter 4
AT5G48160	0.2	NA	2.6	22.1	-0.2	0.2	0.5	0.6	0.4	nucleus	Protein of unknown function (DUF1423)
AT5G54160	0.8	0.5	2.6	1.5	1.3	2.1	2.5	4.0	4.1	cytosol	O-methyltransferase 1
AT3G07780	1.0	NA	2.5	NA	0.6	0.7	0.8	0.7	0.4	plastid	Protein of unknown function (DUF1423)
AT5G54710	1.6	24.4	2.4	23.9	1.3	2.0	2.8	2.1	1.7	plasma membrane	Ankyrin repeat family protein
AT4G23190	1.2	1.4	2.3	26.0	2.8	2.2	2.7	2.5	1.4	plasma membrane	cysteine-rich RLK (RECEPTOR-like protein kinase) 11
AT5G25250	1.2	1.2	2.3	0.1	1.7	2.0	3.3	3.2	2.1	cytosol	SPFH/Band 7/PHB domain-containing membrane-associated protein family
AT1G65390	1.0	1.0	2.3	3.4	1.9	1.8	3.5	4.5	3.7	plastid	phloem protein 2 A5
AT4G02880	0.4	NA	2.2	22.8	0.2	0.2	-0.1	0.3	0.7	cytosol	
AT3G29400	1.6	-0.2	2.2	1.4	1.0	1.2	1.5	1.5	0.6	cytosol	exocyst subunit exo70 family protein E1
AT3G26210	23.1	0.7	2.1	4.1	1.7	0.7	1.7	2.1	2.4	endoplasmic reticulum	cytochrome P450, family 71, subfamily B, polypeptide 23
AT5G51070	1.1	0.8	2.1	1.2	1.1	1.1	0.6	0.6	0.4	plastid	Clp ATPase
AT2G37710	1.0	0.9	2.1	1.8	1.8	2.0	2.9	3.2	2.5	plasma membrane	receptor lectin kinase
AT5G47120	1.3	23.3	2.1	24.2	0.7	1.3	1.8	2.0	2.1	endoplasmic reticulum	BAX inhibitor 1
AT4G18880	25.4	NA	2.1	NA	1.6	1.0	1.5	1.0	1.2	nucleus	heat shock transcription factor A4A
AT5G54720	0.8	1.3	2.0	1.7	0.6	0.6	0.8	0.5	NA	cytosol	Ankyrin repeat family protein
AT1G11260	0.8	0.3	2.0	1.7	0.4	1.2	2.6	3.7	3.8	plasma membrane	sugar transporter 1
AT2G18690	1.7	1.2	2.0	1.7	2.0	2.1	2.8	3.3	3.4	plasma membrane	
AT1G22410	1.1	0.7	1.9	1.2	2.4	2.3	2.2	2.5	2.3	plastid	Class-II DAHP synthetase family protein
AT1G34260	0.2	NA	1.9	23.4	0.9	0.9	1.1	1.4	0.6	nucleus	FORMS APLOID AND BINUCLEATE CELLS 1A
AT5G61210	1.0	1.0	1.8	1.2	1.4	1.1	2.1	2.0	1.1	nucleus	soluble N-ethylmaleimide-sensitive factor adaptor protein 33
AT3G06300	0.5	0.8	1.8	1.1	0.7	1.1	1.6	1.4	1.5	extracellular	P4H isoform 2
AT1G13260	2.6	NA	1.8	NA	-0.5	1.0	1.0	0.9	1.5	nucleus	related to ABI3/VP1 1
AT4G08850	0.7	0.7	1.5	1.7	1.8	1.7	3.2	3.2	2.9	plasma membrane	Leucine-rich repeat receptor-like protein kinase family protein
AT1G70520	0.8	0.5	1.5	2.0	1.6	1.7	2.7	2.0	1.3	extracellular	cysteine-rich RLK (RECEPTOR-like protein kinase) 2
AT4G33050	0.9	1.7	1.5	0.8	2.0	2.4	4.1	3.0	1.8	cytosol	calmodulin-binding family protein
AT5G05190	0.7	23.9	1.5	24.3	3.3	3.0	4.0	3.3	2.5	nucleus	Protein of unknown function (DUF3133)
AT4G30600	0.4	0.5	1.5	2.3	0.5	0.4	0.6	1.2	0.8	endoplasmic reticulum	signal recognition particle receptor alpha subunit family protein

AT1G12110	-1.3	24.0	1.4	24.5	-0.8	-0.9	-0.7	0.5	2.0	plasma membrane	nitrate transporter 1.1
AT2G30490	0.7	0.6	1.4	1.2	2.7	2.5	3.2	4.2	3.6	endoplasmic reticulum	cinnamate-4-hydroxylase
AT3G45620	0.1	22.6	1.4	0.6	-0.1	-0.1	0.1	0.5	0.4	nucleus	Transducin/WD40 repeat-like superfamily protein
AT4G18950	1.5	0.8	1.2	0.9	2.4	1.4	2.7	2.6	1.0	nucleus	Integrin-linked protein kinase family
AT5G44290	1.4	-0.7	1.2	0.9	1.2	1.6	2.0	2.0	1.3	nucleus	Protein kinase superfamily protein
AT5G09420	-0.2	0.4	1.2	1.1	1.0	0.3	0.4	0.2	0.7	mitochondrion	translocon at the outer membrane of chloroplasts 64-V
AT4G30190	0.2	0.1	1.1	1.4	0.3	1.9	3.1	4.1	3.6	plasma membrane	H(+)-ATPase 2
AT4G33910	0.3	NA	1.1	23.7	0.7	1.0	1.1	1.1	0.7	golgi	2-oxoglutarate (2OG) and Fe(II)-dependent oxygenase superfamily protein
AT1G13110	0.3	0.3	1.1	1.3	1.7	1.9	3.5	3.2	2.3	endoplasmic reticulum	cytochrome P450, family 71 subfamily B, polypeptide 7
AT1G71880	-0.5	-0.6	1.1	0.9	-1.0	-0.6	0.5	1.5	2.2	plasma membrane	sucrose-proton symporter 1
AT1G14880	-0.1	0.2	1.1	0.4	0.0	-0.4	-0.4	0.3	1.1	plasma membrane	PLANT CADMIUM RESISTANCE 1
AT3G48570	0.2	-0.5	1.1	0.4	0.9	1.4	2.1	2.3	2.1	cytosol	secE/sec61-gamma protein transport protein
AT2G41100	0.7	0.5	1.0	1.3	1.2	1.0	1.8	1.8	1.8	nucleus	Calcium-binding EF hand family protein
AT4G01090	0.1	NA	1.0	NA	0.6	1.1	1.4	0.9	0.8	nucleus	Protein of unknown function (DUF3133)
AT3G05970	0.5	0.0	1.0	0.5	-0.3	-0.3	0.0	0.5	0.6	peroxisome	long-chain acyl-CoA synthetase 6
AT4G38550	0.9	1.3	1.0	1.3	1.6	1.8	3.6	2.2	1.2	nucleus	Arabidopsis phospholipase-like protein (PEARLI 4) family
AT3G04210	-0.2	-0.3	-1.0	-0.3	0.3	-0.5	-0.2	-1.0	-0.9	plasma membrane	Disease resistance protein (TIR-NBS class)
AT4G24780	-1.0	-0.1	-1.0	-0.5	-0.5	0.5	0.4	-0.3	-1.0	extracellular	Pectin lyase-like superfamily protein
AT4G04340	-0.9	-0.8	-1.1	-1.0	-0.8	-2.5	-2.4	-2.4	-1.2	plasma membrane	ERD (early-responsive to dehydration stress) family protein
AT5G25460	-0.4	-0.1	-1.1	-0.3	-1.0	-1.4	-1.0	-1.8	-2.1	extracellular	Protein of unknown function, DUF642
AT2G36870	-1.3	0.1	-1.1	-1.1	-0.6	-0.7	-1.0	-0.8	-0.5	extracellular	xyloglucan endotransglucosylase/hydrolase 32
AT1G48570	0.0	-0.2	-1.2	-0.4	-0.2	-0.4	-0.9	-0.6	0.0	plastid	zinc finger (Ran-binding) family protein
AT5G49720	-0.3	-0.4	-1.2	-1.1	-1.7	-0.8	-0.6	-0.7	-0.5	cytosol	glycosyl hydrolase 9A1
AT2G16280	-0.5	-0.6	-1.3	-0.9	-1.0	-0.7	-0.9	-0.8	-0.9	plasma membrane	3-ketoacyl-CoA synthase 9
AT3G27180	-0.1	-0.3	-1.3	-0.3	-0.1	-0.2	-0.6	-1.0	-0.5	plastid	S-adenosyl-L-methionine-dependent methyltransferases superfamily protein
AT4G22690	-0.1	0.0	-1.3	-1.9	1.5	-0.3	0.5	-1.0	-1.0	endoplasmic reticulum	cytochrome P450, family 706, subfamily A, polypeptide 1
AT5G23210	-0.5	0.1	-1.3	-0.2	-0.7	-0.7	-0.8	-1.4	-1.1	extracellular	serine carboxypeptidase-like 34
AT3G61820	-0.8	-0.1	-1.3	-0.4	-0.9	-0.4	-0.1	-0.7	-0.4	extracellular	Eukaryotic aspartyl protease family protein
AT5G13630	-0.4	-0.6	-1.4	-1.3	-0.4	-0.7	-2.0	-2.8	-1.6	plastid	magnesium-chelatase subunit chlH, chloroplast, putative / Mg-protoporphyrin IX chelatase, putative (CHLH)
AT5G14060	0.0	-0.1	-1.4	-0.9	-0.1	-0.4	-1.5	-1.6	-0.9	plastid	Aspartate kinase family protein
AT4G34980	-0.6	-0.2	-1.4	-0.6	-1.0	-1.8	-1.5	-1.4	-1.5	extracellular	subtilisin-like serine protease 2

AT2G39670	-0.3	-0.1	-1.4	-0.9	-0.3	-0.4	-1.1	-1.0	-0.4	plastid	Radical SAM superfamily protein
AT3G06980	0.0	-0.2	-1.5	-1.7	0.1	-0.4	-1.2	-1.6	-1.2	nucleus	DEA(D/H)-box RNA helicase family protein
AT3G47960	-0.7	-0.5	-1.5	-0.7	-0.4	0.4	-0.3	-0.4	-0.1	plasma membrane	Major facilitator superfamily protein
AT5G08330	0.0	-0.5	-1.5	-24.2	-0.4	-0.9	-1.0	-1.3	-1.2	nucleus	TCP family transcription factor
AT5G64840	-1.2	-0.5	-1.5	-1.5	-0.3	-0.9	-0.7	-0.7	0.2	mitochondrion	general control non-repressible 5
AT1G47900	-0.5	-22.8	-1.5	NA	-0.1	-0.2	-0.6	-0.3	-0.5	nucleus	Plant protein of unknown function (DUF869)
AT3G02060	-0.2	NA	-1.6	25.5	-0.4	-0.7	-1.2	-1.0	-0.6	plastid	DEAD/DEAH box helicase, putative
AT1G73600	0.2	-0.1	-1.8	-0.8	NA	0.1	0.0	0.0	-0.2	cytosol	S-adenosyl-L-methionine-dependent methyltransferases superfamily protein
AT3G18390	-0.5	-0.3	-1.9	-0.7	-0.3	-0.6	-1.1	-2.0	-1.4	plastid	CRS1 / YhbY (CRM) domain-containing protein
AT5G62340	-1.9	-0.2	-2.0	-0.7	NA	NA	NA	NA	NA	extracellular	Plant invertase/pectin methylesterase inhibitor superfamily protein
AT3G07010	-1.4	-0.2	-2.2	-0.9	-0.3	-0.2	-0.1	-0.5	-1.1	extracellular	Pectin lyase-like superfamily protein
AT1G01300	-0.7	-0.4	-2.2	-0.6	-1.0	-1.1	-0.7	-0.6	-0.4	extracellular	Eukaryotic aspartyl protease family protein
AT1G68560	-0.8	-0.1	-2.4	-0.4	-1.5	-2.7	-2.4	-2.1	-1.3	extracellular	alpha-xylosidase 1
AT3G18080	-0.6	-0.2	-2.6	-0.5	-0.1	-1.5	-2.1	-2.7	-2.1	extracellular	B-S glucosidase 44
AT5G62350	-2.2	-0.3	-2.6	-0.8	-1.4	-1.3	-1.2	-2.2	-1.3	extracellular	Plant invertase/pectin methylesterase inhibitor superfamily protein
AT3G09210	-0.3	-0.3	-2.6	-0.8	-0.5	-0.8	-1.0	-1.5	-0.5	plastid	plastid transcriptionally active 13
AT2G05920	-1.2	-0.3	-2.7	-0.4	-1.0	-1.0	-1.4	-1.3	-1.3	extracellular	Subtilase family protein
AT1G76160	-1.6	-0.1	-4.0	-0.5	-1.1	0.1	0.8	0.8	0.6	extracellular	SKU5 similar 5

Table S3 (C): Differentially expressed proteins in total fraction at 3 h

Protein ID	Ratio[a]				Ratio[b]					SUBAcon	Description
	Proteome				Transcriptome						
	3h		9h								
	Nuc	Tot	Nuc	Tot	1h	2h	3h	5h	9h		
AT5G64120	28.5	5.4	27.8	7.7	3.6	3.3	4.3	6.1	7.1	extracellular	Peroxidase superfamily protein
AT5G52640	5.7	4.2	5.4	3.9	0.1	2.9	3.7	1.9	1.0	cytosol	heat shock protein 90.1
AT1G66090	27.5	4.2	4.1	27.0	1.6	2.6	1.4	1.6	1.4	plastid	Disease resistance protein (TIR-NBS class)
AT1G23170	3.7	4.0	5.7	4.9	0.4	1.9	2.5	1.3	0.1	cytosol	Protein of unknown function DUF2359, transmembrane
AT3G12580	4.4	3.6	2.9	2.9	0.2	2.9	3.3	0.9	0.5	cytosol	heat shock protein 70
AT5G25260	2.2	3.6	4.4	5.1	1.9	2.6	3.8	3.7	2.9	cytosol	SPFH/Band 7/PHB domain-containing membrane-associated protein family
AT4G20860	24.4	3.3	23.2	4.7	2.7	3.1	4.5	5.1	4.6	plasma membrane	FAD-binding Berberine family protein
AT4G15610	24.1	3.2	25.0	3.0	1.6	1.9	2.1	2.6	2.3	plasma membrane	Uncharacterised protein family (UPF0497)
AT3G50480	2.2	3.2	29.8	5.4	1.4	1.5	2.2	3.3	3.0	cytosol	homolog of RPW8 4
AT2G43620	26.5	3.1	26.2	5.0	4.3	3.4	3.1	4.0	6.0	extracellular	Chitinase family protein
AT5G50200	3.1	3.0	30.0	4.7	2.6	2.8	3.6	4.4	4.4	extracellular	nitrate transmembrane transporters
AT1G51820	4.1	2.9	27.7	27.0	2.8	2.7	3.6	3.5	NA	plasma membrane	Leucine-rich repeat protein kinase family protein
AT2G37040	3.5	2.6	1.4	3.0	1.9	3.0	4.0	3.7	3.7	cytosol	PHE ammonia lyase 1
AT1G71697	1.5	2.5	0.3	2.5	1.7	1.6	2.4	2.3	1.7	golgi	choline kinase 1
AT5G02490	2.5	2.5	3.5	4.0	0.4	2.0	3.0	2.3	2.1	cytosol	Heat shock protein 70 (Hsp 70) family protein
AT2G40000	26.0	2.3	24.7	23.1	1.9	1.5	2.0	0.6	0.8	nucleus	ortholog of sugar beet HS1 PRO-1 2
AT4G01700	2.8	2.2	3.2	3.0	3.3	3.9	5.2	5.3	4.0	extracellular	Chitinase family protein
AT3G53260	25.5	2.0	NA	0.6	2.4	2.2	2.1	1.4	1.4	cytosol	phenylalanine ammonia-lyase 2
AT1G02930	23.5	1.7	24.2	2.8	1.7	1.6	2.8	3.8	3.3	cytosol	glutathione S-transferase 6
AT3G22060	26.4	1.6	25.5	2.1	3.6	3.4	3.6	3.8	3.2	extracellular	Receptor-like protein kinase-related family protein
AT3G25780	NA	1.6	NA	1.3	1.7	1.3	0.3	0.6	1.0	plastid	allene oxide cyclase 3
AT1G51800	4.1	1.5	6.0	3.1	3.0	3.0	4.7	5.2	4.7	plasma membrane	Leucine-rich repeat protein kinase family protein
AT5G48540	2.6	1.3	2.8	1.7	2.8	3.1	3.9	3.8	3.1	extracellular	receptor-like protein kinase-related family protein
AT3G51660	NA	1.3	NA	1.8	1.5	1.5	2.4	2.8	2.0	peroxisome	Tautomerase/MIF superfamily protein
AT2G18690	1.7	1.2	2.0	1.7	2.0	2.1	2.8	3.3	3.4	plasma membrane	
AT5G48570	NA	1.2	23.2	26.4	0.5	4.0	4.1	0.2	0.1	cytosol	FKBP-type peptidyl-prolyl cis-trans isomerase family protein
AT4G36500	0.5	1.2	0.5	-0.1	1.6	1.2	1.5	0.4	0.1	mitochondrion	
AT1G76680	NA	1.0	NA	1.0	0.7	1.0	2.1	0.7	0.0	cytosol	12-oxophytodienoate reductase 1
AT4G21960	-24.8	-1.7	-27.6	-2.1	-0.9	-1.8	-2.7	-2.6	-2.2	extracellular	Peroxidase superfamily protein

Table S3 (D): Differentially expressed proteins in total fraction at 9 h

Protein ID	Ratio[a]				Ratio[b]					SUBAcon	Description
	Proteome				Transcriptome						
	3h		9h								
	Nuc	Tot	Nuc	Tot	1h	2h	3h	5h	9h		
AT5G64120	28.5	5.4	27.8	7.7	3.6	3.3	4.3	6.1	7.1	extracellular	Peroxidase superfamily protein
AT3G05500	0.4	0.9	4.6	5.6	0.2	0.4	0.7	1.5	3.2	cytosol	Rubber elongation factor protein (REF)
AT3G50480	2.2	3.2	29.8	5.4	1.4	1.5	2.2	3.3	3.0	cytosol	homolog of RPW8 4
AT5G25260	2.2	3.6	4.4	5.1	1.9	2.6	3.8	3.7	2.9	cytosol	SPFH/Band 7/PHB domain-containing membrane-associated protein family
AT2G43620	26.5	3.1	26.2	5.0	4.3	3.4	3.1	4.0	6.0	extracellular	Chitinase family protein
AT1G23170	3.7	4.0	5.7	4.9	0.4	1.9	2.5	1.3	0.1	cytosol	Protein of unknown function DUF2359, transmembrane
AT5G50200	3.1	3.0	30.0	4.7	2.6	2.8	3.6	4.4	4.4	extracellular	nitrate transmembrane transporters
AT4G20860	24.4	3.3	23.2	4.7	2.7	3.1	4.5	5.1	4.6	plasma membrane	FAD-binding Berberine family protein
AT2G39210	2.6	1.2	4.1	4.1	1.2	1.5	3.5	4.4	3.6	plasma membrane	Major facilitator superfamily protein
AT2G38870	NA	2.1	NA	4.1	3.2	3.0	3.6	4.5	4.8	cytosol	Serine protease inhibitor, potato inhibitor I-type family protein
AT5G02490	2.5	2.5	3.5	4.0	0.4	2.0	3.0	2.3	2.1	cytosol	Heat shock protein 70 (Hsp 70) family protein
AT5G52640	5.7	4.2	5.4	3.9	0.1	2.9	3.7	1.9	1.0	cytosol	heat shock protein 90.1
AT3G29034	24.5	2.2	23.2	3.5	2.1	2.5	3.8	3.8	3.2	cytosol	
AT1G65390	1.0	1.0	2.3	3.4	1.9	1.8	3.5	4.5	3.7	plastid	phloem protein 2 A5
AT1G51800	4.1	1.5	6.0	3.1	3.0	3.0	4.7	5.2	4.7	plasma membrane	Leucine-rich repeat protein kinase family protein
AT5G19230	NA	1.9	NA	3.0	2.3	2.3	3.2	3.0	2.8	extracellular	Glycoprotein membrane precursor GPI-anchored
AT4G01700	2.8	2.2	3.2	3.0	3.3	3.9	5.2	5.3	4.0	extracellular	Chitinase family protein
AT4G15610	24.1	3.2	25.0	3.0	1.6	1.9	2.1	2.6	2.3	plasma membrane	Uncharacterised protein family (UPF0497)
AT4G23210	3.1	25.5	29.6	3.0	1.2	1.7	2.2	3.2	3.8	plasma membrane	cysteine-rich RLK (RECEPTOR-like protein kinase) 13
AT2G37040	3.5	2.6	1.4	3.0	1.9	3.0	4.0	3.7	3.7	cytosol	PHE ammonia lyase 1
AT3G52400	2.2	2.0	3.3	2.9	1.6	1.7	3.6	2.9	2.3	plasma membrane	syntaxin of plants 122
AT3G12580	4.4	3.6	2.9	2.9	0.2	2.9	3.3	0.9	0.5	cytosol	heat shock protein 70
AT5G40780	1.4	1.8	2.6	2.8	1.7	1.4	2.1	3.6	4.0	plasma membrane	lysine histidine transporter 1
AT1G02930	23.5	1.7	24.2	2.8	1.7	1.6	2.8	3.8	3.3	cytosol	glutathione S-transferase 6
AT5G21900	26.9	1.1	NA	2.8	0.1	0.2	0.2	0.5	0.6	nucleus	RNI-like superfamily protein
AT1G27020	NA	-0.2	NA	2.8	0.5	-0.2	0.4	1.2	2.4	cytosol	
AT3G19930	0.6	24.6	2.6	2.7	0.5	1.1	1.9	2.4	2.1	plasma membrane	sugar transporter 4
AT1G22400	NA	1.9	NA	2.6	1.3	2.4	1.5	1.7	1.9	cytosol	UDP-Glycosyltransferase superfamily protein

AT1G71697	1.5	2.5	0.3	2.5	1.7	1.6	2.4	2.3	1.7	golgi	choline kinase 1
AT1G28380	0.9	1.3	-0.7	2.4	1.6	1.7	2.5	1.8	1.2	cytosol	MAC/Perforin domain-containing protein
AT5G55050	NA	1.1	NA	2.3	0.2	1.5	2.1	2.5	2.2	extracellular	GDSL-like Lipase/Acylhydrolase superfamily protein
AT2G17720	1.7	0.7	3.7	2.3	0.9	1.3	1.9	2.3	2.3	endoplasmic reticulum	2-oxoglutarate (2OG) and Fe(II)-dependent oxygenase superfamily protein
AT4G34230	NA	1.1	NA	2.3	0.8	1.5	2.2	3.1	2.9	cytosol	cinnamyl alcohol dehydrogenase 5
AT4G30600	0.4	0.5	1.5	2.3	0.5	0.4	0.6	1.2	0.8	endoplasmic reticulum	signal recognition particle receptor alpha subunit family protein
AT4G23570	0.8	1.5	0.9	2.3	0.5	2.2	1.8	0.9	1.0	cytosol	phosphatase-related
AT3G50930	1.5	1.3	1.3	2.2	1.5	0.8	0.1	0.8	0.7	mitochondrion	cytochrome BC1 synthesis
AT3G22060	26.4	1.6	25.5	2.1	3.6	3.4	3.6	3.8	3.2	extracellular	Receptor-like protein kinase-related family protein
AT1G70520	0.8	0.5	1.5	2.0	1.6	1.7	2.7	2.0	1.3	extracellular	cysteine-rich RLK (RECEPTOR-like protein kinase) 2
AT3G13790	2.5	0.7	3.7	2.0	0.5	2.0	2.7	3.4	3.9	extracellular	Glycosyl hydrolases family 32 protein
AT5G37600	26.3	0.7	25.5	2.0	1.9	1.8	2.7	4.4	4.3	cytosol	glutamine synthase clone R1
AT2G39200	5.0	3.1	29.8	1.9	4.0	3.6	6.0	6.2	5.3	plasma membrane	Seven transmembrane MLO family protein
AT3G51660	NA	1.3	NA	1.8	1.5	1.5	2.4	2.8	2.0	peroxisome	Tautomerase/MIF superfamily protein
AT2G37710	1.0	0.9	2.1	1.8	1.8	2.0	2.9	3.2	2.5	plasma membrane	receptor lectin kinase
AT4G08850	0.7	0.7	1.5	1.7	1.8	1.7	3.2	3.2	2.9	plasma membrane	Leucine-rich repeat receptor-like protein kinase family protein
AT5G54720	0.8	1.3	2.0	1.7	0.6	0.6	0.8	0.5	NA	cytosol	Ankyrin repeat family protein
AT5G48540	2.6	1.3	2.8	1.7	2.8	3.1	3.9	3.8	3.1	extracellular	receptor-like protein kinase-related family protein
AT3G55450	0.9	0.7	0.5	1.7	1.1	0.6	1.2	1.1	0.7	plasma membrane	PBS1-like 1
AT2G37130	NA	-24.9	NA	1.7	-0.7	0.1	0.1	0.6	1.0	extracellular	Peroxidase superfamily protein
AT2G18690	1.7	1.2	2.0	1.7	2.0	2.1	2.8	3.3	3.4	plasma membrane	
AT1G11260	0.8	0.3	2.0	1.7	0.4	1.2	2.6	3.7	3.8	plasma membrane	sugar transporter 1
AT4G23300	NA	-0.1	26.4	1.6	0.1	0.8	1.1	1.7	2.9	plasma membrane	cysteine-rich RLK (RECEPTOR-like protein kinase) 22
AT3G19010	NA	1.2	22.2	1.6	2.4	2.2	3.5	2.9	1.9	golgi	2-oxoglutarate (2OG) and Fe(II)-dependent oxygenase superfamily protein
AT3G21630	0.3	0.4	0.2	1.5	1.7	1.7	2.1	2.2	1.4	plasma membrane	chitin elicitor receptor kinase 1
AT5G54160	0.8	0.5	2.6	1.5	1.3	2.1	2.5	4.0	4.1	cytosol	O-methyltransferase 1
AT5G03160	-0.2	0.3	1.5	1.4	-0.3	0.6	2.2	1.7	1.2	endoplasmic reticulum	homolog of mamallian P58IPK
AT4G13510	1.1	0.2	2.1	1.4	1.2	1.2	2.5	2.3	2.1	plasma membrane	ammonium transporter 1;1
AT4G30190	0.2	0.1	1.1	1.4	0.3	1.9	3.1	4.1	3.6	plasma membrane	H(+)-ATPase 2
AT5G22060	0.4	1.0	0.6	1.3	0.2	1.6	1.9	0.9	0.4	cytosol	DNAJ homologue 2
AT3G25780	NA	1.6	NA	1.3	1.7	1.3	0.3	0.6	1.0	plastid	allene oxide cyclase 3
AT5G59730	0.5	0.7	0.6	1.3	0.7	0.3	1.0	0.3	0.1	golgi	exocyst subunit exo70 family protein H7
AT3G07090	NA	1.0	NA	1.3	0.4	2.1	1.4	1.3	0.8	cytosol	PPPDE putative thiol peptidase family protein
AT4G38550	0.9	1.3	1.0	1.3	1.6	1.8	3.6	2.2	1.2	nucleus	Arabidopsis phospholipase-like protein (PEARLI 4) family
AT2G41100	0.7	0.5	1.0	1.3	1.2	1.0	1.8	1.8	1.8	nucleus	Calcium-binding EF hand family protein

AT1G02360	NA	1.0	NA	1.3	3.4	3.4	3.8	4.0	3.1	extracellular	Chitinase family protein
AT1G60420	NA	0.1	NA	1.3	0.2	0.4	1.1	1.3	1.5	cytosol	DC1 domain-containing protein
AT1G13110	0.3	0.3	1.1	1.3	1.7	1.9	3.5	3.2	2.3	endoplasmic reticulum	cytochrome P450, family 71 subfamily B, polypeptide 7
AT4G02480	0.1	0.0	0.7	1.3	-0.3	0.3	0.3	0.0	0.2	plastid	AAA-type ATPase family protein
AT1G22410	1.1	0.7	1.9	1.2	2.4	2.3	2.2	2.5	2.3	plastid	Class-II DAHP synthetase family protein
AT1G03370	0.5	0.5	0.5	1.2	1.5	1.3	1.8	1.8	0.9	plasma membrane	C2 calcium/lipid-binding and GRAM domain containing protein
AT2G30490	0.7	0.6	1.4	1.2	2.7	2.5	3.2	4.2	3.6	endoplasmic reticulum	cinnamate-4-hydroxylase
AT1G69410	24.9	0.2	2.0	1.2	0.5	1.0	1.7	2.3	2.3	cytosol	eukaryotic elongation factor 5A-3
AT5G51070	1.1	0.8	2.1	1.2	1.1	1.1	0.6	0.6	0.4	plastid	Clp ATPase
AT5G58430	0.2	1.0	0.7	1.2	1.0	0.8	0.8	0.3	0.4	plasma membrane	exocyst subunit exo70 family protein B1
AT2G04550	NA	0.3	NA	1.1	0.0	0.0	-0.1	0.0	-0.1	nucleus	indole-3-butyric acid response 5
AT1G74020	NA	0.6	NA	1.1	1.3	1.5	1.9	1.9	1.6	vacuole	strictosidine synthase 2
AT3G06300	0.5	0.8	1.8	1.1	0.7	1.1	1.6	1.4	1.5	extracellular	P4H isoform 2
AT5G45510	-0.1	0.1	0.4	1.1	0.1	0.6	1.0	1.1	1.6	cytosol	Leucine-rich repeat (LRR) family protein
AT3G53180	2.3	0.5	2.6	1.1	1.9	2.0	2.1	1.9	1.4	cytosol	glutamate-ammonia ligases;catalytics;glutamate-ammonia ligases
AT3G61580	-0.4	-0.1	1.2	1.1	0.5	0.7	1.9	1.6	0.4	endoplasmic reticulum	Fatty acid/sphingolipid desaturase
AT2G23810	0.3	0.1	1.0	1.1	1.4	0.6	1.6	2.0	2.1	plasma membrane	tetraspanin8
AT1G55450	0.7	0.7	1.0	1.1	3.1	2.1	3.5	2.7	1.1	cytosol	S-adenosyl-L-methionine-dependent methyltransferases superfamily protein
AT3G01290	0.3	0.5	0.9	1.1	0.6	0.9	2.4	2.7	2.6	plasma membrane	SPFH/Band 7/PHB domain-containing membrane-associated protein family
AT4G20830	26.6	0.7	25.5	1.0	2.1	2.2	2.6	3.3	2.7	plasma membrane	FAD-binding Berberine family protein
AT2G36580	23.7	0.2	NA	1.0	1.4	1.8	2.7	3.0	2.4	cytosol	Pyruvate kinase family protein
AT2G01600	-0.3	-0.1	0.0	1.0	0.3	0.7	0.6	0.8	0.1	cytosol	ENTH/ANTH/VHS superfamily protein
AT5G13490	0.1	0.6	0.2	1.0	1.5	2.4	2.8	2.2	1.7	mitochondrion	ADP/ATP carrier 2
AT4G04340	-0.9	-0.8	-1.1	-1.0	-0.8	-2.5	-2.4	-2.4	-1.2	plasma membrane	ERD (early-responsive to dehydration stress) family protein
AT3G59400	-0.4	-0.6	-24.7	-1.0	-0.3	-1.1	-1.6	-1.5	-0.3	plastid	enzyme binding;tetrapyrrole binding
AT1G62180	-0.3	-0.1	-2.4	-1.0	-1.2	-0.1	-0.5	-0.2	-0.6	plastid	5'adenylylphosphosulfate reductase 2
AT5G49720	-0.3	-0.4	-1.2	-1.1	-1.7	-0.8	-0.6	-0.7	-0.5	cytosol	glycosyl hydrolase 9A1
AT1G55140	-0.1	-0.5	-23.6	-1.2	-0.2	-0.3	-1.0	-1.5	-0.8	plastid	Ribonuclease III family protein
AT5G13630	-0.4	-0.6	-1.4	-1.3	-0.4	-0.7	-2.0	-2.8	-1.6	plastid	magnesium-chelatase subunit chlH, chloroplast, putative / Mg-protoporphyrin IX chelatase, putative (CHLH)
AT4G15560	-0.9	-0.3	-25.5	-1.3	-0.3	-0.7	-1.2	-0.9	-0.2	plastid	Deoxyxylulose-5-phosphate synthase
AT3G22235	-0.5	-0.5	-0.5	-1.4	0.1	-0.7	-0.7	0.1	-0.7	plastid	

AT4G30440	-0.5	-0.9	-0.8	-1.6	-0.6	-0.7	-0.7	-0.9	-0.5	golgi	UDP-D-glucuronate 4-epimerase 1
AT2G33830	NA	-0.7	NA	-1.6	-1.0	-2.3	-1.5	-2.5	-2.2	nucleus	Dormancy/auxin associated family protein
AT2G38170	-0.5	-0.4	-0.5	-1.6	-0.4	-2.1	-3.3	-2.9	-2.0	plastid	cation exchanger 1
AT4G22690	-0.1	0.0	-1.3	-1.9	1.5	-0.3	0.5	-1.0	-1.0	endoplasmic reticulum	cytochrome P450, family 706, subfamily A, polypeptide 1
AT5G54770	-0.1	-0.5	-25.5	-1.9	-0.5	-1.2	-2.3	-3.4	-3.1	plastid	thiazole biosynthetic enzyme, chloroplast (ARA6) (THI1) (THI4)
AT4G21960	-24.8	-1.7	-27.6	-2.1	-0.9	-1.8	-2.7	-2.6	-2.2	extracellular	Peroxidase superfamily protein
AT1G16410	-25.5	-27.3	-26.3	-4.2	-1.1	-1.5	-2.1	-1.9	-1.9	endoplasmic reticulum	cytochrome p450 79f1

Table S3: List of proteins showing quantitative change in response to flg22. Proteins that are differentially expressed (|log2 value| > 1; q-value < 0.05) in the nuclear fraction at 3 h **(A)** and/or 9 h **(B)**, and total fraction at 3 h **(C)** and/or 9 h **(D)** after 1 µM flg22-treatment.

Table S4:

Table S4 (A): Proteins showing consistent present/absent expression profile in nuclear fraction at 3 h

Protein ID	Ratio[a]				Ratio[b]					SUBAcon	Description
	Proteome				Transcriptome						
	3h		9h								
	Nuc	Tot	Nuc	Tot	1h	2h	3h	5h	9h		
AT5G26920	28.6	23.4	28.6	NA	1.9	2.2	3.2	3.6	3.0	mitochondrion	Cam-binding protein 60-like G
AT5G64120	28.5	5.4	27.8	7.7	3.6	3.3	4.3	6.1	7.1	extracellular	Peroxidase superfamily protein
AT4G23550	28.2	24.6	26.4	24.3	1.3	2.9	3.5	3.7	1.7	nucleus	WRKY family transcription factor
AT4G01250	28.1	NA	26.4	NA	2.2	3.2	4.0	3.5	2.4	nucleus	WRKY family transcription factor
AT5G64750	28.1	22.3	0.0	NA	0.7	1.9	3.2	3.3	1.5	nucleus	Integrase-type DNA-binding superfamily protein
AT2G19190	28.1	26.4	29.9	28.7	2.0	3.1	4.4	5.9	4.3	plasma membrane	FLG22-induced receptor-like kinase 1
AT1G62300	28.1	NA	27.3	NA	2.7	2.0	2.5	1.7	1.4	nucleus	WRKY family transcription factor
AT1G51850	27.9	26.6	28.4	28.2	3.0	3.5	4.8	4.9	4.4	plasma membrane	Leucine-rich repeat protein kinase family protein
AT3G55150	27.8	24.9	26.5	23.9	NA	3.9	4.6	4.3	NA	nucleus	exocyst subunit exo70 family protein H1
AT1G66090	27.5	4.2	4.1	27.0	1.6	2.6	1.4	1.6	1.4	plastid	Disease resistance protein (TIR-NBS class)
AT2G22880	27.4	NA	25.8	NA	1.5	1.7	2.7	2.9	1.7	nucleus	VQ motif-containing protein
AT2G44370	27.2	24.5	29.0	25.7	2.4	4.0	5.6	5.0	4.3	nucleus	Cysteine/Histidine-rich C1 domain family protein
AT2G17740	26.8	24.4	28.1	26.6	2.5	4.8	6.8	6.5	4.9	nucleus	Cysteine/Histidine-rich C1 domain family protein
AT2G26560	26.5	2.9	25.0	1.7	3.6	2.3	2.1	0.5	-0.3	cytosol	phospholipase A 2A
AT2G43620	26.5	3.1	26.2	5.0	4.3	3.4	3.1	4.0	6.0	extracellular	Chitinase family protein
AT3G22060	26.4	1.6	25.5	2.1	3.6	3.4	3.6	3.8	3.2	extracellular	Receptor-like protein kinase-related family protein
AT4G24230	26.3	24.4	0.4	25.2	0.7	0.6	1.5	1.2	0.5	extracellular	acyl-CoA-binding domain 3
AT5G37600	26.3	0.7	25.5	2.0	1.9	1.8	2.7	4.4	4.3	cytosol	glutamine synthase clone R1
AT3G46280	26.1	27.4	26.2	28.4	3.2	4.3	6.0	6.3	5.7	extracellular	protein kinase-related
AT5G02790	25.6	0.0	NA	0.0	-0.3	-0.6	-1.0	-0.8	-0.7	cytosol	Glutathione S-transferase family protein
AT1G09970	25.4	NA	25.4	NA	0.4	1.1	1.1	1.3	1.0	plasma membrane	Leucine-rich receptor-like protein kinase family protein
AT4G18880	25.4	NA	2.1	NA	1.6	1.0	1.5	1.0	1.2	nucleus	heat shock transcription factor A4A
AT1G30755	25.3	23.3	25.6	23.5	2.7	2.4	3.1	2.5	1.9	nucleus	Protein of unknown function (DUF668)
AT3G21070	25.3	21.4	25.6	21.7	4.2	1.4	1.2	0.8	0.0	cytosol	NAD kinase 1

AT1G53625	25.0	22.9	25.4	NA	3.1	3.4	4.2	3.6	2.6	nucleus	
AT4G11890	24.9	24.0	2.7	25.6	2.1	2.0	2.2	2.5	2.4	cytosol	Protein kinase superfamily protein
AT2G39380	24.6	22.2	24.3	22.4	1.0	3.4	4.8	NA	NA	plastid	exocyst subunit exo70 family protein H2
AT4G18170	24.6	NA	NA	NA	1.9	1.0	1.4	1.1	0.3	nucleus	WRKY DNA-binding protein 28
AT5G57710	24.5	21.0	25.4	NA	0.8	0.9	1.2	1.6	1.7	plastid	Double Clp-N motif-containing P-loop nucleoside triphosphate hydrolases superfamily protein
AT4G20860	24.4	3.3	23.2	4.7	2.7	3.1	4.5	5.1	4.6	plasma membrane	FAD-binding Berberine family protein
AT4G21120	24.2	NA	25.1	24.4	1.4	2.5	3.4	3.4	2.9	plasma membrane	amino acid transporter 1
AT3G58620	23.8	NA	24.1	23.7	0.5	1.1	1.4	1.2	1.0	cytosol	tetratricopetide-repeat thioredoxin-like 4
AT1G20370	23.3	NA	NA	-22.7	-0.2	-0.4	-0.2	0.1	0.2	nucleus	Pseudouridine synthase family protein
AT2G22540	-23.9	NA	-0.2	NA	-0.6	-1.9	-1.2	-1.3	-0.8	nucleus	K-box region and MADS-box transcription factor family protein
AT1G04680	-24.7	-0.2	-24.4	-0.2	-1.0	-0.7	-0.3	-0.4	0.0	extracellular	Pectin lyase-like superfamily protein
AT2G38580	-24.7	NA	25.2	NA	0.0	-0.2	-0.1	0.5	0.4	nucleus	Mitochondrial ATP synthase D chain-related protein
AT4G23620	-25.0	0.5	0.3	0.0	-0.3	-0.3	-0.3	0.3	0.3	mitochondrion	Ribosomal protein L25/Gln-tRNA synthetase, anti-codon-binding domain
AT1G75380	-25.6	-0.7	0.4	0.7	-1.8	-2.4	-1.9	-1.2	0.3	mitochondrion	bifunctional nuclease in basal defense response 1
AT1G28440	-25.8	NA	-26.1	NA	-0.3	-1.0	-0.8	-0.8	-0.5	plasma membrane	HAESA-like 1
AT1G74270	-27.5	-0.9	0.4	26.6	0.0	-0.4	-0.2	0.0	0.2	cytosol	Ribosomal protein L35Ae family protein
AT5G39560	-28.5	NA	-0.4	NA	NA	NA	NA	NA	NA	plasma membrane	Galactose oxidase/kelch repeat superfamily protein

Table S4(B): Proteins showing consistent present/absent expression profile in nuclear fraction at 9 h

Protein ID	Ratio[a]				Ratio[b]					SUBAcon	Description
	Proteome				Transcriptome						
	3h		9h								
	Nuc	Tot	Nuc	Tot	1h	2h	3h	5h	9h		
AT5G50200	3.1	3.0	30.0	4.7	2.6	2.8	3.6	4.4	4.4	extracellular	nitrate transmembrane transporters
AT2G19190	28.1	26.4	29.9	28.7	2.0	3.1	4.4	5.9	4.3	plasma membrane	FLG22-induced receptor-like kinase 1
AT2G39200	5.0	3.1	29.8	1.9	4.0	3.6	6.0	6.2	5.3	plasma membrane	Seven transmembrane MLO family protein
AT3G50480	2.2	3.2	29.8	5.4	1.4	1.5	2.2	3.3	3.0	cytosol	homolog of RPW8 4
AT4G23210	3.1	25.5	29.6	3.0	1.2	1.7	2.2	3.2	3.8	plasma membrane	cysteine-rich RLK (RECEPTOR-like protein kinase) 13
AT2G44370	27.2	24.5	29.0	25.7	2.4	4.0	5.6	5.0	4.3	nucleus	Cysteine/Histidine-rich C1 domain family protein
AT5G26920	28.6	23.4	28.6	NA	1.9	2.2	3.2	3.6	3.0	mitochondrion	Cam-binding protein 60-like G
AT1G51850	27.9	26.6	28.4	28.2	3.0	3.5	4.8	4.9	4.4	plasma membrane	Leucine-rich repeat protein kinase family protein
AT4G36670	1.4	25.3	28.3	27.8	0.9	1.5	3.0	4.5	4.8	plasma membrane	Major facilitator superfamily protein
AT2G39518	27.0	25.7	28.2	28.1	3.0	4.0	5.6	6.2	5.6	extracellular	Uncharacterised protein family (UPF0497)
AT2G17740	26.8	24.4	28.1	26.6	2.5	4.8	6.8	6.5	4.9	nucleus	Cysteine/Histidine-rich C1 domain family protein
AT1G10340	3.0	24.5	27.9	24.4	1.7	1.3	1.8	1.9	1.9	plasma membrane	Ankyrin repeat family protein
AT3G28540	NA	NA	27.9	2.0	0.0	-0.3	-0.4	0.8	1.7	plasma membrane	P-loop containing nucleoside triphosphate hydrolases superfamily protein
AT5G64120	28.5	5.4	27.8	7.7	3.6	3.3	4.3	6.1	7.1	extracellular	Peroxidase superfamily protein
AT1G51820	4.1	2.9	27.7	27.0	2.8	2.7	3.6	3.5	NA	plasma membrane	Leucine-rich repeat protein kinase family protein
AT1G30900	25.1	1.1	27.4	3.6	0.6	0.9	1.1	1.9	1.7	vacuole	VACUOLAR SORTING RECEPTOR 6
AT1G62300	28.1	NA	27.3	NA	2.7	2.0	2.5	1.7	1.4	nucleus	WRKY family transcription factor
AT2G39530	NA	23.7	27.2	27.1	0.8	3.0	4.5	5.1	4.5	extracellular	Uncharacterised protein family (UPF0497)
AT3G47480	25.2	NA	27.2	NA	0.4	1.1	1.3	2.2	2.5	plasma membrane	Calcium-binding EF-hand family protein
AT3G21080	NA	NA	27.1	22.7	-0.1	0.0	1.0	2.1	2.9	plasma membrane	ABC transporter-related
AT1G52200	2.3	25.7	27.0	26.5	1.6	2.5	4.7	4.8	4.2	plasma membrane	PLAC8 family protein
AT1G51890	26.5	23.6	27.0	26.3	1.8	2.9	4.1	4.1	3.7	extracellular	Leucine-rich repeat protein kinase family protein
AT3G01830	2.3	25.5	26.8	25.5	3.2	3.0	3.2	2.6	2.1	nucleus	Calcium-binding EF-hand family protein

AT1G08050	26.5	23.5	26.8	24.9	0.8	1.6	1.8	1.8	1.0	nucleus	Zinc finger (C3HC4-type RING finger) family protein
AT3G55150	27.8	24.9	26.5	23.9	NA	3.9	4.6	4.3	NA	nucleus	exocyst subunit exo70 family protein H1
AT4G23550	28.2	24.6	26.4	24.3	1.3	2.9	3.5	3.7	1.7	nucleus	WRKY family transcription factor
AT4G01250	28.1	NA	26.4	NA	2.2	3.2	4.0	3.5	2.4	nucleus	WRKY family transcription factor
AT4G23200	0.3	0.4	26.3	0.0	0.7	1.3	0.6	0.8	0.5	plasma membrane	cysteine-rich RLK (RECEPTOR-like protein kinase) 12
AT5G57480	24.1	NA	26.3	NA	0.9	0.7	1.2	1.7	1.6	endoplasmic reticulum	P-loop containing nucleoside triphosphate hydrolases superfamily protein
AT3G46280	26.1	27.4	26.2	28.4	3.2	4.3	6.0	6.3	5.7	extracellular	protein kinase-related
AT2G43620	26.5	3.1	26.2	5.0	4.3	3.4	3.1	4.0	6.0	extracellular	Chitinase family protein
AT1G68840	2.5	NA	26.0	NA	1.6	1.7	2.8	1.8	1.9	nucleus	related to ABI3/VP1 2
AT5G52830	NA	NA	25.9	NA	0.9	1.7	1.6	2.2	1.5	nucleus	WRKY DNA-binding protein 27
AT3G56170	24.0	NA	25.9	24.6	-0.2	0.5	1.0	1.5	1.4	mitochondrion	Ca-2+ dependent nuclease
AT1G80840	4.3	25.1	25.8	NA	3.4	2.1	2.0	1.7	1.3	nucleus	WRKY DNA-binding protein 40
AT2G16900	25.2	NA	25.8	22.7	1.4	1.8	2.4	2.4	1.2	nucleus	Arabidopsis phospholipase-like protein (PEARLI 4) family
AT3G44630	0.2	NA	25.8	NA	0.7	-0.1	-0.3	-0.3	0.2	nucleus	Disease resistance protein (TIR-NBS-LRR class) family
AT1G30755	25.3	23.3	25.6	23.5	2.7	2.4	3.1	2.5	1.9	nucleus	Protein of unknown function (DUF668)
AT5G42050	24.9	NA	25.5	NA	0.8	0.9	1.5	1.7	1.5	nucleus	DCD (Development and Cell Death) domain protein
AT5G37600	26.3	0.7	25.5	2.0	1.9	1.8	2.7	4.4	4.3	cytosol	glutamine synthase clone R1
AT5G57710	24.5	21.0	25.4	NA	0.8	0.9	1.2	1.6	1.7	plastid	Double Clp-N motif-containing P-loop nucleoside triphosphate hydrolases superfamily protein
AT5G54860	0.13	22.58	25.42	23.23	1.35	0.96	1.90	1.43	0.63	plasma membrane	Major facilitator superfamily protein
AT5G46520	NA	NA	25.33	NA	0.73	0.75	0.75	0.85	1.05	cytosol	Disease resistance protein (TIR-NBS-LRR class) family
AT4G12490	NA	24.96	25.31	28.50	-0.18	0.39	3.63	5.89	6.59	extracellular	Bifunctional inhibitor/lipid-transfer protein/seed storage 2S albumin superfamily protein
AT2G38580	-24.73	NA	25.23	NA	0.05	-0.18	-0.11	0.49	0.39	nucleus	Mitochondrial ATP synthase D chain-related protein
AT1G69740	25.87	0.03	25.20	-0.06	-0.21	-0.10	-0.16	-0.14	0.36	plastid	Aldolase superfamily protein
AT2G42280	NA	NA	25.17	NA	-0.12	0.10	0.09	0.44	0.43	nucleus	basic helix-loop-helix (bHLH) DNA-binding superfamily protein
AT3G09830	25.60	22.14	25.15	22.34	2.25	1.01	1.32	1.41	0.78	nucleus	Protein kinase superfamily protein
AT4G21120	24.16	NA	25.15	24.39	1.37	2.52	3.36	3.41	2.93	plasma membrane	amino acid transporter 1
AT5G06560	-1.22	NA	25.06	NA	0.96	0.62	1.01	0.84	0.35	nucleus	Protein of unknown function, DUF593

AT5G45110	24.89	NA	25.05	NA	1.39	0.67	0.89	1.43	1.49	nucleus	NPR1-like protein 3
AT4G12250	24.73	NA	25.02	NA	0.36	0.31	0.50	0.34	0.41	golgi	UDP-D-glucuronate 4-epimerase 5
AT3G45060	26.06	NA	25.01	NA	1.28	1.93	2.42	2.58	1.62	plasma membrane	high affinity nitrate transporter 2.6
AT2G38940	NA	NA	24.98	24.44	0.10	1.82	3.28	4.19	4.02	plasma membrane	phosphate transporter 1;4
AT4G15610	24.09	3.24	24.97	2.97	1.63	1.94	2.11	2.65	2.31	plasma membrane	Uncharacterised protein family (UPF0497)
AT3G08970	24.77	22.31	24.96	22.75	0.32	2.13	2.28	1.56	0.70	endoplasmic reticulum	DNAJ heat shock N-terminal domain-containing protein
AT4G00300	25.32	-24.18	24.96	24.53	0.35	0.51	0.46	0.74	0.68	vacuole	fringe-related protein
AT5G15130	23.21	NA	24.77	NA	0.19	NA	NA	NA	1.44	nucleus	WRKY DNA-binding protein 72
AT3G52190	23.66	0.27	24.76	1.33	0.96	1.23	1.97	2.26	1.99	endoplasmic reticulum	phosphate transporter traffic facilitator1
AT4G32650	NA	23.09	24.60	NA	0.73	1.30	2.37	3.24	3.00	plastid	potassium channel in Arabidopsis thaliana 3
AT2G23770	NA	24.01	24.54	24.76	0.71	0.72	0.75	0.66	0.26	plasma membrane	protein kinase family protein / peptidoglycan-binding LysM domain-containing protein
AT3G22310	NA	NA	24.41	NA	0.18	0.25	0.47	0.85	0.79	mitochondrion	putative mitochondrial RNA helicase 1
AT5G66675	23.99	23.56	24.40	24.18	1.32	1.14	1.07	0.83	0.59	plasma membrane	Protein of unknown function (DUF677)
AT2G39380	24.56	22.19	24.30	22.41	1.03	3.37	4.77	NA	NA	plastid	exocyst subunit exo70 family protein H2
AT2G44380	NA	NA	24.12	NA	1.07	2.23	3.84	3.57	2.89	nucleus	Cysteine/Histidine-rich C1 domain family protein
AT1G14870	23.69	24.08	24.10	24.53	2.32	2.87	3.86	3.86	3.59	plasma membrane	PLANT CADMIUM RESISTANCE 2
AT5G18750	NA	NA	24.06	-25.39	0.15	0.08	0.74	0.59	0.11	nucleus	DNAJ heat shock N-terminal domain-containing protein
AT2G28890	23.62	NA	23.53	NA	1.56	1.50	2.19	2.55	1.84	nucleus	poltergeist like 4
AT4G09420	21.68	NA	22.50	23.80	0.03	0.71	0.75	1.41	1.66	cytosol	Disease resistance protein (TIR-NBS class)
AT1G01930	-0.24	-0.28	-24.04	0.12	0.13	0.12	0.04	-0.08	-0.01	nucleus	zinc finger protein-related
AT1G68520	NA	NA	-24.14	NA	-2.47	-2.58	-2.72	-2.25	-0.97	nucleus	B-box type zinc finger protein with CCT domain
AT4G08950	-0.41	-0.91	-24.16	-1.16	-1.87	-0.49	-0.28	-0.01	0.16	extracellular	Phosphate-responsive 1 family protein
AT5G05690	-24.69	NA	-24.25	NA	-0.93	-1.39	-1.60	-1.89	-1.24	endoplasmic reticulum	Cytochrome P450 superfamily protein
AT2G43010	-0.12	NA	-24.28	NA	-0.82	-1.00	-1.62	-2.23	-1.37	nucleus	phytochrome interacting factor 4
AT4G01130	-1.95	0.17	-25.04	-0.35	0.02	-0.61	-0.77	-0.87	-0.64	extracellular	GDSL-like Lipase/Acylhydrolase superfamily protein

AT2G39140	0.32	-0.52	-25.11	-23.45	-0.37	-0.43	-0.74	-0.99	-0.47	plastid	pseudouridine synthase family protein
AT2G15970	-24.98	-25.03	-25.27	-25.36	-1.54	-2.21	-2.39	-3.30	-2.35	plasma membrane	cold regulated 413 plasma membrane 1
AT3G28040	-1.48	-0.72	-25.33	-0.01	-0.07	-1.24	-1.56	-1.43	-0.94	plasma membrane	Leucine-rich receptor-like protein kinase family protein
AT1G52190	-25.59	NA	-25.64	NA	-0.68	-1.39	-0.42	-1.42	-1.23	plasma membrane	Major facilitator superfamily protein
AT4G33480	-0.05	NA	-25.75	NA	-0.24	-0.62	-1.12	-0.93	-0.60	plastid	
AT1G16410	-25.48	-27.28	-26.34	-4.20	-1.14	-1.50	-2.10	-1.86	-1.87	endoplasmic reticulum	cytochrome p450 79f1
AT1G65590	-1.21	-0.06	-27.13	-0.39	-0.22	-0.28	-0.42	-0.78	-0.43	extracellular	beta-hexosaminidase 3
AT4G21960	-24.79	-1.69	-27.64	-2.08	-0.88	-1.84	-2.68	-2.61	-2.25	extracellular	Peroxidase superfamily protein

Table S4(C): Proteins showing consistent present/absent expression profile in total fraction at 3 h

Protein ID	Ratio[a]				Ratio[b]					SUBAcon	Description
	Proteome				Transcriptome						
	3h		9h								
	Nuc	Tot	Nuc	Tot	1h	2h	3h	5h	9h		
AT3G46280	26.1	27.4	26.2	28.4	3.2	4.3	6.0	6.3	5.7	extracellular	protein kinase-related
AT1G30700	NA	27.3	NA	28.9	2.4	5.0	5.6	5.7	3.8	extracellular	FAD-binding Berberine family protein
AT5G48430	26.1	26.6	25.5	28.7	4.4	5.2	6.5	6.2	NA	extracellular	Eukaryotic aspartyl protease family protein
AT1G51850	27.9	26.6	28.4	28.2	3.0	3.5	4.8	4.9	4.4	plasma membrane	Leucine-rich repeat protein kinase family protein
AT3G21230	NA	26.5	NA	26.4	2.1	2.5	2.6	3.3	2.3	peroxisome	4-coumarate:CoA ligase 5
AT2G27660	3.4	26.4	4.8	26.0	3.1	3.0	4.1	3.4	2.9	nucleus	Cysteine/Histidine-rich C1 domain family protein
AT2G19190	28.1	26.4	29.9	28.7	2.0	3.1	4.4	5.9	4.3	plasma membrane	FLG22-induced receptor-like kinase 1
AT1G21120	NA	26.1	NA	26.3	4.2	2.3	3.3	2.3	1.0	cytosol	O-methyltransferase family protein
AT1G74310	24.7	26.0	24.9	25.3	0.5	3.7	1.5	0.0	-0.4	cytosol	heat shock protein 101
AT1G52200	2.3	25.7	27.0	26.5	1.6	2.5	4.7	4.8	4.2	plasma membrane	PLAC8 family protein
AT3G01830	2.3	25.5	26.8	25.5	3.2	3.0	3.2	2.6	2.1	nucleus	Calcium-binding EF-hand family protein
AT4G36670	1.4	25.3	28.3	27.8	0.9	1.5	3.0	4.5	4.8	plasma membrane	Major facilitator superfamily protein
AT4G12400	24.7	25.2	25.0	26.0	0.4	3.0	2.4	0.3	0.1	nucleus	stress-inducible protein, putative
AT1G19380	1.1	25.1	0.1	24.3	1.0	1.4	2.8	2.7	2.3	plasma membrane	Protein of unknown function (DUF1195)
AT3G09350	25.2	25.0	0.6	25.2	0.1	3.3	1.6	0.1	0.5	cytosol	Fes1A
AT3G07195	3.1	25.0	1.6	24.6	2.6	2.5	3.1	2.1	1.5	nucleus	RPM1-interacting protein 4 (RIN4) family protein
AT2G24850	24.1	24.9	NA	NA	1.5	1.9	1.6	0.9	0.0	plastid	tyrosine aminotransferase 3
AT3G55150	27.8	24.9	26.5	23.9	NA	3.9	4.6	4.3	NA	nucleus	exocyst subunit exo70 family protein H1
AT2G02010	NA	24.8	NA	25.2	3.4	2.8	1.4	0.6	0.7	cytosol	glutamate decarboxylase 4
AT4G15417	NA	24.6	24.7	26.4	NA	2.0	2.7	NA	NA	cytosol	RNAse II-like 1
AT1G10340	3.0	24.5	27.9	24.4	1.7	1.3	1.8	1.9	1.9	plasma membrane	Ankyrin repeat family protein
AT2G17740	26.8	24.4	28.1	26.6	2.5	4.8	6.8	6.5	4.9	nucleus	Cysteine/Histidine-rich C1 domain family protein
AT2G42620	0.0	23.3	NA	0.0	-0.6	-0.2	-0.2	0.0	-0.1	plastid	RNI-like superfamily protein
AT5G44380	NA	22.9	NA	24.9	0.9	3.3	3.6	NA	3.5	extracellular	FAD-binding Berberine family protein
AT4G37760	-0.1	-22.9	-0.2	0.3	-0.1	0.0	-0.6	-0.4	-0.2	plasma membrane	squalene epoxidase 3
AT5G62360	NA	-25.3	NA	-25.9	-1.7	-0.9	-1.1	-1.2	-0.1	extracellular	Plant invertase/pectin methylesterase inhibitor superfamily protein

Table S4(D): Proteins showing consistent present/absent expression profile in total fraction at 9 h

Protein ID	Ratio[a]				Ratio[b]					SUBAcon	Description
	Proteome				Transcriptome						
	3h		9h								
	Nuc	Tot	Nuc	Tot	1h	2h	3h	5h	9h		
AT1G30700	NA	27.3	NA	28.9	2.4	5.0	5.6	5.7	3.8	extracellular	FAD-binding Berberine family protein
AT1G30720	NA	2.8	NA	28.9	2.8	3.7	4.8	5.3	4.9	extracellular	FAD-binding Berberine family protein
AT4G22470	24.4	3.8	NA	28.8	2.3	3.0	4.5	5.4	5.3	extracellular	protease inhibitor/seed storage/lipid transfer protein (LTP) family protein
AT5G48430	26.1	26.6	25.5	28.7	4.4	5.2	6.5	6.2	NA	extracellular	Eukaryotic aspartyl protease family protein
AT2G19190	28.1	26.4	29.9	28.7	2.0	3.1	4.4	5.9	4.3	plasma membrane	FLG22-induced receptor-like kinase 1
AT4G12490	NA	25.0	25.3	28.5	-0.2	0.4	3.6	5.9	6.6	extracellular	Bifunctional inhibitor/lipid-transfer protein/seed storage 2S albumin superfamily protein
AT3G46280	26.1	27.4	26.2	28.4	3.2	4.3	6.0	6.3	5.7	extracellular	protein kinase-related
AT1G51850	27.9	26.6	28.4	28.2	3.0	3.5	4.8	4.9	4.4	plasma membrane	Leucine-rich repeat protein kinase family protein
AT2G39518	27.0	25.7	28.2	28.1	3.0	4.0	5.6	6.2	5.6	extracellular	Uncharacterised protein family (UPF0497)
AT4G36670	1.4	25.3	28.3	27.8	0.9	1.5	3.0	4.5	4.8	plasma membrane	Major facilitator superfamily protein
AT5G39580	NA	26.8	NA	27.6	2.3	3.0	4.9	NA	NA	extracellular	Peroxidase superfamily protein
AT4G36430	NA	NA	NA	27.3	NA	0.3	3.2	5.5	5.6	extracellular	Peroxidase superfamily protein
AT2G39530	NA	23.7	27.2	27.1	0.8	3.0	4.5	5.1	4.5	extracellular	Uncharacterised protein family (UPF0497)
AT1G51820	4.1	2.9	27.7	27.0	2.8	2.7	3.6	3.5	NA	plasma membrane	Leucine-rich repeat protein kinase family protein
AT1G66090	27.5	4.2	4.1	27.0	1.6	2.6	1.4	1.6	1.4	plastid	Disease resistance protein (TIR-NBS class)
AT4G24690	0.2	NA	3.4	26.9	-0.2	-0.2	0.3	0.6	1.7	nucleus	ubiquitin-associated (UBA)/TS-N domain-containing protein / octicosapeptide/Phox/Bemp1 (PB1) domain-containing protein
AT5G26340	1.7	1.7	3.0	26.8	1.9	1.6	2.4	2.6	2.8	plasma membrane	Major facilitator superfamily protein
AT1G64170	-0.6	NA	0.5	26.8	0.5	0.9	2.2	3.6	2.4	plasma membrane	cation/H+ exchanger 16
AT3G47380	NA	25.2	24.2	26.6	2.0	2.5	3.2	2.9	2.2	extracellular	Plant invertase/pectin methylesterase inhibitor superfamily protein
AT3G03640	NA	NA	NA	26.6	0.1	-0.5	-0.8	-0.6	2.1	extracellular	beta glucosidase 25

AT2G17740	26.8	24.4	28.1	26.6	2.5	4.8	6.8	6.5	4.9	nucleus	Cysteine/Histidine-rich C1 domain family protein
AT1G52200	2.3	25.7	27.0	26.5	1.6	2.5	4.7	4.8	4.2	plasma membrane	PLAC8 family protein
AT4G12470	NA	25.2	25.5	26.5	0.2	0.7	2.3	3.7	5.8	extracellular	azelaic acid induced 1
AT3G11340	NA	NA	NA	26.5	0.0	-0.3	0.6	2.9	3.4	golgi	UDP-Glycosyltransferase superfamily protein
AT3G21230	NA	26.5	NA	26.4	2.1	2.5	2.6	3.3	2.3	peroxisome	4-coumarate:CoA ligase 5
AT3G51330	NA	NA	NA	26.4	1.0	2.3	3.2	3.5	3.1	extracellular	Eukaryotic aspartyl protease family protein
AT5G48570	NA	1.2	23.2	26.4	0.5	4.0	4.1	0.2	0.1	cytosol	FKBP-type peptidyl-prolyl cis-trans isomerase family protein
AT4G15417	NA	24.6	24.7	26.4	NA	2.0	2.7	NA	NA	cytosol	RNAse II-like 1
AT1G51890	26.5	23.6	27.0	26.3	1.8	2.9	4.1	4.1	3.7	extracellular	Leucine-rich repeat protein kinase family protein
AT1G65690	NA	NA	26.6	26.2	3.1	3.5	4.3	4.4	3.3	plasma membrane	Late embryogenesis abundant (LEA) hydroxyproline-rich glycoprotein family
AT4G12400	24.7	25.2	25.0	26.0	0.4	3.0	2.4	0.3	0.1	nucleus	stress-inducible protein, putative
AT2G27660	3.4	26.4	4.8	26.0	3.1	3.0	4.1	3.4	2.9	nucleus	Cysteine/Histidine-rich C1 domain family protein
AT4G23190	1.2	1.4	2.3	26.0	2.8	2.2	2.7	2.5	1.4	plasma membrane	cysteine-rich RLK (RECEPTOR-like protein kinase) 11
AT3G54420	NA	24.9	NA	26.0	2.3	2.5	3.1	4.4	4.0	extracellular	homolog of carrot EP3-3 chitinase
AT2G45220	NA	26.1	NA	25.9	0.5	1.7	2.6	3.3	3.5	extracellular	Plant invertase/pectin methylesterase inhibitor superfamily
AT2G44370	27.2	24.5	29.0	25.7	2.4	4.0	5.6	5.0	4.3	nucleus	Cysteine/Histidine-rich C1 domain family protein
AT5G41750	0.4	0.8	26.7	25.6	0.9	0.7	0.8	1.1	1.0	mitochondrion	Disease resistance protein (TIR-NBS-LRR class) family
AT2G45290	NA	24.1	NA	25.6	1.9	2.2	2.1	1.9	0.7	plastid	Transketolase
AT4G01750	NA	24.5	NA	25.6	2.2	3.0	4.2	3.7	2.3	mitochondrion	rhamnogalacturonan xylosyltransferase 2
AT4G11890	24.9	24.0	2.7	25.6	2.1	2.0	2.2	2.5	2.4	cytosol	Protein kinase superfamily protein
AT5G35735	1.0	25.2	1.4	25.5	2.0	2.6	3.3	2.5	2.1	plasma membrane	Auxin-responsive family protein
AT3G01830	2.29	25.54	26.83	25.46	3.21	3.04	3.19	2.64	2.09	nucleus	Calcium-binding EF-hand family protein
AT3G57550	NA	0.73	NA	25.34	2.05	1.95	2.51	2.27	1.74	cytosol	guanylate kinase
AT1G74310	24.67	26.02	24.93	25.29	0.55	3.67	1.52	0.02	-0.36	cytosol	heat shock protein 101
AT3G09350	25.21	25.01	0.62	25.21	0.07	3.28	1.60	0.09	0.45	cytosol	Fes1A
AT4G24230	26.29	24.39	0.45	25.21	0.66	0.62	1.49	1.24	0.54	extracellular	acyl-CoA-binding domain 3
AT2G20880	NA	NA	25.33	25.19	0.21	-0.35	0.49	0.68	0.77	nucleus	Integrase-type DNA-binding superfamily protein

AT1G66880	0.91	23.09	24.93	25.15	1.79	0.74	1.63	1.48	1.45	plasma membrane	Protein kinase superfamily protein
AT1G76930	NA	24.03	NA	25.01	1.16	3.04	3.31	3.78	4.73	extracellular	extensin 4
AT4G29740	NA	24.76	NA	24.97	1.80	1.64	2.11	2.71	2.44	endoplasmic reticulum	cytokinin oxidase 4
AT1G08050	26.51	23.52	26.81	24.93	0.78	1.57	1.77	1.79	0.99	nucleus	Zinc finger (C3HC4-type RING finger) family protein
AT1G29690	NA	0.93	NA	24.91	1.31	1.12	1.74	1.48	1.11	cytosol	MAC/Perforin domain-containing protein
AT5G44380	NA	22.87	NA	24.90	0.94	3.30	3.61	NA	3.48	extracellular	FAD-binding Berberine family protein
AT4G14440	NA	0.08	NA	24.77	-0.02	0.50	0.39	0.11	0.14	peroxisome	3-hydroxyacyl-CoA dehydratase 1
AT2G30750	23.80	24.40	23.27	24.67	0.48	0.67	1.23	NA	1.92	endoplasmic reticulum	cytochrome P450, family 71, subfamily A, polypeptide 12
AT4G24160	0.88	0.65	23.79	24.63	0.71	0.80	1.13	1.03	0.70	mitochondrion	alpha/beta-Hydrolases superfamily protein
AT4G00300	25.32	-24.18	24.96	24.53	0.35	0.51	0.46	0.74	0.68	vacuole	fringe-related protein
AT5G25440	NA	24.42	NA	24.51	1.18	2.07	2.48	3.17	2.10	nucleus	Protein kinase superfamily protein
AT4G21410	1.20	24.51	25.84	24.38	1.99	2.16	2.93	2.44	1.76	plasma membrane	cysteine-rich RLK (RECEPTOR-like protein kinase) 29
AT4G22530	NA	23.77	NA	24.34	0.63	1.41	1.14	0.90	0.49	golgi	S-adenosyl-L-methionine-dependent methyltransferases superfamily protein
AT5G05190	0.74	23.91	1.47	24.25	3.26	2.99	4.01	3.35	2.54	nucleus	Protein of unknown function (DUF3133)
AT2G17760	NA	NA	NA	24.22	0.69	0.92	1.86	1.96	1.50	extracellular	Eukaryotic aspartyl protease family protein
AT1G51790	24.29	NA	23.90	24.21	1.63	2.09	3.33	3.15	3.10	plasma membrane	Leucine-rich repeat protein kinase family protein
AT4G24240	1.61	23.19	3.85	23.91	1.21	1.72	3.28	2.56	2.18	nucleus	WRKY DNA-binding protein 7
AT1G30755	25.35	23.25	25.56	23.46	2.72	2.41	3.13	2.52	1.89	nucleus	Protein of unknown function (DUF668)
AT5G42830	NA	22.79	NA	22.65	2.35	1.69	2.67	2.10	1.53	cytosol	HXXXD-type acyl-transferase family protein
AT1G43130	0.15	0.02	-0.04	22.59	0.07	0.31	0.19	0.73	0.30	plasma membrane	like COV 2
AT5G45650	NA	NA	NA	-23.02	0.23	-0.62	-1.25	-1.18	-0.37	extracellular	subtilase family protein
AT3G18680	-0.47	0.14	-24.12	-25.01	-0.19	-0.43	-1.10	-1.85	-1.45	plastid	Amino acid kinase family protein

Table S4: List of proteins showing consistent presence/absence pattern in response to flg22. Proteins which are consistently present in flg22 samples (in six replicates) and absent (in six replicates) in mock are defined as “Increased” and vice-versa (as “Decreased”) in abundance.

Table S5:

Table S5(A): Proteins showing greater increase or decrease in abundance in the nuclear fraction than the total fraction upon flg22 treatment at 3h

Protein ID	Ratio[a] Proteome		Ratio[b] Transcriptome					SUBAcon	Description
	Difference	p.val	1h	2h	3h	5h	9h		
AT1G16820	4.13	0.00	-0.02	-0.12	-0.06	-0.28	-0.10	cytosol	vacuolar ATP synthase catalytic subunit-related / V-ATPase-related / vacuolar proton pump-related
AT3G21070	2.88	0.00	4.22	1.41	1.20	0.83	0.04	cytosol	NAD kinase 1
AT1G64280	2.79	0.00	0.88	0.55	0.52	0.65	0.22	cytosol	regulatory particle non-ATPase subunit 5B
AT5G37600	2.61	0.00	1.94	1.81	2.69	4.39	4.25	cytosol	glutamine synthase clone R1
AT5G64760	2.58	0.01	0.55	0.27	0.50	0.19	0.13	cytosol	regulatory particle non-ATPase subunit 5B
AT5G02790	2.55	0.00	-0.25	-0.61	-1.03	-0.80	-0.71	cytosol	Glutathione S-transferase family protein
AT5G11670	2.46	0.00	2.11	2.52	3.18	2.54	1.58	cytosol	NADP-malic enzyme 2
AT1G09310	2.19	0.00	-1.03	-0.81	-1.24	-1.87	-2.38	cytosol	Protein of unknown function, DUF538
AT5G52640	2.10	0.00	0.12	2.91	3.73	1.95	1.03	cytosol	heat shock protein 90.1
AT3G33520	2.09	0.00	-0.28	-0.36	-0.51	-0.20	0.00	cytosol	actin-related protein 6
AT3G53180	1.84	0.00	1.95	2.02	2.12	1.93	1.39	cytosol	glutamate-ammonia ligases;catalytics;glutamate-ammonia ligases
AT1G28350	1.52	0.00	0.32	0.34	0.52	0.09	0.48	cytosol	Nucleotidylyl transferase superfamily protein
AT2G40840	1.33	0.00	0.12	-0.59	-1.94	-2.67	-2.44	cytosol	disproportionating enzyme 2
AT1G10870	1.30	0.00	-0.22	-0.24	-0.20	-0.12	0.07	cytosol	ARF-GAP domain 4
AT3G07690	1.15	0.01	-0.02	-0.18	-0.21	0.05	0.42	cytosol	6-phosphogluconate dehydrogenase family protein
AT1G71780	1.81	0.01	-0.08	-0.06	0.38	0.36	0.24	reticulum	unknown

AT3G13790	2.94	0.00	0.53	1.98	2.75	3.42	3.91	extracellular	Glycosyl hydrolases family 32 protein
AT5G62360	2.69	0.00	-1.67	-0.94	-1.10	-1.22	-0.10	extracellular	Plant invertase/pectin methylesterase inhibitor superfamily protein
AT5G19280	2.35	0.00	0.04	0.03	-0.02	-0.12	0.18	extracellular	kinase associated protein phosphatase
AT4G24230	1.92	0.01	0.66	0.62	1.49	1.24	0.54	extracellular	acyl-CoA-binding domain 3
AT1G09750	1.48	0.00	-0.34	-0.28	-0.64	-1.01	-1.12	extracellular	Eukaryotic aspartyl protease family protein
AT5G48540	1.47	0.00	2.83	3.07	3.91	3.80	3.09	extracellular	receptor-like protein kinase-related family protein
AT3G22060	1.39	0.00	3.60	3.38	3.60	3.80	3.15	extracellular	Receptor-like protein kinase-related family protein
AT3G14310	1.14	0.01	-1.36	-1.75	-1.66	-1.62	-1.89	extracellular	pectin methylesterase 3
AT1G50200	2.41	0.00	0.08	-0.05	-0.05	-0.11	0.24	mitochondrion	Alanyl-tRNA synthetase
AT5G26920	5.61	0.00	1.89	2.17	3.19	3.59	2.99	mitochondrion	Cam-binding protein 60-like G
AT5G61670	1.51	0.00	-0.49	-0.90	-1.13	-0.59	-0.53	mitochondrion	
AT4G01250	4.83	0.00	2.24	3.24	4.04	3.49	2.35	nucleus	WRKY family transcription factor
AT5G64750	4.69	0.00	0.69	1.85	3.16	3.34	1.50	nucleus	Integrase-type DNA-binding superfamily protein
AT2G22880	4.66	0.00	1.45	1.67	2.70	2.94	1.72	nucleus	VQ motif-containing protein
AT1G62300	4.26	0.00	2.69	2.04	2.47	1.69	1.38	nucleus	WRKY family transcription factor
AT4G23550	3.88	0.00	1.31	2.90	3.46	3.73	1.73	nucleus	WRKY family transcription factor
AT4G01720	3.74	0.00	0.82	1.36	2.92	2.75	2.65	nucleus	WRKY family transcription factor
AT2G38470	3.67	0.00	1.16	2.11	2.61	1.60	1.53	nucleus	WRKY DNA-binding protein 33
AT1G13260	3.22	0.00	-0.49	0.95	1.05	0.86	1.51	nucleus	related to ABI3/VP1 1
AT1G61140	3.03	0.00	0.69	0.49	0.84	1.19	0.56	nucleus	SNF2 domain-containing protein / helicase domain-containing protein / zinc finger protein-related
AT2G03340	2.89	0.00	-0.77	-0.69	-0.32	-0.42	-0.34	nucleus	WRKY DNA-binding protein 3

AT1G68840	2.80	0.00	1.56	1.74	2.82	1.82	1.94	nucleus	related to ABI3/VP1 2
AT3G09830	2.46	0.01	2.25	1.01	1.32	1.41	0.78	nucleus	Protein kinase superfamily protein
AT3G55150	2.30	0.00	NA	3.93	4.58	4.34	NA	nucleus	exocyst subunit exo70 family protein H1
AT4G18880	2.21	0.00	1.61	1.05	1.46	0.99	1.16	nucleus	heat shock transcription factor A4A
AT4G31550	2.19	0.01	1.99	2.66	3.03	2.51	2.07	nucleus	WRKY DNA-binding protein 11
AT2G44370	2.13	0.01	2.39	4.02	5.64	5.03	4.31	nucleus	Cysteine/Histidine-rich C1 domain family protein
AT1G05805	1.95	0.00	0.14	0.52	0.39	0.37	0.37	nucleus	basic helix-loop-helix (bHLH) DNA-binding superfamily protein
AT2G38250	1.89	0.00	0.67	0.92	0.87	0.94	0.90	nucleus	Homeodomain-like superfamily protein
AT5G59870	1.87	0.00	0.52	0.34	0.25	0.30	-0.06	nucleus	histone H2A 6
AT3G09360	1.62	0.01	-0.14	-0.24	-0.09	-0.09	0.31	nucleus	Cyclin/Brf1-like TBP-binding protein
AT4G05410	1.20	0.00	0.02	0.07	0.60	0.30	0.28	nucleus	Transducin/WD40 repeat-like superfamily protein
AT4G03080	1.14	0.01	0.09	0.16	0.13	-0.05	0.03	nucleus	BRI1 suppressor 1 (BSU1)-like 1
AT1G64170	3.64	0.01	0.48	0.86	2.21	3.56	2.38	plasma membrane	cation/H+ exchanger 16
AT1G09970	2.94	0.00	0.37	1.08	1.14	1.27	1.00	plasma membrane	Leucine-rich receptor-like protein kinase family protein
AT1G51800	2.59	0.00	2.97	3.00	4.67	5.16	4.71	plasma membrane	Leucine-rich repeat protein kinase family protein
AT4G21410	2.52	0.01	1.99	2.16	2.93	2.44	1.76	plasma membrane	cysteine-rich RLK (RECEPTOR-like protein kinase) 29
AT4G26550	2.00	0.00	-0.22	-0.16	0.12	0.40	0.52	plasma membrane	Got1/Sft2-like vescicle transport protein family
AT4G21120	1.94	0.00	1.37	2.52	3.36	3.41	2.93	plasma membrane	amino acid transporter 1
AT3G47480	1.63	0.00	0.45	1.05	1.26	2.16	2.51	plasma membrane	Calcium-binding EF-hand family protein
AT1G36390	1.91	0.00	-0.40	-0.31	-0.73	-0.68	-0.41	plastid	Co-chaperone GrpE family protein
AT1G69740	2.79	0.00	-0.21	-0.10	-0.16	-0.14	0.36	plastid	Aldolase superfamily protein

AT5G57710	2.26	0.00	0.75	0.90	1.17	1.60	1.71	plastid	Double Clp-N motif-containing P-loop nucleoside triphosphate hydrolases superfamily protein
AT2G05990	1.79	0.00	-0.12	-0.20	-0.84	-1.14	-0.93	plastid	NAD(P)-binding Rossmann-fold superfamily protein
AT1G62960	1.66	0.01	-0.29	-0.20	-0.21	0.12	0.47	plastid	ACC synthase 10
AT3G54050	1.15	0.01	-0.46	-0.84	-2.11	-2.82	-2.32	plastid	high cyclic electron flow 1
AT5G55220	1.08	0.00	0.14	-0.21	-0.90	-1.85	-2.00	plastid	trigger factor type chaperone family protein
AT3G55270	-2.60	0.01	-0.09	0.43	0.08	0.45	0.13	nucleus	mitogen-activated protein kinase phosphatase 1
AT5G60850	-2.38	0.00	-0.76	-1.44	-0.59	-0.74	-0.49	nucleus	OBF binding protein 4
AT2G15270	-2.14	0.01	-0.04	0.06	-0.02	0.23	0.02	nucleus	
AT2G28550	-2.05	0.00	-1.46	-0.92	-0.83	-0.85	-0.55	nucleus	related to AP2.7

Table S5(B): Proteins showing greater increase or decrease in abundance in the nuclear fraction than the total fraction upon flg22 treatment at 9 h

Protein ID	Ratio[a]		Ratio[b]					SUBAcon	Description
	Proteome		Transcriptome						
	Difference	p.val	1h	2h	3h	5h	9h		
AT1G53310	4.25	0.00	-0.14	-0.19	0.43	1.13	1.68	cytosol	phosphoenolpyruvate carboxylase 1
AT1G62820	2.14	0.01	-0.37	0.04	0.10	0.51	0.03	cytosol	Calcium-binding EF-hand family protein
AT5G52640	1.88	0.00	0.12	2.91	3.73	1.95	1.03	cytosol	heat shock protein 90.1
AT5G11670	1.81	0.00	2.11	2.52	3.18	2.54	1.58	cytosol	NADP-malic enzyme 2
AT3G53180	1.78	0.00	1.95	2.02	2.12	1.93	1.39	cytosol	glutamate-ammonia ligases;catalytics;glutamate-ammonia ligases
AT5G46520	1.72	0.01	0.73	0.75	0.75	0.85	1.05	cytosol	Disease resistance protein (TIR-NBS-LRR class) family
AT4G02880	1.54	0.00	0.21	0.18	-0.13	0.35	0.68	cytosol	
AT5G58200	1.53	0.00	-0.16	-0.48	-0.69	-0.45	-0.50	cytosol	Calcineurin-like metallo-phosphoesterase superfamily protein
AT5G54160	1.49	0.01	1.29	2.09	2.51	4.02	4.09	cytosol	O-methyltransferase 1
AT2G05830	1.24	0.01	-0.21	-0.17	-0.87	-1.39	-1.07	cytosol	NagB/RpiA/CoA transferase-like superfamily protein
AT5G57480	3.59	0.00	0.85	0.70	1.24	1.75	1.60	endoplasmic reticulum	P-loop containing nucleoside triphosphate hydrolases superfamily protein
AT5G52420	2.01	0.01	-0.22	-0.66	-0.98	-1.41	-1.03	endoplasmic reticulum	
AT5G62360	4.44	0.00	-1.67	-0.94	-1.10	-1.22	-0.10	extracellular	Plant invertase/pectin methylesterase inhibitor superfamily protein
AT5G50200	2.17	0.00	2.55	2.77	3.58	4.44	4.41	extracellular	nitrate transmembrane transporters
AT3G13790	1.81	0.00	0.53	1.98	2.75	3.42	3.91	extracellular	Glycosyl hydrolases family 32 protein
AT5G65760	1.57	0.01	0.02	-0.33	-0.78	-0.94	-0.49	extracellular	Serine carboxypeptidase S28 family protein

AT4G12250	2.78	0.00	0.36	0.31	0.50	0.34	0.41	golgi	UDP-D-glucuronate 4-epimerase 5
AT5G26920	5.89	0.00	1.89	2.17	3.19	3.59	2.99	mitochondrion	Cam-binding protein 60-like G
AT4G20010	2.30	0.00	0.51	0.25	0.45	1.06	0.82	mitochondrion	plastid transcriptionally active 9
AT4G01720	5.81	0.00	0.82	1.36	2.92	2.75	2.65	nucleus	WRKY family transcription factor
AT1G62300	3.62	0.00	2.69	2.04	2.47	1.69	1.38	nucleus	WRKY family transcription factor
AT2G38470	3.56	0.00	1.16	2.11	2.61	1.60	1.53	nucleus	WRKY DNA-binding protein 33
AT5G52830	3.54	0.00	0.91	1.66	1.64	2.20	1.47	nucleus	WRKY DNA-binding protein 27
AT4G01250	3.52	0.00	2.24	3.24	4.04	3.49	2.35	nucleus	WRKY family transcription factor
AT5G61560	3.28	0.00	1.58	2.56	3.49	3.19	1.96	nucleus	U-box domain-containing protein kinase family protein
AT5G64750	3.23	0.00	0.69	1.85	3.16	3.34	1.50	nucleus	Integrase-type DNA-binding superfamily protein
AT3G44630	3.14	0.00	0.75	-0.06	-0.28	-0.25	0.19	nucleus	Disease resistance protein (TIR-NBS-LRR class) family
AT2G16900	3.08	0.00	1.44	1.78	2.36	2.38	1.18	nucleus	Arabidopsis phospholipase-like protein (PEARLI 4) family
AT1G13260	3.02	0.00	-0.49	0.95	1.05	0.86	1.51	nucleus	related to ABI3/VP1 1
AT4G18880	3.00	0.00	1.61	1.05	1.46	0.99	1.16	nucleus	heat shock transcription factor A4A
AT2G27660	2.93	0.00	3.06	3.04	4.13	3.38	2.91	nucleus	Cysteine/Histidine-rich C1 domain family protein
AT1G27470	2.91	0.00	-0.01	0.56	0.87	1.03	0.59	nucleus	transducin family protein / WD-40 repeat family protein
AT5G42050	2.77	0.00	0.78	0.95	1.49	1.67	1.47	nucleus	DCD (Development and Cell Death) domain protein
AT5G04020	2.69	0.00	0.13	0.66	0.88	0.71	0.48	nucleus	calmodulin binding
AT1G68840	2.68	0.00	1.56	1.74	2.82	1.82	1.94	nucleus	related to ABI3/VP1 2
AT3G21295	2.60	0.00	0.84	0.34	0.46	0.81	0.37	nucleus	Tudor/PWWP/MBT superfamily protein
AT3G55150	2.55	0.00	NA	3.93	4.58	4.34	NA	nucleus	exocyst subunit exo70 family protein H1
AT5G48160	2.52	0.00	-0.20	0.18	0.54	0.59	0.38	nucleus	Protein of unknown function (DUF1423)
AT1G73805	2.34	0.00	0.53	-0.02	0.07	0.58	0.75	nucleus	Calmodulin binding protein-like

AT2G38250	2.32	0.00	0.67	0.92	0.87	0.94	0.90	nucleus	Homeodomain-like superfamily protein
AT2G25000	2.21	0.00	-0.09	-0.07	1.38	1.57	1.72	nucleus	WRKY DNA-binding protein 60
AT3G27260	2.17	0.00	0.15	0.42	0.24	0.33	0.21	nucleus	global transcription factor group E8
AT2G44370	2.15	0.00	2.39	4.02	5.64	5.03	4.31	nucleus	Cysteine/Histidine-rich C1 domain family protein
AT2G42280	2.14	0.00	-0.12	0.10	0.09	0.44	0.43	nucleus	basic helix-loop-helix (bHLH) DNA-binding superfamily protein
AT3G09830	2.00	0.00	2.25	1.01	1.32	1.41	0.78	nucleus	Protein kinase superfamily protein
AT1G80840	1.93	0.00	3.43	2.07	2.01	1.72	1.29	nucleus	WRKY DNA-binding protein 40
AT4G31800	1.93	0.00	0.60	0.39	1.06	1.27	1.79	nucleus	WRKY DNA-binding protein 18
AT5G15130	1.60	0.01	0.19	NA	NA	NA	1.44	nucleus	WRKY DNA-binding protein 72
AT3G01830	1.34	0.01	3.21	3.04	3.19	2.64	2.09	nucleus	Calcium-binding EF-hand family protein
AT5G20050	5.97	0.00	1.16	2.01	3.46	3.11	2.08	plasma membrane	Protein kinase superfamily protein
AT3G47480	4.75	0.00	0.45	1.05	1.26	2.16	2.51	plasma membrane	Calcium-binding EF-hand family protein
AT1G10340	4.16	0.00	1.72	1.34	1.81	1.85	1.86	plasma membrane	Ankyrin repeat family protein
AT3G21080	4.05	0.00	-0.05	0.03	0.96	2.15	2.92	plasma membrane	ABC transporter-related
AT1G51800	3.28	0.00	2.97	3.00	4.67	5.16	4.71	plasma membrane	Leucine-rich repeat protein kinase family protein
AT4G23200	3.20	0.00	0.74	1.30	0.57	0.83	0.50	plasma membrane	cysteine-rich RLK (RECEPTOR-like protein kinase) 12
AT2G39200	3.05	0.00	4.01	3.57	6.05	6.22	5.28	plasma membrane	Seven transmembrane MLO family protein
AT3G28540	2.78	0.00	-0.03	-0.33	-0.44	0.76	1.66	plasma membrane	P-loop containing nucleoside triphosphate hydrolases superfamily protein
AT1G09970	2.53	0.00	0.37	1.08	1.14	1.27	1.00	plasma membrane	Leucine-rich receptor-like protein kinase family protein
AT5G54710	2.46	0.00	1.33	2.00	2.85	2.06	1.68	plasma membrane	Ankyrin repeat family protein
AT2G18690	1.90	0.01	1.99	2.09	2.78	3.29	3.36	plasma membrane	
AT5G57710	2.08	0.00	0.75	0.90	1.17	1.60	1.71	plastid	Double Clp-N motif-containing P-loop nucleoside triphosphate hydrolases superfamily protein

AT3G07780	1.90	0.00	0.61	0.72	0.76	0.69	0.36	plastid	Protein of unknown function (DUF1423)
AT2G46910	1.81	0.00	-0.14	-0.72	-0.85	-1.21	-1.28	plastid	Plastid-lipid associated protein PAP / fibrillin family protein
AT2G37020	1.70	0.01	-0.08	-0.30	-0.24	-0.26	-0.07	plastid	Translin family protein
AT1G69740	1.66	0.00	-0.21	-0.10	-0.16	-0.14	0.36	plastid	Aldolase superfamily protein
AT2G17972	1.53	0.01	-0.21	-0.97	-0.97	-1.37	-0.55	plastid	
AT2G27680	1.40	0.01	-0.19	-0.43	-1.03	-1.57	-1.65	plastid	NAD(P)-linked oxidoreductase superfamily protein
AT5G36210	1.21	0.00	-0.08	-0.69	-0.60	-1.02	-0.19	plastid	alpha/beta-Hydrolases superfamily protein
AT4G21750	-2.34	0.01	-0.14	-0.02	-0.42	-0.48	-0.47	nucleus	Homeobox-leucine zipper family protein / lipid-binding START domain-containing protein
AT2G43010	-2.32	0.00	-0.82	-1.00	-1.62	-2.23	-1.37	nucleus	phytochrome interacting factor 4
AT5G28300	-2.06	0.00	-1.90	-1.44	-1.12	-1.06	-0.51	nucleus	Duplicated homeodomain-like superfamily protein
AT1G47900	-1.81	0.00	-0.06	-0.18	-0.55	-0.29	-0.49	nucleus	Plant protein of unknown function (DUF869)
AT5G60850	-1.62	0.00	-0.76	-1.44	-0.59	-0.74	-0.49	nucleus	OBF binding protein 4

Table S5: Table showing potential candidates involved in relaying flg22 perception. Proteins that shows change in nuclear abundance but no change in the total protein fraction at 3 h **(A)** or 9 h **(B)** in the nuclear fraction. Proteome changes in nuclear (Nuc) and total (Tot) fractions and difference between them (Difference) are shown. A two-tailed *t*-test was used to calculate p-values (pval) corresponding to the difference between protein abundance change in the nuclear and total fraction calculated over 6-biological replicates. Ratio[a] represents protein abundance change in Col-0 plants in response to flg22 vs mock treatment. Ratio[b] represents transcriptome change in Col-0 vs *fls2* plants in response to flg22 treatment over indicated time-points. SUBA4 predicted subcellular localizations (SUBAcon) and descriptions are indicated for the proteins shown.

Table S6:

Table S6 (A): Correlation among replicates in the nuclear fraction at 15 min

Nuclear			flg 1	flg 2	flg 3	flg 4	flg 5	flg 6	mock 1	mock 2	mock 3	mock 4	mock 5	mock6
	flg22 15min	flg 1	1.00											
		flg 2	0.96	1.00										
		flg 3	0.94	0.94	1.00									
		flg 4	0.87	0.85	0.83	1.00								
		flg 5	0.86	0.84	0.81	0.94	1.00							
		flg 6	0.89	0.88	0.89	0.90	0.89	1.00						
	mock 15min	mock 1	0.87	0.85	0.81	0.85	0.85	0.81	1.00					
		mock 2	0.87	0.86	0.82	0.86	0.85	0.83	0.93	1.00				
		mock 3	0.91	0.90	0.89	0.85	0.84	0.87	0.91	0.93	1.00			
		mock 4	0.88	0.87	0.85	0.95	0.94	0.92	0.84	0.85	0.86	1.00		
		mock 5	0.88	0.86	0.85	0.95	0.94	0.92	0.85	0.86	0.87	0.96	1.00	
		mock6	0.90	0.89	0.89	0.92	0.91	0.95	0.83	0.85	0.87	0.94	0.94	1.00
			flg 1	flg 2	flg 3	flg 4	flg 5	flg 6	mock 1	mock 2	mock 3	mock 4	mock 5	mock6
			flg22 15min						mock 15min					
			Nuclear											

Table S6 (B): Correlation among replicates in the nuclear fraction at 30 min

Nuclear			flg 1	flg 2	flg 3	mock 1	mock 2	mock 3
	flg22 30min	flg 1	1.00					
		flg 2	0.96	1.00				
		flg 3	0.95	0.96	1.00			
	mock 30min	mock 1	0.96	0.97	0.96	1.00		
		mock 2	0.95	0.97	0.97	0.97	1.00	
		mock 3	0.95	0.96	0.97	0.97	0.97	1.00
			flg 1	flg 2	flg 3	mock 1	mock 2	mock 3
			flg22 30min			mock 30min		
			Nuclear					

Table S6 (C): Correlation among replicates in the nuclear fraction at 60 min

Nuclear			flg 1	flg 2	flg 3	mock 1	mock 2	mock 3
	flg22 60min	flg 1	1.00					
		flg 2	0.95	1.00				
		flg 3	0.95	0.97	1.00			
	mock 60min	mock 1	0.95	0.96	0.95	1.00		
		mock 2	0.96	0.97	0.97	0.97	1.00	
		mock 3	0.95	0.96	0.96	0.96	0.97	1.00
			flg 1	flg 2	flg 3	mock 1	mock 2	mock 3
			flg22 60min			mock 60min		
			Nuclear					

Table S6 (D): Correlation among replicates in the nuclear fraction at 60 min after CHX treatment

Nuclear			flg 1	flg 2	flg 3	mock 1	mock 2	mock 3
	CHX 60min	flg 1	1.00					
		flg 2	0.97	1.00				
		flg 3	0.95	0.95	1.00			
	CHX 60min	mock 1	0.97	0.96	0.95	1.00		
		mock 2	0.95	0.95	0.96	0.95	1.00	
		mock 3	0.95	0.94	0.95	0.95	0.95	1.00
			flg 1	flg 2	flg 3	mock 1	mock 2	mock 3
			CHX 60min			CHX 60min		
			Nuclear					

Table S6 (E): Correlation among replicates in the total fraction at 15 min

Total														
	flg22 15min	flg 1	1.00											
		flg 2	0.89	1.00										
		flg 3	0.93	0.89	1.00									
		flg 4	0.92	0.84	0.90	1.00								
		flg 5	0.91	0.84	0.90	0.96	1.00							
		flg 6	0.91	0.84	0.90	0.97	0.96	1.00						
	mock 15min	mock 1	0.93	0.89	0.91	0.89	0.89	0.89	1.00					
		mock 2	0.92	0.91	0.90	0.86	0.86	0.86	0.91	1.00				
		mock 3	0.94	0.89	0.95	0.91	0.91	0.92	0.93	0.92	1.00			
		mock 4	0.92	0.84	0.90	0.95	0.96	0.96	0.89	0.86	0.91	1.00		
		mock 5	0.91	0.84	0.90	0.96	0.96	0.96	0.89	0.86	0.91	0.96	1.00	
		mock6	0.91	0.83	0.89	0.97	0.97	0.96	0.89	0.86	0.91	0.96	0.97	1.00
			flg 1	flg 2	flg 3	flg 4	flg 5	flg 6	mock 1	mock 2	mock 3	mock 4	mock 5	mock6
			flg22 15min						mock 15min					
			Total											

Table S6 (F): Correlation among replicates in the total fraction at 30 min

Total								
	flg22 30min	flg 1	1.00					
		flg 2	0.95	1.00				
		flg 3	0.95	0.93	1.00			
	mock 30min	mock 1	0.97	0.94	0.95	1.00		
		mock 2	0.96	0.96	0.94	0.96	1.00	
		mock 3	0.93	0.91	0.95	0.93	0.91	1.00
			flg 1	flg 2	flg 3	mock 1	mock 2	mock 3
			flg22 30min			mock 30min		
			Total					

Table S6 (G): Correlation among replicates in the total fraction at 60 min

Total								
	flg22 60min	flg 1	1.00					
		flg 2	0.94	1.00				
		flg 3	0.93	0.93	1.00			
	mock 60min	mock 1	0.96	0.94	0.93	1.00		
		mock 2	0.95	0.95	0.92	0.95	1.00	
		mock 3	0.92	0.92	0.96	0.93	0.92	1.00
			flg 1	flg 2	flg 3	mock 1	mock 2	mock 3
			flg22 60min			mock 60min		
			Total					

Table S6 (H): Correlation among replicates in the total fraction at 60 min after CHX treatment

Total								
	CHX 60min	flg 1	1.00					
		flg 2	0.94	1.00				
		flg 3	0.95	0.92	1.00			
	CHX 60min	mock 1	0.93	0.91	0.92	1.00		
		mock 2	0.95	0.95	0.93	0.93	1.00	
		mock 3	0.94	0.92	0.96	0.91	0.93	1.00
			flg 1	flg 2	flg 3	mock 1	mock 2	mock 3
			CHX 60min			CHX 60min		
			Total					

Table S6: Table showing level of correlation between samples for each treatment and replicate. LFQ intensities were used to calculate correlation (R^2 values) in Perseus (version 1.5.2.6). The R^2 values are indicated for nuclear fraction at 15 min **(A)**, 30 min **(B)**, 60 min **(C)** and total fraction at 15 min **(E)**, 30 min **(F)**, 60 min **(G)** after 1 µM-flg22 or mock treatment. The R^2 values after 60 min of 100 µM-CHX or mock (DMSO) treatment are indicated for nuclear **(D)** and total **(E)** fractions. Total and nuclear proteins were isolated from Col-0 seedlings (12-day old). For 15 min samples six replicates (protein samples were prepared in two different days each containing three replicates prepared from independent plant materials) were prepared for each condition. For 30 and 60 min and CHX/DMSO treated samples three replicates (from independent plant materials) were prepared for each condition.

Table S7:

Table S7(A): Differentially expressed proteins in nuclear fraction at 15 min after flg22 treatment

Protein ID	Proteome								SUBAcon	Description
	Nuc				Tot					
	15min	30min	60min	CHX	15min	30min	60min	CHX		
AT3G02550	2.62	0.32	1.05	-2.54	NA	NA	NA	NA	nucleus	LOB domain-containing protein 41
AT1G33790	2.25	0.01	-24.77	-24.71	-0.34	0.42	-0.29	0.36	cytosol	jacalin lectin family protein
AT2G35540	2.05	-0.13	-0.11	0.08	NA	NA	NA	NA	nucleus	DNAJ heat shock N-terminal domain-containing protein
AT3G52250	1.70	0.06	0.02	-0.07	NA	NA	NA	NA	nucleus	Duplicated homeodomain-like superfamily protein
AT5G21010	1.64	-0.11	-0.19	-0.14	NA	0.19	0.32	0.19	cytosol	BTB-POZ and MATH domain 5
AT5G64220	1.60	1.10	0.95	1.51	-0.21	-0.14	0.04	-0.40	nucleus	Calmodulin-binding transcription activator protein with CG-1 and Ankyrin domains
AT3G21810	1.58	-0.11	-0.10	0.05	NA	NA	NA	NA	nucleus	Zinc finger C-x8-C-x5-C-x3-H type family protein
AT1G51720	1.56	0.12	0.20	-0.04	NA	NA	NA	NA	cytosol	Amino acid dehydrogenase family protein
AT3G06340	1.48	-0.02	-0.03	0.05	NA	NA	NA	NA	nucleus	DNAJ heat shock N-terminal domain-containing protein
AT4G38495	1.46	0.18	-0.34	-0.03	NA	NA	NA	NA	cytosol	
AT3G16650	1.40	0.05	0.21	-0.12	NA	NA	NA	NA	cytosol	Transducin/WD40 repeat-like superfamily protein
AT4G32620	1.37	0.18	0.07	-0.19	NA	NA	NA	NA	nucleus	Enhancer of polycomb-like transcription factor protein
AT2G22300	1.32	0.45	0.18	0.97	-0.22	0.20	-0.42	-0.51	nucleus	signal responsive 1
AT1G19485	1.24	-0.08	-0.11	-0.10	NA	NA	NA	NA	nucleus	Transducin/WD40 repeat-like superfamily protein
AT5G35210	1.10	-0.13	0.08	-0.06	NA	NA	NA	NA	nucleus	metalloendopeptidases;zinc ion binding;DNA binding
AT5G10810	1.05	0.09	0.04	-0.01	NA	NA	NA	NA	cytosol	enhancer of rudimentary protein, putative
AT3G10390	1.05	-0.06	0.03	-0.09	22.11	NA	NA	NA	plastid	Flavin containing amine oxidoreductase family protein
AT5G62270	1.02	0.10	-0.29	0.00	-0.42	0.26	-0.60	0.60	mitochondrion	
AT1G51830	-1.00	0.05	-0.01	0.30	NA	NA	NA	NA	plasma membrane	Leucine-rich repeat protein kinase family protein
AT4G01050	-1.00	0.34	0.16	0.07	0.03	0.04	-0.21	-0.02	plastid	thylakoid rhodanese-like
AT1G48090	-1.02	-0.01	-0.54	0.31	-1.00	0.29	0.22	0.13	golgi	calcium-dependent lipid-binding family protein
AT5G20350	-1.03	-0.32	-0.30	0.10	0.54	-0.13	0.54	0.26	golgi	Ankyrin repeat family protein with DHHC zinc finger domain
ATCG00280	-1.05	0.27	0.46	0.31	0.04	0.37	0.02	-0.07	plastid	photosystem II reaction center protein C
AT5G58710	-1.05	-0.15	0.16	0.35	0.03	0.35	0.20	-0.35	endoplasmic reticulum	rotamase CYP 7
AT3G47930	-1.06	-0.05	0.06	0.64	-0.20	-0.04	0.28	0.12	mitochondrion	L-galactono-1,4-lactone dehydrogenase
AT1G74730	-1.06	-0.17	-0.04	-0.49	0.19	0.44	0.16	-0.58	plastid	Protein of unknown function (DUF1118)
AT4G11960	-1.06	0.52	0.03	0.39	0.04	0.10	-0.13	0.15	plastid	PGR5-like B

AT1G74470	-1.07	0.25	0.27	0.18	-0.07	0.08	-0.11	0.29	plastid	Pyridine nucleotide-disulphide oxidoreductase family protein
AT2G47380	-1.07	-0.13	0.04	-0.35	0.73	-0.34	-0.26	-0.87	mitochondrion	Cytochrome c oxidase subunit Vc family protein
AT1G77590	-1.07	0.12	-0.16	0.53	-0.18	0.07	0.18	-0.20	plastid	long chain acyl-CoA synthetase 9
AT1G35620	-1.08	-0.31	-0.15	0.16	-0.04	-0.15	-0.14	-0.12	endoplasmic reticulum	PDI-like 5-2
AT2G30695	-1.09	1.23	0.13	1.91	0.14	-0.07	0.00	-0.20	plastid	
AT2G35190	-1.09	-1.02	-0.45	-0.75	0.31	-0.31	0.14	0.07	cytosol	novel plant snare 11
AT1G14345	-1.09	0.09	0.53	0.30	0.00	0.15	-0.16	-0.16	plastid	NAD(P)-linked oxidoreductase superfamily protein
AT4G25450	-1.09	0.48	0.09	0.16	-0.06	-0.14	0.28	0.13	plastid	non-intrinsic ABC protein 8
AT2G20940	-1.10	-0.09	0.17	-0.03	0.16	0.07	0.01	-0.08	mitochondrion	Protein of unknown function (DUF1279)
AT2G27730	-1.11	-0.04	-0.13	0.06	0.12	-0.11	0.18	-0.21	mitochondrion	copper ion binding
AT2G26280	-1.12	-0.30	-0.76	-0.55	-0.14	-0.25	-0.28	0.10	nucleus	CTC-interacting domain 7
AT3G59780	-1.13	0.29	-0.06	0.02	-0.09	0.24	0.04	0.22	plastid	Rhodanese/Cell cycle control phosphatase superfamily protein
AT3G13150	-1.14	-0.78	-0.34	-0.78	-0.06	-0.20	-0.21	0.00	nucleus	Tetratricopeptide repeat (TPR)-like superfamily protein
AT1G73990	-1.15	0.42	0.01	0.04	-0.10	0.16	0.05	0.28	plastid	signal peptide peptidase
AT5G66570	-1.16	0.42	0.16	0.17	-0.09	0.09	-0.14	-0.15	plastid	PS II oxygen-evolving complex 1
AT5G65950	-1.16	-0.06	0.05	0.70	0.15	0.20	-0.01	0.08	cytosol	
AT5G63980	-1.16	NA	NA	NA	-0.02	0.01	0.09	-0.03	plastid	Inositol monophosphatase family protein
AT1G06530	-1.19	-0.03	-0.02	0.44	0.11	-0.28	0.09	0.07	mitochondrion	Tropomyosin-related
ATCG00680	-1.20	0.34	0.65	0.14	-0.18	0.20	0.09	0.17	plastid	photosystem II reaction center protein B
AT3G25070	-1.21	-0.49	-0.14	-0.33	-0.28	0.28	-0.32	-0.19	plasma membrane	RPM1 interacting protein 4
AT3G43540	-1.21	0.15	0.78	0.57	0.00	0.19	0.27	0.05	plastid	Protein of unknown function (DUF1350)
AT5G11860	-1.21	0.58	0.80	0.08	NA	NA	NA	NA	cytosol	SCP1-like small phosphatase 5
AT3G23530	-1.22	0.03	-0.06	0.29	-0.07	0.12	-0.22	0.09	plasma membrane	Cyclopropane-fatty-acyl-phospholipid synthase
AT1G64430	-1.22	-0.08	-0.32	0.13	0.36	0.15	0.12	-0.01	plastid	Pentatricopeptide repeat (PPR) superfamily protein
AT4G13200	-1.23	-0.02	-0.12	0.10	0.26	-0.14	-0.20	0.07	plastid	
AT4G00585	-1.24	-0.93	-0.88	-0.15	-0.07	-0.23	0.31	0.75	mitochondrion	
AT5G04900	-1.26	0.31	0.51	0.58	-0.71	-0.27	0.32	0.23	plastid	NYC1-like
AT2G18770	-1.27	-0.23	0.30	0.47	0.24	0.21	0.18	0.03	endoplasmic reticulum	P-loop containing nucleoside triphosphate hydrolases superfamily protein
AT5G03880	-1.28	0.09	-0.04	0.16	-0.04	0.18	-0.05	0.21	plastid	Thioredoxin family protein
AT1G55340	-1.29	-0.13	-0.24	-0.17	NA	NA	NA	NA	nucleus	Protein of unknown function (DUF1639)
AT4G15560	-1.31	0.49	0.77	-0.08	-0.27	0.38	0.18	0.34	plastid	Deoxyxylulose-5-phosphate synthase
ATCG00580	-1.32	0.72	1.33	0.50	-0.05	-0.07	-0.05	0.03	plastid	photosystem II reaction center protein E
ATCG01110	-1.35	-0.14	0.76	0.15	-0.17	0.17	0.27	0.22	plastid	NAD(P)H dehydrogenase subunit H

ATCG00270	-1.35	0.22	0.49	0.08	-0.05	0.23	-0.06	0.08	plastid	photosystem II reaction center protein D
AT5G03160	-1.35	0.44	-0.67	-0.54	-0.48	-0.22	0.26	0.01	endoplasmic reticulum	homolog of mamallian P58IPK
AT1G31330	-1.35	0.01	0.17	-0.17	0.14	0.21	0.03	0.19	plastid	photosystem I subunit F
AT3G16480	-1.38	-0.18	0.28	0.00	0.07	-0.32	0.00	-0.07	mitochondrion	mitochondrial processing peptidase alpha subunit
AT5G57030	-1.38	-0.49	0.89	-0.41	-0.25	-0.16	-0.13	0.26	plastid	Lycopene beta/epsilon cyclase protein
AT2G32240	-1.38	-0.13	-0.28	-0.04	0.06	-0.08	0.02	-0.04	cytosol	
ATCG00340	-1.39	0.12	0.49	0.10	-0.11	0.16	0.02	0.19	plastid	Photosystem I, PsaA/PsaB protein
AT4G02770	-1.41	0.09	0.36	0.17	-0.03	0.23	0.08	0.04	plastid	photosystem I subunit D-1
AT2G20890	-1.43	0.47	0.47	0.12	0.00	-0.06	0.05	0.32	plastid	photosystem II reaction center PSB29 protein
AT2G22795	-1.49	-0.60	-0.23	-0.45	-0.15	-0.02	-0.24	-0.27	golgi	
AT5G42150	-1.49	0.62	0.38	-0.23	-0.20	-0.18	0.16	-0.23	mitochondrion	Glutathione S-transferase family protein
AT1G76550	-1.50	0.05	0.15	0.42	-0.13	0.24	0.12	-0.12	cytosol	Phosphofructokinase family protein
AT2G30740	-1.50	NA	NA	NA	-0.14	0.10	0.23	-0.08	cytosol	Protein kinase superfamily protein
ATCG00350	-1.52	-0.02	0.32	0.31	0.03	0.36	-0.03	0.19	plastid	Photosystem I, PsaA/PsaB protein
AT1G74880	-1.57	-0.01	0.62	0.15	-0.07	-0.09	-0.23	0.17	plastid	NAD(P)H:plastoquinone dehydrogenase complex subunit O
AT5G67030	-1.59	0.15	0.11	0.10	0.12	0.29	0.01	0.17	plastid	zeaxanthin epoxidase (ZEP) (ABA1)
AT5G14600	-1.63	NA	NA	NA	-0.73	NA	NA	NA	endoplasmic reticulum	S-adenosyl-L-methionine-dependent methyltransferases superfamily protein
AT2G32480	-1.63	0.15	0.10	0.15	0.06	0.15	-0.08	-0.63	plastid	ARABIDOPSIS SERIN PROTEASE
AT5G02120	-1.65	0.57	0.29	0.22	-0.07	0.68	0.06	0.75	plastid	one helix protein
AT2G42310	-1.65	-0.08	-0.72	-0.73	0.15	0.53	1.45	0.83	mitochondrion	
AT5G58260	-1.74	0.07	0.69	0.12	0.05	0.35	-0.02	0.09	plastid	oxidoreductases, acting on NADH or NADPH, quinone or similar compound as acceptor
AT3G21865	-1.74	0.13	0.42	0.33	-0.27	0.09	0.42	0.35	nucleus	peroxin 22
AT2G18710	-1.80	0.02	0.13	-0.15	0.27	0.04	-0.02	0.38	plastid	SECY homolog 1
AT1G19580	-1.85	0.15	0.04	0.07	-0.21	-0.60	-0.85	-0.12	mitochondrion	gamma carbonic anhydrase 1
AT1G01170	-1.94	0.62	-0.02	0.69	0.20	0.24	-0.13	-0.05	plasma membrane	Protein of unknown function (DUF1138)
AT1G52410	-1.97	0.26	0.06	-1.01	-0.80	0.16	0.00	-0.44	extracellular	TSK-associating protein 1
AT2G14750	-2.09	0.05	0.00	0.55	-0.61	-0.16	0.32	-0.23	plastid	APS kinase
ATCG00430	-2.19	-0.30	-0.52	0.87	-0.03	0.25	-0.28	0.09	plastid	photosystem II reaction center protein G
AT3G08920	-2.19	-0.37	0.03	0.61	0.16	0.29	-0.03	-0.01	plastid	Rhodanese/Cell cycle control phosphatase superfamily protein
AT3G03100	-2.34	-0.51	-0.36	0.33	0.88	-0.19	0.56	0.25	mitochondrion	NADH:ubiquinone oxidoreductase, 17.2kDa subunit
AT5G57345	-2.59	-0.27	-0.15	0.63	0.22	0.65	-0.22	0.09	plastid	
AT1G14150	-2.59	0.18	0.04	0.18	0.38	0.17	0.02	0.42	plastid	PsbQ-like 2
AT4G31390	-2.88	-0.14	0.06	0.17	-0.04	0.14	0.09	0.22	plastid	Protein kinase superfamily protein
AT4G23890	-2.94	-1.04	-0.11	-0.25	0.21	0.15	-0.06	0.04	plastid	
AT4G39710	-3.08	22.45	0.31	-0.17	0.18	0.04	0.13	-0.06	plastid	FK506-binding protein 16-2
AT1G02910	-3.48	-0.49	0.28	0.88	0.18	-0.05	-0.08	0.06	plastid	tetratricopeptide repeat (TPR)-containing protein
AT5G42270	-4.13	1.29	0.42	0.54	-0.10	0.00	-0.05	0.21	plastid	FtsH extracellular protease family

Table S7(B): Differentially expressed proteins in nuclear fraction at 30 min after flg22 treatment

Protein ID	Proteome								SUBAcon	Description
	Nuc				Tot					
	15min	30min	60min	CHX	15min	30min	60min	CHX		
AT2G22880	NA	3.08	4.62	-0.01	NA	NA	NA	NA	nucleus	VQ motif-containing protein
AT5G59820	NA	2.72	25.39	-1.21	NA	NA	NA	NA	nucleus	C2H2-type zinc finger family protein
AT1G08420	26.04	2.42	1.20	1.57	-0.33	-0.04	0.04	0.14	nucleus	BRI1 suppressor 1 (BSU1)-like 2
AT2G35040	25.50	1.66	0.08	-0.16	-0.02	0.01	0.13	-0.04	plastid	AICARFT/IMPCHase bienzyme family protein
AT3G10670	0.24	1.40	0.31	-0.01	0.06	0.20	-0.12	-0.10	plastid	non-intrinsic ABC protein 7
AT3G11960	NA	1.35	-0.35	0.92	NA	NA	NA	NA	nucleus	Cleavage and polyadenylation specificity factor (CPSF) A subunit protein
AT5G55220	0.54	1.31	0.52	0.62	-0.05	-0.08	-0.04	0.22	plastid	trigger factor type chaperone family protein
AT4G29780	0.54	1.20	2.28	-0.41	NA	NA	22.04	NA	cytosol	
AT1G76080	0.23	1.18	1.13	1.34	-0.12	0.12	0.21	-0.10	plastid	chloroplastic drought-induced stress protein of 32 kD
AT1G09750	NA	1.15	1.32	-0.43	0.24	0.09	-0.05	0.11	extracellular	Eukaryotic aspartyl protease family protein
AT3G19480	-0.46	1.14	0.98	0.72	0.05	0.33	0.27	0.48	plastid	D-3-phosphoglycerate dehydrogenase
AT5G64220	1.60	1.10	0.95	1.51	-0.21	-0.14	0.04	-0.40	nucleus	Calmodulin-binding transcription activator protein with CG-1 and Ankyrin domains
AT5G27030	1.32	1.08	0.75	0.64	24.49	-0.12	0.20	-0.68	extracellular	TOPLESS-related 3
AT2G25840	0.42	1.07	0.08	-0.21	0.19	0.08	-0.01	0.12	plastid	Nucleotidylyl transferase superfamily protein
AT5G42390	0.63	1.03	0.30	0.52	0.03	0.16	0.05	0.14	plastid	Insulinase (Peptidase family M16) family protein
AT2G35190	-1.09	-1.02	-0.45	-0.75	0.31	-0.31	0.14	0.07	cytosol	novel plant snare 11
AT1G07250	0.50	-1.02	0.23	-0.13	-0.31	0.00	0.04	0.06	cytosol	UDP-glucosyl transferase 71C4
AT5G18800	-26.70	-1.12	-0.61	-0.07	-0.08	0.09	-0.05	-0.35	cytosol	Cox19-like CHCH family protein
AT2G06510	-0.51	-1.14	0.00	-0.03	NA	NA	NA	NA	nucleus	replication protein A 1A
AT5G64400	NA	-1.26	0.01	-0.45	-0.61	0.02	0.26	0.35	mitochondrion	
AT1G33750	23.51	-1.27	-0.22	-0.06	NA	NA	NA	NA	mitochondrion	Terpenoid cyclases/Protein prenyltransferases superfamily protein
AT3G62870	-0.54	-1.34	-0.09	-0.09	0.05	-0.14	0.12	-0.21	cytosol	Ribosomal protein L7Ae/L30e/S12e/Gadd45 family protein
AT3G12915	-0.29	-1.35	-0.35	0.43	-0.27	0.69	0.00	-0.53	cytosol	Ribosomal protein S5/Elongation factor G/III/V family protein
AT5G14280	NA	-1.38	-0.86	-1.37	NA	0.88	0.21	0.38	nucleus	DNA-binding storekeeper protein-related
AT5G62340	-21.30	-1.44	-0.07	-0.83	-0.74	24.40	0.15	-0.48	extracellular	Plant invertase/pectin methylesterase inhibitor superfamily protein
AT4G12600	-0.03	-1.54	0.44	0.46	-0.08	-0.48	-0.18	-0.32	cytosol	Ribosomal protein L7Ae/L30e/S12e/Gadd45 family protein
AT4G34610	NA	-1.61	0.11	-0.69	NA	NA	NA	NA	nucleus	BEL1-like homeodomain 6
AT3G05490	NA	-2.25	-1.89	0.43	NA	NA	NA	NA	extracellular	ralf-like 22

Table S7(C): Differentially expressed proteins in nuclear fraction at 60 min after flg22 treatment

Protein ID	Proteome								SUBAcon	Description
	Nuc				Tot					
	15min	30min	60min	CHX	15min	30min	60min	CHX		
AT2G22880	NA	3.08	4.62	-0.01	NA	NA	NA	NA	nucleus	VQ motif-containing protein
AT1G80840	22.43	0.99	3.15	-1.30	NA	NA	NA	NA	nucleus	WRKY DNA-binding protein 40
AT5G64660	NA	-23.51	2.80	-25.47	NA	NA	NA	NA	nucleus	CYS, MET, PRO, and GLY protein 2
AT1G65390	NA	0.53	2.46	-1.06	NA	NA	NA	NA	plastid	phloem protein 2 A5
AT4G29780	0.54	1.20	2.28	-0.41	NA	NA	22.04	NA	cytosol	
AT2G38470	0.18	0.82	2.27	-0.16	NA	NA	NA	NA	nucleus	WRKY DNA-binding protein 33
AT5G14590	NA	0.44	1.52	0.26	0.01	0.09	0.11	-0.02	mitochondrion	Isocitrate/isopropylmalate dehydrogenase family protein
AT4G31550	NA	-0.08	1.50	-1.39	NA	NA	NA	NA	nucleus	WRKY DNA-binding protein 11
AT4G31800	0.58	0.74	1.41	-0.86	NA	NA	NA	NA	nucleus	WRKY DNA-binding protein 18
AT1G68840	0.32	0.84	1.40	-1.74	NA	NA	NA	NA	nucleus	related to ABI3/VP1 2
AT4G17900	NA	0.36	1.36	-0.11	NA	NA	NA	NA	nucleus	PLATZ transcription factor family protein
ATCG00580	-1.32	0.72	1.33	0.50	-0.05	-0.07	-0.05	0.03	plastid	photosystem II reaction center protein E
AT1G09750	NA	1.15	1.32	-0.43	0.24	0.09	-0.05	0.11	extracellular	Eukaryotic aspartyl protease family protein
AT3G54810	25.28	0.67	1.32	-2.82	NA	NA	NA	NA	nucleus	Plant-specific GATA-type zinc finger transcription factor family protein
AT1G08420	26.04	2.42	1.20	1.57	-0.33	-0.04	0.04	0.14	nucleus	BRI1 suppressor 1 (BSU1)-like 2
AT1G76080	0.23	1.18	1.13	1.34	-0.12	0.12	0.21	-0.10	plastid	chloroplastic drought-induced stress protein of 32 kD
AT2G42600	-0.07	0.55	1.12	1.02	-0.06	0.03	0.03	0.03	cytosol	phosphoenolpyruvate carboxylase 2
AT5G08790	0.17	0.29	1.09	-0.81	-0.99	NA	NA	NA	nucleus	NAC (No Apical Meristem) domain transcriptional regulator superfamily protein
AT2G47800	-0.15	-0.14	1.02	-0.04	-0.03	-0.36	0.00	0.05	plasma membrane	multidrug resistance-associated protein 4
AT3G52840	NA	0.28	1.00	-0.70	0.05	0.12	0.21	-0.06	extracellular	beta-galactosidase 2
AT2G03340	0.60	-0.78	-1.24	-0.31	NA	NA	NA	NA	nucleus	WRKY DNA-binding protein 3
AT3G57090	NA	-23.11	-1.25	-0.29	0.01	0.15	-0.12	-0.02	mitochondrion	Tetratricopeptide repeat (TPR)-like superfamily protein
AT4G32160	NA	0.00	-1.31	-0.86	NA	1.14	0.00	-0.54	nucleus	Phox (PX) domain-containing protein
AT2G30590	24.22	-0.82	-1.32	0.05	NA	NA	NA	NA	nucleus	WRKY DNA-binding protein 21
AT1G54580	0.65	-0.58	-1.51	1.90	-0.31	-2.76	1.02	0.65	plastid	acyl carrier protein 2
AT5G40440	-24.35	-0.03	-1.69	0.20	0.20	0.32	-0.30	-0.47	cytosol	mitogen-activated protein kinase kinase 3
AT5G28220	NA	0.40	-1.82	23.67	NA	0.69	0.09	-0.48	cytosol	Protein prenylyltransferase superfamily protein
AT3G05490	NA	-2.25	-1.89	0.43	NA	NA	NA	NA	extracellular	ralf-like 22
AT5G51440	NA	-0.96	-2.13	-0.29	NA	-23.38	-23.87	-0.73	mitochondrion	HSP20-like chaperones superfamily protein

Table S7(D): Differentially expressed proteins in nuclear fraction at 60 min after CHX treatment

Protein ID	Proteome								SUBAcon	Description
	Nuc				Tot					
	15min	30min	60min	CHX	15min	30min	60min	CHX		
AT5G47390	NA	0.19	0.19	1.75	NA	-0.35	23.13	-0.13	nucleus	myb-like transcription factor family protein
AT5G64220	1.60	1.10	0.95	1.51	-0.21	-0.14	0.04	-0.40	nucleus	Calmodulin-binding transcription activator protein with CG-1 and Ankyrin domains
AT1G65410	-0.05	0.04	-0.09	1.17	-0.29	-0.28	0.25	0.64	plastid	non-intrinsic ABC protein 11
AT2G01350	-0.35	0.22	0.27	1.15	0.05	-0.29	0.04	0.11	cytosol	quinolinate phoshoribosyltransferase
AT4G18480	0.39	0.41	0.53	1.13	-0.14	0.00	0.00	-0.01	plastid	P-loop containing nucleoside triphosphate hydrolases superfamily protein
AT5G60600	-0.05	0.16	0.38	1.03	0.01	-0.03	0.01	0.06	plastid	4-hydroxy-3-methylbut-2-enyl diphosphate synthase
AT1G52410	-1.97	0.26	0.06	-1.01	-0.80	0.16	0.00	-0.44	cytosol	TSK-associating protein 1
AT2G26890	-0.77	0.35	0.40	-1.05	0.51	-0.03	-0.33	0.01	cytosol	DNAJ heat shock N-terminal domain-containing protein
AT4G36440	-22.88	-0.53	-0.25	-1.06	-24.31	-1.33	-0.09	0.06	plasma membrane	
AT1G13260	0.63	0.35	0.28	-1.29	NA	NA	NA	NA	nucleus	related to ABI3/VP1 1
AT1G80840	22.43	0.99	3.15	-1.30	NA	NA	NA	NA	nucleus	WRKY DNA-binding protein 40
AT3G17860	22.73	-0.18	-0.35	-1.31	NA	NA	NA	NA	nucleus	jasmonate-zim-domain protein 3
AT4G31550	NA	-0.08	1.50	-1.39	NA	NA	NA	NA	nucleus	WRKY DNA-binding protein 11
AT1G25560	NA	0.35	0.15	-1.45	NA	NA	NA	NA	nucleus	AP2/B3 transcription factor family protein
AT1G72450	0.56	0.20	-0.44	-1.52	NA	NA	NA	NA	nucleus	jasmonate-zim-domain protein 6
AT4G28910	1.28	0.32	-0.04	-1.61	23.88	-0.22	-0.41	0.06	nucleus	novel interactor of JAZ
AT2G22430	-0.10	-0.41	-0.70	-1.68	NA	NA	NA	NA	nucleus	homeobox protein 6
AT1G68840	0.32	0.84	1.40	-1.74	NA	NA	NA	NA	nucleus	related to ABI3/VP1 2
AT4G19003	NA	-0.52	0.52	-1.76	25.21	-0.31	1.42	-0.07	cytosol	E2F/DP family winged-helix DNA-binding domain
AT3G08630	0.57	-0.92	-0.57	-2.33	0.07	0.14	0.03	0.04	plastid	Protein of unknown function (DUF3411)
AT1G28280	-25.16	-25.81	-1.23	-2.38	-22.82	NA	NA	NA	nucleus	VQ motif-containing protein
AT2G29990	NA	-23.13	-23.39	-2.40	24.50	0.63	-25.33	-0.01	mitochondrion	alternative NAD(P)H dehydrogenase 2
AT3G02550	2.62	0.32	1.05	-2.54	NA	NA	NA	NA	nucleus	LOB domain-containing protein 41
AT3G54810	25.28	0.67	1.32	-2.82	NA	NA	NA	NA	nucleus	Plant-specific GATA-type zinc finger transcription factor family protein

Table S7: List of proteins showing quantitative change in the nuclear fraction at early time points. Proteins that are differentially expressed (|log2 value| > 1; p-value < 0.05) in the nuclear fraction at 15 min **(A),** 30 min **(B)**, and 60 min **(C)** respectively after 1µM-fl22/mock treatment or at 60 min **(C)** after 100µM CHX/mock (DMSO) treatment.

7. Acknowledgments

I would like to express my deepest gratitude to my direct supervisor Prof. Dr. Kenichi Tsuda for his excellent supervision and support till the very end of my thesis. I am extremely thankful that you always took time for discussions and constantly pushed me to further my critical thinking skills which helped me to successfully submit my thesis. I would also like to extend my deepest gratitude to my TAC members- Dr. Imre Somssich and Prof. Dr. Iris Finkemeier for their critical comments and constructive inputs during my TAC meetings. I am also grateful to our PhD coordinator Dr. Stephan Wagner for being a tremendous support during my PhD studies at the MPIPZ and also joining my thesis examination committee.

I am highly grateful to Prof. Dr. Stanislav Kopriva, Prof. Dr. Iris Finkemeier, and Prof. Dr. Achim Tresch for joining my thesis examination committee as first examiner, second examiner, and the chair of my thesis examination committee, respectively. I am thankful for the financial support from DAAD (Deutscher Akademischer Austauschdienst) for my PhD study. I would also like to thank Dr. Hirofumi Nakagami and my collaborators at the Protein Mass Spectrometry group for their support.

I am extremely thankful to all my Tsuda lab members for their support and making my stay at the MPIPZ one of the most enjoyable experiences of my academic career. A special thanks to Prof. Dr. Yiming Wang and Dr. Thomas Winkelmüller for allowing me to use their data. Many thanks to Dieter Becker for providing a fun atmosphere in the lab and many after work get togethers.

Finally, I am greatly thankful to my parents, sister and Carina for their belief in me and their continuous support throughout the ups and downs during my PhD which helped me to keep going till the very end.

8. Erklärung zur Dissertation

„Hiermit versichere ich an Eides statt, dass ich die vorliegende Dissertation selbstständig und ohne die Benutzung anderer als der angegebenen Hilfsmittel und Literatur angefertigt habe. Alle Stellen, die wörtlich oder sinngemäß aus veröffentlichten und nicht veröffentlichten Werken dem Wortlaut oder dem Sinn nach entnommen wurden, sind als solche kenntlich gemacht. Ich versichere an Eides statt, dass diese Dissertation noch keiner anderen Fakultät oder Universität zur Prüfung vorgelegen hat; dass sie - abgesehen von unten angegebenen Teilpublikationen und eingebundenen Artikeln und Manuskripten - noch nicht veröffentlicht worden ist sowie, dass ich eine Veröffentlichung der Dissertation vor Abschluss der Promotion nicht ohne Genehmigung des Promotionsausschusses vornehmen werde. Die Bestimmungen dieser Ordnung sind mir bekannt. Darüber hinaus erkläre ich hiermit, dass ich die Ordnung zur Sicherung guter wissenschaftlicher Praxis und zum Umgang mit wissenschaftlichem Fehlverhalten der Universität zu Köln gelesen und sie bei der Durchführung der Dissertation zugrundeliegenden Arbeiten und der schriftlich verfassten Dissertation beachtet habe und verpflichte mich hiermit, die dort genannten Vorgaben bei allen wissenschaftlichen Tätigkeiten zu beachten und umzusetzen. Ich versichere, dass die eingereichte elektronische Fassung der eingereichten Druckfassung vollständig entspricht."

Teilpublikationen:

Stuttmann J, Peine N, Garcia AV, Wagner C, Choudhury SR, Wang Y, et al. (2016) Arabidopsis thaliana DM2h (R8) within the Landsberg RPP1-like Resistance Locus Underlies three different cases of EDS1-conditioned autoimmunity. PLoS Genet 12(4):e1005990.

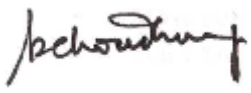

Köln, 25.01.2021